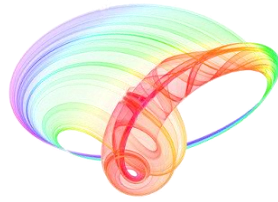


# **Book of abstracts**



## **PHOTONICA2021**

VIII International School and Conference on Photonics

& HEMMAGINERO workshop

23 - 27 August 2021,

Belgrade, Serbia

*Editors*

Mihailo Rabasović, Marina Lekić and Aleksandar Krmpot

Institute of Physics Belgrade, Serbia

Belgrade, 2021

ABSTRACTS OF TUTORIAL, KEYNOTE, INVITED LECTURES,  
PROGRESS REPORTS AND CONTRIBUTED PAPERS

of

VIII International School and Conference on Photonics  
PHOTONICA2021

23 - 27 August 2021

Belgrade Serbia

*Editors*

Mihailo Rabasović, Marina Lekić and Aleksandar Krmpot

*Publisher*

Institute of Physics Belgrade

Pregrevica 118

11080 Belgrade, Serbia

*Printed by*

Serbian Academy of Sciences and Arts

*Number of copies*

200

ISBN 978-86-82441-53-3

CIP - Каталогизација у публикацији - Народна библиотека Србије, Београд

535(048)

621.37/.39:535(048)

621.37/.39:535]:61(048)

66.017/.018(048)

INTERNATIONAL School and Conference on Photonic (8; 2021; Beograd)

Book of abstracts / VIII International School and Conference on Photonics PHOTONICA2021 & HEMMAGINERO workshop, 23 - 27 August 2021, Belgrade, Serbia; editors Mihailo Rabasović, Marina Lekić and Aleksandar Krmpot. - Belgrade: Institute of Physics, 2021 (Belgrade: SASA). - V, 192 str.: ilustr.; 30 cm

Tiraž 200. - Bibliografija uz većinu apstrakata. - Registar.

ISBN 978-86-82441-53-3

1. Hemmaginero Workshop (2021; Beograd)

а) Оптика -- Апстракти б) Оптички материјали -- Апстракти в) Оптоелектроника -- Апстракти г) Оптоелектроника -- Биомедицина -- Апстракти д) Телекомуникације -- Апстракти

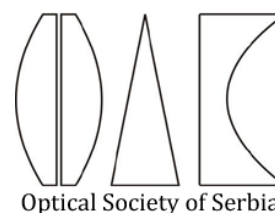
COBISS.SR-ID 44290057

PHOTONICA 2021 (VIII International School and Conference on Photonics - [www.photonica.ac.rs](http://www.photonica.ac.rs)) is organized by Institute of Physics Belgrade, University of Belgrade ([www.ipb.ac.rs](http://www.ipb.ac.rs)), Serbian Academy of Sciences and Arts ([www.sanu.ac.rs](http://www.sanu.ac.rs)), and Optical Society of Serbia ([www.ods.org.rs](http://www.ods.org.rs)).



PHOTONICA 2021 is organized under auspices and with support of the Ministry of Education, Science and Technological Development, Serbia ([www.mpd.gov.rs](http://www.mpd.gov.rs)).

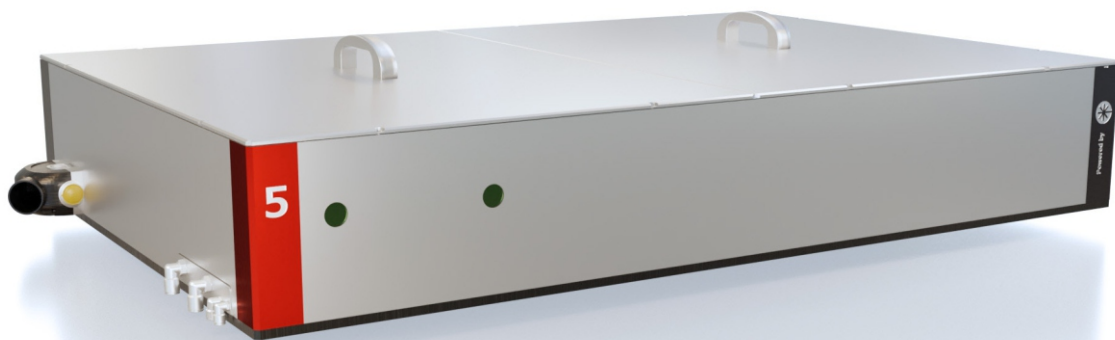
The support of the sponsors of PHOTONICA 2021 is gratefully acknowledged:



# WHITE DWARF OPCPA 5 W

## for few-cycle pulse

The **White Dwarf** OPCPA offers extremely short pulse durations with optional CEP stability in a compact, robust package.



### AVERAGE POWER

5 W

### WAVELENGTH OPTIONS

800 nm — 2000 nm

### PULSE DURATION

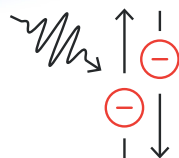
9 fs

### PUMPED BY

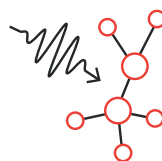
Coherent Monaco

### CEP stability

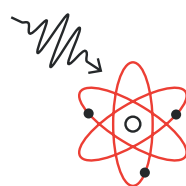
Optional



- Spin dynamics
- Superconductivity



- Cluster and gasphase dynamics



- Attosecond dynamics in solids and gases



## Committees

### Scientific Committee

- Aleksandar Krmpot, Serbia
- Aleksandra Maluckov, Serbia
- Bojan Resan, Switzerland
- Boris Malomed, Israel
- Branislav Jelenković, Serbia
- Carsten Ronning, Germany
- Concita Sibilica, Italy
- Darko Zibar, Denmark
- Dmitry Budker, Germany
- Dragan Inđin, United Kingdom
- Edik Rafailov, United Kingdom
- Francesco Cataliotti, Italy
- Giannis Zacharakis, Greece
- Goran Isić, Serbia
- Goran Mašanović, United Kingdom
- Ivana Vasić, Serbia
- Jasna Crnjanski, Serbia
- Jelena Radovanović, Serbia
- Jelena Stašić, Serbia
- Jerker Widengren, Sweden
- Jovan Bajić, Serbia
- Ljupčo Hadžievski, Serbia
- Luca Antonelli, UK
- Marco Canepari, France
- Marko Krstić, Serbia
- Marko Spasenović, Serbia
- Milan Kovačević, Serbia
- Milena Milošević, Serbia
- Milivoj Belić, Qatar
- Mirjana Novaković, Serbia
- Nikola Stojanović, Germany
- Nikola Vuković, Serbia
- Nikos Pleros, Greece
- Pavle Andjus, Serbia
- Petra Beličev, Serbia
- Sergei Turitsyn, UK
- Vladan Pavlović, Serbia
- Vladan Vuletić, USA
- Vladana Vukojević, Sweden
- Zoran Grujić, Serbia

### Organizing Committee

- Marina Lekić, Institute of Physics Belgrade (Chair)
- Aleksandar Krmpot, Institute of Physics Belgrade (Co-Chair)
- Danica Pavlović, Institute of Physics Belgrade (Secretary)
- Stanko Nikolić, Institute of Physics Belgrade (Webmaster)
- Mihailo Rabasović, Institute of Physics Belgrade
- Tanja Pajić, Faculty of Biology, University of Belgrade
- Aleksandra Gočanin, Faculty of Physics, University of Belgrade
- Jadranka Vasiljević, Institute of Physics Belgrade
- Uroš Ralević, Institute of Physics Belgrade

### Technical Organizer



**Lufthansa City Center**  
Panacomp Wonderland  
Travel

<http://www.panacomp.net/>  
Tel: +381 21 466 075  
Tel: +381 21 466 076  
Tel: +381 21 466 077

Dear Colleagues, friends of photonics,

We are honored by your participation at our PHOTONICA 2021 and your contribution to the tradition of this event. This year PHOTONICA will be a hybrid event. It means the Conference will comprise both an in-person conference and a virtual conference. Welcome to the world of photonics.

**The International School and Conference on Photonics- PHOTONICA**, is a biennial event held in Belgrade since 2007. The first meeting in the series was called ISCOM (International School and Conference on Optics and Optical Materials), but it was later renamed to PHOTONICA to reflect more clearly the aims of the event as a forum for education of young scientists, exchanging new knowledge and ideas, and fostering collaboration between scientists working within emerging areas of photonic science and technology. A particular educational feature of the program is to enable students and young researchers to benefit from the event, by providing introductory lectures preceding most recent results in many topics covered by the regular talks. In other words, tutorial and keynote speakers will give lectures specifically designed for students and scientists starting in this field. Apart from the oral presentations PHOTONICA hosts vibrant poster sessions. A significant number of best posters will be selected and the authors will have opportunity to present their work through short oral presentations – contributed talks.

The wish of the organizers is to provide a platform for discussing new developments and concepts within various disciplines of photonics, by bringing together researchers from academia, government and industrial laboratories for scientific interaction, the showcasing of new results in the relevant fields and debate on future trends.

PHOTONICA 2021 will host HEMMAGINERO workshop which is dedicated to hemoglobin and erythrocytes imaging and spectroscopy in various aspects. The Workshop is related to HEMMAGINERO project funded by the Science fund of Republic of Serbia, within PROMIS program. In addition, the representatives of the companies related to photonics will have significant role at the event by presenting the new trends in research and development sector. Following the official program, the participants will also have plenty of opportunities to mix and network outside of the lecture theatre with planned free time and social events

This book contains 161 abstracts of all presentations at the VIII International School and Conference on Photonics, PHOTONICA2021. Authors from all around the world, from all the continents, will present their work at this event. There will be five tutorial and seven keynote lectures to the benefits of students and early stage researches. The most recent results in various research fields of photonics will be presented through sixteen invited lectures and twelve progress reports of early-stage researchers. Within the poster sessions and a number of contributed talks, authors will present 122 poster presentations on their new results in a cozy atmosphere of the building of Serbian Academy of Science and Arts.

Belgrade, August 2021

Editors

# Table of Contents

<b>Tutorial Lectures.....</b>	<b>9</b>
T.1 Advancing Photonics with Machine Learning.....	10
T.2 Revealing details of cellular dynamics - a super-resolution fluorescence spectroscopy story ...	11
T.3 Progress in InP-based Photonic Integration.....	12
<b>Keynote Lectures.....</b>	<b>13</b>
K.1 The amazing effectiveness of fluorescence as a tool to understand structure and dynamics of molecules .....	14
K.2 Ultrafast Measurements and Extreme Events in Nonlinear Fibre Optics .....	15
K.3 Quantum gases in optical boxes .....	16
K.4 Nanophotonics: an enabling tool for basic research and technology.....	17
K.5 Photonic and plasmonic semiconductor nanowire lasers.....	18
K.6 Programmable Quantum Simulator with 256 Atoms .....	19
K.7 Smart and Responsive Photonic Materials .....	20
<b>Invited Lectures.....</b>	<b>21</b>
I.1 Non-linear Detection of THz radiation using a Metasurface Enhanced Sensor .....	22
I.2 Recent machine-learning applications in ultrafast nonlinear fibre photonics.....	23
I.3 Ultrafast processes at laser material processing: Toward more knowledge and better control .	24
I.4 Nonlinear topological phenomena in photorefractive photonic lattices .....	25
I.5 Diode pumped alkali laser – current status and prospects .....	26
I.6 Subwavelength Optical Lattices .....	27
I.7 Topological machine learning for photonics .....	28
I.8 Multiphysics modelling of infrared photodetectors based on graphene .....	29
I.9 Light sheet microscopy for fast 3D imaging of living samples .....	30
I.10 Mixed-dimensional van der Waals heterointerfaces.....	31
I.11 Gamma Factory, or how the largest accelerator facility is bringing atomic physics to its extreme .....	32
I.12 Quantum Information Hardware Based on Color Center Nanophotonics .....	33
I.13 Nonlinear photonic states in topological systems.....	34
I.14 Apertureless scanning near field microscopy and applications .....	35
I.15 Quantitative single molecule localization microscopy for precision medicine .....	36
I.16 Photoacoustic imaging: Listening to laser light interactions with matter.....	37
I.17 Compact, commercial 200 kHz few-cycle OPCPA at 800 nm with stable CEP .....	38

<b>Progress Reports.....</b>	<b>39</b>
P.1 Carbon nanocomposites as advantageous antibacterial surfaces .....	40
P.2 Terahertz Quantum-Cascade Lasers: Physics of the Electrons Transport, Design Review and Temperature Performance Optimization .....	41
P.3 Proposal for realizing quantum scars in the tilted 1D Fermi-Hubbard model.....	42
P.4 The Influence of Ion Implantation of Iron on the Surface Properties of High Density Polyethylene .....	43
P.5 Unsupervised method for time-series classification of signals obtained from calcium imaging	44
P.6 Live-cell cartography: spatial mapping of biomolecular information by functional Fluorescence Microscopy Imaging (fFMI).....	45
P.7 Pixel categorization based on resonance energy transfer between fluorescent molecules: a pathway towards localization of functionalized metal nanoparticles in individual cells by fluorescence microscopy .....	46
P.8 Microspectroscopy and adaptive laser tools for fluorescence based retinal tissue diagnostics and therapy .....	47
P.9 How to create 2D magnets from non-magnetic 2D crystals .....	48
P.10 Langmuir-Blodgett films from liquid phase exfoliated 2D materials: surface modification and optoelectronic properties .....	49
P.11 Faraday and Resonant Waves in Dipolar Cigar-Shaped Bose-Einstein Condensates .....	50
P.12 XUV-driven plasma switch for THz: new spatio-temporal overlap tool for XUV–THz pump–probe experiments at FELs .....	51
<b>1. Quantum optics and ultracold systems .....</b>	<b>53</b>
Q.O.1 Using a mapping as a probe for heating suppression in periodically driven many-body quantum systems: a mean-field example with Bose gases.....	54
Q.O.2 Autler-Townes spectroscopy in a Mn-dopedInGaAs/GaAs quantum dot.....	55
Q.O.3 Bend-free photonic integrated circuits with the crosstalk as a resource .....	56
Q.O.4 Control of entanglement between driven three-level atom in ladder-type configuration and its spontaneous emission.....	57
Q.O.5 Intensity squeezed states of light by four wave mixing in potassium vapor.....	58
Q.O.6 Quantum droplets in dipolar ring-shaped Bose-Einstein condensates .....	59
Q.O.7 Non-equilibrium evolution of Bose-Einstein condensate deformation in temporally controlled weak disorder .....	60
Q.O.8 Slow light under double-double EIT regime in spherical quantum dot with hydrogen impurity .....	61
Q.O.9 Search for topological defects of bosonic ultralight field with optically pumped magnetometer: design, calibration, and sensitivity of the Belgrade GNOME station .....	62

<b>2. Nonlinear optics .....</b>	<b>63</b>
N.O.1 Stability of necklace beams in media with cubic-quintic nonlinearity .....	64
N.O.2 Strong-field ionization of diatomic molecules and molecular anions: interferences and classical model .....	65
N.O.3 On the propagation of twin beam pulses in four-way-mixing medium – cause for asymmetric broadening and splitting.....	66
N.O.4 Mobility of localized solutions in a nonlinear graphene ribbon.....	67
N.O.5 Optical vortices in waveguides with spatial dependence of the nonlinear refractive index.....	68
N.O.6 Compact localized modes in the flux dressed 2D octagonal-diamond photonic lattice in the presence of nonlinearity .....	69
N.O.7 Spatio-temporal solitary and traveling wave solutions to the Kundu–Mukherjee–Naskar equation.....	70
N.O.8 Active multi-core fibers – photonic platform for development of a topological charge switching device.....	71
N.O.9 The nature, origin, and properties of the one- and two-dimensional optical rogue waves.....	72
N.O.10 Bright solitons under the influence of third-order dispersion and self-steepening effect .....	73
<b>3. Optical materials .....</b>	<b>74</b>
O.M.1 Narrowing of laser beam propagating through biological suspension .....	75
O.M.2 2D silver-bismuth-iodide rudorffitenanomaterials for photovoltaic devices: a novel route for chemical synthesis of $Ag_3BiI_6$ nanosheets.....	76
O.M.3 Influence of boundary conditions on electronic and transport properties in monolayer low – buckled HgTe nanoribbons.....	77
O.M.4 Structural and Optical Characterization of titanium-carbide and polymethyl methacrylate based nanocomposite.....	78
O.M.5 Nickel vertical posts: Influence of thickness on magnetic and optical properties.....	79
O.M.6 Consideration and definition of optical phenomena and properties of ultrathin crystalline films.....	80
O.M.7 Nanoscopy of van der Waals heterostructures fabricated by the wet transfer method.....	81
O.M.8 Thulium-doped titanate-germanate glasses for infrared photonics.....	82
O.M.9 Light-induced optical effects in phosphorus, nitrogen and boron doped diamonds.....	83
O.M.10 Effect of Au/Ag ion implantation and subsequent thermal annealing on optical properties of titanium nitride thin films.....	84
O.M.11 Influence of the protective layer on the photoacoustic response of transparent samples .....	85
O.M.12 Plasma-assisted nitrogen doping of Langmuir-Blodgett self-assembled graphene films.....	86
O.M.13 Enhanced photoluminescence of gamma-irradiated S, N graphene quantum dots.....	87
O.M.14 A cluster of bilayer diodesmodel for bulk heterojunction organic solar cells .....	88

O.M.15	Influencing on optical properties of buffered TiO <sub>2</sub> -Au thin film systems by deposition and annealing parameters .....	89
O.M.16	Hard-templated porous Nb <sub>2</sub> O <sub>5</sub> thin films for chemiresistive VOC sensing .....	90
O.M.17	Determination of refractive index of ultrathin dielectric films prepared via layer-by-layer polyelectrolyte deposition .....	91
O.M.18	Interplay between ordered multilayer structure and randomly distributed nanospheres and nanopillars in dichromated pullulan increases the width of the photonic bandgap .....	92
O.M.19	Diamond-based nanocomposites as sources of fast X-ray luminescence in the visible and near-IR range .....	93
O.M.20	High-resolution terahertz and infrared spectroscopy of hybrid perovskite CH <sub>3</sub> NH <sub>3</sub> PbI <sub>3</sub> .....	94
O.M.21	Organic framework engineering for VOC sensing in mesoporous SiO <sub>2</sub> films.....	95
O.M.22	Acetone sensing with optical readout using SiO <sub>2</sub> thin films .....	96

**4. Biophotonics..... 97**

B.1	A new tool for measuring local temperature gradients on a submicron scale .....	98
B.2	Natural waveguides on <i>Hoplia argentea</i> elytra .....	99
B.3	Thermoresponsive, biocompatible hydrogels for rapid prototyping of biomimetic microchannels .....	100
B.4	Coupled substitutions of fluorapatite crystals in the engineering of optically-active bionanomaterials.....	101
B.5	Influence of light guide type on dental composite polymerization shrinkage – a holographic and thermographic study .....	102
B.6	The metal-doped TiO <sub>2</sub> nanoparticles as photosensitizers in photodynamic therapy of melanoma .....	103
B.7	Laser Microsurgery of Filamentous Fungi: The Latest Protocol Enabling Patch-Clamp Amenable Protoplasts .....	104
B.8	Boosting surface plasmon resonances of thin golden film by bio photonic crystals .....	105
B.9	Mapping of fluorescent compounds in lyophilized blackcurrant ( <i>Ribes nigrum L.</i> ) fruits using spectroscopy and nonlinear microscopy .....	106
B.10	Interaction of ultrashort laser pulses with hemoglobin as a tool for selective erythrocytes photo-labeling .....	107
B.11	Discovering abnormal erythrocyte membranes - optical approaches.....	108
B.12	Visible light-responsiveness of the nanocarrier/drug complex based on the TiO <sub>2</sub> nanoparticles and Ru complex .....	109
B.13	The use of Raman microspectroscopy for characterization of tumor and tumor margin cell populations.....	110
B.14	First glance at a multitude of ion currents on filamentous fungus <i>P. blakesleeanus</i> protoplasts obtained by femtosecond laser microsurgery .....	111
B.15	Surface roughness and topography of dentin characterized by AFM.....	112

B.16 Secondary structure of *Ginkgo biloba* chlorophyll catabolites by circular dichroism spectroscopy ..... 113

B.17 Altered organization of collagen fibers in the uninvolved human colon mucosa 10 cm and 20 cm away from the colorectal cancer ..... 114

B.18 Label-free Third Harmonic Generation Imaging of Lipid Droplets in Live Filamentous Fungi ..... 115

B.19 Nonlinear Imaging of Dentin-Adhesive Interface Treated by Cold Atmospheric Plasma ..... 116

**5. Devices and components..... 117**

D.C.1 Modeling of intersubband transitions in ZnO/ZnMgO Coupled QuantumWells ..... 118

D.C.2 Surface recombination influence on photocurrent spectra of organic photovoltaic devices ..... 119

D.C.3 Measuring the Spectrally-Resolved Linewidth Enhancement Factor..... 120

D.C.4 Interband cascade lasers: overcoming intersubband transitions in the valence band ..... 121

D.C.5 Bend-free photonic integrated circuits with the crosstalk as a resource..... 122

D.C.6 Influence of vacancy defects on electronic structure of graphene nanoribbons ..... 123

D.C.7 High-power diffraction-limited laser systems oscillating in middle infrared spectral range on strontium atomic self-terminating transitions ..... 124

D.C.8 Fiber optic sensor system for intrusion location detection based on Sagnac interferometer ..... 125

D.C.9 Frequency combs generated by a Bloch gain induced giant Kerr nonlinearity ..... 126

D.C.10 Advanced model of Mid-IR quantum cascade laser active region with anisotropy effects included ..... 127

D.C.11 GST loaded silicon-on-insulator diffraction grating..... 128

D.C.12 The electron coherent transport in nonpolar m-plane ZnO/MgZnO resonant tunneling diodes ..... 129

D.C.13 High-power high-beam quality laser systems oscillating in visible spectral range on copper atomic self-terminating transitions ..... 130

**6. Optical communications..... 131**

O.C.1 Experimental observation of edge states in dimerized Stub photonic lattices ..... 132

O.C.2 An estimation of the far-field intensity distribution for novel hollow photonic crystal optical fibers..... 133

**7. Laser spectroscopy and metrology..... 134**

L.S.M.1 Time-spatial resolved LIBS of atomic and molecular carbon in laser ablation plasma.... 135

L.S.M.2 Colorimetric system based on CCD array spectrometer ..... 136

L.S.M.3 Effects of laser heating on luminescent properties of Gd<sub>2</sub>O<sub>3</sub>:Er,Yb nanophosphor ..... 137

L.S.M.4	Optical Phase Locked Loop for Quantum Cascade Laser Frequency Combs .....	138
L.S.M.5	Approaching the Heisenberg limit in a many-spin system .....	139
<b>8. Ultrafast optical phenomena .....</b>		<b>140</b>
U.O.1	Ultrashort quasi-non-diffracting long-range Gauss-Bessel beams .....	141
U.O.2	Femtosecond laser spectroscopy for Exploration of Space: Introduction of new research group at German Aerospace Center.....	142
U.O.3	Ultrafast Laser Control of Interatomic-Coulomb-Decay Dynamics.....	143
U.O.4	Upgrading of the THz beamline for pump-probe experiments in FLASH2020+.....	144
U.O.5	Single-shot THz characterization for a new THz/XUV endstation in FLASH2020+ .....	145
<b>9. Laser - material interaction.....</b>		<b>146</b>
L.M.I.1	Sulphur concentration influence on morphology and optical properties of MoS <sub>2</sub> monolayers .....	147
L.M.I.2	Optical breakdown of liquid media triggered by a wide range of laser pulse durations and its analytical application.....	148
L.M.I.3	Morphological study of silver in the conditions of ultrashort laser ablation in liquid.....	149
L.M.I.4	Analysis of Chitosan/ Hydroxyapatite spin-coated fs microstructured Poly Lactic Acid (PLA) temporary cell scaffolds .....	150
L.M.I.5	Neodymium-doped ZnO nanoparticles for NIR II biomarkers .....	151
L.M.I.6	Dynamic interference of photoelectrons at multiphoton ionization of atoms by short laser pulses .....	152
L.M.I.7	Laser surface texturing of Ti/Cu/Ti/Si and Ti/Cu/Zr/Ti/Si multilayer thin films.....	153
L.M.I.8	Raman spectroscopy and multivariate classification as a tool for different ketchup samples discrimination .....	154
L.M.I.9	Implementation of general Bessel beam scattering using the discrete dipole approximation .....	155
L.M.I.10	The surface array structures induced by femtosecond laser modifications of Ti/Cr multilayer thin films for biomedical applications .....	156
L.M.I.11	Direct laser writing waveguides in CR-39 polymer .....	157
<b>10. Optical metamaterials and plasmonics .....</b>		<b>158</b>
O.M.P.1	Active terahertz metamaterial for polarization manipulation and biosensing .....	159
O.M.P.2	Light absorption in two-dimensional crystals covered by randomly distributed plasmonic nanoparticles.....	160
O.M.P.3	Fibonacci sequence design for MXene based metasurface with enhanced optical absorption in the visible range.....	161
O.M.P.4	Hyperbolic Metamaterials via Hierarchical Block Copolymer Nanostructures .....	162

O.M.P.5 Optical properties of surface plasmon polaritons launched via metallic groves ..... 163

O.M.P.6 Dependence of loss parameters on circularly polarized terahertz wave propagation through graphene gated metamaterial ..... 164

O.M.P.7 Bio-inspired holey submicrometer plasmonic core-shell particles as generalized synthetic brochosomes ..... 165

**11. Machine learning in photonics ..... 166**

M.L.1 Deep learning for analysis of optical maps of CVD-grown TMDs ..... 167

M.L.2 Design and optimization of fiber-optic colorimetric probe based on ANN for estimating spectrum of color samples..... 168

M.L.3 Electronic Semiconductor Characterization Using Reverse-Back Procedure Based on Neural Networks and Photoacoustic Response ..... 169

M.L.4 Deep learning solutions for cross-phase modulation dominated channels..... 170

M.L.5 Using SOLO software package for classification of temperature dependent luminescence spectra ..... 171

M.L.6 Reducing number of measuring points for estimating reflected spectrum of colorimetric probe ..... 172

M.L.7 Influence of data scaling and normalization on overall neural network performances in photoacoustics ..... 173

M.L.8 Trace gases analysis in pulsed photoacoustics based on swarm intelligence optimization.... 174

**12. Other topics in photonics..... 175**

O.P.1 Localization-delocalization transition in compressed Lieb ribbon lattices ..... 176

O.P.2 Transport properties and localized edge modes arising at imperfect kagome lattices..... 177

O.P.3 Bipartite lattice of domain wall junction states in photonic lattices ..... 178

O.P.4 Calculation of transition amplitude in two levels systems by application of an adiabatic approximation..... 179

O.P.5 Influence of UV radiation on the time response of a resistive gas sensor based on liquid-phase exfoliated graphene ..... 180

O.P.6 Observation of inter-orbital coupling ..... 181

O.P.7 Microstructural characterization of Al-Cu alloy with optical microscopy in bright field and polarized light..... 182

O.P.8 Tracking of the temporal dependency of fading of the human footprint temperature contrast ..... 183

O.P.9 Optimization of Optoelectronic Properties of Electrochemically Exfoliated Graphene by Cascade Centrifugation ..... 184

O.P.10 Relevance of incoherent light-induced coherences for photosynthetic energy transfer ..... 185

O.P.11 Coupled waveguide arrays ring resonators..... 186

**Index ..... 187**

# **Tutorial Lectures**

## Advancing Photonics with Machine Learning

Alexandra Boltasseva

School of Electrical and Computer Engineering, Birck Nanotechnology Center and Purdue Quantum Science and Engineering Institute, Purdue University, West Lafayette, IN 47906, USA

and

The Quantum Science Center (QSC), a National Quantum Information Science Research Center of the U.S. Department of Energy (DOE), Oak Ridge, TN 37931  
aeb@purdue.edu

Discovering unconventional optical designs via machine-learning promises to advance on-chip circuitry, imaging, sensing, energy, and quantum information technology. In this talk, photonic design approaches and emerging material platforms will be discussed showcasing machine-learning-assisted topology optimization for thermophotovoltaic metasurface designs as well as machine learning algorithms for speeding-up quantum measurements and quantum device integration and prototyping.

## Revealing details of cellular dynamics - a super-resolution fluorescence spectroscopy story

F. Reina<sup>1,2</sup>, C. Lagerholm<sup>3</sup> and C. Eggeling<sup>1-3</sup>

<sup>1</sup>*Friedrich-Schiller-University Jena, Institute of Applied Optics and Biophysics, Jena, Germany*

<sup>2</sup>*Leibniz Institute of Photonic Technology e.V., Department Biophysical Imaging, Jena, Germany*

<sup>3</sup>*University of Oxford, MRC Human Immunology Unit & Wolfson Imaging Center Oxford, Oxford, United Kingdom*

e-mail:christian.eggeling@uni-jena.de

Molecular interactions are key in cellular signaling. They are usually ruled by the organization and mobility of the involved molecules. A key issue is the limited availability of photonic detection techniques with enough spatial and temporal resolution. We present different optical tools that are able to determine such organization and extract diffusion and interaction dynamics. These tools are based on advanced microscopy approaches such as the combination of super-resolution STED microscopy with fluorescence correlation spectroscopy (STED-FCS) or spectral detection, or ultrafast single-molecule tracking employing interferometric scattering (iSCAT) or recent Minflux microscopy. We highlight how these tools can reveal novel aspects of membrane bioactivity such as of the existence and function of potential lipid rafts.

### REFERENCES

- [1] E. Sezgin, I. Levental, S. Mayor, C. Eggeling, *Nat Rev Mol Cell Biol* 18, 361-374 (2017).
- [2] L. Schermelleh, A. Ferrand, T. Huser, C. Eggeling, M. Sauer, O. Biehlmaier, G.P.C. Drummen, *Nat Cell Biol* 21, 72-84 (2019).

## Progress in InP-based Photonic Integration

Meint K. Smit

*Institute for Photonic Integration, Eindhoven University of Technology, Eindhoven, 5600MB, The Netherlands*

The application market for Photonic Integrated Circuits (PICs) is rapidly growing. Photonic Integration is the dominant technology in high bandwidth and long-distance tele-communications and is increasingly applied in shorter distances and within data centers. It is set to become dominant in many other fields of photonics. PICs offer compelling performance advances in terms of precision, bandwidth and energy efficiency. To enable uptake in new sectors, the availability of highly standardized (generic) photonic integration platform technologies is of key importance as this separates design from technology, reducing barriers for new entrants. Another major challenge is low-cost and energy-efficient integration of photonics with the electronic circuitry that is used for driving and controlling the photonic IC and processing its information. The major platform technologies today are Indium Phosphide (InP)-based monolithic integration and Silicon Photonics. InP-based technology offers integration of the full suite of photonic components, including lasers, optical amplifiers and high-performance modulators. In this paper we describe the current status and future developments of InP-based generic integration and we discuss the potential of InP-based Photonics for integration with electronics.

# **Keynote Lectures**

## The amazing effectiveness of fluorescence as a tool to understand structure and dynamics of molecules

A.H.A. Clayton<sup>1</sup>,

<sup>1</sup>Optical Sciences Centre, Swinburne University of Technology, Melbourne, Australia

e-mail: aclayton@swin.edu.au

Fluorescence is the radiative emission resulting a transition from an excited singlet state to the ground state. Fluorescence is highly sensitive to structure and dynamics. This is mainly because of the nanosecond timescale a fluorescence probe molecule spends in the excited state. Judicious choice and placement of fluorescent molecule(s) within a biological macromolecule(s) enables the experimentalist to obtain information at a specific site(s) in the macromolecular (complex) of interest. Moreover, the inherent multi-dimensional nature of fluorescence signals across color (wavelength), orientation (polarization), space and time enables the design of experiments that give direct information on macromolecular structure and dynamics in biological environments, such as living cells [1].

In this talk, I will present a brief tour of methods developed in my laboratory that address structure and dynamics using fluorescence-based imaging techniques [1-6].

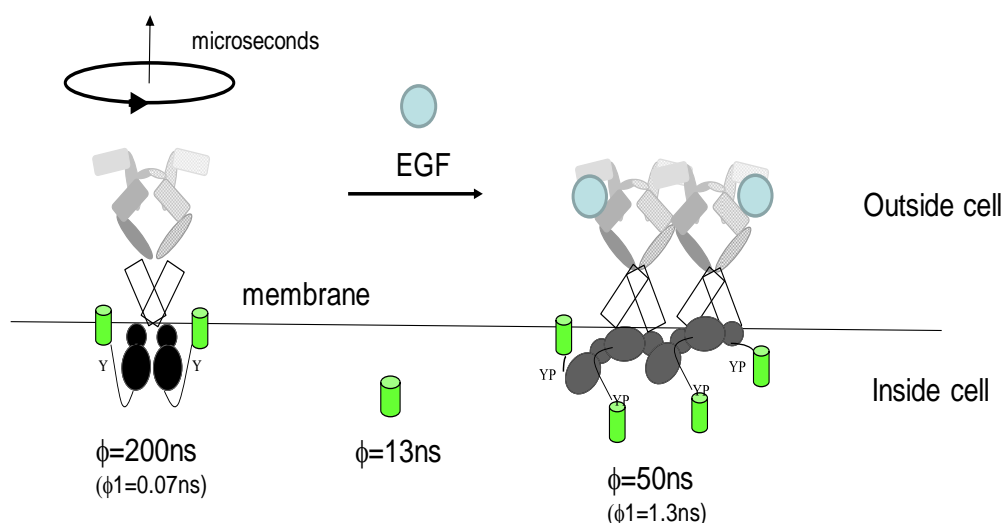


Figure 1. Structural dynamics of a membrane receptor on the surface of living cells [2] using polarized phasor ellipse approach [3]

### REFERENCES

- [1] A.H.A. Clayton, *Journal of Biosciences* 43 (3), 463-469 (2018).
- [2] N. Kozler, A.H.A. Clayton, *European Biophysics Journal*, 49(1), 29-27 (2020).
- [3] N. Kozler, A.H.A. Clayton, *Methods and applications in fluorescence* 4 (2), 024005 (2018).
- [4] A. Lajevardipour *et al*, *Scientific reports* 6 (1), 1-10 (2016).
- [5] A. Lajevardipour, J.W.M. Chon, A.H.A. Clayton, *AIMS Biophysics*, 2, 1-7, (2015).
- [6] N. Kozler *et al*, *Biochemistry* 53 (16), 2594-2604, (2014).

## Ultrafast Measurements and Extreme Events in Nonlinear Fibre Optics

J. M. Dudley,<sup>1</sup> F. Meng,<sup>1</sup> C. Lapre,<sup>1</sup> M. Mabed,<sup>1</sup> C. Finot,<sup>2</sup> G. Genty<sup>3</sup>

<sup>1</sup> *Institut FEMTO-ST, Université Bourgogne Franche-Comté CNRS UMR 6174, Besançon, 25000, France*

<sup>2</sup> *Laboratoire Interdisciplinaire Carnot de Bourgogne, Université Bourgogne Franche-Comté CNRS UMR 6303, Dijon, 21078, France*

<sup>3</sup> *Photonics Laboratory, Tampere University, Tampere, FI-33104, Finland*  
e-mail:john.dudley@univ-fcomte.fr

The year 2021 represents 60 years since the birth of nonlinear optics, and with continued developments in sources, materials, and waveguides, the field is more active than ever. An area of much recent interest has focused on studying extreme nonlinear pulse propagation in optical fibre and fibre lasers, and experiments have revealed a rich landscape of complex interactions due to the interplay of nonlinearity, dispersion and dissipation. In the past, however, these dynamics have not been able to be measured completely because of experimental limitations, but new techniques have now opened up the possibility to analyze a range of novel nonlinear processes, including the generation of spontaneous “rogue wave” events with analogies to the giant and destructive waves on the surface of the ocean [1]. After giving a general introduction to the field and an overview of the measurement techniques used, we will discuss a range of recent results in both fibre propagation and fibre laser systems [2,3]. We will also describe how tools from artificial intelligence such as neural networks are providing further new methodologies to study and understand such complex dynamics [4-6].

### REFERENCES

- [1] J. M. Dudley, G. Genty, A. Mussot, A. Chabchoub, F. Dias, Rogue waves and analogies in optics and oceanography, *Nature Reviews Physics* 1 675-689 (2019).
- [2] C. Lapre, C. Billet, F. Meng, P. Ryczkowski, T. Sylvestre, C. Finot, G. Genty, J. M. Dudley, Real-time characterization of spectral instabilities in a mode-locked fibre laser exhibiting soliton-similariton dynamics, *Scientific Reports* 9, 13950 (2019)
- [3] F. Meng, C. Lapre, C. Billet, G. Genty, J. M. Dudley, Instabilities in a dissipative soliton-similariton laser using a scalar iterative map, *Optics Letters* 45, 1232-1235 (2020)
- [4] L. Salmela, C. Lapre, J. M. Dudley, G. Genty, Machine learning analysis of rogue solitons in supercontinuum generation, *Scientific Reports* 10, 9596 (2020)
- [5] G. Genty, L. Salmela, J. M. Dudley, D. Brunner, A. Kokhanovskiy, S. Kobtsev, S. K. Turitsyn. Machine Learning and Applications in Ultrafast Photonics, *Nature Photonics* 15, 91-101 (2021)
- [6] L. Salmela, N. Tzipinakis, A. Foi, C. Billet, J. M. Dudley, G. Genty, Predicting ultrafast nonlinear dynamics in fibre optics with a recurrent neural network. *Nature Machine Intelligence* 3 (4), 344-354 (2021)

## Quantum gases in optical boxes

Zoran Hadzibabic

*Cavendish Laboratory, University of Cambridge, UK*

e-mail: zh10001@cam.ac.uk

For the past 25 years ultracold atomic gases have been used with great success to study fundamental many-body phenomena such as Bose-Einstein condensation and superfluidity. While traditionally they were produced in harmonic electromagnetic traps, it is now also possible to create them in the uniform potential of an optical box trap [1]. This has opened many new possibilities, allowing closer connections with other many-body systems and textbook theories. I will give an overview of some of our experiments with these novel systems, which range from verifications of old theories of equilibrium interacting 3D [2] and 2D [3] systems, to studies of nonequilibrium phenomena such as critical dynamics [4] and turbulence [5, 6], to still open-ended searches for universal behavior in far-from-equilibrium quantum systems [7, 8].

### REFERENCES

- [1] A. L. Gaunt, T. F. Schmidutz, I. Gotlibovych, R. P. Smith, and Z. Hadzibabic, *Phys. Rev. Lett.* **110**, 200406 (2013).
- [2] R. Lopes, C. Eigen, N. Navon, D. Clément, R. P. Smith, and Z. Hadzibabic, *Phys. Rev. Lett.* **119**, 190404 (2017).
- [3] P. Christodoulou, M. Galka, N. Dogra, R. Lopes, J. Schmitt, and Z. Hadzibabic, *Nature* **594**, 191 (2021).
- [4] N. Navon, A. L. Gaunt, R. P. Smith, and Z. Hadzibabic, *Science* **347**, 167 (2015).
- [5] N. Navon, A. L. Gaunt, R. P. Smith, and Z. Hadzibabic, *Nature* **539**, 72 (2016).
- [6] N. Navon, C. Eigen, J. Zhang, R. Lopes, A. L. Gaunt, K. Fujimoto, M. Tsubota, R. P. Smith, and Z. Hadzibabic, *Science* **366**, 382 (2019).
- [7] C. Eigen, J. A. P. Glidden, R. Lopes, E. A. Cornell, R. P. Smith, and Z. Hadzibabic, *Nature* **563**, 221 (2018).
- [8] J. A. P. Glidden, C. Eigen, L. H. Dogra, T. A. Hilker, R. P. Smith, and Z. Hadzibabic, *Nat. Phys.* **17**, 457 (2021).

## Nanophotonics: an enabling tool for basic research and technology

R. Quidant <sup>1</sup>

<sup>1</sup>*Nanophotonic Systems Laboratory, Department of Mechanical and Process Engineering, ETH Zurich, Switzerland*  
[rquidant@ethz.ch](mailto:rquidant@ethz.ch)

Twenty years of extensive research in the field of nanooptics have enabled us to considerably advance light control on the nanometer scale. Following the early *peak of inflated expectation*, the assets of nanooptics over other technologies, along with its limitations, became clearer. More recently, the field has entered into the *slope of enlightenment* in which its actual contribution to both basic research and novel technologies has been better identified. In this talk, following a general introduction on the main assets of nano-optics, we will review different aspects of our research where nano-optical resonators, both metallic and dielectric, are used as an enabling technology, which benefits a wide range of scientific disciplines, all the way from Lab-on-a-chip technology [1-4], reconfigurable planar optics [5,6] to additive manufacturing [7,8].

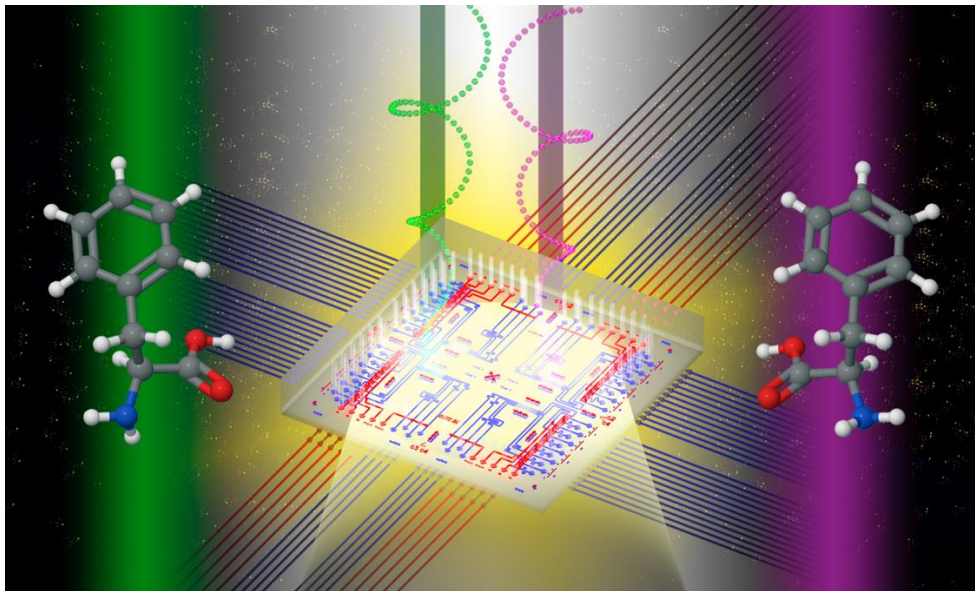


Figure 1. 3D sketch of on-chip chiral biosensing using dielectric nanoresonators

### REFERENCES

- [1] O. Yavas, M. Svedendahl, P. Dobosz, V. Sanz, R. Quidant, *Nano Lett.* **17**, 4421 (2017)
- [2] O. Yavas, M. Svedendahl, R. Quidant, *ACS Nano* **13**, 4582 (2019)
- [3] J. García-Guirado, M. Svedendahl, J. Puigdollers, R. Quidant, *Nano Lett.* **20**, 585 (2020)
- [4] B. Ciraulo, J. Garcia Guirado, I. de Miguel, J. Ortega, R. Quidant, *Nature Comm.* **12**, 2001 (2021)
- [5] A. Afridi, J. Canet, L. Philippet, J. Osmond, P. Berto, R. Quidant, *ACS Photonics* **5**, 4497 (2018)
- [6] P. Berto, L. Philippet, J. Osmond, C. F. Liu, A. Afridi, M. Montagut, B. Molero, G. Tessier, R. Quidant, *Nature Photon.* **13**, 649 (2019)
- [7] A. Powell, A. Stavrinadis, I. de Miguel, G. Konstantatos, R. Quidant, *NanoLett.* **18**, 6660 (2018)
- [8] A. Powell, A. Stavrinadis, S. Christodoulou, R. Quidant, G. Konstantatos, *NanoLett.* **20**, 3485 (2020)

## Photonic and plasmonic semiconductor nanowire lasers

Carsten Ronning<sup>1</sup>

<sup>1</sup>*Institute of Solid State Physics, Friedrich Schiller University Jena, Germany*  
carsten.ronning@uni-jena.de

The miniaturization of light sources, the confinement and manipulation of light on a sub-wavelength scale as well as the detection of single photons are key challenges for the realization of future photonic circuits. Here, semiconductor nanowires are of major interest as a serving material platform, since they do not only offer superior photonic properties, but can also bridge the interface to electronic circuits enabled by their semiconducting properties. The efficient and sub-wavelength waveguiding of light is one of such superior photonic properties specifying nanowires as truly one-dimensional systems for photons [1]. It is also an important prerequisite and defines the geometrical diameter limit for enabling lasing oscillations within nanowire cavities [2,3]. High pumping powers and gain values are necessary in order to overcome the thresholds for amplified spontaneous emission (ASE) and laser oscillations. We determined those thresholds for both ZnO and CdS nanowires as well as the geometrical limitations [3,4]. Furthermore, the laser output originating out of the end facet of a single nanowire was detected “head-on”, and a double pump technique was applied to measure the laser dynamics [5-7]. Finally, I will present in this presentation the possibility of coupling such lasing nanowires with plasmonic structures in order to accelerate the dynamics and confine the light field even into much smaller structures [8,9], which provides a useful benchmark for the future development of these nanoscale devices.

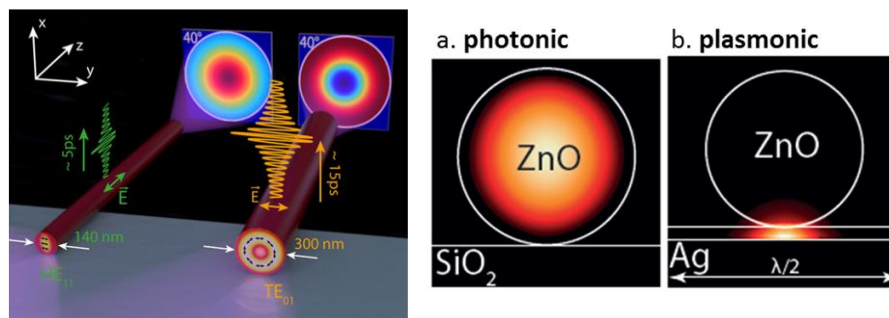


Figure 1. (left) Emission pattern, polarization and dynamics of photonic nanowire lasers as a function of their diameter, (right) field distributions in photonic and plasmonic nanowire lasers.

### REFERENCES

- [1] T. Voss, et al., *Nano Letters* 7, 3675 (2007)
- [2] M. Zimmler, et al., *Appl. Phys. Lett.* 93, 051101 (2008).
- [3] M. Zimmler, et al., *Semi. Sci. and Techn.* 25, 024001 (2010) - review.
- [4] S. Geburt, et al., *Nanotechnology* 23, 365204 (2012)
- [5] R. Röder, et al., *Nano Letters* 15, 4638 (2015)
- [6] R. Röder, et al., *Nano Letters* 16, 2878 (2016)
- [7] M. Zapf, et al., *Advanced Optical Materials* 7, 1900504 (2019)
- [9] T.P.H. Sidiropoulos, et al., *Nature Physics* 10, 870 (2014)
- [9] V. Sorger, et al., *Nano Letters* 11, 4907 (2011)

## Programmable Quantum Simulator with 256 Atoms

S. Ebadi<sup>1</sup>, T.T. Wang<sup>1</sup>, H. Levine<sup>1</sup>, A. Keesling<sup>1</sup>, G. Semeghini<sup>1</sup>,  
A. Omran<sup>1,2</sup>, D. Bluvstein<sup>1</sup>, R. Samajdar<sup>1</sup>, H. Pichler<sup>3</sup>, W.W. Ho<sup>1,4</sup>,  
S. Choi<sup>5,6</sup>, S. Sachdev<sup>1</sup>, M. Greiner<sup>1</sup>, M. Lukin<sup>1</sup>, and V. Vuletić<sup>6</sup>

<sup>1</sup> *Department of Physics, Harvard University, Cambridge, MA 02138, USA*

<sup>2</sup> *QuEra Computing Inc., Boston, MA 02135, USA*

<sup>3</sup> *Institute for Theoretical Physics, University of Innsbruck, Innsbruck A-6020, Austria*

<sup>4</sup> *Department of Physics, Stanford University, Stanford, CA 94305, USA*

<sup>5</sup> *Department of Physics, University of California Berkeley, Berkeley, CA 94720, USA*

<sup>6</sup> *Department of Physics and Research Laboratory of Electronics,  
Massachusetts Institute of Technology, Cambridge, MA 02139, USA*

e-mail:vuletic@mit.edu

Quantum simulation with individually trapped and controlled neutral ultracold atoms holds great promise for understanding complex many-body quantum processes in physics and chemistry. Here, we demonstrate a programmable quantum simulator based on deterministically prepared two-dimensional arrays of neutral atoms, featuring strong interactions controlled via coherent atomic excitation into Rydberg states. For sufficiently high quantum number, Rydberg atoms can interact over optically resolvable length scales, enabling individual control and readout of atomic spins.

Using this approach, we realize a quantum spin model with tunable interactions for system sizes ranging up to 256 qubits [1]. We benchmark the system by creating and characterizing high-fidelity antiferromagnetically ordered states, demonstrate universal properties of an Ising quantum phase transition in one and two dimensions, and study the dynamics after a sudden quench of the strongly interacting many-body system. We then create and study several new quantum phases that arise from the interplay between interactions and coherent laser excitation, experimentally map the phase diagram, and investigate the role of quantum fluctuations. We also demonstrate quantum gates between pairs of atoms with high fidelity [2].

### REFERENCES

- [1] Quantum Phases of Matter on a 256-Atom Programmable Quantum Simulator. S. Ebadi, T.T. Wang, Levine, A. Keesling, G. Semeghini, A. Omran, D. Bluvstein, R. Samajdar, H. Pichler, W.W. Ho, S. Choi, S. Sachdev, M. Greiner, V. Vuletić, and M.D. Lukin, *Nature* **595**, 227-232 (2021).
- [2] Parallel implementation of high-fidelity multi-qubit gates with neutral atoms. H. Levine, A. Keesling, G. Semeghini, A. Omran, T. T. Wang, S. Ebadi, H. Bernien, M. Greiner, V. Vuletić, H. Pichler, and M. D. Lukin, *Phys. Rev. Lett.* **123**, 170503 (2019).



## **Invited Lectures**

## Non-linear Detection of THz radiation using a Metasurface Enhanced Sensor

Hakan Altan

Department of Physics, Middle East Technical University, Cankaya 06800, Ankara, Turkey  
haltan@metu.edu.tr

The arrangements of subwavelength inclusions in a metasurface can serve as an effective absorber for the terahertz region. Furthermore, depending on the geometry such structures can lead to strong field confinement effects. When such an absorber that has such inclusions which exhibit field confinement is combined with a unique material, the absorption can induce effects that can lead to a change in the material's electrical properties. The optimization of such structures is key to the development of a new class of sensors and detectors in the THz region. To realize such a vision, the use of materials which exhibit conductive changes is necessary. Vanadium dioxide shows a passive and reversible change from monoclinic insulator phase to metallic tetragonal rutile structure by using external stimuli such as temperature (340K), photo excitation, electric field, mechanical strain or magnetic field [1,2]. Upon absorption of the THz radiation, the high electric fields that are generated inside the gaps of the metasurface can serve as trigger points, as was shown previously using kV strength THz E-fields [1]. By designing a better sensor which takes advantage of this non-linear enhancement one can lower this value to more accessible THz electric field strengths. Utilizing various metasurface designs we examined the insulator to metal transition in VO<sub>2</sub> when illuminated by THz radiation. For a unique unit-cell design based on a SRR-like structure we found that field enhancement is not necessarily related to the resonant frequency of the unit cell structure. The inclusion of gaps whose lengths were varied as 0.5, 1, 1.5 μm that are oriented perpendicularly to the polarized THz fields served as field enhancement centers. Comparisons are made for single and double notched gaps. Typically, we found maximum in-gap field enhancement values near 100 for a 1.0 μm gap size. The multiplication shows that the non-linear enhancement is highly dependent on the geometry of the electrodes for a fixed unit cell wall thickness. Such enhancements can be exploited in designing detectors in the sub-1 THz region where many applications from communications to sensing are taking place.

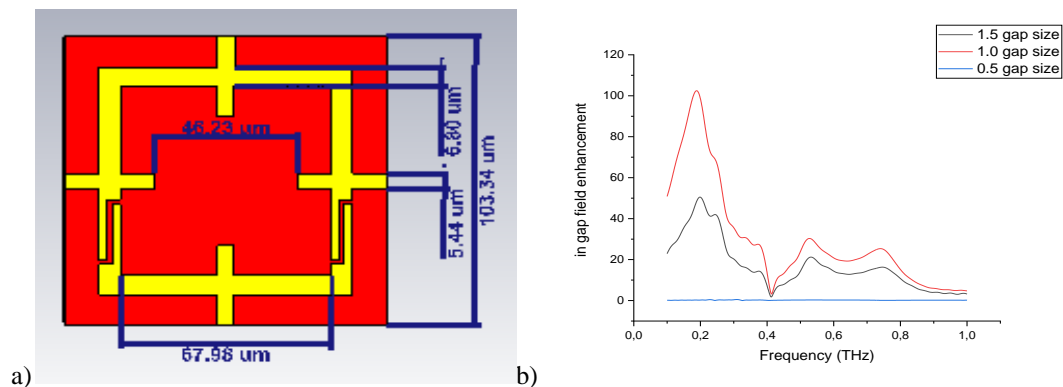


Figure 1. The metasurface unit cell is comprised of a gold patterned layer deposited on VO<sub>2</sub> and is designed to have a resonant absorption below 1 THz. To explore non-linear enhancement behavior two cases were analyzed: a) single notched b) in-gap field enhancement values

### REFERENCES

- [1] M. Liu, Y.H. Hwang, H. Tao, A.C., Strikwerda, K. Fan, G.R. Keiser, A.J. Sternbach, K.G. West, S. Kittiwatanakul, J. Lu, S.A. Wolf, F.G. Omenetto, X. Zhang, K.A. Nelson, and R.D. Averitt, "Terahertz Field-Induced Insulator-to-Metal Transition in Vanadium Dioxide Metamaterial," *Nature*. 487, 345-348 (2012).
- [2] S. Lysenko, A.J. Rua, V. Vikhmin, J. Jimenez, F. Fernandez and H. Liu, "Light-Induced Ultrafast Phase Transitions in VO<sub>2</sub> Thin Film," *Applied Surface Science*. 252, 5512-5515 (2006)

## Recent machine-learning applications in ultrafast nonlinear fibre photonics

Sonia Boscolo<sup>1</sup>, Christophe Finot<sup>2</sup> and Junsong Peng<sup>3</sup>

<sup>1</sup>*Aston Institute of Photonic Technologies, Aston University, Birmingham B4 7ET, United Kingdom*

<sup>2</sup>*Laboratoire Interdisciplinaire Carnot de Bourgogne, Université de Bourgogne-Franche Comté,  
21078 Dijon Cedex, France*

<sup>3</sup>*State Key Laboratory of Precision Spectroscopy, East China Normal University, Shanghai 200062, China*

e-mail: [s.a.boscolo@aston.ac.uk](mailto:s.a.boscolo@aston.ac.uk)

Recent years have seen the rapid growth and development of the field of smart photonics, where machine-learning algorithms are being matched to optical systems to add new functionalities and to enhance performance. Ultrafast photonics areas where the promise of machine learning is being realised include the design and operation of pulsed lasers, and the characterisation and control of ultrafast propagation dynamics [1].

Here, we review our recent results and advances in the field, by describing the use of a supervised feedforward neural network (NN) paradigm to solve the direct and inverse problems relating to nonlinear pulse shaping in optical fibres, bypassing the need for direct numerical solution of the governing propagation model [2]. Specifically, we show how the network accurately predicts the temporal and spectral intensity profiles of the pulses that form upon nonlinear propagation in fibres with both anomalous and normal dispersion. Further, we demonstrate the ability of the NN to determine the nonlinear propagation properties from the pulses observed at the fibre output, and to classify the output pulses according to the initial pulse shape. We also expand our analysis to the case of pulse propagation in the presence of distributed gain or loss, with a special focus on the generation of self-similar parabolic pulses [3]. The network can accommodate to and maintain high accuracy for a wide dynamic range of system parameters. Our results show that a properly trained network can greatly help the characterisation and inverse-engineering of fibre-based shaping systems by providing immediate and sufficiently accurate solutions.

Further, we demonstrate an evolutionary algorithm (EA) for the self-optimisation of the breathing-soliton regime in a mode-locked fibre laser, based on the optimal four-parameter tuning of the intracavity nonlinear transfer function through electronically driven polarisation control [4]. We define compound merit functions relying on the characteristic features of the radiofrequency spectrum of the laser output, which are capable to locate various self-starting breather regimes in the laser, including single breathers with controllable breathing ratio and period, and breather molecular complexes with a controllable number of elementary constituents. Contrary to the generation regimes of stationary pulses of ultrafast lasers that have been mainly addressed by previous works using EAs, breathing solitons exhibit a fast evolutionary behaviour [5]. In this respect, our work opens novel opportunities for the exploration of highly dynamic, non-stationary operating regimes of ultrafast lasers, such as soliton explosions, non-repetitive rare events and intermittent nonlinear regimes [6].

### REFERENCES

- [1] G. Genty et al., *Nat. Photon.* 15, 91 (2021).
- [2] S. Boscolo, C. Finot, *Opt. Laser Technol.* 131, 106439 (2020).
- [3] S. Boscolo, J.M. Dudley, C. Finot, *Res. Opt.* 3, 100066 (2021).
- [4] X. Wu, J. Peng, S. Boscolo, Y. Zhang, C. Finot, H. Zeng, Submitted (2021).
- [5] J. Peng, S. Boscolo, Z. Zhao, H. Zeng, *Sci. Adv.* 5, eaax1110 (2019).
- [6] C. Lapre et al., *Sci. Rep.* 9, 13950 (2019).

## Ultrafast processes at laser material processing: Toward more knowledge and better control

N.M. Bulgakova

*HiLASE Centre, Institute of Physics of the Czech Academy of Sciences, Dolní Břežany, Czech Republic*  
e-mail: [bulgakova@fzu.cz](mailto:bulgakova@fzu.cz)

When high-power laser pulses act on a solid material, being focused on the surface or inside the bulk, they trigger a large body of processes occurring simultaneously and/or sequentially. At ultrashort laser pulses, some material properties start to change swiftly already at femtosecond time scale, exhibiting strong variation of material optical response, emerging defect states, ultrafast “cold” melting, etc. that strongly depends on a material kind. Furthermore, modifications of material properties can be localized at nanometer spatial scales. There are no experimental methods, which would allow simultaneously to directly follow the complexity of the processes at such temporal and spatial scales. Only indirect techniques are available that give a valuable but far incomplete information which must be analyzed and properly understood. On the other hand, deep understanding of the fundamental phenomena involved in the laser action on materials of different kinds makes possible the elaboration of new approaches, new methodologies, and novel applications.

In this talk, the fundamental processes in ultrashort-laser-irradiated materials will be analyzed, starting from material excitation during the laser pulse, continuing with material relaxation routes, and finishing with imprinting modification features into material surface or bulk [1]. The following effects will be discussed based on comparison of theories and experiments: photoionization of bandgap materials in the regimes of surface and volumetric modification; formation of laser-induced periodic surface structures (LIPSS) with the role of surface plasmon polaritons; role of swift change of optical properties of materials, including metals, in laser energy coupling. Finally, new results on laser annealing of amorphous titania nanotubes [2], functionalization of graphene by using LIPSS imprinting to graphene supporting substrates [3], and formation of hollow tips on silicon by doughnut-shaped laser pulses will be presented. Further perspectives of laser-matter interaction studies will be also discussed, including new types of lasers under development with broad irradiation parameters, which widen the spectrum of viable laser applications in various fields of science, industry, and medicine.

### REFERENCES

- [1] N.M. Bulgakova, In: *Ultrafast Laser Processing: From Micro- to Nanoscale*, Chapter 3, Eds. Koji Sugioka and Ya Cheng (Pan Stanford Publishing, 2013). – P. 99–182.
- [2] H. Sopha, I. Mirza, H. Turčičová, et al., *RSC Adv.*10, 22126 (2020).
- [3] K.A. Drogowska-Horna, I. Mirza, A. Rodriguez, et al. *Nano Research* 13, 2332–2339 (2020).

## Nonlinear topological phenomena in photorefractive photonic lattices

Hrvoje Buljan

*Department of Physics, Faculty of Science, University of Zagreb, 10000 Zagreb, Croatia, and  
MOE Key Laboratory of Weak-Light Nonlinear Photonics, TEDA Applied Physics Institute and School of  
Physics, Nankai University, Tianjin 300457, China.*

In this talk I will present some of the recently addressed (theoretically and experimentally) nonlinear topological phenomena in photorefractive photonic lattices including (i) nonlinear tuning of PT symmetry and non-Hermitian topological states [1], (ii) nonlinear control of photonic higher-order topological bound states in the continuum [2], (iii) nontrivial coupling of light into a defect: the interplay of nonlinearity and topology [3], and the concepts of inherited and emergent nonlinear topological phenomena [3,4]. It should be emphasized that although the phenomena are demonstrated in photorefractive lattices, they are universal and they should exist in other platforms in optics, in ultracold atomic gases and condensed matter systems, where pertinent Hamiltonians can be experimentally realized.

### REFERENCES

- [1] S. Xia, D. Kaltsas, D. Song, I. Komis, J. Xu, A. Szameit, H. Buljan, K.G. Makris, Z. Chen, *Science* 372, 72 (2021).
- [2] Z. Hu, D. Bongiovanni, D. Jukić, E. Jajtic, S. Xia, D. Song, J. Xu, R. Morandotti, H. Buljan, and Z. Chen, <https://arxiv.org/abs/2106.00360>
- [3] S. Xia, D. Jukić, N. Wang, D. Smirnova, L. Smirnov, L. Tang, D. Song, A. Szameit, D. Leykam, J. Xu, Z. Chen, and H. Buljan, *Light Sci. Appl.* 9, 147 (2020).
- [4] D. Bongiovanni, D. Jukić, Z. Hu, F. Lunić, Y. Hu, D. Song, R. Morandotti, Z. Chen, and H. Buljan, <https://arxiv.org/abs/2103.08378>

## Diode pumped alkali laser – current status and prospects

M. Endo<sup>1</sup>, Hiroki Nagaoka<sup>2</sup>, and Fumio Wani<sup>2</sup>

<sup>1</sup>*Department of Physics, Tokai University, Hiratsuka, Japan*

<sup>2</sup>*Aerospace Systems Company, Kawasaki Heavy Industries, Ltd., Kakamigahra, Japan.*

e-mail: endo@tokai.ac.jp

Diode-pumped alkali lasers (DPALs) are optically pumped, near-infrared, continuous-wave (CW) gas lasers. A vaporized alkali metal—such as potassium, rubidium, or cesium—mixed with helium buffer gas at nearly atmospheric pressure serves as the active medium. A DPAL is optically pumped by a narrow-band laser diode at the D<sub>2</sub> transition, and it lases at the D<sub>1</sub> transition. Figure 1 shows an energy diagram and the transition paths of a Cs DPAL. In a Cs DPAL, methane or ethane is added to the medium to facilitate upper-state mixing.

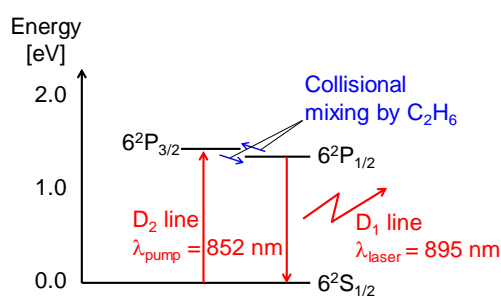


Figure 1. Energy diagram of a Cs DPAL.

There are two distinct advantages of DPAL over current high-energy solid-state laser sources. Because of this simple three-level construction, DPALs are inherently highly efficient. Optical-to-optical slope efficiency of more than 80% has been reported [1]. Therefore, DPALs are often referred to as a “beam quality converter,” in which output of the bunch of low-quality diode lasers are converted to a single, high-power, diffraction limited laser beam. The other benefit of DPALs comes from their gaseous laser medium. When the output power of solid-state lasers or fiber lasers exceeds a 10-kW level, heat generated in their solid-state material poses serious beam-quality degradation. On the other hand, beam quality issues are greatly eased for gas lasers such as DPALs. In addition to that, circulating the gas inside the optical cavity further reduces the index gradients inside the cavity that is not expected for solid-state media.

Because of these advantages, DPALs have been extensively studied in the past decade as a potential source for extremely high-average-power applications, especially, for directed energy weapons. In the United States, a 30-kW output power has been demonstrated [2]. Because DPALs are scalable to megawatts, they are expected to be useful also as high-energy, ground-based laser drivers for the removal of space debris from orbit.

We have been studying DPAL with the aforementioned civil application as our goal. The method includes a simulation code that combines a three-dimensional Navier-Stokes Equation solver and Fresnel-Kirchhoff wave propagation solver to design a large-scale device [3]. Our recent achievement includes a 38-fold enhancement of the peak power with a cavity dumping technique [4].

### REFERENCES

- [1] V. Zhdanov, T. Ehrenreich, and R. J. Knize, *Optics Communications* 260, 696 (2006).
- [2] P. J. Wisoff, LLNL-TR-730237 (2017)
- [3] M. Endo, R. Nagaoka, H. Nagaoka, T. Nagai, and F. Wani, *Jpn. J. Appl. Phys.* 59, 022002 (2020).
- [4] M. Endo, *Opt. Express* 28, 33994 (2020).

## Subwavelength Optical Lattices

E. Gvozdiovas, P. Račkauskas and G. Juzeliūnas

*Institute of Theoretical Physics and Astronomy, Vilnius University, Saulėtekio 3, Vilnius LT-10257, Lithuania*

e-mail: gediminas.juzeliunas@tfai.vu.lt

Traditionally, optical lattices are created by interfering two or more light beams, so that atoms are trapped at minima or maxima of the emerging interference pattern depending on the sign of the atomic polarizability [1]. Optical lattices are highly tunable and play an essential role in manipulation of ultracold atoms [2–3]. The characteristic distances over which optical lattice potentials change are limited by diffraction and thus cannot be smaller than half of the optical wavelength  $\lambda$ . Yet the diffraction limit does not necessarily apply to optical lattices [4–7] relying on coherent coupling between atomic internal states. It was demonstrated theoretically [4,5] and experimentally [6] that a periodic array of sub-wavelength barriers can be formed for atoms populating a long lived dark state of the  $\Lambda$ -type atom-light coupling scheme. The  $\Lambda$  scheme has a single dark state, so no spin (or quasi-spin) degree of freedom is involved for the atomic motion in the dark state manifold affected by the sub-wavelength barriers.

In the present talk we will discuss various ways of producing subwavelength optical lattices. In particular, we demonstrate that a tripod atom light coupling scheme shown in Fig. 1 can be used to create a lattice with spin-dependent sub-wavelength barriers [8,9]. The tripod scheme is characterized by two dark states playing the role of quasi-spin states. Inclusion of the spinor degree of freedom provides new possibilities for controlling the spectral and kinetic properties of atoms in the lattice. The tripod lattice can be realized using current experimental techniques.

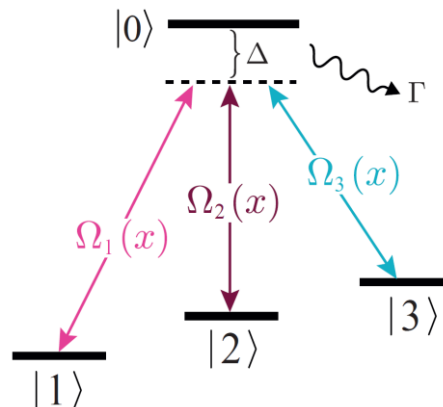


Figure 1. Tripod atom-light coupling scheme.

### REFERENCES

- [1] I. Bloch, *Nature Physics* 1(1), 23 (2005).
- [2] M. Lewenstein et al., *Advances in Physics* 56(2), 243 (2007).
- [3] I. Bloch, J. Dalibard and W. Zwerger, *Rev. Mod. Phys* 80, 885 (2008).
- [4] M. Łački et al., *Phys. Rev. Lett.* 117, 233001 (2016).
- [5] F. Jendrzejewski et al., *Phys. Rev. A* 94, 063422 (2016).
- [6] Y. Wang et al, *Phys. Rev. Lett.* 120, 083601 (2018).
- [7] R. P. Anderson et al, *Physical Review Research* 2, 013149 (2020).
- [8] E. Gvozdiovas, P. Račkauskas, G. Juzeliūnas, <https://arxiv.org/abs/2105.15148>.
- [9] P. Kubala, J. Zakrzewski and M. Łački, <https://arxiv.org/abs/2106.04709>.

## Topological machine learning for photonics

D. Leykam<sup>1</sup> and D. G. Angelakis<sup>1,2</sup>

<sup>1</sup>*Centre for Quantum Technologies, National University of Singapore, 3 Science Drive 2, Singapore 117543*

<sup>2</sup>*School of Electrical and Computer Engineering, Technical University of Crete, Chania, Greece 73100*

e-mail: cqtdani@nus.edu.sg

Machine learning approaches are promising for the automated solution of various problems in photonics including inverse design of photonic crystals, image reconstruction, and finding optimal experimental parameters [1]. However, the flexibility of popular techniques such as artificial neural networks often comes at a large computational cost, due to the complexity of the underlying models. Moreover, it becomes difficult to understand how the trained model works and when it may fail. These limitations motivate studies of explainable machine learning techniques based on easily-interpretable features of the input data.

Topological data analysis is a powerful approach for discovering robust nonlocal features of complex datasets which attracts growing interest in the physical sciences [2,3]. The approach taken by topological data analysis is to study the persistence of various topological features of the data (e.g. clusters and cycles) across a range of scales in order to infer its shape in a manner which is robust to noise. The most significant features persist over a wide range of scales. This information can be encoded in a persistence diagram which tracks the birth and death scales of the topological features. Persistence diagrams can then be used to construct feature vectors for various machine learning techniques.

In this talk I will provide a brief introduction to topological data analysis and some of its potential applications in photonics. First, I will show how persistent homology can be used to reliably quantify the abstract “shapes” of photonic band structures including their isofrequency contours and the winding numbers of the Bloch wave eigenstates, enabling the optimization of these features [4].

Second, I will show how topological data analysis can be used for the automated detection of topological features of experimental images from a large publicly-available dataset of Bose-Einstein condensate density images [5]. Using the identified features as inputs to simple supervised classification approaches such as logistic regression enables the rapid and reliable detection of dark solitons at a fraction of the computational cost of neural network-based approaches.

### REFERENCES

- [1] G. Carleo, I. Cirac, K. Cranmer, L. Daudet, M. Schuld, N. Tishby, L. Vogt-Maranto, and L. Zdeborova, Machine learning and the physical sciences, *Rev. Mod. Phys.* 91, 045002 (2019).
- [2] G. Carlsson, Topological methods for data modelling, *Nature Rev. Phys.* 2, 697 (2020).
- [3] J. Murugan and D. Robertson, An introduction to topological data analysis for physicists: from LGM to FRBs, arXiv:1904.11044.
- [4] D. Leykam and D. G. Angelakis, Photonic band structure design using persistent homology, *APL Photon.* 6, 028102 (2021).
- [5] S. Guo, A. R. Fritsch, C. Greenberg, I. B. Spielman, and J. P. Zwolak, Machine-learning enhanced dark soliton detection in Bose-Einstein condensates, *Mach. Learn.: Sci. Technol.* 2, 035020 (2021).

## Multiphysics modelling of infrared photodetectors based on graphene

E. Lidorikis

*Department of Materials Science and Engineering, University of Ioannina, 45110 Ioannina, Greece*  
*Institute of Materials Science and Computing, University Research Center of Ioannina, 45110 Ioannina, Greece*  
 e-mail: elidorik@uoi.gr

Graphene's optical response is characterized by constant absorption in the visible, electrically tunable absorption in the NIR-SWIR and plasmonic excitations in the midIR-LWIR spectrum. These traits make for interesting applications in photodetection, light modulation and sensing. To make the response more efficient and competitive, however, the small overall absorption in graphene must be overcome by integrating graphene with resonant photonic or plasmonic cavities. Strong light absorption within the resonators creates hot electrons and temperature gradients. In a comprehensive modeling and design scheme of graphene-based optoelectronic applications, the optical, thermal, and electrical responses must be considered within a self-consistent approach: absorption creates hot carriers, whose temperature distribution is determined by the thermal properties of graphene and the appropriate relaxation pathways and corresponding rates. But the thermal properties and the absorption in graphene are themselves functions of the temperature. After a short introduction in graphene physics and computational methods, we will go over our recent studies on several graphene-based optoelectronic devices. An example is shown in Fig. 1, where a free-space MIR detector based on hBN-encapsulated graphene with plasmonic antenna and p-n lateral split gates was simulated, with modelled responsivities showing remarkable agreement to experimental measurements [1].

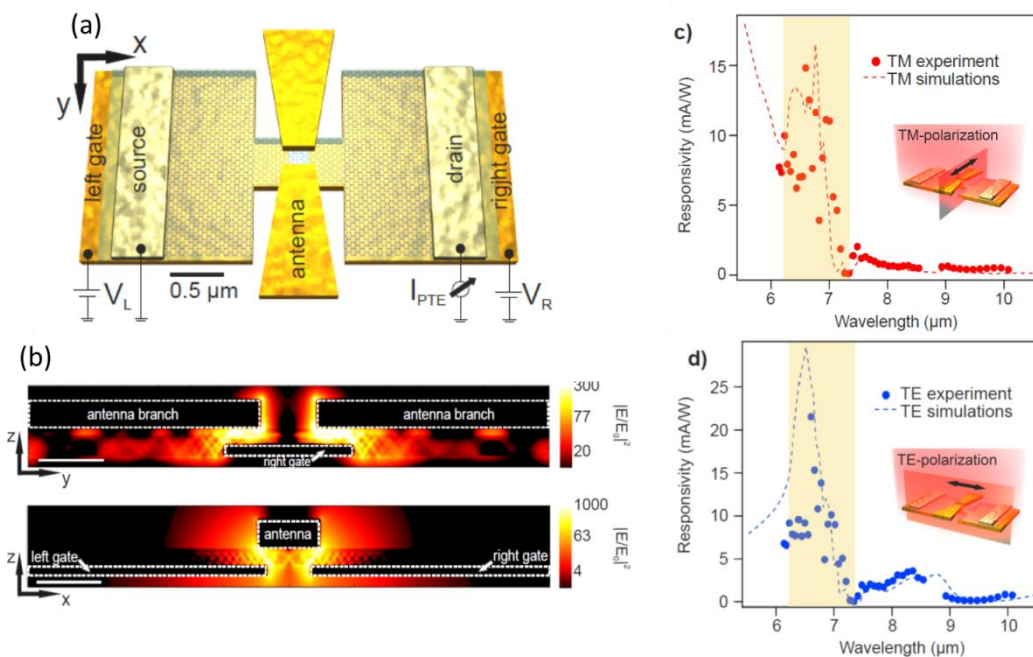


Figure 1: (a) schematic of a free space MIR photodetector based on hBN-encapsulated graphene with plasmonic antenna and p-n lateral split gates. (b) Plasmonically enhanced field intensity, where the transmission lines of hBN hyperbolic phonon-polaritons are shown. (c)-(d) Measured and simulated responsivities for the TM and TE polarizations respectively.

### REFERENCES

[1] S. Castilla, I. Vangelidis, V.-V. Pusapati, J. Goldstein, M. Autore, T. Slipchenko, K. Rajendran, S. Kim, K. Watanabe, T. Taniguchi, L. Martín-Moreno, D. Englund, K.J. Tielrooij, R. Hillenbrand, E. Lidorikis, F.H.L Koppens, "Plasmonic antenna coupling to hyperbolic phonon-polaritons for sensitive and fast mid-infrared photodetection with graphene", *Nature Communications* 11, 4872 (2020).

## Light sheet microscopy for fast 3D imaging of living samples

Pablo Loza-Alvarez

*ICFO-Instituto de Ciencias Fotónicas, Av. Carl Friedrich Gauss, 3,  
08860 Castelldefels (Barcelona), Spain*

In Light Sheet Fluorescence Microscopy (LSFM), a sheet of excitation light is produced into the sample plane and the generated fluorescence is then collected using a microscope objective placed orthogonally to the excitation light sheet plane. LSFM allows for a highly efficient excitation and collection of the generated signal. Altogether, such scheme minimise light dose onto the sample and results in a decreased photobleaching, reducing thus phototoxic effects. Therefore LSFM is ideal for 3D imaging and long term observation of in vivo biological samples.

I will present our efforts for achieving high throughput, long term imaging of different samples. In this case, our setup is based a fluidic system based on the use of a FEP tube and a syringe pump. Other modalities allowed by the setup will be explained. Then, I will present a LSFM microscope for fast volumetric imaging. In this case, the observation arm of the microscope contains an electrically tuneable lens (ETL). I will present our results for 3D imaging the spontaneous  $\text{Ca}^{2+}$  activity in of primary neuron cultures in hydrogels. The field of view is of  $300\mu\text{m} \times 300\mu\text{m} \times 1\text{mm}$ . The imaging speeds allows a proper sampling of the propagation of GCaMP signal in the full observation volume. The obtained data is then processed to calculate the connectivity maps in the 3D neuron cultured in hydrogels.

## Mixed-dimensional van der Waals heterointerfaces

A. Matković<sup>1</sup>

<sup>1</sup> *Institute of Physics, Montanuniversitaet Leoben,  
Leoben, Austria*

e-mail: Aleksandar.matkovic@unileoben.ac.at

Two-dimensional (2D) materials have attracted wide attention by the research community in the past decades. Usually referred to as van der Waals (vdW) materials, they own many of their interesting properties and applications to their inherent 2D nature, i.e. the fact that their building blocks are 2D sheets. However, there are other vdW building blocks besides 2D sheets. One example are molecular crystals. Made out of individual molecules, effectively zero-dimensional (0D) building blocks, their 3D solids are held together in virtually all directions by vdW forces. VdW interfaces are atomically abrupt and tend to preserve most of the intrinsic properties of their components. These facts have played a key role in creation of 2D vdW heterostructures. The benefits of vdW interfaces hold regardless of the inherent building blocks dimensionality. Therefore, combining crystalline organic nanostructures and 2D materials opens one of the pathways into mixed-dimensional vdW heterostructures [1].

This talk will focus on heterostructures between 2D materials – mainly graphene, hexagonal boron nitride, and molybdenum disulphide – with small rod-like molecules. The two main considered molecular species are parahexaphenyl (6P) and dihydrotetraazaheptacene (DHTA7), as representatives with phenylene (armchair-like) and acene (zigzag-like) backbones. These molecules form elongated crystalline needle-like nanostructures. As a consequence of the epitaxial relation, these organic nanostructures exhibit self-alignment with high symmetry directions of the 2D material substrates [2]. Organic molecules can be engineered with desired opto-electronic properties. One such case is DHTA7. Electrical conductivity of DHTA7 organic crystals can be photo enhanced by more than two orders of magnitude [3]. However, their optical absorption is highly anisotropic. Due to their rod-like structure, the molecules (and consequently their crystallites) can absorb only the light component which is parallel to their molecular backbone. Both their photo conductivity and anisotropic optical response can be harnessed in mixed-dimensional vdW heterostructures. By growing elongated crystallites on hBN using multi-layer graphene as contacts light polarization can be used as “gate” signal in these hybrid devices [3].

The fact that organic nanostructures self-assemble and self-align with respect to their 2D material substrates, can be utilized to pattern 2D materials and 2D material-based field effect devices (FETs) into networks of nanoribbons. Such approach opens even more device design possibilities for mixed-dimensional vdW heterostructures, especially for opto-electronics and sensing applications. We will present monolithic ribbon networks of graphene and MoS<sub>2</sub>, integrated into fully operational FETs. Due to an extreme increase of the edge-to-surface ratio, the devices were found to exhibit extremely pronounced gate-dependent polarity switching [4], mimicking behavior of ferroelectric-supported 2D FETs [5].

### REFERENCES

- [1] D. Jariwala, T.J. Marks, M.C. Hersam, *Nat. Mater.* **16**, 170 (2017).
- [2] A. Matković, et.al., *Sci. Rep.* **6**, 38519 (2016).
- [3] A. Matković, et.al., *Adv. Funct. Mater.* **29**, 1903816 (2019).
- [4] M.A. Aslam, et.al. (*manuscript in preparation*)
- [5] J. Chu, et.al. *Adv. Mater.* **33**, 2004469 (2021).

## **Gamma Factory, or how the largest accelerator facility is bringing atomic physics to its extreme**

Szymon Pustelny (for the Gamma Factory collaboration)  
*Marian Smoluchowski Institute of Physics, Jagiellonian University in Kraków*  
*Lojasiewicza 11, 30-348 Kraków, Poland*  
*e-mail:pustelny@uj.edu.pl*

Modern accelerators represent one of the most spectacular examples of the success of the human intellect over matter. The development of accelerator systems over the past decades has led to many important discoveries, with the last one being the discovery of the God particle - the Higgs boson. Paradoxically, this great discovery put high-energy physics in a crisis, as none of the existing high-energy physics theories provides predictions that could be confirmed with the available, or even envisioned accelerators. This poses an inevitable question about the legitimacy of the existence of accelerator facilities but also stimulates searches of novel applications ranging far beyond their current framework.

While high-energy physics seems to be on the defensive, atomic physics on the other hand has enjoyed enormous successes over recent years. New, more and more precise experiments not only provide knowledge about the surrounding Universe and its laws, but also offer tools that are used in other branches of physics, as well as astronomy, chemistry, biology, archeology, medicine, etc. However, even that does not change the fact that atomic physics must also face specific challenges. For instance, numerous quantum phenomena could be better studied and possibly understood if it was possible to interact with electrons of the inner electron shells of heavy atoms. Unfortunately, due to large energy gaps between energy levels of the strongly-bounded electrons, until now, such studies have been extremely difficult due to the lack of available light sources.

During the talk, I will present a new proposal at the interphase at atomic and high-energy physics called Gamma Factory [1]. I will show how these two disciplines may lead to a qualitative change in science, offering yet unavailable research opportunities. Specifically, I will discuss how, based on the interaction of ultrarelativistic strongly ionized heavy ions with laser light, spectroscopy of hydrogen-, helium-, lithium-like lead, at transition energies of hundreds or even thousands eV becomes possible [2]. I will also talk about how such scheme allows to boost photon energies over 10,000,000 times, making the system intense source of megaelectronvolts photons and hence enabling applications in atomic, nuclear and high energy physics, but also in chemistry and biology.

### REFERENCES

- [1] W. Płaczek *et al.*, *Acta Phys. Pol. B* 50, 1191 (2019).
- [2] J. Bieroń, M. W. Krasny, W. Płaczek, and S. Pustelny, arXiv:2106.00330.
- [3] D. Budker *et al.*, *Ann. Phys. (Berlin)*, 532, 2000204 (2020).

## Quantum Information Hardware Based on Color Center Nanophotonics

Marina Radulaski

Department of Electrical and Computer Engineering, University of California, Davis, USA  
mradulaski@ucdavis.edu

Color centers in wide band gap materials have been prominently studied for applications as quantum bits, quantum light sources, quantum sensors, and spin-photon interfaces [1]. Silicon carbide, in particular, has been an attractive host of color centers due their NIR single photon emission, long spin-coherence times, nonlinear optical properties, and commercial substrate availability. Integration of color centers with nanophotonic devices has been a challenging task, but significant progress has been made with demonstrations up to 120-fold resonant emission enhancement of emitters embedded in photonic crystal cavities [2].

In this talk, I will discuss new geometries for silicon carbide quantum device integration [3], including waveguides, photonic crystal cavities, and photonic crystal molecules which can be applied in quantum light generation, quantum repeaters, integrated quantum circuits, and quantum simulation. Using the parameters of the state-of-the-art color center-cavity systems, we explore the light and matter interaction using open quantum system modeling. By carefully including the inhomogeneous broadening in emitter frequencies into the Tavis-Cummings-Hubbard model, we explore multi-emitter interactions in coupled cavity arrays evaluating cavity-protection, localization and superfluid phase transition effects.

### REFERENCES

- [1] V. A. Norman, S. Majety, Z. Wang, W. H. Casey, N. Curro, M. Radulaski, “Novel color center platforms enabling fundamental scientific discovery,” *InfoMat*, 1-24 (2020).
- [2] D. M. Lukin, C. Dory, M. A. Guidry, K. Y. Yang, S. D. Mishra, R. Trivedi, M. Radulaski, S. Sun, D. Vercruyssen, G. H. Ahn, J. Vučković, “4H-Silicon-Carbide-on-Insulator for Integrated Quantum and Nonlinear Photonics,” *Nature Photonics***14**, 330-334 (2020).
- [3] S. Majety, V. A. Norman, L. Li, M. Bell, P. Saha, M. Radulaski, “Quantum photonics in triangular-cross-section nanodevices in silicon carbide,” *J. Phys. Photonics***3**, 034008 (2021).

## Nonlinear photonic states in topological systems

Daria Smirnova

*Research School of Physics, The Australian National University, Canberra, ACT 2601, Australia*  
e-mail:daria.smirnova@anu.edu.au

Photonic topological insulators represent a novel class of crystalline structures that support robust propagation of light along edges [1]. They show special promise for numerous applications in optical communications and computing technologies, due to the topological protection of their transport properties against disorder, including the ability of electromagnetic pulses to overcome structural imperfections without back-reflection. Since nonlinearity is an inherent feature of materials employed in topological photonics, the wave processes in such structures can be accompanied by a variety of nonlinear effects, such as harmonic generation [2], self-action effects [3], and modulational instability [4].

In this talk, we will discuss the propagation of slowly-varying wavepackets along the topological domain walls in nonlinear photonic valley-Hall insulators. As a specific example, we consider a dimerized graphene lattice composed of single-mode dielectric waveguides with local nondispersive Kerr nonlinearity. We show that in the continuum limit the nonlinear evolution of a spinor wavefunction in such a system is governed by the nonlinear Dirac equations. It is analytically demonstrated that the evolution of finite wavepackets propagating along the domain wall is accompanied by steepening of the trailing wavefront up to the development of a gradient catastrophe. To illustrate this key effect we also model numerically the temporal dynamics of edge wavepackets. Taking the weak spatial dispersion into account stipulates then the formation of stable edge quasi-solitons. Our results are validated by full-wave numerical modeling of beam propagation along a valley-Hall domain wall in realistic staggered honeycomb lattices of laser-written waveguides.

Beyond the specific example we considered, our findings are instructive for other emerging experimental studies of nonlinear dynamic phenomena in a variety of topological platforms spanning from metamaterials to optical lattices and exciton-polariton condensates.

### REFERENCES

- [1] T. Ozawa et al, *Reviews of Modern Physics* 91, 015006 (2019).
- [2] D. Smirnova, S. Kruk, D. Leykam, E. Melik-Gaykazyan, D.Y. Choi, and Y. Kivshar, *Physical Review Letters* 123, 103901 (2019).
- [3] D.A. Smirnova, L.A. Smirnov, D. Leykam, and Y.S. Kivshar, *Laser & Photonics Reviews* 13, 1900223 (2019).
- [4] D. Leykam, E. Smolina, A. Maluckov, S. Flach, and D.A. Smirnova, *Physical Review Letters* 126, 073901 (2021).

## Apertureless scanning near field microscopy and applications

George A. Stanciu

Center for Microscopy-Microanalysis and Information Processing,  
University Politehnica of Bucharest, 313 Splaiul Independentei, 060042, Bucharest, Romania  
e-mail: [stanciu@physics.pub.ro](mailto:stanciu@physics.pub.ro), web: [www.cmmip-upb.org](http://www.cmmip-upb.org)

The superresolution techniques based on far field are stimulated emission depletion microscopy (STED), fluorescence photoactivation localization microscopy (f-PALM) and stochastic optical reconstruction microscopy (STORM). They require fluorescent labels and the main disadvantages of them are the connection between laser wavelength and fluorescent marker and difficulty to attach the marker to the interesting region of the samples. Moreover they may not attach to correct molecule or functional group of interest that create problems in interpreting images.

In the case of densely distributed nanoscale objects, optical measurements require an optical field confined to the same scale for obtaining the necessary high lateral spatial resolution. According to Minsky's ideas [1] near-field optics make possible investigations of the optical interaction produced by emerging light from a subwavelength aperture or scattered light by a subwavelength metallic or semiconductor tip of an object in the immediate vicinity, within a fraction of the radiation wavelength of the aperture or of scattering source. The near field is a nonpropagating evanescent wave, which decays exponentially with the distance from the aperture or the scattering source. Near field optical microscopy is based on the exploitation of the evanescent components of the electromagnetic field to overcome the limitations imposed by the diffraction phenomena. Scanning near field optical microscopy (SNOM) is a label free technique able to overcome the optical diffraction limit. SNOM techniques are divided into two branches: aperture-SNOM (a-SNOM) and apertureless-SNOM (A-SNOM). In a-SNOM the aperture has a double role, to 'illuminate' the sample surface with near field and to collect the near field after interaction with the sample. The use of an aperture such as the tapered fiber opening poses several experimental limitations, the most important is related with the resolution which is limited at around 50 nm.

A-SNOM exploits the field enhancing nano-antenna properties of sharp metallic tips. In this technique usually, the sample is raster scanned under an oscillating probe of an atomic force microscope (AFM). The probe serves as a nanoscale light confiner, enhancer, and scatterer. Basically, the operating principle of the A-SNOM is to use an external laser beam to illuminate the tip of a standard atomic force microscope (AFM) probe and to detect the light having information about tip-surface interaction. There are several techniques in the A-SNOM family, the most used among them are: scattering-SNOM (s-SNOM), tip enhanced fluorescence-SNOM (TEF-SNOM) and second harmonic generation-SNOM (SHG-SNOM).

One of the most useful applications of s-SNOM relates to the local measurement of the local dielectric function [2]. The possibility to locally measure the dielectric function in the visible domain, with nanoscale resolution opens a wide range of applications in Material Science and Life Sciences.

### REFERENCES

- [1] E. Synge, A suggested method for extending microscopic resolution into the ultra-microscopic region, *Philosophical Magazine and Journal of Science*, 6(35) (1928)
- [2] D.E. Tranca DE, Stanciu SG, Hristu R and Stanciu GA, 2018, *Nanomedicine and Nanotechnology, Biology and Medicine*, 14, 47 (2018)

## Quantitative single molecule localization microscopy for precision medicine

Kathleen M. Lennon<sup>1</sup>, Andras Saftics<sup>1</sup>, Adam L. Maddox<sup>1</sup>, Reem Bagabas<sup>1</sup>, Devin L. Wakefield<sup>1</sup>, Steven J. Tobin<sup>1</sup>, Matthew S. Brehove<sup>1</sup>, Gagandeep Singh<sup>2</sup>, Joanne Mortimer<sup>2</sup>, Veronica Jones<sup>2</sup>, Daniel Schmolze<sup>2</sup>, Saumya Das<sup>3</sup>, Kendall Van Keuren-Jensen<sup>4</sup>, Tijana Jovanovic-Talisman<sup>1</sup>

<sup>1</sup>*Beckman Research Institute, City of Hope Comprehensive Cancer Center, Duarte, CA, USA*

<sup>2</sup>*City of Hope Comprehensive Cancer Center, Duarte, CA, USA*

<sup>3</sup>*Massachusetts General Hospital, Harvard Medical School, Boston, MA, USA.*

<sup>4</sup>*Translational Genomics Research Institute, Phoenix, AZ, USA*

A fluorescence-based imaging method, called quantitative single molecule localization microscopy (qSMLM), can detect individual molecules with nanoscale precision. qSMLM has been typically used in cultured cells and has rarely quantified biomolecules in human specimens: patient tissues and extracellular vesicles secreted by patient cells. By tailoring methodology for sample preparation, imaging, and data analysis, we can probe density and organization of biomolecules in these clinical samples. Using advanced qSMLM approaches, we assessed human epidermal growth factor receptor 2 (HER2) in tissues from breast cancer patients. When an anti-HER2 therapeutic antibody called trastuzumab was used as a fluorescent reporter, qSMLM was able to quantify HER2 receptors that harbor an available drug binding site [1]. We also quantified size and cargo of extracellular vesicles from plasma of pancreatic cancer patients. Compared to healthy controls, patients with pancreatic cancer exhibited a distinct population of larger extracellular vesicles enriched in two biomarkers: epidermal growth factor receptor and carbohydrate antigen 19-9 [2]. Ultimately, when qSMLM is paired with traditional methods, it may advance precision medicine.

### REFERENCES

[1] S.J. Tobin, D.L. Wakefield, V. Jones, X. Liu, D. Schmolze, T. Jovanovic-Talisman, *Sci. Reports*, 8, 15154 (2018).

[2] K.M. Lennon, D.L. Wakefield, A.L. Maddox, M.S. Brehove, A.N. Willner, K. Garcia-Mansfield, B. Meechoovet, R. Reiman, E. Hutchins, M.M. Miller, A. Goel, P. Pirrotte, K. Van Keuren-Jensen, T. Jovanovic-Talisman, *J. Extracell. Vesicles*, 8, 1685634 (2019).

## Photoacoustic imaging: Listening to laser light interactions with matter

G.J. Tserevelakis

*Foundation for Research and Technology Hellas, Institute of Electronic Structure and Laser, N. Plastira 100,  
Heraklion, Crete, Greece, GR-70013*

e-mail: tserevel@iesl.forth.gr

With a history spanning over more than three centuries, optical microscopy has been considered to be the most vital tool for the *in vivo* observation of complex biological processes. Driven by the most recent groundbreaking advances in biomedical research such as the molecular decryption of cancer formation and the elucidation of fundamental aging mechanisms, optical microscopy has evolved into numerous approaches able to fulfill a large range of diagnostic requirements including non-invasiveness, high spatial resolution, and exceptional contrast specificity. Nevertheless, pure light techniques are highly restricted to superficial investigations as a result of heavy tissue scattering. In this context, the recently developed photoacoustic microscopy systems have the potential to offer optical absorption contrast at depths totally inaccessible to traditional optical microscopy, significantly complementing the capabilities of existing methods.

In the first part of this talk, I will discuss about the development of novel hybrid microscopy systems exploiting different interactions between light and biomolecules, including the photoacoustic effect and single-photon excitation fluorescence, aiming to provide label-free information as regards melanin accumulation in marine organisms, vegetative pigment production and distribution [1], as well as, bacterial infection effects on plant tissues. Furthermore, I will demonstrate the applications that multimodal imaging can have in ophthalmic diagnosis and research, by focusing on the investigation of the ocular accommodation system [2] and the early detection of highly aggressive malignant intraocular tumors [3].

In the second part of the presentation, I will demonstrate how photoacoustic imaging can break through the barriers of biomedical research, and find innovative applications in cultural heritage diagnostics. In particular, the advantages of photoacoustic imaging are utilized to establish a radically new, non-destructive methodology for the uncovering and differentiation of well-hidden features in multi-layered objects such as paintings and documents [4,5]. Finally, I will present the capabilities of photoacoustic signal detection on the *in situ* real-time monitoring of laser cleaning interventions, which has the potential to promote an improved conservation outcome by safeguarding artworks' original surfaces [6].

### REFERENCES

- [1] G.J. Tserevelakis, M. Tsagkaraki, G. Zacharakis, *Journal of microscopy* 263 (3), 300-306 (2016).
- [2] G.J. Tserevelakis, S. Avtzi, M.K. Tsilimbaris, G. Zacharakis *Journal of biomedical optics* 22 (6), 060501 (2017).
- [3] G.J. Tserevelakis, K.G. Mavrakis, D. Pantazopoulou et al., *Optics Letters* 45 (20), 5748-5751 (2020)
- [4] G.J. Tserevelakis, I. Vrouvaki, P. Siozos, et al., *Scientific reports* 7 (1), 1-11 (2017).
- [5] G.J. Tserevelakis, M. Tsagkaraki, P. Siozos, G. Zacharakis, *Strain* 55 (2), e12289 (2019).
- [6] G.J. Tserevelakis, J.S. Pozo-Antonio, P. Siozos, et al., *Journal of Cultural Heritage* 35, 108-115 (2019)

## Special Invited Talk

## Compact, commercial 200 kHz few-cycle OPCPA at 800 nm with stable CEP

Ekaterina Zapolnova<sup>1</sup>, Thomas Braatz<sup>1</sup>, Sebastian Starosielec<sup>1</sup>,  
Torsten Golz<sup>1</sup>, Mark J. Prandolini<sup>1,2</sup>, Jan Heye Buss<sup>1</sup>, Michael Schulz<sup>1</sup>, and Robert Riedel<sup>1</sup>

<sup>1</sup>Class 5 Photonics GmbH, Notkestraße 85, 22607 Hamburg, Germany

<sup>2</sup>Institut für Experimentalphysik, Universität Hamburg, Luruper Chaussee 149, 22761 Hamburg, Germany

e-mail: robert.riedel@class5photonics.com

For attosecond technology, carrier envelope phase (CEP) stabilization in the few-cycle regime combined with high repetition rates is essential for studying ultrafast electronic processes in atoms, molecules, solids, and complex many body systems [1-3]. Therefore, a laser system was designed, where the laser pulses are generated from a single white-light generation (WLG) source operating at 200 kHz, providing CEP stable pulses at 800 nm with pulse durations of < 10 fs, and pulse energies of 15  $\mu\text{J}$ . A passive CEP jitter over 10 min was measured with an f-to-2f interferometer below 170 mrad rms.

Additionally, a second output is optionally available providing simultaneously CEP stable pulses at 2  $\mu\text{m}$  which allows for pump-probe measurements.

The system is robust and compact, with a footprint of less than a square meter, and commercially available from Class 5 Photonics GmbH.

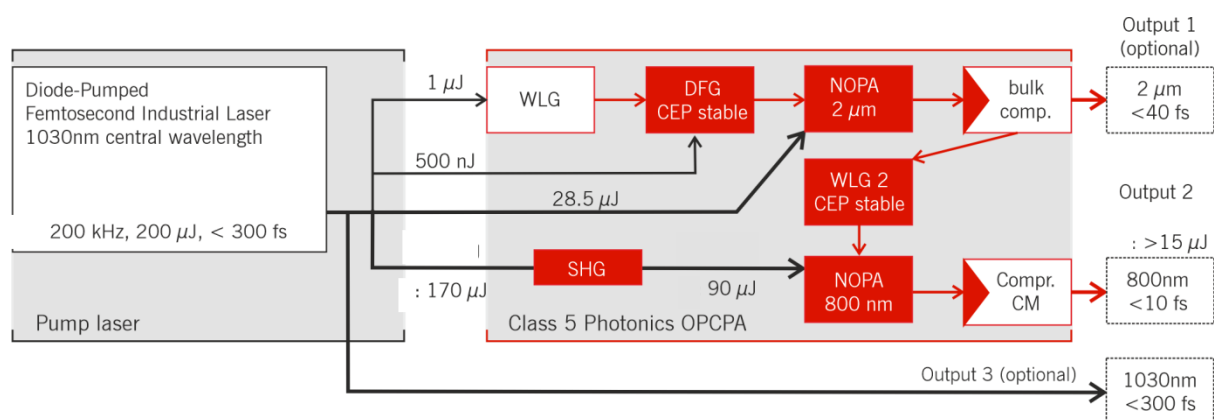


Figure 1. Schematic of the laser system with white-light generation (WLG), second-harmonic generation (SHG), non-colinear optical-parametric chirped-pulse amplifier (NOPA), chirped-mirror (CM) compressor.

### REFERENCES

- [1] Calegari, F., et-al. “Ultrafast electron dynamics in phenylalanine initiated by attosecond pulses”, *Science*, 336-339 (2014)
- [2] Uzan, A.J, et al. “Attosecond spectral singularities in solid-state high-harmonic generation.”, *Nat. Photonics* 14, 183–187 (2020).
- [3] Harth, A., et.-al. “Compact 200 kHz HHG source driven by a few-cycle OPCPA”, *Journal of Optics* 20, 014007 (2017)

# **Progress Reports**

## Carbon nanocomposites as advantageous antibacterial surfaces

M. D. Budimir<sup>1</sup>, Z.M. Marković<sup>1</sup>, B. Todorović Marković<sup>1</sup>

<sup>1</sup>Vinca Institute of Nuclear Sciences - National Institute of the Republic of Serbia, University of Belgrade, Serbia  
e-mail: budimir@vin.bg.ac.rs

Microbial contamination is a major problem that impacts many facets of our lives, including health care, water purification systems, food storage, etc. Decades of inadequate use and disposal of antibiotics have led to the emergence of antibiotic-resistant bacteria strains. Therefore, it's critical to develop new antibacterial materials that can successfully combat both planktonic Gram-positive and Gram-negative bacteria, as well as their biofilms. Antibacterial materials can inhibit biofilm formation and overcome difficulties associated with the use of conventional antimicrobial agents, such as residual toxicity, short-term antibacterial activity, and the development of antimicrobial resistance [1].

The application of carbon nanomaterials is an emerging area of nanoscience and nanotechnology in the last few decades. When material dimensions are reduced to the nanoscale, they display unique physical, chemical, electrical and optical properties compared to their macro-scaled counterparts. Recently, researchers have focused on their biological properties, owing to their great potential as antibacterial agents and low toxicity [2]. In this regard, the goal of this work is to present several carbon/polymer nanocomposites with outstanding antibacterial properties, using two alternative approaches: photothermal and photodynamic effects.

The first strategy for successful bacteria capture and eradication that will be presented here exploits the photothermal effect. The developed device consists of a flexible Kapton interface modified with gold nanoholes (Au NH) substrate, coated with reduced graphene oxide-polyethyleneimine thin films (K/Au NH/rGO-PEI) [3]. The K/Au NH/rGO-PEI device is efficient in capturing and eliminating both planktonic Gram-positive *Staphylococcus aureus* (*S. aureus*) and Gram-negative *Escherichia coli* (*E. coli*) bacteria after 10 min of NIR (980 nm) irradiation. Additionally, the developed device could effectively destroy and eradicate *Staphylococcus epidermidis* (*S. epidermidis*) biofilms after 30 min of irradiation.

In the second experiment, a photoactive nanocomposite with excellent antibacterial properties was formed by incorporating hydrophobic quantum dots (hCQDs) in the polyurethane (PU) matrix. In this nanocomposite, a photodynamic effect is exploited, through the generation of reactive oxygen species (ROS) in hCQDs upon irradiation with low-power blue light (470 nm). Additionally, gamma-irradiation of various doses (1, 10, and 200 kGy) in the air environment was applied to the formed nanocomposite to alter its physical and chemical properties and improve its antibacterial efficacy. After the pre-treatment with gamma-irradiation, the antibacterial activity of the presented nanocomposite was greatly improved, and the best result was achieved for the irradiation dose of 200kGy. In this sample, total bacteria elimination was achieved after 15 min of irradiation by blue light, for both Gram-positive and Gram-negative strains [4].

Both of the developed nanocomposites are simple and rather universal in terms of eradication of different microorganisms, with a potential application in biomedicine, industry, or daily-used objects.

### REFERENCES

- [1] J. Hasan, R.J. Crawford, E.P. Ivanova, Trends Biotechnol. 31 (2013) 295–304.
- [2] S. Szunerits, R. Boukherroub, J. Mater. Chem. B 4 (2016) 6892–6912.
- [3] M. Budimir, R. Jijie, R. Ye, A. Barras, S. Melinte, A. Silhanek, Z. Markovic, S. Szunerits, R. Boukherroub, J. Mater. Chem. B 7 (2019) 2771–2781.
- [4] M. Budimir, Z. Marković, J. Vajdak, S. Jovanović, P. Kubat, P. Humpoliček, M. Mičušik, M. Danko, A. Barras, D. Milivojević, Z. Špitalsky, R. Boukherroub, B.T. Marković, Radiat. Phys. Chem. 185 (2021) 109499.

## Terahertz Quantum-Cascade Lasers: Physics of the Electrons Transport, Design Review and Temperature Performance Optimization

A. Demić<sup>1</sup>, Z. Ikonić<sup>1</sup>, P. Dean<sup>1</sup>, and D. Indjin<sup>1</sup>

<sup>1</sup> *School of Electronic and Electrical Engineering,  
University of Leeds, U.K.*

e-mail:A.Demic@leeds.ac.uk

The paradigm of exploiting intra-band electron transport and maintaining population inversion via resonant tunnelling, combined with semiconductor band structure engineering has yielded state of the art sources in far-infrared spectrum: Terahertz-frequency quantum cascade lasers (THz QCLs). Since their first demonstration [1], a variety of designs provided devices lasing in the range 1.2 – 5.6 THz, with high output power and operating temperature up to 250 K in pulsed regime [2-4]. There is a great interest of achieving room temperature performance and this possibility seems exhausted after 20 years of research and development with GaAs/AlGaAs material system.

In this work we present a detail review of THz QCL designs and discuss temperature degradation mechanisms which outline their strengths and weaknesses.

Our density matrix transport model [5] has demonstrated very high quality and reliability in predicting the cut-off temperature across various designs and we have recently employed it in temperature optimization procedure [6].

The current record structure employs a three level system where lower lasing level is efficiently extracted via interaction between electrons and longitudinal optical (LO) phonons. This design has proven its temperature performance robustness over the years, however latest record device [4] employed extraction transition of 51 meV which is much higher from the LO phonon resonant energy (36 meV). We attribute this behaviour to a known disadvantage of using LO phonon scattering mechanism for assistance in lasing process at THz frequencies. This scattering process is most efficient at resonant energy of 36 meV, however it may persist up to 60 meV and as THz lasing energy is typically 12-16 meV it is clear that in a three level system, this process may inadvertently extract the upper lasing level (the LO phonon scattering leakage).

In [5,6] we presented a novel design which does not suffer from LO phonon scattering leakage and simulated over 4 million devices in a search for optimal structure. Our focus in [6] was to generate a structure with lower threshold and in this work we present novel designs which in contrast have higher thresholds, however exploit extraction transition in 46 – 51 meV range offering better temperature degradation efficiency.

### REFERENCES

- [1] R. Köhler, A. Tredicucci, F. Beltram, H. E. Beere, E. H. Linfield, A. G. Davies, D. A. Ritchie, R. C. Iotti, and F. Rossi, *Nature* 417(6885), 156–159 (2002).
- [2] C. Walther, M. Fischer, G. Scalari, R. Terazzi, N. Hoyler, and J. Faist, *Applied Physics Letters*, vol. 91, no. 13, p. 131122(2007).
- [3] M. Wienold, B. Röben, X. Lü, G. Rozas, L. Schrottke, K. Biermann, and H. T. Grahn, *Appl. Phys. Lett.*, vol. 107, no. 20, p. 202101(2015).
- [4] A. Khalatpour, A. K. Paulsen, C. Deimert, Z. R. Wasilewski, and Q. Hu, *Nature Photonics*, vol. 15, no. 1, pp. 16–20(2021).
- [5] A. Demić, Z. Ikonić, R. W. Kelsall, and D. Indjin, *AIP Adv.* 9(9), 095019 (2019).
- [6] A. Demić, Z. Ikonić, P. Dean, and D. Indjin, *Optics Express*, vol. 28, no. 26, pp. 38788–38812, (2020).

## Proposal for realizing quantum scars in the tilted 1D Fermi-Hubbard model

J.-Y. Desaulès<sup>1</sup>, A. Hudomal<sup>1,2</sup>, C. J. Turner<sup>1</sup>, Z. Papić<sup>1</sup>

<sup>1</sup>*School of Physics and Astronomy, University of Leeds, United Kingdom*

<sup>2</sup>*Institute of Physics Belgrade, University of Belgrade, Serbia*

e-mail:ana.hudomal@ipb.ac.rs

Understanding how closed many-body quantum systems evolve in time when taken out of their equilibrium state is an active field of research. While many such systems rapidly return to their equilibrium state, in accordance with fundamental principles of quantum statistical mechanics, much of recent work has focused on systems that fail to do so as a consequence of ergodicity breaking. The inability of nonergodic systems to act as heat reservoirs for their smaller parts has been traditionally known to affect the entire spectrum of the system. However, there has been a flurry of interest in weak ergodicity breaking phenomena. The latter refers to the emergence of a dynamically decoupled subspace within the many-body Hilbert space, in general without any underlying symmetry, spanned by ergodicity-breaking eigenstates. In recent experiments on interacting Rydberg atom arrays, weak ergodicity breaking was observed via persistent revivals following the global quench of the system, prompting the name “quantum many-body scarring” by analogy with the phenomenon of quantum scars in single-particle system.

Motivated by recent observations of ergodicity breaking due to Hilbert space fragmentation in 1D Fermi-Hubbard chains with a tilted potential [1], we show that the same system also hosts quantum many-body scars in a regime  $U \approx \Delta \gg J$  at electronic filling factor  $\nu=1$  [2]. We numerically demonstrate that the scarring phenomenology in this model is similar to other known realizations such as Rydberg atom chains, including persistent dynamical revivals and ergodicity-breaking many-body eigenstates. At the same time, we show that the mechanism of scarring in the Fermi-Hubbard model is different from other examples in the literature: the scars originate from a subgraph, representing a free spin-1 paramagnet, which is weakly connected to the rest of the Hamiltonian’s adjacency graph. Our work demonstrates that correlated fermions in tilted optical lattices provide a platform for understanding the interplay of many-body scarring and other forms of ergodicity breaking, such as localization and Hilbert space fragmentation.

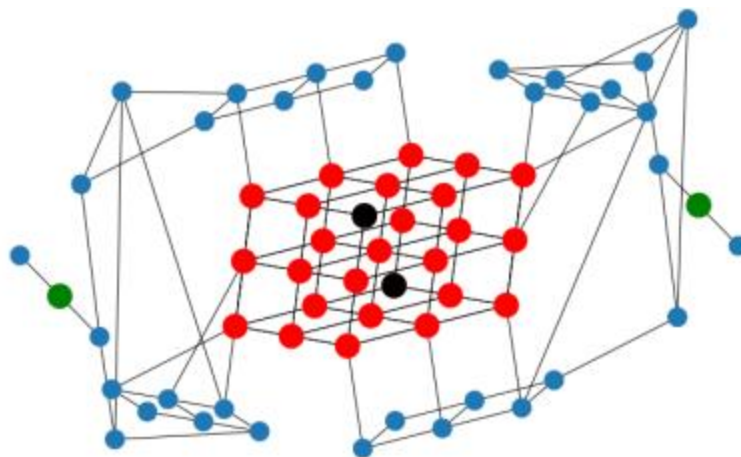


Figure 1. Adjacency graph of the effective model.

### REFERENCES

[1] S. Scherg et al., arXiv:2010.12965 (2020).

[2] J.-Y. Desaulès, A. Hudomal, C. J. Turner, Z. Papić, Phys. Rev. Lett. 126, 210601 (2021).

## The Influence of Ion Implantation of Iron on the Surface Properties of High Density Polyethylene

D. Kisić, M. Nenadović, M. Novaković, J. Potočnik  
*Vinca Institute of Nuclear Sciences,  
Belgrade, Serbia*

In this study, iron-polyethylene nanocomposites were synthesized, by ion implantation with different fluences, in the range from  $5 \times 10^{16}$  ions/cm<sup>2</sup> to  $5 \times 10^{17}$  ions/cm<sup>2</sup>, and at the energy of 95 keV. Rutherford backscattering spectroscopy confirmed the presence of iron in the implanted samples, and the calculated fluences matched with those predicted, except for the highest implantation fluence, where a significant difference was due to the sputtering effect. It was also found that the depth of damage was slightly lower than predicted by the SRIM simulation [1]. X-ray photoelectron spectroscopy has revealed that implanted iron is in the form of pure metallic iron - Fe (0), and multiple iron oxides. On the other hand, carbon was mostly transformed from a sp<sup>3</sup> hybridized, to a sp<sup>2</sup> hybridized, indicating that the carbonization of polyethylene and the degassing of hydrogen took place. Infrared spectroscopy has indicated that aldehydes and ketones are formed after implantation, and that many organic compounds are likely to form upon implantation with the highest fluence. Atomic force microscopy confirmed that implantation led to considerable destruction of the surface, resulting in changes of surface morphology, and a considerable increase of surface roughness [2]. Transmission electron microscopy microphotographs show that after implantation, iron nanoparticles are formed, and the particle sizes have a characteristic depth distribution, according to which they can be classified into three zones. However, a continuous layer is formed in the case of the highest implantation fluence. Energy dispersive spectrophotometric analysis of a single particle indicated that the nanoparticle interior was mainly composed of pure metallic iron, and that the iron oxides probably dominated near the very surface of the nanoparticles [1]. From the measurements of the sheet resistivity by the 4-point contact probe method, it was observed that between the  $1 \times 10^{17}$  ions/cm<sup>2</sup> and  $2 \times 10^{17}$  ions/cm<sup>2</sup> fluences, a transition occurs in which the metal phase takes a dominant role in the mechanism of electric conduction and that percolation most likely is achieved for fluences in the range between  $2 \times 10^{17}$  ions/cm<sup>2</sup> and  $5 \times 10^{17}$  ions/cm<sup>2</sup> [2]. Measurements by Kerr magneto-optical magnetometry have indicated that the magnetic properties change in accordance with the applied implantation fluence and the morphology of the iron nanoparticles formed in the surface layer. The occurrence of the ferromagnetic phase can be observed for the two higher fluences, with a coercivity of only 20 Oe for the fluence of  $2 \times 10^{17}$  ions/cm<sup>2</sup>, whereas for the highest fluence of  $5 \times 10^{17}$  ions/cm<sup>2</sup>, the coercivity is 57 Oe. The shape of hysteresis loop is typical of a mixture of single and multi-domain particles. UV-VIS spectroscopy showed that, as a consequence of implantation, the peaks in the Kubelka - Munk spectra of remission function appear [1], most likely originating from localized surface plasmon resonance of the iron nanoparticles [3,4]. Surface energy changes with the implantation fluence, in a way that it increases up to a fluence of  $1 \times 10^{17}$  ions/cm<sup>2</sup>, and then decreases with increasing fluence. It was also found that the hydrophobic, i.e. dispersive character of the surface does not change significantly as a consequence of implantation [2].

### REFERENCES

- [1] D. Kisić, M. Nenadović, J. Potočnik, M. Novaković, P. Noga, D. Vaňa, A. Závacká, Z. Rakočević, *Vacuum* 171, 109016 (2020)
- [2] D. Kisić, M. Nenadović, T. Barudžija, P. Noga, D. Vaňa, M. Muška, Z. Rakočević, *Nucl. Instrum. Methods Phys. Res. B* 462, 143 (2020)
- [3] U. Kreibig, M. Vollmer, *Optical Properties of Metal Clusters*, Springer, Verlag, Berlin, Heidelberg, (1995)
- [4] F. Mashayekhi, A. Shafiekhani, S.A. Sebt, *Eur. Phys. J. Appl. Phys.* 74, 30402 (2016)

## Unsupervised method for time-series classification of signals obtained from calcium imaging

Andrej Korenić<sup>1</sup>, Dunja Bijelić<sup>1</sup>, Bilal Ersen Kerman<sup>2</sup>, Abdulkerim Çapar<sup>3</sup>, Pavle Andjus<sup>1</sup>

<sup>1</sup> *Institute of Physiology and Biochemistry “Jean Gaja”, Faculty of Biology, University of Belgrade*

<sup>2</sup> *İstanbul Medipol University, İstanbul*

<sup>3</sup> *İstanbul Technical University, İstanbul*

andrej.korenica@bio.bg.ac.rs

**Introduction:** Automated Quantitative Live Cell Fluorescence Microscopy utilizes high throughput screening and aims to analyze responses from large cell numbers which is expectedly hampered by demanding processes of classifying cells' responses. On the other hand, Time Series Classification (TSC) is an important and challenging problem of defining labels that cluster time-series in similar sets. Most methods that have so far led to significant progress in the accuracy of time-series classifiers have high computational complexity, requiring significant training time even for smaller data sets.

**Materials and Methods:** The raw data for the analysis came from the primary rat cortical astrocytes recorded for calcium imaging. Without focusing on a single type of feature such as shape or frequency, we are aiming to develop and test Unsupervised Machine Learning approach in order to characterize traces, cluster them and if any groups could be found, train a classifier to reliably predict a class for any given test trace. By using maximum entropy modeling [1] we aim to construct a training and validation set for the classifier and use subsequently the rest of the traces as a test set. Based on classification results, Markov clustering [2] and hierarchical clustering will be conducted for community detection.

**Results & Conclusion:** Our preliminary results show that traces are grouped as expected according to the shape and characteristics of the signal, as when grouping was performed by taking into the account prominent features of the signal (e.g., amplitude, rise, decay, number of peaks etc.). The overarching goal would be to adapt a method of sparse dictionary learning framework for time-series imaging by successively adding constraints based on the hierarchical architecture of trace communities, while requiring minimum preprocessing. From a medical point of view, this method can give us a deeper insight into the variability of the obtained signals, and, for example, grounds for a possible correlation of the results with data on patients and their disease.

### REFERENCES

[1] Vinod H.D. López-de-Lacalle J. Stat. Softw. (2009)

[2] Van Dongen S. PhD thesis, University of Utrecht. (2000)

*Acknowledgment:* This study was supported by H2020 MSCA RISE project 778405 “AUTOIGG”

## Live-cell cartography: spatial mapping of biomolecular information by functional Fluorescence Microscopy Imaging (fFMI)

S. Oasa<sup>1</sup>, A.J. Krmpot<sup>2</sup>, S.N. Nikolić<sup>2</sup>, A.H.A. Clayton<sup>3</sup>, I.F. Tsigelny<sup>4</sup>,  
J.-P. Changeux<sup>5</sup>, L. Terenius<sup>1</sup>, R. Rigler<sup>6</sup> and V. Vukojević<sup>1</sup>

<sup>1</sup>*Department of Clinical Neuroscience (CNS), Karolinska Institutet, Stockholm Sweden*

<sup>2</sup>*Institute of Physics Belgrade, University of Belgrade, Belgrade, Serbia*

<sup>3</sup>*Optical Science Centre, Department of Physics and Astronomy, School of Science, Swinburne University of Technology, Melbourne, Australia*

<sup>4</sup>*Department of Neurosciences, University of California San Diego, CA, USA*

<sup>5</sup>*Institut Pasteur, Department of Neuroscience, Unité Neurobiologie Intégrative des Systemés, Paris France*

<sup>6</sup>*Department of Medical Biochemistry and Biophysics (MBB), Karolinska Institutet, Stockholm Sweden*

e-mail: sho.oasa@ki.se

Live cells convey key information and control their vital functions *via* molecular interactions and transporting processes. Through molecular interactions and transporting processes, they precisely control, spatially and timewise, the concentration and mobility of biomolecules, and their local environment (pH, ionic strength, charge density). To understand the dynamic integration of molecular interactions through transport processes, quantitative methods with high sensitivity, spatial and temporal resolution are needed. Fluorescence microscopy- and correlation spectroscopy based methods have proven to be invaluable for this purpose, and advanced methods such as Image Correlation Spectroscopy (ICS) [1] and Single Plane Illumination Microscopy (SPIM; also called Light Sheet Microscopy)/Total Internal Reflection (TIR)-based Fluorescence Correlation Spectroscopy (SPIM-FCS/TIR-FCS) [2] have been recently developed. However, both methods, while very powerful, also have limitations. ICS is based on Confocal Laser Scanning Microscopy (CLSM), thus relying on the analysis of fluorescence signal acquired with a time lag (dwell time between pixels). In SPIM-FCS, fluorescence intensity is simultaneously read-out; but light sheet propagation may be affected by obstacles in the sample, giving rise to an uneven fluorescence excitation across the specimen. Also the observation volume elements are larger than in conventional single-point FCS due to light-sheet thickness. Finally, TIR-FCS use is limited as it only can be used to study processes at the basal plasma membrane. With this in mind, we were motivated to develop scanning-free massively parallel FCS with high spatio-temporal resolution (~240 nm and ~ 10  $\mu$ s, respectively) and single-molecule sensitivity, which will allow us to quantitatively characterize fast dynamic processes and precisely measure the concentration of fluorescently-tagged biomolecules in live cells and in solution [3]. To this aim, fluorescence intensity from 256 or 1024 excitation foci generated by the diffractive optical element (DOE) are recorded by a position-matched individual single-photon avalanche detector (SPAD) in a 2D SPAD camera. Autocorrelation curves are computed from time series of fluorescence intensity fluctuation to determine the concentration (reciprocal to the amplitude of the autocorrelation curve) and diffusion time (decay time of the autocorrelation curve). Our instrument allows also Fluorescence Lifetime Imaging Microscopy (FLIM), to characterize the immediate surroundings of the fluorescent tags *via* fluorescence lifetime, and FLIM-based Förster Resonance Energy Transfer (FRET), to assess the biomolecular interaction via donor-acceptor interaction. We have applied mpFCS/FLIM to spatially map in live cells the local concentration, diffusion and local environment of a transcription factor in the cell nucleus and have characterised the effects of an allosteric inhibitor of transcription factor dimerization [4].

### REFERENCES

1. Wiseman, P.W., *Image correlation spectroscopy: principles and applications*. Cold Spring Harb Protoc, 2015. **2015**(4): p. 336-48.
2. Sankaran, J., et al., *Simultaneous spatiotemporal super-resolution and multi-parametric fluorescence microscopy*. Nat Commun, 2021. **12**(1): p. 1748.
3. Krmpot, A.J., et al., *Functional Fluorescence Microscopy Imaging: Quantitative Scanning-Free Confocal Fluorescence Microscopy for the Characterization of Fast Dynamic Processes in Live Cells*. Anal Chem, 2019. **91**(17): p. 11129-11137.
4. Oasa, S., et al., *A strategy for designing allosteric modulators of transcription factor dimerization*. Proc Natl Acad Sci U S A, 2020. **117**(5): p. 2683-2686.

## **Pixel categorization based on resonance energy transfer between fluorescent molecules: a pathway towards localization of functionalized metal nanoparticles in individual cells by fluorescence microscopy**

J. Pajović<sup>1,2</sup>, R. Dojčilović<sup>3,4</sup>, S. Kaščakova<sup>5,6</sup>, M. Refregiers<sup>2,7</sup>, D. K. Božanić<sup>3</sup> and V. Djoković<sup>3</sup>

<sup>1</sup>*Faculty of Physics, University of Belgrade, Belgrade, Serbia*

<sup>2</sup>*DISCO beamline, Synchrotron SOLEIL, Gif sur Yvette, France*

<sup>3</sup>*"VINČA" Institute of Nuclear Sciences - National Institute of the Republic of Serbia, University of Belgrade, Belgrade, Serbia*

<sup>4</sup>*Department of Experimental and Health Sciences, Pompeu Fabra University, Barcelona, Spain*

<sup>5</sup>*Inserm Unité 1193, F-94800 Villejuif, France*

<sup>6</sup>*University Paris-Sud XI, UMR-S1193, F-94800 Villejuif, France*

<sup>7</sup>*Centre de Biophysique Moléculaire, CNRS UPR4301, Orléans, France*

e-mail: jelena@ff.bg.ac.rs

Molecular resonance energy transfer (RET) is a basis of a half-century-old tool known as the molecular ruler, used for inference of mutual distances of two spectrally-coupled fluorophores usually relevant in biological contexts [1]. RET influences not only the absolute intensities of fluorescence signals of the molecular pair, but also their other optical characteristics, e.g. the valence electrons' excited states. On the other hand, metal-based hybrid nanostructures show great promise as future multifunctional nanoplatfroms, due to their superior sensitivity to external perturbations [2]. The metal components of the nanostructures influence the optical properties of fluorescent molecules in the vicinity, similarly as bulk metals do, which often presents a drawback. Here we want to demonstrate how this particular feature in metal-based nanosystems can be used as an advantage point in conventional biophysical imaging if the beneficial underlying physical mechanisms are identified [3].

In this talk, we will first explain the influence of gold nanoparticles on resonance energy transfer between tryptophan, essential amino acid, and riboflavin, vitamin B2, in an aqueous environment. We will show that the relative change of the signal in the tryptophan spectral channel is more pronounced when the biomolecules are attached to the nanoparticles. Afterward, we will demonstrate how time-lapse fluorescence imaging of nanoparticle-incubated liver cancer cells can be used for inferring subcellular areas of nanoparticle accumulation. By exposing the incubated cell to continuous UV radiation, the photobleaching of the fluorescent molecules in the sample occurs. Being sensitive to the electronic structure of the fluorophore, the photobleaching rates of different subareas in the cell show distinctive trends, depending on the chemical composition. As the nanoparticles promote RET between tryptophan and riboflavin, the nanostructures exhibit a particular photobleaching trend compared to the cells' endogenous fluorescent species [4]. Thus, by separating areas of fluorescence images into different classes based on their photobleaching rates, i.e. grouping the pixels of the same signal trends, we are able to infer the preferential accumulation sites of bifunctionalized gold nanoparticles by using fluorescence microscopy of lower lateral resolution than the size of the nanoparticles. In this way, we demonstrate a potent auxiliary detection modality of metal-based hybrid nanostructures in optical imaging.

### REFERENCES

- [1] P. J. Walla, *Modern Biophysical Chemistry: Detection and Analysis of Biomolecules*, John Wiley & Sons (2014).
- [2] C. Lai-Kwan, H.-T. Chang, *From Bioimaging to Biosensors: Noble Metal Nanoparticles in Biodetection*, Pan Stanford, (2012).
- [3] S. J. Sahl, S. W. Hell, S. Jakobs, *Nat. Rev. Mol. Cell Biol.* 18, 685 (2017).
- [4] R. M. Young, J. K. Arnette, D. A. Roess, B. G. Barisas, *Biophys. J.* 67, 881–888 (1994).

## Microspectroscopy and adaptive laser tools for fluorescence based retinal tissue diagnostics and therapy

R. Podlipec<sup>1,2</sup>, Z. Arsov<sup>1</sup>, I. Urbančič<sup>1</sup>, T. Koklič<sup>1</sup>, J. Mur<sup>3</sup>, R. Petkovšek<sup>3</sup>, J. Štrancar<sup>1</sup>

<sup>1</sup> *Laboratory of Biophysics, Condensed Matter Physics Department, Jožef Stefan Institute, Ljubljana, Slovenia*

<sup>2</sup> *Helmholtz-Zentrum Dresden-Rossendorf e.V., Ion Beam Center, Dresden, Germany*

<sup>3</sup> *Faculty of Mechanical Engineering, University of Ljubljana, Ljubljana, Slovenia*

e-mail: rok.podlipec@ijs.si

New autofluorescence-based imaging and spectroscopy techniques have been found particularly useful for many diagnostics applications in ophthalmology due to their molecular sensitivity and non-invasiveness. Besides improved diagnostics, the ultimate goal in this field for the coming years presents also an improved and automated laser-induced therapy coupled with the recognition of pathologies by highly resolved imaging using reliable algorithms for image processing. In our talk, we will present two of our recent studies focused on the applications of advanced microspectroscopy and adaptive laser approaches for detailed retinal pathology diagnostics and treatment based on tissue autofluorescence detection and image analysis.

By fluorescence hyperspectral imaging of whole fresh ex-vivo porcine eyes exposed to laser treatment inducing rupture of the retinal vessel to mimic blood leakage, we characterized blood coagulation dynamics in relation to oxygenation and found new insights into the active role of erythrocytes in the coagulation cascade (Figure 1A) [1]. This study was important within the scope of an early diagnosis and better understanding of blood leakage and coagulation mechanisms which are the key to prevent critical illness of e.g. diabetic retinopathy. The disease can cause visual loss and affects 80 percent of those with diabetes for more than 20 years and it progresses through vessel leakage, abnormal vessel growth and is accompanied by coagulation disorders. Another severe eye disease causing the visual loss is age-related macular degeneration (AMD). It is commonly treated by short laser pulses inducing thermal and mechanical stress that can as well cause unwanted damage to the surrounding retinal tissue. To properly adapt the laser treatment to minimize side effects, real-time controlled diagnostics and therapy should be applied. In our latest study, we show a new smart approach for real-time retinal theranostics based on tissue fluorescence lifetime information and adaptable pulsed laser therapy (Figure 1B).

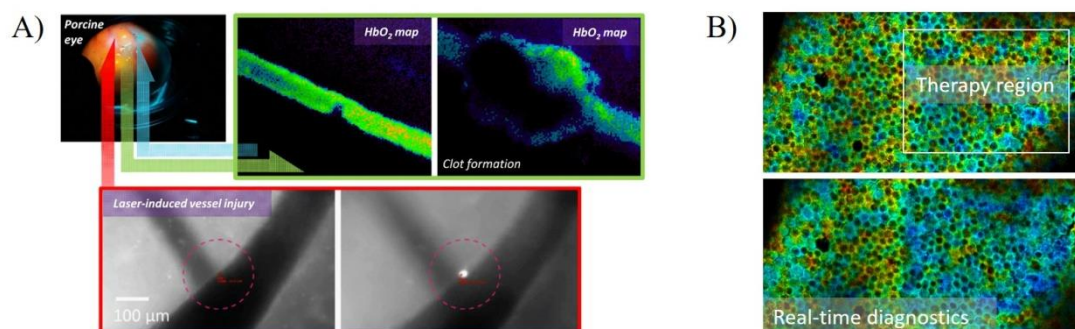


Figure 1. A) real-time fluorescence hyperspectral monitoring of blood coagulation in intact retinal vessels; B) real-time fluorescence lifetime based diagnostics of retinal tissue therapy

### REFERENCES

[1] R. Podlipec, Z. Arsov, T. Koklič, J. Štrancar, *Journal. of Biophotonics*, e202000021 (2020).

## How to create 2D magnets from non-magnetic 2D crystals

S. Stavrić<sup>1,2</sup>, B. N. Šoškić<sup>3</sup> and Ž. Šljivančanin<sup>2</sup>

<sup>1</sup>Physics Department, University of Trieste, via A. Valerio 2, Trieste 34127, Italy

<sup>2</sup>Vinča Institute of Nuclear Sciences, National Institute of the Republic of Serbia, University of Belgrade, P.O. Box 522, RS-11001 Belgrade, Serbia

<sup>3</sup>Faculty of Natural Sciences and Mathematics, University of Montenegro, Džordža Vašingtona bb, 81000 Podgorica, Montenegro  
e-mail: stavric@vinca.rs

The introduction of point defects offers manifold possibilities to induce a magnetic response in intrinsically non-magnetic two-dimensional (2D) materials. In graphene, the presence of vacancies leads to notable paramagnetism, yet no long-range magnetic ordering has been experimentally achieved due to low defect concentration. Another approach to induce magnetism in 2D crystals is to adsorb magnetic transition metal atoms. However, when deposited on graphene, transition metal atoms tend to cluster due to strong metal-metal attraction [1], making it challenging to control the shape and size of obtained nanostructures and their magnetic properties. One route to suppress the unfavorable clusterization is to attach the metal adatoms to the vacancies, acting as the trapping sites. The embedded metal atoms might carry out non-zero magnetic moments, yet the random distribution of these defects across the 2D sheet makes the long-range ordering of localized magnetic moments highly unlikely. In this lecture, we show that with the use of borophene, a 2D boron crystal recently synthesized on Ag(111) substrate, these obstacles can be overcome [2]. Borophene, unlike graphene, possesses a regular pattern of hexagonal holes which can be used as a template to grow 2D magnets when filled with Fe atoms. We show that the obtained Fe nanostructures are composed of close-packed Fe wires featuring ferromagnetism within the chain and the inter-chain antiferromagnetic coupling. Using density functional theory calculations, we extract the exchange and single-ion anisotropy constants needed to describe the magnetic properties of these systems with the classical Ising and Heisenberg models. The corresponding Monte Carlo simulations revealed finite temperature magnetic ordering, with the estimates of critical temperatures of 105 K and 30 K derived from the anisotropic Heisenberg model, for the Fe-based magnets grown above and under the borophene.

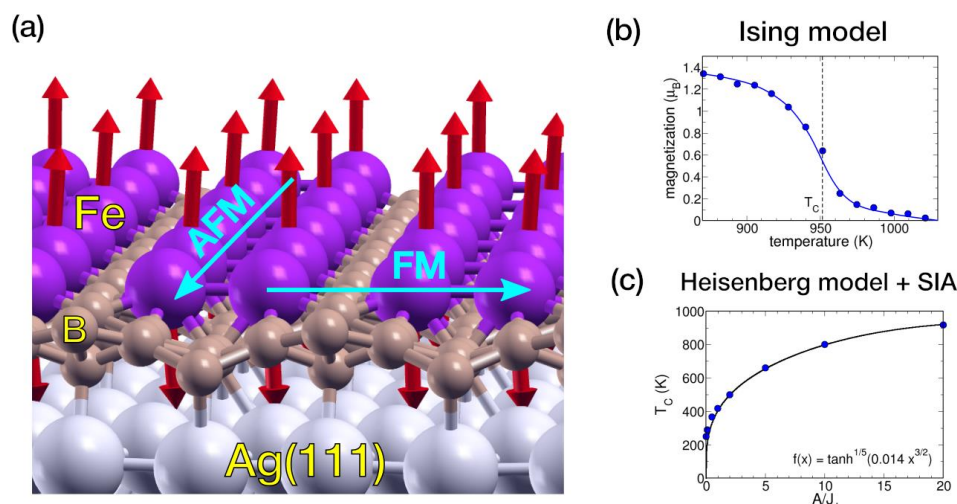


Figure 1. 2D magnet made from Fe wires grown above borophene/Ag(111) (a) and the critical temperatures obtained from Monte Carlo simulations employing Ising (b) and anisotropic Heisenberg model (c).

### REFERENCES

[1] S. Stavrić, M. Belić, Ž. Šljivančanin, Carbon **96**, 216 (2016)

[2] B. N. Šoškić, S. Stavrić, Ž. Šljivančanin, accepted for publishing in Phys. Rev. Materials (2021)

## Langmuir-Blodgett films from liquid phase exfoliated 2D materials: surface modification and optoelectronic properties

T. Tomasević-Ilić<sup>1</sup>, M. Spasenović<sup>2</sup>

<sup>1</sup>*Institute of Physics Belgrade, University of Belgrade, Pregrevica 118, 11080 Belgrade, Serbia*

<sup>2</sup>*Center for Microelectronic Technologies, Institute of Chemistry, Technology and Metallurgy, University of Belgrade, Njegoševa 12, 11000 Belgrade, Serbia*  
e-mail:ttijana@ipb.ac.rs

Liquid phase exfoliation is an important production technique to obtaining a high yield of two-dimensional nanosheets in solution. It can be applied to numerous layered materials and satisfies practical applications. Langmuir-Blodgett deposition is a simple and versatile method based on self-organization of nanostructures that brings large surfaces of thin films on the substrate of choice. Although, Langmuir-Blodgett self-assembly (LBSA) of 2D materials in solution allows facile fabrication of highly transparent graphene films, the high density of defects that causes high sheet resistance of these films is unavoidable. Identifying the type of defect of these films and understanding how they can be manipulated is crucial for development of new strategies to adapt their electrical properties to the requirements of the optoelectronic industry. In this talk, the structure and optoelectronic properties of LBSA graphene films, the change and subsequent enhancement of their sheet conductivity with surface modification/functionalization by chemical doping, annealing, photochemical oxidation, and plasma exposure will be summarized [1-3]. Surface modification of these films results in a multifold reduction in sheet resistance of the films without changing their high transmittance. Edges are the dominant type of defect of these films and play a crucial role in defect patching and enhancing of electrical properties of modified LBSA graphene films. For materials beyond graphene, the properties and the encapsulation capability of LBSA films of h-BN for high-quality CVD graphene, ideal for transparent electronics but highly degradable in extreme environments such as photochemical oxidation, will be discussed.

[1] A. Matković, et al., *2D Mater.* 3, 015002 (2016)

[2] T. Tomašević-Ilić, J. Pešić, I. Milošević, J. Vujin, A. Matković, M. Spasenović, R. Gajić, *Opt. Quant. Electron.* 48, 319 (2016)

[3] T. Tomašević-Ilić, Đ. Jovanović, I. Popov, R. Fandan, J. Pedrós, M. Spasenović, R. Gajić, *Appl. Surf. Sci.* 458, 446–453 (2018)

## Faraday and Resonant Waves in Dipolar Cigar-Shaped Bose-Einstein Condensates

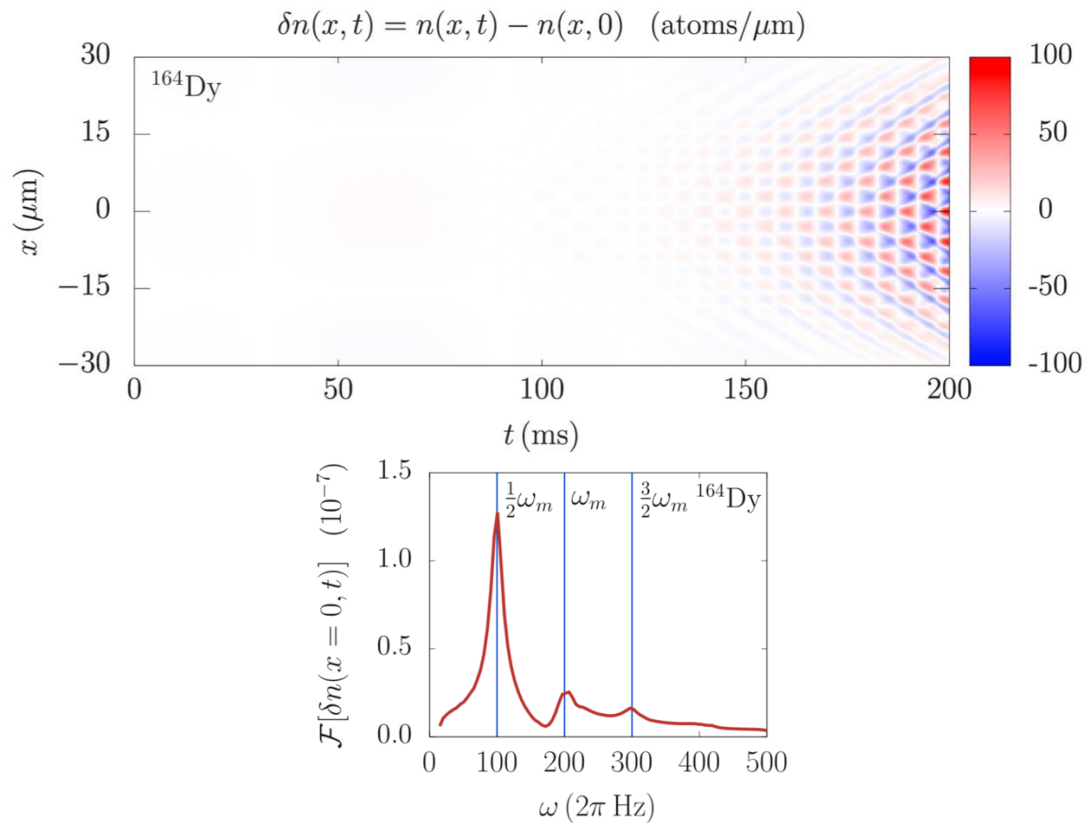
Dušan Vudragović

*Scientific Computing Laboratory, Center for the Study of Complex Systems,*

*Institute of Physics Belgrade, University of Belgrade, Serbia*

e-mail:dusan@ipb.ac.rs

Faraday and resonant density waves emerge in Bose-Einstein condensates as a result of harmonic driving of the system [1-3]. They represent nonlinear excitations and are generated due to the interaction-induced coupling of collective oscillation modes and the existence of parametric resonances. Using a mean-field variational and a full numerical approach, we study density waves in dipolar condensates at zero temperature [1], where breaking of the symmetry due to anisotropy of the dipole-dipole interaction plays an important role. We derive variational equations of motion for the dynamics of a driven dipolar system and identify the most unstable modes that correspond to the Faraday and resonant waves. Based on this, we also derive the analytical expressions for spatial periods of both types of density waves as functions of the contact and the dipole-dipole interaction strength. Finally, we compare the obtained variational results with the results of extensive numerical simulations that solve the dipolar Gross-Pitaevskii equation in 3D.



### REFERENCES

- [1] D. Vudragović and A. Balaž, *Symmetry* **11**, 1090 (2019).
- [2] A. Balaž, R. Paun, A. I. Nicolin, et al., *Phys. Rev. A* **89**, 023609 (2014).
- [3] A. Balaž and A. I. Nicolin, *Phys. Rev. A* **85**, 023613 (2012).

## XUV-driven plasma switch for THz: new spatio-temporal overlap tool for XUV–THz pump–probe experiments at FELs

E. Zapolnova<sup>1,4</sup>, R. Pan<sup>1</sup>, T. Golz<sup>1</sup>, M. Sindik<sup>1</sup>, M. Nikolic<sup>1</sup>, M. Temme<sup>1</sup>, M. Rabasovic<sup>2</sup>, D. Grujic<sup>2</sup>, Z. Chen<sup>3</sup>, S. Toleikis<sup>1</sup> and N. Stojanovic<sup>1</sup>

<sup>1</sup>Deutsches Elektronen-Synchrotron (DESY), Notkestrasse 85, 22607 Hamburg, Germany,

<sup>2</sup>Institute of Physics Belgrade, Pregrevica 118, 11080 Belgrade, Serbia, and

<sup>3</sup>SLAC National Accelerator Laboratory, Menlo Park, CA 94025, USA

<sup>4</sup>Class 5 Photonics GmbH, Notkestrasse 85, 22607 Hamburg, Germany

e-mail: ekaterina.zapolnova@@class5photonics.com

Intense THz pulses combined with synchronized X-ray pulses enable investigation of the dynamics of the light–matter interaction, non-linear response of materials and control of the properties of matter selectively on femtosecond time scales. Therefore, achieving the temporal overlap between pump and probe pulses in the femtosecond range is essential for both at table top high harmonic sources and Free Electron Lasers (FELs) [1].

A simple and robust tool for spatio-temporal overlap of THz and XUV pulses in in-vacuum pump–probe experiments is presented. The technique exploits ultrafast changes of the optical properties in semiconductors (i.e. silicon) driven by ultrashort XUV pulses that are probed by THz pulses. It enables the measurements of the arrival time between XUV and THz pulses with temporal resolution on the scale of the duration of the THz pulse. It enables the single shot measurement of the optical constants of the excited materials with the variable XUV wavelength [2].

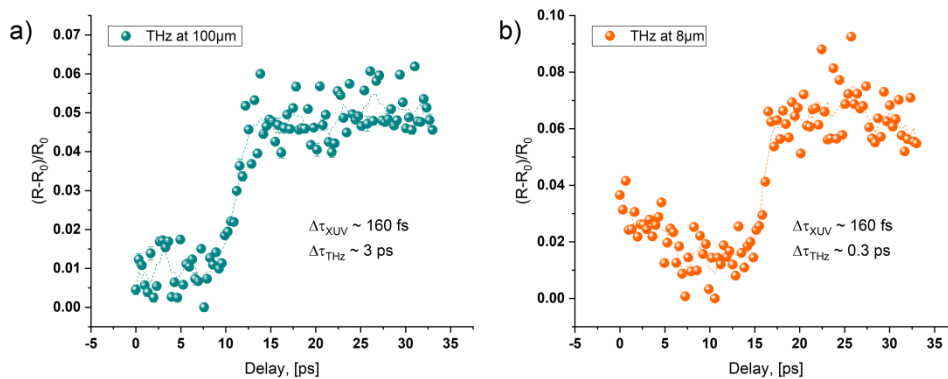


Figure 1. Transient THz reflectivity change of Si, excited by 13.5 nm XUV pulse probed with THz wavelengths of 100  $\mu\text{m}$  and 8  $\mu\text{m}$ .

### REFERENCES

- [1] E. Zapolnova, R. Pan, T. Golz, M. Sindik, M. Nikolic, M. Temme, M. Rabasovic, D. Grujic, Z. Chen, S. Toleikis and N. Stojanovic, *Journal of Synchrotron Radiation*, Vol. 27, p.1 (11-16) 2020  
 [2] Z. Chen, et. al., *Nature Communications*, 12 (1638), 2021

# Contributed papers

1. Quantum optics and ultracold systems
2. Nonlinear optics
3. Optical materials
4. Biophotonics
5. Devices and components
6. Optical communications
7. Laser spectroscopy and metrology
8. Ultrafast optical phenomena
9. Laser - material interaction
10. Optical metamaterials and plasmonics
11. Machine learning in photonics
12. Other topics in photonics

# **1. Quantum optics and ultracold systems**

## Using a mapping as a probe for heating suppression in periodically driven many-body quantum systems: a mean-field example with Bose gases

E. Wamba<sup>1</sup>, A. Pelster<sup>2</sup> and J. Anglin<sup>2</sup>

<sup>1</sup>*Faculty of Engineering and Technology, University of Buea, P.O. Box 63 Buea, Cameroon*

<sup>2</sup>*State Research Center OPTIMAS and Department of Physics, Technische Universität Kaiserslautern, 67663 Kaiserslautern, Germany*

e-mail: axel.pelster@physik.uni-kl.de

Experiments on periodically driven quantum systems have effectively realized quasi-Hamiltonians, in the sense of Floquet theory, that are otherwise inaccessible in static condensed matter systems. Although the Floquet quasi-Hamiltonians are time-independent, however, these continuously driven systems can still suffer from heating due to a secular growth in the expectation value of the time-dependent physical Hamiltonian. Here we use an exact space-time mapping [1,2] to construct a class of many-body systems with rapid periodic driving which we nonetheless prove to be completely free of heating, by mapping them exactly onto time-independent systems. The absence of heating despite the periodic driving occurs in these cases of harmonically trapped dilute Bose gas because the driving is a certain periodic but anharmonic modulation of the two-body contact interaction. Although we prove that the absence of heating is exact within full quantum many-body theory, we then use mean-field theory to simulate ‘Floquet heating spectroscopy’ and compute the heating rate when the driving frequency is varied away from the critical value for zero heating. The heating rate as a function of driving frequency appears to show a Fano resonance, suggesting that the exactly proven absence of heating at the critical frequency may be explained in terms of destructive interferences between excitation modes.

### REFERENCES

- [1] E. Wamba, A. Pelster, and J. Anglin, *Phys. Rev. A* **94**, 043628 (2016).
- [2] E. Wamba and A. Pelster, *Phys. Rev. A* **102**, 043320 (2020)

## Autler-Townes spectroscopy in a Mn-doped InGaAs/GaAs quantum dot

J. Filipovic, A. Lemaître and O. Krebs

<sup>1</sup>Centre for Nanosciences and Nanotechnology, CNRS, University Paris-Saclay, France

e-mail:jovana.filipovic@universite-paris-saclay.fr

For more than a decade, doping of semiconductor quantum dots (QDs) with a single magnetic atom has provided the unique possibility to investigate exchange interaction in the quantum regime [1,2] and to manipulate the corresponding spin states with light [3, 4]. In particular, the optical Stark effect induced by a strong optical excitation was demonstrated in II–VI QDs [4]. Here, we investigate similar effects in a self-assembled InGaAs/GaAs QD doped with a single Mn atom. This point defect in a III–V matrix forms a neutral acceptor  $A^0$  with a spin=1 [2]. In our present experiment, it is further coupled to a resident single hole giving rise to ferromagnetic (FM) and antiferromagnetic (AFM) levels split by about 1 meV. Under inter-band optical excitation, the QD exhibits thus a specific scheme of transitions consisting in a double lambda-system (Fig.1a). A continuous-wave (cw) tunable laser can be used to drive successively two transitions from the FM ground state, whereas the excited populations are directly monitored via the micro-photoluminescence ( $\mu$ PL) towards the AFM level (Fig.1b). In this sample, the observed resonance line widths are dominated by spectral diffusion ( $\sim 20 \mu\text{eV}$ ) and does not reveal the QD natural linewidth ( $\sim 1.5 \mu\text{eV}$ ). Still, optical Stark shift was clearly observed, and far above the saturation regime, an Autler-Townes splitting was spectrally resolved with the expected  $\propto \sqrt{P}$  power dependence. More interestingly, by driving the system with a weak probe laser at resonance with the upper transition, while a stronger pump laser is scanned through the lower transition (Fig.1c), it is possible to spectrally resolve the Autler-Townes effect experienced by the FM ground state, much below the spectral diffusion broadening limit. In this regime, the probe signal shows a Lorentzian dip with typical  $10 \mu\text{eV}$  spectral width, near the pump laser resonance (Fig.1d). This is a signature of the Autler-Townes effect in the ground state, which moreover reveals that the spin coherence of the two excited states is essentially unaffected by the spectral diffusion.

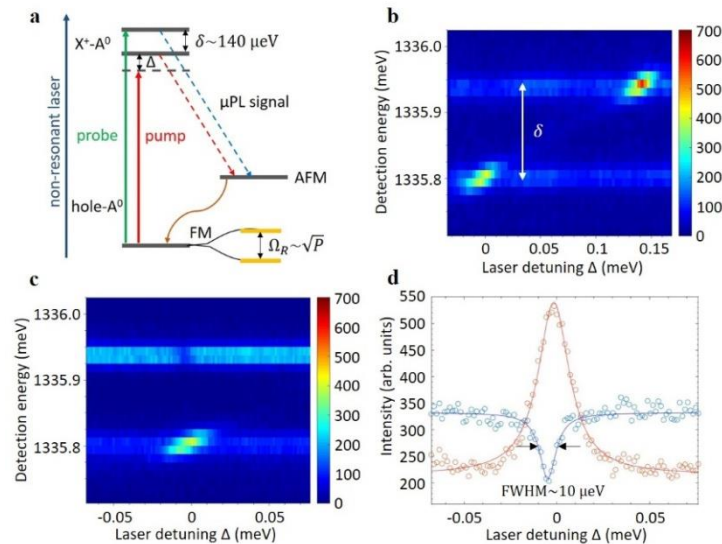


**Figure 1.** **a)** Energy levels of single positively charged Mn-doped QD driven by probe and pump cw lasers. Under strong resonant driving, dressed states are indicated (orange) for the ground state with Rabi frequency  $\Omega_R$ . **b)**  $\mu$ PL spectra against detuning of a single scanning laser ( $P=16 \mu\text{W}$ ). **c)**  $\mu$ PL spectra for a fix resonant probe laser ( $P=1.3 \mu\text{W}$ ) and a scanning pump laser ( $P=11 \mu\text{W}$ ). **d)** Intensities of the two transitions extracted from **c** (circles) fit with Lorentzian curves (solid lines).

### REFERENCES

- [1] L. Besombes, et al., Phys. Rev. Lett. 93, 207403 (2004).
- [2] A. Kudelski, et al., Phys. Rev. Lett. 99, 247209 (2007).
- [3] E. Baudin, et al., Phys. Rev. Lett. 107, 197402 (2011).
- [4] C. Le Gall et al., Phys. Rev. Lett. 107, 057401 (2011).

## Bend-free photonic integrated circuits with the crosstalk as a resource

J. Petrovic<sup>1,2</sup>, J. Krsic<sup>2</sup>, J.J.P Veerman<sup>3</sup>, A. Maluckov<sup>2</sup>

<sup>1</sup>*Institut für Optik und Atomare Physik, Technische Universität Berlin, Germany*

<sup>2</sup>*"VINCA" Institute of Nuclear Sciences, University of Belgrade, Serbia*

<sup>3</sup>*Fariborz Maseeh Department of Mathematics and Statistics, Portland State University, Portland, OR, USA*

e-mail: jovana.petrovic@tu-berlin.de

We challenge the current thinking and approach to design of photonic integrated circuits (PICs), which are marked as drivers of the future information processing.

Standard quantum PICs are composed of the unit cells based on directional couplers. The couplers typically consist of two waveguides bent to exhibit coupling in the proximity region. They conveniently produce the maximally entangled Bell state and have been used to construct functional optical quantum PICs [1]. However, their full exploitation faces the conceptual and technical challenges including the non-intrinsic scalability that requires waveguide branching, the radiation loss at waveguide bends and the therewith associated high-density packaging limit [2].

Arrays of linearly coupled parallel waveguides have been considered a viable alternative. However, the intricate inverse design of the corresponding Hamiltonians has limited their applications to the particular instances of the quantum logic gates obtained by numerical optimization procedures and machine learning [3, 4] and the simulators of the condensed matter systems, such as spin and Bloch arrays with the Wannier-Stark ladder spectrum [5]. A generic design solution based on a common physical and mathematical principle has not been reached.

We propose a new concept for the design of bend-free high-density PICs composed exclusively of the linearly coupled *commensurable* waveguide arrays (CWGA). Their operation is based on the *periodic continuous quantum walk of photons* and leverages on the engineered waveguide coupling. We discuss the class of analytically accessible designs with the eigenspectra that randomly sample the Wannier-Stark ladder [6, 7]. *The free choice of eigenfrequencies marks a clear distinction from the current photonic simulators and provides a variety of novel circuit layouts and functionalities.* In particular, we rework the designs of interconnects for qubits and qudits, multiport couplers, entanglement generators and interferometers. The analytical results are corroborated numerically. Finally, we test the robustness of the proposed building blocks to the random variations in design parameters, with a view to defining acceptable fabrication tolerances.

### REFERENCES

- [1] J. Wang, et al. *Science* 360, 285 (2018).
- [2] W. Song, et al., *Nat. Commun.* 6, 2027 (2015).
- [3] Y. Lahini, et al., *npj Quantum Inf.* 4, 2 (2018).
- [4] A. Youssry, et al., *Quant. Sci. Technol.* 5, 025001 (2020).
- [5] M. Gräfe, A. Szameit, *J. Phys. B: Atom. Mol. Opt. Phys.* 53, 073001 (2020).
- [6] J. Petrovic, J. J. P. Veerman, *Ann. Phys.* 392, 128 (2018).
- [7] J. Petrovic, *Opt. Lett.* 40, 139 (2015).

## Control of entanglement between driven three-level atom in ladder-type configuration and its spontaneous emission

Lj. Stevanović and N. Andrejić

*Department of Physics, Faculty of Sciences and Mathematics, University of Niš, Serbia*

e-mail:ljstevanovic@junis.ni.ac.rs

Investigation of atom – photon entanglement attracts the attention in the past decades due to its application in the areas of quantum communication and quantum computing [1]. The numerous papers, dealing with that subject, are devoted to entanglement between the atom and its spontaneous emission. The study is based on the model of multi-level atom in different configurations dressed by coherent field [2], [3].

Here, we study the entanglement between the three-level atom and its spontaneous emission. The atom is driven by two coherent laser fields: one field induces transition between the ground and the first excited level, while the other field induces transition between the excited levels, making the ladder-type configuration. The optical Bloch equations, describing the density matrix evolution, are derived in semiclassical approach under rotating wave approximation and then solved numerically in the steady-state regime. Reduced entropy, based on atomic density matrix, is used as the measure of entanglement.

The effect of the system parameters, like spontaneous decay rates of the excited levels, Rabi frequencies and detunings of the laser fields, on entanglement is investigated in details. The influence of Rabi frequencies is studied in two cases: when one of them is much less than the other and when they are comparable. Also, the effect of detunings is considered in the case of two-photon resonance and beyond it. Another way in investigation is devoted to the control of entanglement by the vacuum induced coherence, which is achieved in the quantum system with equidistant levels.

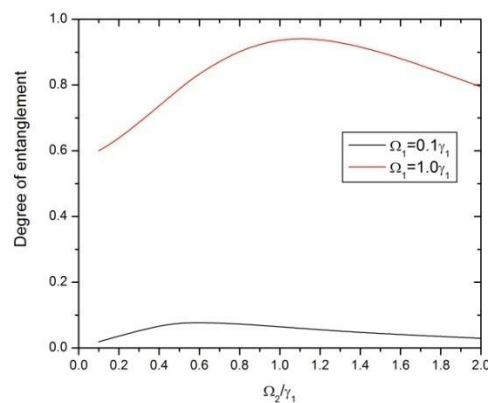


Figure 1. Effect of Rabi frequencies of the laser fields on the degree of entanglement.

### REFERENCES

- [1] S. Chen, Y. A. Chen, B. Zhao, Z. S. Yuan, J. Schmiedmayer, J. W. Pan, *Phys. Rev. Lett.* **99**, 180505 (2007).
- [2] A. Mortezaipoor, M. Abedi, M. Mahmoudi, M. R. H. Khajehpor, *J. Phys. B: At. Mol. Opt. Phys.* **44**, 085501 (2011)
- [3] Z. Kordi, S. Ghanbari, M. Mahmoudi, *Quant. Inf. Process* **15**, 199 (2016)

## Intensity squeezed states of light by four wave mixing in potassium vapor

M. Curcic, B. Jelenkovic  
*Institute of Physics, Belgrade, Serbia*  
e-mail:marijac@ipb.ac.rs

We will present our recent results of intensity difference squeezing generated by four wave mixing (FWM) in high density potassium vapor. Squeezed light with the noise level of several dB below standard quantum limit is observed in the difference signal between correlated probe and conjugate beams. Previous studies of the squeezing in alkalis were done mainly for Rb and Cs [1, 2].

For the FWM process we used non-degenerate double  $\Lambda$  scheme, with nearly co-propagating pump and probe beams. The source for the pump and the probe was the high power MBR (Coherent) laser. The vapor is contained in the vacuum K cell. For the difference of the probe and conjugate beam's intensities after the cell we used balanced detectors with a gain of  $10^5$  V/A. The signal difference was analysed using the spectrum analyzer.

We have varied number of parameters: pump one photon detuning (OPD), two pump-probe detuning (TPD), temperature, pump and probe powers, angle between the beams and the length of the cell. The best squeezing, we obtained so far, is about  $-5.5$  dBm, before the correction for losses on the cell window, optics used behind the cell and the detection efficiency. This level of squeezing was obtained at pump and probe powers of 800 mW and 6  $\mu$ W, OPD and TPD of 1.2 GHz and 6 MHz, at the cell temperature of 122  $^{\circ}$ C. We analysed effects of all mentioned parameters on the relative intensity squeezing and on the gains of the twin beams, and compare them with the behavior of squeezing found in Rb and Cs.

### REFERENCES

- [1] C. F. McCormick, A. M. Marino, V. Boyer, and P.D. Lett, , Phys. Rev. A 78, 043816 (2008).
- [2] R. Ma, W. Liu, Z. Qin, X. Jia and Ji. Gao, Phys. Rev. A 96, 043843 (2017).

## Quantum droplets in dipolar ring-shaped Bose-Einstein condensates

M. Šindik<sup>1</sup>, A. Pelster<sup>2</sup> and A. Balaž<sup>1</sup>

<sup>1</sup>*Institute of Physics Belgrade, University of Belgrade, Serbia*

<sup>2</sup>*Department of Physics, Technical University of Kaiserslautern, Germany*

e-mail: [marijas@ipb.ac.rs](mailto:marijas@ipb.ac.rs)

We study the formation of quantum droplets in dipolar Bose-Einstein condensates in a ring-shaped geometry using numerical techniques. A condensate is initially prepared in a stable ground state of the system, and droplet formation is triggered by a sudden quench of the contact interaction. We investigate how the number of the obtained droplets depend on the total number of atoms in the system, as well as on the strength of the contact and the dipole-dipole interaction. These results can be used in experiments to fine-tune parameters of the system in order to produce droplets of desired size. Furthermore, we study the emergence of supersolidity in the system, when droplets are formed due to the contact interaction quench, but the common phase is still preserved among spatially separated droplets. The quasi-1D geometry imposes additional constraints in the system, in particular when the particle density is higher, such that quantum fluctuation effects become more prominent. We use the Bogoliubov-Popov theory for dipolar Bose systems, including the dipolar analogue of the Lee-Huang-Yang correction, and take into account the condensate depletion due to quantum fluctuations.

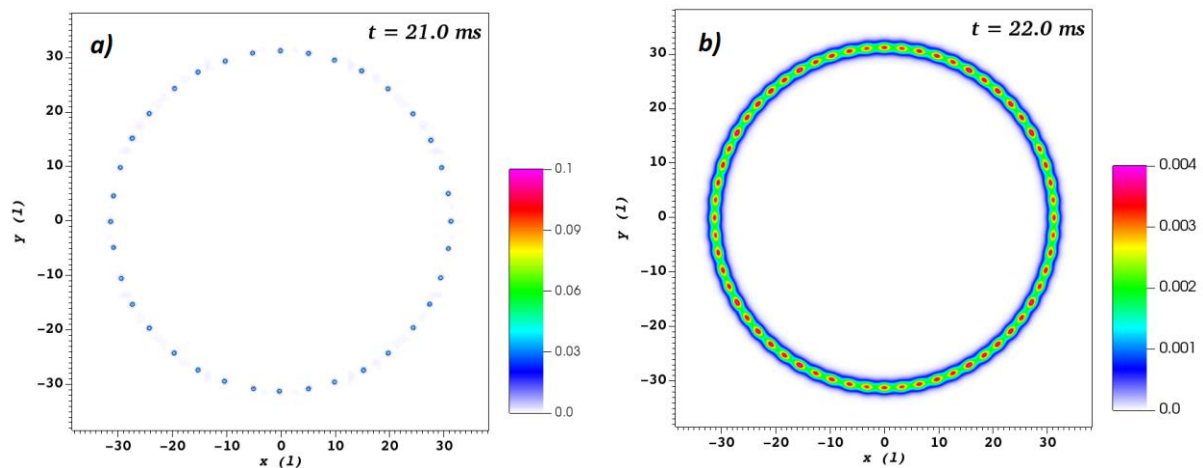


Figure 1. Density distribution in case of a) isolated droplets, b) supersolid state.

## Non-equilibrium evolution of Bose-Einstein condensate deformation in temporally controlled weak disorder

Milan Radonjić<sup>1,2</sup> and Axel Pelster<sup>1</sup>

<sup>1</sup>*Physics Department and Research Center OPTIMAS, Technical University of Kaiserslautern,  
Erwin-Schrödinger Straße 46, 67663 Kaiserslautern, Germany*

<sup>2</sup>*Institute of Physics Belgrade, University of Belgrade, Pregrevica 118,  
11080 Belgrade, Serbia*

e-mail: milanr@ipb.ac.rs

We consider a time-dependent extension of a perturbative mean-field approach to the homogeneous dirty boson problem by considering how switching on and off a weak disorder potential affects the stationary state of an initially equilibrated Bose-Einstein condensate by the emergence of a disorder-induced condensate deformation. We find that in the switch on scenario the stationary condensate deformation turns out to be a sum of an equilibrium part [1], that actually corresponds to adiabatic switching on the disorder, and a dynamically-induced part, where the latter depends on the particular driving protocol [2]. If the disorder is switched off afterwards, the resulting condensate deformation acquires an additional dynamically-induced part in the long-time limit, while the equilibrium part vanishes. We also present an appropriate generalization to inhomogeneous trapped condensates. Our results demonstrate that the condensate deformation represents an indicator of the generically non-equilibrium nature of steady states of a Bose gas in a temporally controlled weak disorder.

### REFERENCES

- [1] K. Huang and H. F. Meng, *Phys. Rev. Lett.* **69**, 644 (1992).
- [2] M. Radonjić and A. Pelster, *SciPost Phys.* **10**, 008 (2021).

## Slow light under double-double EIT regime in spherical quantum dot with hydrogen impurity

N. Filipović and V. Pavlović

Department of Physics, Faculty of Sciences and Mathematics, University of Niš, Serbia

e-mail: nikola.filipovic@pmf.edu.rs

Throughout the decades, a lot of attention has been devoted to the study of the light manipulation, with various applications in quantum optics and photonics [1]. One prosperous application is slow light, obtained by reducing the group velocity of light by several orders of magnitude [2,3]. The technique largely used to achieve such an effect is via the electromagnetically induced transparency (EIT). This phenomenon allows the medium, previously opaque for the weak probe laser, to become transparent in the presence of another, strong control field [4].

Typically, the EIT is obtained with two lasers. However, adding another control field can lead to the formation of two transparency windows, which is called double-double EIT [5]. In this paper, this type of coupling is achieved by using the four-level cascade scheme, with the levels  $1s_0$ ,  $2p_{-1}$ ,  $3d_{-2}$  and  $4f_{-3}$  of the GaAs spherical quantum dot (SQD) with the on-center hydrogen impurity. The probe field  $E_p$  couples the levels  $1s_0$  and  $2p_{-1}$ , while control fields  $E_{c1}$  and  $E_{c2}$  excite transitions  $2p_{-1} \leftrightarrow 3d_{-2}$  and  $3d_{-2} \leftrightarrow 4f_{-3}$ , respectively. Using semiconductor quantum dots, where the charge carriers are confined in all three dimensions, improves the implementation and controllability of the experimental setup [6].

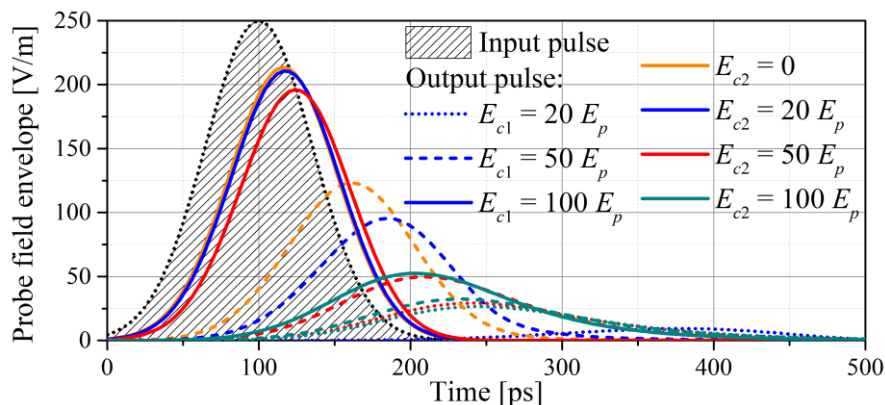


Figure 1. The temporal profile of the input and output probe pulse envelope for several values of the electric field of the two control lasers.

To investigate the weak probe pulse propagation through the SQD under the presence of two strong cw control fields, Maxwell-Bloch equations are solved by using the Fourier transform method. The central result is shown in Fig. 1. The group velocity of the output pulse can be reduced by decreasing  $E_{c1}$ , which also reduces the efficiency. On the other hand, the switch-on and further increase of  $E_{c2}$  leads to the formation and increase of the middle absorption peak height, respectively. The position of this peak can be altered by applying the external static magnetic field, which can increase the output pulse efficiency. All the conclusions can be further utilized to contribute to the fields of magnetometry, quantum telecommunications and quantum information processing.

### REFERENCES

- [1] M. O. Scully, M. S. Zubairy, Quantum Optics, Cambridge University Press, 1997.
- [2] L. V. Hau, S. E. Harris, Z. Dutton, C. H. Behroozi, Nature 397, 594 (1999).
- [3] D. Budker, D. F. Kimball, S. M. Rochester, V. V. Yashchuk, Phys. Rev. Lett. 83, 1767 (1999).
- [4] S. E. Harris, Phys. Today 50, 36 (1997).
- [5] H. M. M. Alotaibi, B. C. Sanders, Phys. Rev. A 89, 021802 (2014).
- [6] P. C. Ku, C. J. Chang-Hasnain, S. L. Chuang, J. Phys. D Appl. Phys. 40, R93 (2007).

## Search for topological defects of bosonic ultralight field with optically pumped magnetometer: design, calibration, and sensitivity of the Belgrade GNOME station

S. Topić<sup>1,2</sup>, and Z. D Grujić<sup>1</sup>

<sup>1</sup>*Institute of Physics, Belgrade, Serbia*

<sup>2</sup>*Faculty of Physics, University of Belgrade, Serbia*

e-mail: [sasa.topic.sale@gmail.com](mailto:sasa.topic.sale@gmail.com)

We present the design and calibration of optically pumped magnetometer (OPM), based on a paraffin coated cesium cell, and estimate its ultimate reach in terms of mass and interaction strength of hypothetical axionic or axion-like dark matter fields in form of a topological defects. Hypothetical axions or Axion Like Particles (ALP's) are form of ultralight bosonic matter that are postulated in order to solve strong CP problem, matter-antimatter imbalance in the Universe and maybe even solve current  $\Lambda$  Cold Dark Matter ( $\Lambda$ CDM) observational discrepancies and  $H_0$  tensions. Dark matter problem, exacerbated by negative results of search for WIMP's, core-cusp problem, missing satellites problem and others may be solved by a type of ultralight matter model which can reconcile GR and MOND paradigms.

This model has several detectable signatures, one being in the form of axionic field couplings to Standard Model fermions via the pseudomagnetic fields that are generated during passage through topological defects. The GNOME experiment is designed as a GPS referenced worldwide distributed network of quantum cross-correlated sensors that increases its sensitivity, discovery reach and excludes false positives by methodology similar to LIGO network. Belgrade GNOME station is built around a double resonant optical cesium magnetometer in Mx configuration and is functioning as a scalar magnetometer with a sensitivity less than  $100 \text{ fT}/\sqrt{\text{Hz}}$ . We will present different modes of operations, give an overview of atomic magnetometry and quantify various noise contributions. Special attention will be given to PSD, sensitivities, and stability over short and long baselines of the setup. Guidelines for future work and a foreseen improvements shall also be mentioned.

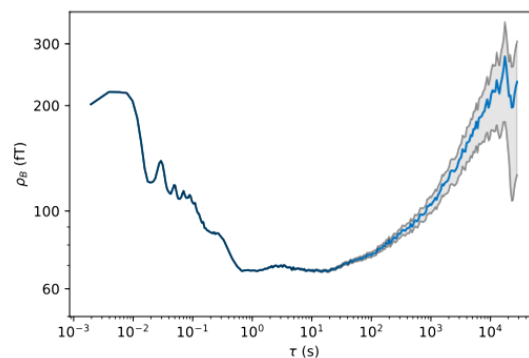


Figure 1. Allan standard deviation of magnetic field recorded by OPM in phase-locked loop.

### REFERENCES

- [1] D. Budker and M.V. Romalis, *Nat. Phys.*, 23 (2007), 229
- [2] M. Pospelov, et al., *Phys. Rev. Lett.*, 110 (2013), 021803
- [3] J. Preskill, M. B. Wise and F. Wilczek, *Phys. Lett.*, B120 (1983), 127
- [4] S. M. Carroll, *Phys. Rev. Lett.*, 81 (1998), 3067
- [5] Pustelny et al., *Ann. Phys.*, 525 (2013), 659-670
- [6] M.P. Ledbetter, M.V. Romalis and D.F. Jackson Kimball, *Phys. Rev. Lett.*, 110 (2013), 040402

## **2. Nonlinear optics**

## Stability of necklace beams in media with cubic-quintic nonlinearity

A. I. Strinić<sup>1,2</sup>, M. S. Petrović<sup>3</sup>, B. N. Aleksić<sup>4</sup>, N. B. Aleksić<sup>5</sup>, and M. R. Belić<sup>2</sup>

<sup>1</sup>*Institute of Physics, University of Belgrade, P.O. Box 68, 11080 Belgrade, Serbia*

<sup>2</sup>*Texas A&M University at Qatar, PO Box 23874, Doha, Qatar*

<sup>3</sup>*Institute of Physics, P. O. Box 57, Belgrade 11001, Serbia*

<sup>4</sup>*Weill Cornell Medicine Qatar, Doha, Qatar*

<sup>5</sup>*Moscow State Technological University "STANKIN", Moscow, Russia*

e-mail: strinic@ipb.ac.rs

In this paper, we have studied numerically the stability of two-dimensional soliton-like clusters in the form of necklaces in media with cubic-quintic nonlinearity. We have tested their stability against initial perturbations, as well as their robustness with respect to variation of parameters [1, 2].

### REFERENCES

- [1] N. B. Aleksić, A. I. Strinić, M. M. Petroski and M. S. Petrović, *Opt. Quant. Electron.* 52, 73 (2020). <https://doi.org/10.1007/s11082-019-2189-x>
- [2] A. I. Strinić, N. B. Aleksić, M. R. Belić and M. S. Petrović, *Opt. Quant. Electron.* 52, 310 (2020). <https://doi.org/10.1007/s11082-020-02382-w>

## Strong-field ionization of diatomic molecules and molecular anions: interferences and classical model

D. Habibović<sup>1</sup>, A. Gazibegović-Busuladžić<sup>1</sup>, M. Busuladžić<sup>2,1</sup> and D. B. Milošević<sup>1,3</sup>

<sup>1</sup>*Faculty of Science, University of Sarajevo, Sarajevo, Bosnia and Herzegovina*

<sup>2</sup>*Faculty of Medicine, University of Sarajevo, Sarajevo, Bosnia and Herzegovina*

<sup>3</sup>*Academy of Sciences and Arts of Bosnia and Herzegovina, Sarajevo, Bosnia and Herzegovina*  
e-mail:dhfizika1@gmail.com

Many interesting phenomena can be observed when the molecular system is exposed to a strong laser field. Among these phenomena, particularly interesting is high-order above-threshold ionization (HATI). In this process the electron ionized under the influence of the laser field propagates in the continuum and, due to the oscillatory character of the laser field, returns to and elastically rescatters off the parent molecular ion. The photoelectron energy spectrum is characterized by a long plateau where the ionization rate changes rather slowly as a function of the electron energy. The characteristics of the process are even more interesting when a two-component driving field is employed instead of a linearly polarized field.

To explain the characteristics of the photoelectron spectra we use the molecular strong-field approximation (MSFA) introduced in [1] and improved in [2,3]. More recently, this theory has been applied to explain HATI spectra obtained exposing diatomic molecules to an orthogonally polarized two-color (OTC) laser field which is a combination of two linearly polarized fields with orthogonal polarizations and commensurable frequencies [4,5]. In [5] we have also developed the improved classical model. The results obtained using this model are in a good agreement with the MSFA theory. The aim of the present work is to analyze the interference of various contributions to the total ionization rate for the case of diatomic molecules exposed to an OTC laser field. These contributions correspond to the situations where the electron is ionized at one and rescattered at the same or at the different atomic center, and they can interfere in a complicated manner. The reason is that for different electron emission angles and different ionization and rescattering centers the photoelectron paths are different. In addition, the electron paths depend on the orientation of the molecule in the laser field. Also, in [6] we have applied the MSFA to molecular anions in a linearly polarized laser field. Now, we apply an improved classical model in order to explain the photoelectron energy distribution and to get an insight into the dynamics of the ionization process. This model allows us to estimate which classical trajectory is responsible for a particular part of the spectrum and to control the ionization process.

### REFERENCES

- [1] D. B. Milošević, *Phys. Rev. A* 74, 063404 (2006).
- [2] M. Busuladžić, A. Gazibegović-Busuladžić, D. B. Milošević, W. Becker, *Phys. Rev. Lett.* 100, 203003 (2008).
- [3] M. Busuladžić, A. Gazibegović-Busuladžić, D. B. Milošević, W. Becker, *Phys. Rev. A* 78, 033412 (2008).
- [4] D. Habibović, A. Gazibegović-Busuladžić, M. Busuladžić, A. Čerkić, D. B. Milošević, *Phys. Rev. A* 102, 023111 (2020).
- [5] D. Habibović, A. Gazibegović-Busuladžić, M. Busuladžić, D. B. Milošević, *Phys. Rev. A* 103, 053101 (2021).
- [6] A. Gazibegović-Busuladžić, D. Habibović, M. Busuladžić, D. B. Milošević, *J. Opt. Soc. Am. B* 37, 813 (2020).

## On the propagation of twin beam pulses in four-way-mixing medium – cause for asymmetric broadening and splitting

D. Arsenovic, Ž. Nikitović, B. Zlatković, A. Krmpot, M. Ćurčić, B. Jelenković  
*Institute of Physics, National Institute of the Republic of Serbia, Belgrade, Serbia*  
e-mail:arsenovic@ipb.ac.rs

Weak probe pulse that propagates a four-way-mixing (FWM) medium is amplified and new conjugate beam is generated as a result of a two pump photon conversion in the nonlinear FWM process. During this propagation, group velocities of these pulses are slowed. The pulses are broadened in respect to the probe pulse, due to dispersion effect on the shape of the pulse – different frequencies of the pulse spectral bandwidth have different group velocities. As the pulses propagate in the medium, asymmetry in pulse broadening, and even strong distortion due to the higher order dispersion, can occur.

Since the applications of the slow light pulses for optical quantum memories and optical switches, requires preservation of initial, usually Gaussian, shape, it is of interest to find parameters for the FWM which maximally preserves the initial shape. The FWM parameters governing the pulse propagation are the pump intensity and medium density, and the detunings of the optical fields from atomic transitions, the pump single photon detuning, and the pump-probe two photon detuning.

Theoretical results for the probe and conjugate pulses propagating through the Potassium vapor, under the effects of FWM, are compared with experimental results. We calculated and measured twin pulses waveforms at the exit of the 4 cm long vacuum cell for the 80 ns probe seed beam, when K vapor density is  $3 \cdot 10^{12} \text{ cm}^{-3}$  (120 °C), and the pump power in the experiment and Ruby frequency in the theoretical model are 220 mW and 1.5 GHz, respectively. Most previous theoretical works on the pulse propagation in the FWM alkali vapor are based on analytical expressions, and therefore on several assumptions in their models [1]. We have done a full numerical calculations of the density matrix elements, and subsequently the atomic polarization that is governing both gains and shapes of initial seed probe and conjugate pulses.

The 80 ns probe pulse has a spectral bandwidth of 550 MHz, and in a dispersive medium, like the K vapor near the two-photon resonance, different spectral components will acquire different phases and different delays. This causes broadening of twin pulses, while different gains associated with different spectral components of the pulse, can distort the pulse, causing even pulse splitting.

We present results of the model and of experiment that show strong dependence of the pulse waveform on the two-photon detuning, for the same pump one photon detuning and vapor density. We also emphasize importance of Doppler line broadening on the results of the model.

### REFERENCES

[1] N. B. Phillips, A. V. Gorshkov and Irina Novikova (2009) *Slow light propagation and amplification via electromagnetically induced transparency and four-wave mixing in an optically dense atomic vapor*, Journal of Modern Optics, 56:18-19, 1916-1925

## Mobility of localized solutions in a nonlinear graphene ribbon

Ignacio Salinas V., Camilo Cantillano, and Rodrigo A. Vicencio

*Departamento de Física and MIRO, Facultad de Ciencias Físicas y Matemáticas, Universidad de Chile, Chile*  
e-mail: ignacio.salinas@ing.uchile.cl

We consider a quasi-one-dimensional graphene ribbon photonic lattice with Kerr-type nonlinearity. Its linear regime presents four dispersive (DBs) and two flat (FBs) bands. The system has two different compact solutions with amplitude different to zero in only four sites, which are known as localized linear FB modes [1]. When the nonlinearity is switched on, the FB modes continues into two families of compact nonlinear modes with the same amplitude and phase structure, and with no power threshold. We characterize different families of nonlinear localized solutions by inspecting their power, frequency, Hamiltonian and participation ratio as a way to predict different regions in parameter space where different nonlinear solutions could interact effectively by exciting them dynamically [2,3]. We also look for different regions of parameters where a coherent transport across the system could emerge. We find several regions where different stationary solutions perturbed by a phase gradient (kick/angle) show controlled mobility with low power radiation losses. We numerically observe how different localized solutions adiabatically transforms into others as dynamical sequence shows in Figure 1.

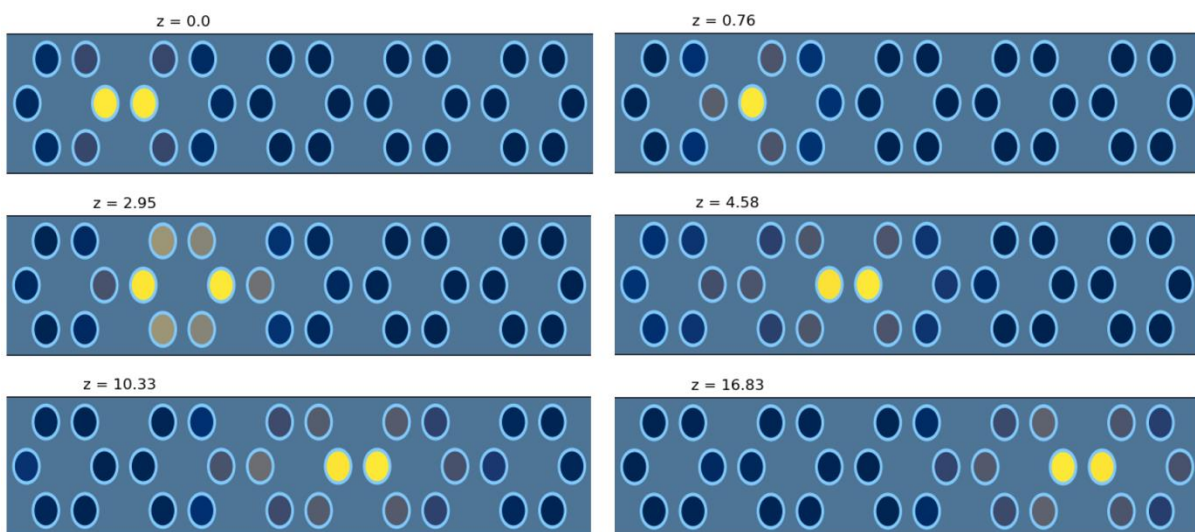


Figure 1. Intensity profiles at different propagation distances, showing mobility of a two-peaks solution.

### REFERENCES

- [1] C. Cantillano et al., *New J. Phys.* 20, 033028 (2018).
- [2] B. Real and R. A. Vicencio, *Phys. Rev. A* 98, 053845 (2018).
- [3] M. G. Stojanović, M. Stojanović Krsić, A. Maluckov, M. Johansson, I. A. Salinas, R. A. Vicencio and M. Stepić. *Phys. Rev. A* 102, 023532 (2020).

## Optical vortices in waveguides with spatial dependence of the nonlinear refractive index

Valeri Slavchev<sup>1,3</sup>, Ivan Bozhikoliev<sup>1</sup>, Zhelyazko Zamanev<sup>2</sup>, Aneliya Dakova<sup>1,2</sup>

<sup>1</sup>*Institute of Electronics, Bulgarian Academy of Sciences, 72 Tzarigradsko shossee, 1784 Sofia, Bulgaria*

<sup>2</sup>*Physics and Technology Faculty, University of Plovdiv "Paisii Hilendarski", 24 Tsar Asen Str., 4000 Plovdiv, Bulgaria*

<sup>3</sup>*Faculty of Pharmacy, Medical University - Plovdiv, 15 Vasil Aprilov Bul., 4002 Plovdiv, Bulgaria*

e-mail: [valerislavchev@yahoo.com](mailto:valerislavchev@yahoo.com)

Optical vortex is referred to beam or pulse that has singularity in the amplitude or phase. The last one is characterized by helical phase front. These light structures are solutions of two-dimensional paraxial scalar equation of Leontovich. They are usually created outside the laser cavity by using optical holograms and different optical masks.

In present work it is studied the formation of optical vortices in waveguides with spatial dependence of the nonlinear refractive index. The propagation of such type of laser pulses is governed by a system of amplitude equations for  $x$  and  $y$  components of the electrical field in which it is taken into account the effects of second order dispersion and self-phase modulation. The corresponding system of equations is solved analytically. New class exact solutions, describing the generation of vortices structures in optical fibers with spatial dependence of the nonlinear refractive index and anomalous dispersion, are found. These vortices admit only amplitude type singularities. Their stability is a result of the balance between diffraction and nonlinearity, as well as nonlinearity and angular distribution. This kind of singularities can be observed as a depolarization of the vector field in the laser spot.

Optical vortices have a number of applications in the field of high resolution microscopy, optical tweezers, quantum information transfer, optical vortex trapping and many others.

**Keywords:** Optical vortices, vector amplitude equation, nonlinear refractive index

### ACKNOWLEDGMENTS

The present work is funded by Bulgarian National Science Fund by grant KP-06-M48/1.

## Compact localized modes in the flux dressed 2D octagonal-diamond photonic lattice in the presence of nonlinearity

M. G. Stojanović<sup>1</sup>, S. Gundogdu<sup>2</sup>, M. Stojanović Krsić<sup>3</sup>, M. Stepić<sup>1</sup>, A. Maluckov<sup>1</sup>

<sup>1</sup>*VINČA Institute of Nuclear Sciences, University of Belgrade, National Institute of the Republic of Serbia, Mike Petrovića Alasa 12-14, 11000 Belgrade, Serbia*

<sup>2</sup>*Center for Theoretical Physics of Complex Systems, Institute for Basic Science, Daejeon 34126, Republic of Korea*

<sup>3</sup>*Faculty of Technology, University of Niš, 16 000 Leskovac, Serbia*

The flat-band lattice systems attract researches in photonics owing to peculiar transport properties and localization of light in the absence of dispersion [1, 2]. Moreover, the photonic flat-band systems are easy manageable platforms for testing the properties of the nearly flat band systems in the context of the condensed matter physics. Here, we extend our previous study [3] of the compact localized modes in the two-dimensional photonic octagonal-diamond lattice (ODL) dressing it with artificial flux.

We provide a routine to change the band structure of the ODL, with two flat-bands interrelated by one dispersive band (flux-free case), to those with one fully gapped flat-band by tuning the value of the artificial flux [4]. The possibility of realization of the proposed system in the laboratory is offered by experiments with optical resonators and the femto-second laser inscribed curved lattices.

The flat-band compact localized linear eigenmodes will be examined numerically. The main aim is to test their robustness to the presence of the local nonlinearity. We investigate dependence of the dynamical properties of the nonlinear localized modes continued by nonlinearity from the linear compacton families on the flux-determined flat-band pattern.

### REFERENCES

- [1] D. Leykam, A. Andreanov, and S. Flach, *Advances in Physics*:X 3, 1 (2018).
- [2] D. Leykam and S. Flach, *APL Photonics* 3, 070901 (2018).
- [3] M. G. Stojanović, M. Stojanović Krsić, A. Maluckov, M. Johansson, I. A. Salinas, R. A. Vicencio, M. Stepić, *Phys. Rev. A* 102, 023532 (2020).
- [4] B. Pal, *Physical Review B* 98, 245116 (2018).

## **Spatio-temporal solitary and traveling wave solutions to the Kundu–Mukherjee–Naskar equation**

Nikola Zoran Petrović<sup>1</sup>

<sup>1</sup>*Institute of Physics, Belgrade, Serbia*

e-mail:nzpetr@ipb.ac.rs

Kundu-Mukherjee-Naskar (KMN) equation [1] is an important variant of the (2+1)-dimensional Nonlinear Schrödinger equation for which the transverse Laplacian is replaced with a mixed partial derivative and the derivative with respect to only one of the transverse directions is present in the nonlinear term, thus breaking the symmetry between the two transverse directions. The primary motivation for the development of the KMN equation was to study soliton pulses in (2+1)-dimensions [2]. The KMN equation admits soliton and breather solutions and, due to an infinite number of conserved quantities which can be established through Lax formalism, it can be established that the equation is integrable [1]. Various methods can be used to find exact solutions to the equation, including the extended trial function method [2], the semi-inverse method [3] and the new extended algebraic expansion method [4].

In this work, we generalize the Jacobi Elliptic function expansion method, developed in [5] and [6], to find exact solutions to the KMN equation. An ansatz which takes into account all asymmetries is considered. One obtains both solitary and travelling wave solutions to the KMN equation, both with and without chirp, which to the best of our knowledge was not considered in any of the previous papers. Chirp is, however, only present in the perpendicular direction to the direction of the derivative in the nonlinear term. These solutions could potentially have many practical applications in the continued study of rogue waves [1].

### REFERENCES

- [1] A. Kundu, A. Mukherjee and T. Naskar, Proc. R. Soc. A. 47020130576 (2014)
- [2] M. Ekici et. al., Chinese J. of Phys. 57, 72 (2019)
- [3] J. He, Res. In Phys. 17, 103031 (2020)
- [4] A. Jhangeer, Res. in Phys. 16, 102816 (2020)
- [5] M. Belić, N. Z. Petrović, et. al., Phys. Rev. Lett. 101, 123904 (2008).
- [6] N. Z. Petrović et. al., Opt. Lett. 34, 1609 (2009)

## Active multi-core fibers – photonic platform for development of a topological charge switching device

P. P. Beličev<sup>1</sup>, G. Gligorić<sup>1</sup>, A. Maluckov<sup>1</sup>, Lj. Hadžievski<sup>1</sup> and S. Turitsyn<sup>2,3</sup>

<sup>1</sup>*PSTAR Group, "VINČA" Institute of Nuclear Sciences, National Institute of the Republic of Serbia, University of Belgrade, P. O. B. 522, 11001 Belgrade, Serbia*

<sup>2</sup>*Aston Institute of Photonic Technologies, Aston University, Birmingham, B4 7ET, UK*

<sup>3</sup>*Aston-NSU Centre for Photonics, Novosibirsk State University, Novosibirsk 630090, Russia*

e-mail:petrab@vin.bg.ac.rs

The multi-core fiber (MCF) is a physical system of high practical importance. In addition to standard exploitation, the MCFs may support discrete vortices that carry orbital angular momentum suitable for spatial-division-multiplexing in high capacity fiber-optic communication systems which may also be attractive for applications in high power lasers. Up to now, the main concern of our study has been related to optimization of the conditions capable to ensure transfer of high coherent light through the MCFs [1]. Regarding this we firstly proved the possibility of nonlinearity managed propagation of highly coherent vortices carrying huge power through the passive circular MCFs, which consist of small number of periphery cores. The central core has been shown to play the role of optional switch/gate of coherent light transfer [1]. In addition, the effects of the presence of central core and material loss/gain of all cores on the linear MCF system eigenvalue commensurability conditions have shown significant impact on the coherent planar and vortex mode dynamics [2]. All these findings stimulated the investigation of possibility to amplify the power transferred through the MCF via vortex carriers by inducing effects of the saturable gain and non-saturable loss in the periphery and/or central cores [3].

We numerically consider three cases of active circular MCFs. In the first case active were only periphery cores. Secondly, we investigated response of the system with only central core active, while the last case included all cores to be active. The light propagation is modeled by the generalized nonlinear difference-differential Schrödinger equations with complex coefficients and saturable gain [3]. Results for MCF with 4, 5 and 6 periphery cores have shown that the active periphery is the most promising candidate for topological charge switch of vortices carrying high powers [4]. In this specific operating regime, MCF provides change of the vortex topological charge value, i.e. transition between different vortex states. Moreover, presented system supports topological charge switch function between non-counterpart vortices by proper tailoring the ratio between gain and loss in periphery. The key condition for this phenomenon is existence of the central core which appears to play role of mode dynamics moderator. Being the ‘singular phase’ point of vortex, the central core which only passively takes part in tunneling energy towards the periphery cores, can support the coherent light amplification through the MCF.

On the top of this, presented system shows to be a promising platform for practical realization of devices covering range of multiple functions in applications: from high-power fiber lasers to coherent beam combiners and selective carriers of vortex beams.

### REFERENCES

- [1] Lj. Hadžievski, A. Maluckov, A. M. Rubenchik, S. Turitsyn, *Light Sci. Appl.* 4, e314 (2015).
- [2] A. Radosavljević, A. Daničić, J. Petrovic, A. Maluckov, Lj. Hadžievski, *JOSA B* 32, 2520 (2015).
- [3] S. K. Turitsyn, *Opt. Express* 17, 11898 (2009).
- [4] P. P. Beličev, G. Gligorić, A. Maluckov, Lj. Hadžievski, S. Turitsyn, accepted for publication in *Ann. Phys.* (2021).

## The nature, origin, and properties of the one- and two-dimensional optical rogue waves

S. Nikolic<sup>1,2</sup>, S. B. A. Alwashahi<sup>3</sup>, N. Aleksic<sup>4</sup>, O. A. Ashour<sup>5</sup>, S. A. Chin<sup>6</sup>, M. Belic<sup>2</sup>

<sup>1</sup>*Institute of Physics Belgrade, University of Belgrade, Serbia*

<sup>2</sup>*Science program, Texas A&M University at Qatar, Doha, Qatar*

<sup>3</sup>*Faculty of Physics, University of Belgrade, Serbia*

<sup>4</sup>*Moscow State Technological University "STANKIN", Moscow, Russia*

<sup>5</sup>*Department of Physics, University of California, Berkeley CA 94720, USA*

<sup>6</sup>*Department of Physics and Astronomy, Texas A&M University, College Station TX 77843, USA*

e-mail: stankon@ipb.ac.rs

The generating mechanism of optical rogue waves (RWs) is the modulation instability (MI). It is the nonlinear optical process in which a weak perturbation of the background pump wave produces an exponential growth of higher order sidebands that constructively interfere to build RWs. We produce RWs in numerical simulations of the cubic nonlinear Schrödinger equation, Hirota, and quintic equation with noisy (or other) inputs on the flat or elliptic background [1,2].

We discuss RWs strange nature, ingrained instability, dynamic generation, and potential applications. We propose the method of mode pruning for suppressing the modulation instability of rogue waves. We further demonstrate how to produce stable Talbot carpets (two dimensional patterns) of rogue waves.

We also present statistical analysis [3] on rogue waves produced by various numerical algorithms using white noise as initial conditions.

### REFERENCES

- [1] S. N. Nikolic, O. A. Ashour, N. B. Aleksic, M. R. Belic, S. A. Chin, *Nonlinear Dyn.* **95**, 2855 (2019).
- [2] S. N. Nikolic, O. A. Ashour, N. B. Aleksic, Y. Zhang, M. R. Belic, S. A. Chin, *Nonlinear Dyn.* **97**, 1215 (2019).
- [3] S. Toenger, T. Godin, C. Billet, F. Dias, M. Erkintalo, G. Genty, J. M. Dudley, *Sci. Rep.* **5**, 10380 (2015).

## Bright solitons under the influence of third-order dispersion and self-steepening effect

Zara Kasapeteva<sup>1,3</sup>, Aneliya Dakova<sup>1,2</sup>, Stefka Krasteva<sup>2</sup>, Valeri Slavchev<sup>1,4</sup>, Diana Dakova<sup>2</sup>, Lubomir Kovachev<sup>1</sup>, Anjan Biswas<sup>5,6,7</sup>

<sup>1</sup>*Institute of Electronics, Bulgarian Academy of Sciences, 72 Tzarigradsko shossee, 1784 Sofia, Bulgaria*

<sup>2</sup>*Physics and Technology Faculty, University of Plovdiv "Paisii Hilendarski", 24 Tsar Asen Str., 4000 Plovdiv, Bulgaria*

<sup>3</sup>*Faculty of Mechanical Engineering, Technical University of Sofia - Branch Plovdiv, 25 Tsanko Diustabanov St, 4000 Plovdiv, Bulgaria*

<sup>4</sup>*Faculty of Pharmacy, Medical University - Plovdiv, 15 Vasil Aprilov Bul., 4002 Plovdiv, Bulgaria*

<sup>5</sup>*Department of Applied Mathematics, National Research Nuclear University, 31 Kashirskoe Hwy, Moscow–115409, Russian Federation*

<sup>6</sup>*Mathematical Modeling and Applied Computation (MMAC) Research Group, Department of Mathematics, King Abdulaziz University, Jeddah–21589, Saudi Arabia*

<sup>7</sup>*Department of Mathematics and Applied Mathematics, Sefako Makgatho Health Sciences University, Medunsa–0204, Pretoria, South Africa*

e-mail: [zarra\\_andreeva@abv.bg](mailto:zarra_andreeva@abv.bg)

The evolution of broad-band laser pulses in nonlinear dispersive media, such as one-dimensional and planar waveguides, attracts a considerable attention in last decades. The well-known nonlinear Schrodinger equation (NSE) is one of the most commonly used in optics to describe the propagation of narrow-band light pulses, but in the frames of ultrashort optics, it is necessary to use the more general nonlinear amplitude equation (NAE). NAE works very well for nanosecond and picosecond as well as attosecond and femtosecond optical pulses. The influence of higher orders of dispersion and nonlinearity of the medium becomes significant for broad-band laser pulses. As a result it is needed to include additional terms in NAE that govern these effects.

In the present work the propagation of bright solitons under the influence of third-order dispersion and self-steepening effect in single-mode fibers is analytically and numerically studied. Such optical pulses can be observed as a result of the dynamic balance between higher orders of dispersive and nonlinear phenomena. New analytical soliton solution of NAE in the form of cnoidal wave is found. The solution is presented by Jacobi elliptic delta function. It is shown that at certain values of the parameter  $\kappa$  the solution can be reduced to *sech*-soliton.

Obtained results are important for better understanding of the propagation of bright optical solitons in nonlinear dispersive media under the influence of third order of linear dispersion and self-steepening effect and they can be used in telecommunications technology for signal transmission across long distances.

**Key words:** nonlinear amplitude equation, optical solitons, cnoidal waves

### ACKNOWLEDGMENTS

The present work is funded by Bulgarian National Science Fund by grant KP-06-M48/1.

### **3. Optical materials**

## Narrowing of laser beam propagating through biological suspension

A. Kovacevic<sup>1</sup>, T. Pajic<sup>2</sup>, D. Pavlovic<sup>1</sup>, M. Stanic<sup>3</sup>, M. Lekic<sup>1</sup>, S. Nikolic<sup>1</sup>, B. Jelenkovic<sup>1</sup>

<sup>1</sup> *Institute of Physics Belgrade, University of Belgrade, Pregrevica 118, 11080 Belgrade, Serbia*

<sup>2</sup> *Faculty of Biology, University of Belgrade, Studentski trg 16, 11000 Belgrade, Serbia*

<sup>3</sup> *Institute for Multidisciplinary Research, University of Belgrade, Bulevar Despota Stefana 142, 11060 Belgrade, Serbia*

e-mail:aleksander.kovacevic@ipb.ac.rs

Recent demonstration of nonlinear self-action of laser beams in suspension of biological materials, like marine bacteria and red blood cells, has been reported [1-3]. In this work, we demonstrate nonlinear optical effects of laser beam propagation through the freshwater green microalga *Chlorella sorokiniana*, cultivated in Bold basal medium with 3-fold nitrogen and vitamins (3N-BBM+V).

*Chlorella sorokiniana* is a species of single-celled freshwater green microalga in the division *Chlorophyta*. Its spherical or ellipsoidal cells (3 x 2  $\mu\text{m}$  in small cells to 4.5 x 3.5  $\mu\text{m}$  in large cells, sometimes >5  $\mu\text{m}$ ) divide rapidly to produce four new cells every 17 to 24 hours [4]. The non-pathogenic species has been chosen as a model organism due to its small cell dimension, rapid growth, non-mobility and non-toxicity. The algae were kept in the light chamber and the temperature was maintained at 22°C. Mid-exponential growth phase of algal culture was used for the experiments.

In the experiments, the 532 nm CW laser beam is directed to the glass cuvette that is filled either with the medium or with algae suspended in the medium. We have monitored the laser beam diameter at the entrance and exit of the cuvette, and its axial profile through entire cell length. The concentration has been determined by optical microscopy and optical density and has been varied between  $10^6$  and  $10^8$   $\text{cm}^{-3}$ .

The concentration of the algae and the laser beam power affect the beam radius. Our preliminary results have shown the effect of light self-trapping, i.e., the decrease of laser diameter when the algae concentration exceeds  $10^6$   $\text{cm}^{-3}$  while laser power is above 1 W. The difference of the refractive indexes of the algae and the medium can induce optical trapping of algae, which subsequently changes the concentration of the algae within the laser beam. This in turn can explain different behavior of the beam in the medium with and without algae.

We discuss the mechanisms which led to narrowing of the beam including nonlinear effects as well as potential applications in waveguiding, medical imaging and optimal propagation of laser beam in biological suspensions.

**Acknowledgments.** The authors appreciate valuable and helpful comments of Dr. Najdan Aleksic from the Moscow State Technological University “STANKIN”.

### REFERENCES

- [1] A. Bezryadina, T. Hansson, R. Gautam, et al. *Phys. Rev Lett.* 119, 058101 (2017).
- [2] R. Gautam, Y. Xiang, J. Lamstein, et al., *Light: Sci. Appl.* 8, 31 (2019).
- [3] R. Gautam, A. Bezryadina, Y. Xiang, et al., *Adv. Phys.* X 5 (2020), doi: 10.1080/23746149.2020.1778526.
- [4] I. Shihira, R. W. Krauss. *Chlorella*. Physiology and taxonomy of forty-one isolates, pp.1-97. Maryland: University of Maryland, College Park (1965).

## 2D silver-bismuth-iodide rudorffitenanomaterials for photovoltaic devices: a novel route for chemical synthesis of $\text{Ag}_3\text{BiI}_6$ nanosheets

Danijela Danilović<sup>1\*</sup>, Dušan K. Božanić<sup>1</sup>, Aleksandar R. Milosavljević<sup>2</sup>, Radovan Dojčilović<sup>1</sup>, Dragana Tošić<sup>1</sup>, Vladimir Djoković<sup>1</sup>, Pitambar Sapkota<sup>3</sup>, Sylwia Ptasinska<sup>3</sup>, Nenad Vukmirović<sup>4</sup>

<sup>1</sup>Vinca Institute of Nuclear Sciences, University of Belgrade, P.O. Box 522, 11001 Belgrade, Serbia

<sup>2</sup>Synchrotron SOLEIL, l'Orme des Merisiers, St. Aubin, BP48, 91192 Gif sur Yvette Cedex, France

<sup>3</sup>Radiation Laboratory and Department of Physics, University of Notre Dame, Notre Dame, Indiana 46556, United States

<sup>4</sup>Institute of Physics Belgrade, University of Belgrade, Pregrevica 118, 11080 Belgrade, Serbia

e-mail: [danijeladanilovic92@gmail.com](mailto:danijeladanilovic92@gmail.com)

Silver-bismuth-iodide (Ag-Bi-I) rudorffite hybrid materials have gained an immense interest in the research for a lead-free, chemically stable and low-cost absorber material in photovoltaic devices [1]. These materials can be fabricated in the form of macroscopic crystals or as thin films, in which case they can be integrated into solar cells that show good photoconversion efficiency [2]. Fabricating Ag-Bi-I in nanocrystal form could facilitate further their integration in the photovoltaic devices and enhance device performance due to size confinement effects. In our previous study, we successfully fabricated ligand-free  $\text{Ag}_3\text{BiI}_6$  nanoparticles in the form of aerosols [3]. Here, we report on the fabrication procedure of 2D Ag-Bi-I nanomaterials in the colloidal form. The results of the structural and morphological investigation of the nanosheets will be presented, as well as reconstruction of the electronic levels of the  $\text{Ag}_3\text{BiI}_6$  nanoparticles from the combined UV-vis absorption and X-ray photoelectron spectroscopy data. In addition, an analysis that shows the relation between the positions of the bands in the  $\text{Ag}_3\text{BiI}_6$  nanosheet absorption spectra and the thickness of the nanosheet will be discussed.

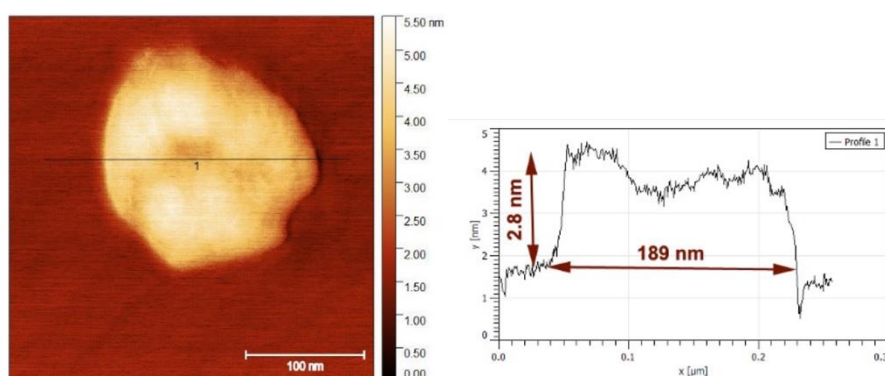


Figure 1. AFM image (left) and corresponding height profile (right) of Ag-Bi-I nanosheets

### REFERENCES

- [1] Kim, Y., Yang, Z., Jain, A., Voznyy, O... *Angew Chem. Int. Ed.* **55**, 9586 (2016).
- [2] Turkevych, I., Kazaoui, S., Ito, E... *ChemSusChem* **10**, 3754 (2017).
- [3] Danilović, D., Božanić, D. K., Dojčilović... *J. Phys. Chem. C* **124**, 23930 (2020).

## Influence of boundary conditions on electronic and transport properties in monolayer low – buckled HgTe nanoribbons

D. B. Topalović<sup>1</sup>, V. V. Arsoški<sup>2</sup>, M. Ž. Tadić<sup>2</sup>, M. Radenković<sup>1</sup>, P. Božović<sup>1</sup>, and F. M. Peeters<sup>3</sup>

<sup>1</sup>*Vinča Institute of Nuclear Sciences, University of Belgrade,  
P. O. Box 522, 11001 Belgrade, Serbia*

<sup>2</sup>*School of Electrical Engineering, University of Belgrade,  
P.O. Box 35 – 54, 11120 Belgrade, Serbia*

<sup>3</sup>*Department of Physics, University of Antwerp,  
Groenenborgerlaan 171, B – 2020 Antwerp, Belgium  
e-mail:dusan.topalovic@vin.bg.ac.rs*

HgTe is a II-VI compound semi-metal with inverted band ordering, low effective mass and high electron mobility [1]. Nanostructures based on this compound are intensively studied due to their specific topological properties [2]. In HgTe based nanostructures an inversion in the band ordering is accompanied by a quantum phase transition from a normal insulator to the phase of a nontrivial two-dimensional (2D) topological insulator or the Quantum Spin Hall insulator [3]. A good dynamic stability of HgTe monolayer is predicted from first-principles methods [4], which opened the possibility to use this material in thin-layer electronic devices. Even before these theoretical findings, HgTe nanoribbons have been experimentally realized [5], and a topological field effect quantum transistor was proposed [6].

We investigate the electronic and transport properties of low-buckled 2D HgTe zig-zag and armchair nanoribbons. Modeling of electronic states was performed by using a single-particle tight-binding model in the nearest-neighbour approximation [7]. The  $sp^3d^5s^*$  basis set in the Slater-Koster notation was used. The spin-orbit interaction was included in the model by using the Chadi formalism [8].

We found specific edge states in the range of energies that define the fundamental band gap of 2D HgTe monolayer. Moreover, we show that the electronic and transport properties of these states depend strongly on nanoribbon width and type of edge, and we demonstrate how external fields can be employed to control them.

### REFERENCES

- [1] E.O. Melezhik, J. V. Gumenjuk – Sichevska, and F. F. Sizov, SpringerPlus. 5, 80 (2016).
- [2] D. B. Topalović, V. V. Arsoški, M. Ž. Tadić, and F. M. Peeters, Phys. Rev. B 100, 125304 (2019).
- [3] B. A. Bernevig, T. L. Hughes, S. C. Zhang, Science 314, 1757 (2006).
- [4] H. Zheng, X. B. Li, N. K. Chen, S. Y. Xie, W. Q. Tian, Y. Chen, H. Xia, S. B. Zhang, and H. B. Sun, Phys. Rev. B 92, 115307 (2015).
- [5] F. S. Sangsefidi, N. Mir, and M. Salavati-Niasari, Mat. Sci. Semicon. Proc. 27, 500 (2014).
- [6] H. H. Fu, J. H. Gao, and K. L. Yao, Nanotechnology 25, 225201 (2014).
- [7] G. Allan and C. Delerue, Phys. Rev. B 86, 165437 (2012).
- [8] D. J. Chadi, Phys. Rev. B 16, 790 (1977).

## Structural and Optical Characterization of titanium-carbide and polymethyl methacrylate based nanocomposite

J. Pešić<sup>1</sup>, A. Šolajić<sup>1</sup>, J. Mitrić<sup>1</sup>, M. Gilić<sup>1</sup>, I. Pešić<sup>2</sup>, N. Paunović<sup>1</sup>, N. Romčević<sup>1</sup>

<sup>1</sup>*Institute of Physics Belgrade, University of Belgrade,  
Pregrevica 118, 11080 Belgrade, Serbia;*

<sup>2</sup>*Faculty of Technology and Metallurgy, University of Belgrade,  
11000 Belgrade, Serbia*

e-mail: yelena@ipb.ac.rs

The rich chemistries and unique morphologies of titanium carbide MXenes made them strong candidates for many applications like sensors and electronic device materials [1]. They can potentially be used as additives to polymers to fabricate composites with outstanding mechanical properties and good electrical conductivities. Presence of titanium-dioxide as a residue of MXene chemical synthesis is researched for its potential benefit on electrochemical properties [2].

In this study we present structural and optical characterization of such polymer nanocomposite titaniumcarbide/PMMA (Polymethyl methacrylate) consisting of  $Ti_3C_2$ ,  $TiC_2$  MXenes and  $TiC$ , and  $TiO_2$  residues of synthesis in PMMA matrix, as a multicomponent nanocomposite. Using XRD, SEM, infrared and Raman spectroscopy, followed by comparative study on the vibrational properties using density functional theory calculations we characterize this nanocomposite.

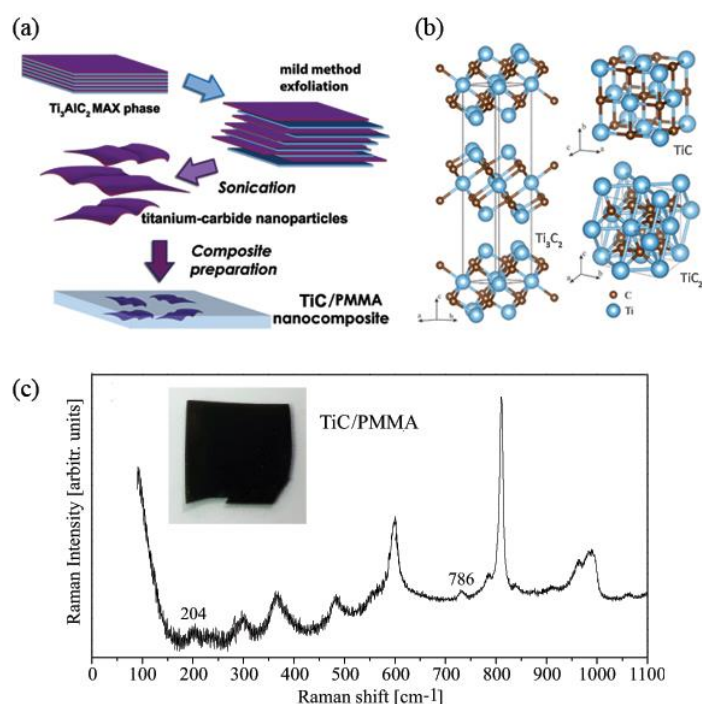


Figure 1. a) Schematic describing the synthesis process and preparation of composite starting from the  $Ti_3AlC_2$  MAX phase b) Schematic representation of titanium-carbide structures present at the composite c) Raman spectrum of  $TiC/PMMA$  nanocomposite with titanium-carbide related peaks marked. Inset: photo of the sample.

### REFERENCES

- [1] Naguib, M.; Kurtoglu, M.; Presser, V.; Lu, J.; Niu, J.; Heon, M.; Hultman, L.; Gogotsi, Y.; Barsoum, M.W., *Advanced Materials* 2011, 23, 4248–4253.  
 [2] Zhu, J.; Tang, Y.; Yang, C.; Wang, F.; Cao, M., *Journal of The Electrochemical Society* 2016, 163, A785–A791.

## Nickel vertical posts: Influence of thickness on magnetic and optical properties

J. Potočnik, M. Popović

*“Vinča” Institute of Nuclear Sciences – National Institute of the Republic of Serbia, University of Belgrade, Belgrade, Serbia*

e-mail: [jpotochnik@vin.bg.ac.rs](mailto:jpotochnik@vin.bg.ac.rs)

In the present study we have investigated the influence of the nickel (Ni) thin films thicknesses on their structural, magnetic and optical properties. Nickel vertical posts were deposited by Glancing Angle Deposition technique, at the angle of  $85^\circ$ . The films were grown to the thicknesses of 50 nm, 80 nm, 110 nm and 140 nm onto the glass slide substrates, which were rotated at the constant rate during the deposition process.

After the deposition, the samples were characterized by Scanning Electron Microscopy (SEM) and it was found that the thin films are porous and that the diameter of the columns increases from 18 nm to 29 nm with increasing thickness. X-ray photoelectron spectroscopy was used in order to determine the chemical composition of the samples, as well as the identification of the compounds present in the deposited thin films. It was shown that the metallic Ni is the dominant component, while the deconvolution of the oxygen line revealed the presence of NiO and Ni(OH)<sub>2</sub>.

Magnetic measurements of Ni thin films were accomplished by Magneto-Optical Kerr effect Microscope at room temperature. Based on the obtained results it can be seen that the deposited nickel samples possess uniaxial magnetic anisotropy. Also, it was noticed that the coercivity increases with thickness up to 150 Oe, for the 110 nm thick sample and then decreases to the value of 115 Oe. For thinner films, magnetic properties are mainly affected by the diameter of the columns, while for the thicker samples, the mechanism of the column growth determines their characteristics.

Optical and electrical properties of nanostructured nickel thin films were investigated by spectroscopic ellipsometry and four-point probe, respectively. According to the ellipsometric measurements it was found that as the thickness of the deposited samples increases plasma frequency ( $\omega_p$ ) also increases, and the damping factor ( $\Gamma_d$ ) decreases. An increase in the plasma frequency means that the density of conducting electrons is higher for the thicker samples, while the decrease in  $\Gamma_d$  indicates their better structural arrangement and lower concentration of defects. From the ellipsometric measurements, also, was observed the decrease of the refractive index values with increasing the film thickness, which is due to the lower optical density of the samples. Besides, higher values of the column width of the thicker Ni films lead to the reduced scattering of the conduction electrons at their boundaries and consequently increase both conductivity and extinction coefficient. Indeed, four-point probe measurements revealed that the electrical resistivity decreases from  $4.98 \times 10^2 \mu\Omega\text{cm}$  to  $0.44 \times 10^2 \mu\Omega\text{cm}$ , with increase film thickness from 50 nm to 140 nm. Lower values of electrical resistivity are probably due to the larger column diameter and lower defects density, as a result of column connecting during the film growth.

## Consideration and definition of optical phenomena and properties of ultrathin crystalline films

N.R. Vojnović<sup>1</sup>, A.J. Šetrajčić-Tomić<sup>2</sup>, S.M. Vučenović<sup>3</sup>,  
I.J. Šetrajčić<sup>1</sup>, S.K. Jaćimovski<sup>4</sup> and J.P. Šetrajčić<sup>2</sup>

<sup>1</sup>*University of Novi Sad, Faculty of Technical Sciences, Novi Sad, Vojvodina – Serbia*

<sup>2</sup>*Academy of Sciences and Arts of the Republic of Srpska, Banja Luka, Bosnia and Herzegovina*

<sup>3</sup>*University of Banja Luka, Faculty of Natural Sciences and Mathematics,  
Banja Luka, Republic of Srpska – Bosnia and Herzegovina*

<sup>4</sup>*University of Criminal Investigation and Police Studies, Zemun – Belgrade, Serbia*

e-mail: [jovan.setrajcic@gmail.com](mailto:jovan.setrajcic@gmail.com)

Today it is very well known and quite clear that the properties of nano-dimensional structures can differ significantly from the same structures of bulk dimensions [1]. What is still a mystery is how to produce purposefully the nanostructures of precisely defined properties, in other words an adequate solution is still being sought to the question which conditions or parameters affect the change of physical properties and to what extent [2].

In this paper the theory of all optical phenomena (refraction, reflection, absorption and transparency) is presented in ultrathin crystal films along the direction in which the film of nanoscopic dimensions is observed. The method of Green's functions and the Kramers-Kronig relation [3] were used to define the indices of refraction, reflection, absorption and transparency. As these indices depend on the position of the crystallographic plane where optical phenomena occur in relation to two boundary planes [4], and in the experiment these values can be seen/measured/determined only for the total film, the question arises as to how to define such values of optical indices. This is exactly what has been done in this paper.

The results of these analyses were applied to a four-layered ultrathin molecular film in two cases: when the boundary planes of the film are free (without environmental influences) and when they are symmetrically perturbed. For the selected models, it has been shown that the effects of dimensional quantization and quantum size effect have a significantly greater impact on the change of optical properties than other boundary – confinement parameters. However, it should be noted that there is a very interesting result that may occur. It is possible that mono-absorption and enormous transparency may occur in the IR region in which such bulk crystals are absolute absorbers.

### REFERENCES

- [1] M. Fox, *Optical Properties of Solids* (2 ed.), ISBN 978-0199573370, Oxford University Press, Oxford 2010, p. 44-46.
- [2] G. Cao, Y. Wang, *Nanostructures and Nanomaterials: Synthesis, Properties, and Applications* (2 ed.), World Scientific Series in Nanoscience and Nanotechnology: Vol. 2, pages 596; doi: 10.1142/7885, 2011.
- [3] M. Fox, *Optical Properties of Solids* (2 ed.). ISBN 978-0199573370, Oxford University Press, Oxford 2010, p. 44-46.
- [4] A.J. Šetrajčić-Tomić, M. Vojnović, J.P. Šetrajčić, S.M. Vučenović, N.R. Vojnović, *Opt. Quant. Electron.* 52, 251 [1-18] (2020); doi: 10.1007/s11082-020-02371-z.

## Nanoscopy of van der Waals heterostructures fabricated by the wet transfer method

J. Obradović<sup>1</sup>, S. Aškračić<sup>2</sup>, D. Čapeta<sup>3</sup>, U. Ralević<sup>2</sup>

<sup>1</sup>*School of Electrical Engineering, University of Belgrade, Serbia*

<sup>2</sup>*Institute of Physics Belgrade, University of Belgrade, Serbia*

<sup>3</sup>*Center for Excellence for Advanced Materials and Sensing Devices, Institute of Physics, Zagreb, Croatia*  
e-mail: uros@ipb.ac.rs

Two dimensional crystals have been in the focus of the scientific research for almost two decades, since the discovery of their first representative, graphene [1]. Among other properties which make these materials interesting for various applications ranging from tribology to optoelectronics, the possibility to combine them at will into vertical stacks, called van der Waals heterostructures (VdWhs), has opened the door to a world of new, equally interesting, and unique materials whose electronic and optical properties can be tailored by changing the VdWh constituents [1].

In this work we investigate VdWhs fabricated from 2D transition metal dichalcogenides ( $WS_2$  and  $MoS_2$ , in particular), which are considered to be strong candidates for various applications in the fields of optics and optoelectronics [2]. The fabrication of these heterostructures was done using a modified variant of the wet transfer method which has proven to be superior to the commonly used procedures in terms of its simplicity and quality of the produced VdWh [3]. The structural and optical properties of the VdWh fabricated by this method were thoroughly investigated by atomic force microscopy, Raman and photoluminescence spectroscopy. The analysis of the results obtained from the aforementioned characterization techniques shows that VdWh have low amount of surface contaminants, unmodified crystal structure, high and uniform photoluminescence intensity. The issue of interlayer contamination, which is inevitable due to the transfer procedure itself, was mitigated by low temperature annealing.

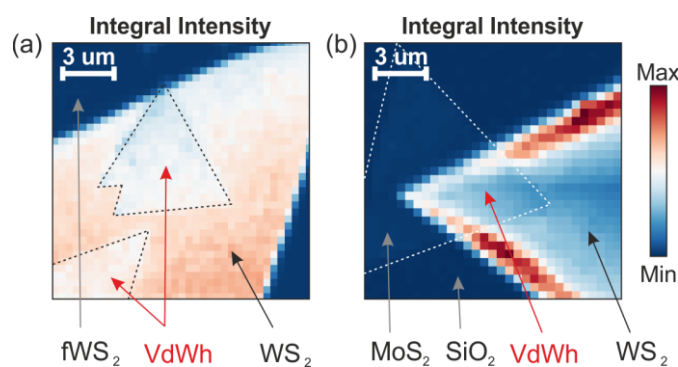


Figure 1. PL maps of  $MoS_2 / WS_2$  VdWh recorded for the VdWhs (a) in the center, (b) at the edge of the large  $WS_2$  monolayer.

### REFERENCES

- [1] K.S. Novoselov, A. Mishchenko, A. Carvalho, A. H. Castro Neto, Science 353, 9439 (2016)
- [2] Y. Liu, N. O. Weiss, X. Duan, H.-C. Cheng, Y. Huang, X. Duan, Nat.Rev.Mater. 1, 16042 (2016)
- [3] I. Niehues, A. Blob, T. Stiehm, R. Schmidt, V. Jadriško, B. Radatović, D. Čapeta, M. Kralj, S. M. de Vasconcellos, R. Bratschitsch, 2D Mater. 5, 031003(2018)

## Thulium-doped titanate-germanate glasses for infrared photonics

K. Kowalska<sup>1</sup>, M. Kuwik<sup>1</sup>, J. Pisarska<sup>1</sup> and W.A. Pisarski<sup>1</sup>

<sup>1</sup>University of Silesia, Institute of Chemistry, Katowice, Poland

e-mail: karolina.kowalska@us.edu.pl

Thulium-doped inorganic glasses have a great deal of attention due to their near-infrared emissions at about 1450 nm and 1800 nm, respectively. The near-infrared luminescence at 1450 nm corresponds to  $^3\text{H}_4 \rightarrow ^3\text{F}_4$  transition of  $\text{Tm}^{3+}$  ions [1] and it is really important for the S-band signal amplification [2]. The second luminescence line at 1800 nm related to the  $^3\text{F}_4 \rightarrow ^3\text{H}_6$  transition of  $\text{Tm}^{3+}$  ions is useful for near-infrared fiber laser applications [3]. The systematic studies indicate that the choice of both the glass-host and activator ( $\text{Tm}^{3+}$ ) concentration is very important to obtain excellent spectroscopic properties and to develop more efficient optical devices based on thulium ions. From literature data it is also well evident that titanium dioxide  $\text{TiO}_2$  has a positive effect on the 1800 nm fluorescence performance of tellurite glass, while the introduction of  $\text{GeO}_2$  has great advantages in enhancing the glass thermal stability [4].

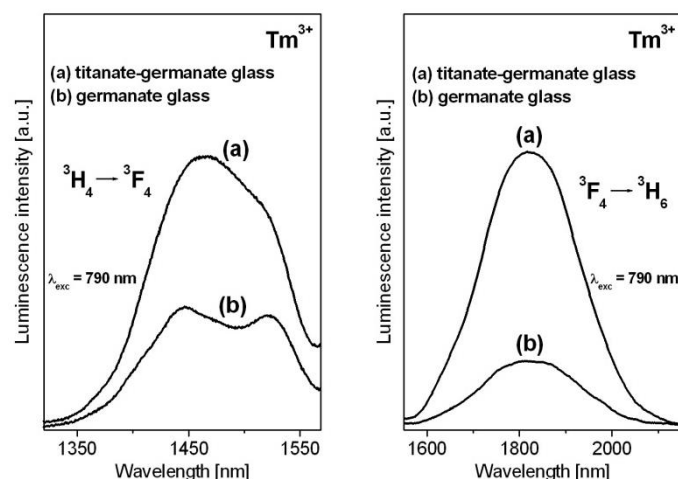


Figure 1. Near-infrared luminescence spectra of  $\text{Tm}^{3+}$  ions in titanate-germanate glass.

Here, we present our preliminary investigations for  $\text{TiO}_2$ -modified germanate glass doped with  $\text{Tm}^{3+}$ . Figure 1 shows two main emission bands at 1450 nm and 1800 nm corresponding to the  $^3\text{H}_4 \rightarrow ^3\text{F}_4$  and  $^3\text{F}_4 \rightarrow ^3\text{H}_6$  transitions of  $\text{Tm}^{3+}$  ions in germanate glass modified by  $\text{TiO}_2$ . In both cases, luminescence bands are enhanced significantly in the presence of  $\text{TiO}_2$ . It confirms our previous results obtained for europium ions in titanate-germanate glass, where orange-reddish emission was increased drastically in comparison to glass sample without  $\text{TiO}_2$  [5]. Our preliminary results suggest that titanate-germanate glass doped with thulium ions is promising candidate for potential near-infrared laser applications.

**Acknowledgment:** This research was funded by National Science Centre (Poland), grant number 2018/31/B/ST8/00166.

### REFERENCES

- [1] R. Balda, LM. Lacha, J. Fernandez, MA. Arriandiaga, JM. Fernandez-Navarro, D. Munoz-Martin, *Opt. Exp.* 16, 11836 (2008).
- [2] D.L. Yang, E.Y.B. Pun, H. Lin, *Appl. Phys. Lett.* 95, 151106 (2009).
- [3] X. Wen, G. Tang, J. Wang, X. Chen, Q. Qian, Z. Yang, *Opt. Exp.* 23, 7722 (2015).
- [4] W. Tang, Y. Tian, B. Li, Y. Xu, Q. Liu, J. Zhang, S. Xu, *Ceram. Int.* 45, 16411 (2019).
- [5] W.A. Pisarski, K. Kowalska, M. Kuwik, J. Polak, E. Pietrasik, T. Goryczka, J. Pisarska, *Materials* 13, 4422 (2020).

## Light-induced optical effects in phosphorus, nitrogen and boron doped diamonds

K. Boldyrev<sup>1</sup>

<sup>1</sup>*Institute of Spectroscopy of the Russian Academy of Sciences, Troitsk, Moscow, Russia*  
e-mail: kn.boldyrev@gmail.com

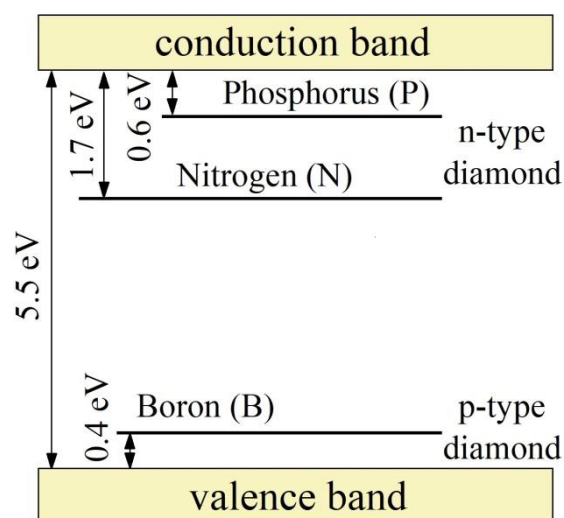
Diamond is a material with many unique properties suitable for the different applications from power electronics to quantum computing. It has an ultra-wide band gap (5.47 eV), high electron and hole mobility, high thermal conductivity, high reflectivity, transparency from RF to UV radiation, and has compelling potential advantages over the most known analogs, such as the narrow-bandgap silicon (Si), in radiation-resistant, high-power, and high-frequency electronics, as well as in deep-UV optoelectronics, synchrotron optics, quantum information, quantum sensing and extreme-environment applications [1]. As well a diamond is an excellent photoconductor, and this property can be used for UV detectors with ultra-high sensitivity [2]. It is known that p-type semiconducting diamond is synthesized by doping boron impurity. However, it used to be almost impossible to make n-type diamond. Phosphorus and nitrogen are impurities for n-type semiconducting diamond established at this moment. But nitrogen level is too deep in the bandgap for the applications (see figure), so phosphorus donor is the best candidate for the n-type diamond. P-donors in a diamond can be used for quantum computing, spin-to-photon conversion, photonic memory, integrated single-photon sources, and all-optical switches because of the read-in/read-out is in the optical region showing extremely high decoherence time up to hours [3]. Earlier studies of the photoconductivity of the phosphorus-doped diamond, which made it possible to register several electronic transitions near 600 meV [4]. These studies gave hope for the presence of photochromic effects in P-doped diamonds, by analogy with such effects in silicon [5]. In addition, based on such effects, it is possible to create a technique for the optical monitoring of the quality and concentration of doping [5,6].

In this work, we report the detail studies of the light-induced effects of the large-sized HPHT-grown high-quality P-, B- and N-doped single-crystal diamonds by the high-resolution spectroscopy. We found a significant light-induced effect on the electronic transitions of phosphorus and boron. A strong intensity measurement in the absorption spectra is observed under the influence of external optical radiation. In addition, there was a redistribution of intensities in the absorption region of boron and phosphorus, by analogy with the dopant of boron and phosphorus in silicon [5,6]. Based on this effect, a method is proposed for determining the real concentration of boron and phosphorus in a diamond.

A financial support by the Russian Science Foundation under Grant № 19-72-10132 is acknowledged.

### REFERENCES

- [1] J. Y. Tsao, S. Chowdhury, M. A. Hollis et al., *Adv. Electron. Mater.* **4**, 1600501 (2018).
- [2] F. Hochedez, W. Schmutz, Y. Stockman et al., *Adv. Space Res.* **37**(2), 303-312 (2006).
- [3] K. Saeedi, S. Simmons, J. Z. Salvail et al., *Science* **342**, 830 (2013).
- [4] K. Haenen, K. Meykens, M. Nesladek et al., *Phys. Stat. Sol. a* **181**, 11 (2000).
- [5] Test method for low temperature FT-IR analysis of single crystal silicon for III-V impurities SEMI MF 1630-0704 (2004).
- [6] K.N. Boldyrev, N.Yu. Boldyrev, R.V. Kirillin, *Bull. Russ. Acad. Sci. Phys.*, **77**(12), 1420 (2013).



## Effect of Au/Ag ion implantation and subsequent thermal annealing on optical properties of titanium nitride thin films

M. Popovic, M. Novakovic and V. Rajic

Department of atomic physics, Vinca Institute of Nuclear Sciences - National Institute of the Republic of Serbia, University of Belgrade, Serbia

e-mail:majap@vin.bg.ac.rs

The control of optical properties of titanium nitride is of great interest especially in the area of plasmonics where titanium nitride can successfully change and overcome most of the drawbacks of plasmonic metals [1,2]. In this study we have investigated the structural and optical changes of 260 nm thick TiN thin film induced by sequential implantation of 200 keV Au and 150 keV Ag ions. During implantation Au ion fluence was kept constant at  $1.0 \times 10^{16}$  ions/cm<sup>2</sup> while the silver ion fluence was varied from  $4.0 \times 10^{16}$  ions/cm<sup>2</sup> to  $13 \times 10^{16}$  ions/cm<sup>2</sup>. After implantation the films were annealed at 500°C, for 1 hour. The samples were analyzed by means of X-ray diffraction and spectroscopic ellipsometry measurements. The changes in dielectric function spectra of TiN induced by Au/Ag ion implantation and post-implantation annealing were analyzed and discussed in detail. The parameters of the fit including screened and unscreened plasma frequency as well as Drude broadening were studied with respect to the ion fluences and annealing temperature, and they were correlated with the structural changes of TiN. It was found that the real part of dielectric constant becomes less negative after implantation (Fig. 1a). Simultaneously, imaginary part decreases meaning that the titanium nitride possesses lower optical losses after implantation (Fig. 1b). Besides this, the overall metallic character of titanium nitride in the visible and near infrared region is retained. Further, we have demonstrated that subsequent annealing at 500°C continues to change the both real and imaginary part of dielectric constant in the same direction as in the case of ion implantation, thus leaving the films with much lower optical losses. Our findings suggest that the optical properties of the TiN films can be tailored by varying the ion fluence of incident metal ions as well as by post-implantation annealing processing.

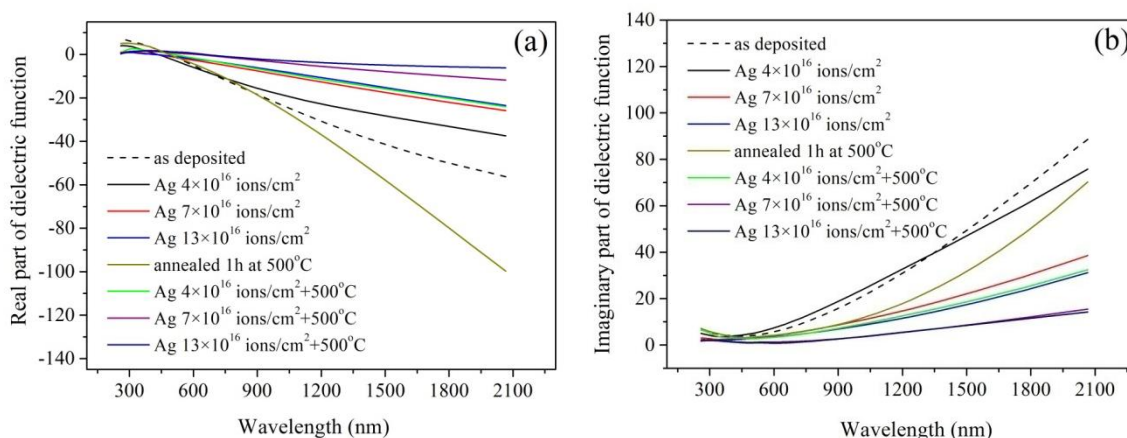


Figure 1. The real (a) and imaginary (b) part of dielectric function of as deposited, Au/Ag sequentially implanted and post-annealed TiN films. Au ion fluence was kept constant at  $1.0 \times 10^{16}$  ions/cm<sup>2</sup> whereas the silver ion fluence was varied; various colors correspond to different silver ion fluencies as indicated in the legend.

### REFERENCES

- [1] K.C. Maurya, V.M. Shalaev, A. Boltasseva, B. Saha, Opt. Mater. Express, 10, 2679 (2020).
- [2] C.C. Chang, J. Nogan, Z.P. Yang, W.J.M. Kort-Kamp, W. Ross, T.S. Luk, D.A.R. Dalvit, A.K. Azad, and H.T. Chen, Sci. Rep. 9(1), 1 (2019).

## **Influence of the protective layer on the photoacoustic response of transparent samples**

**M.N.Popovic<sup>1</sup>, M.V.Nesic<sup>1</sup>, S.P.Galovic<sup>1</sup>, K.Lj.Djordjevic<sup>2</sup>, D.D.Markushev<sup>3</sup>**

<sup>1</sup>*Vinca Institute of Nuclear Sciences – National institute of the Republic of Serbia, University of Belgrade*

<sup>2</sup>*Faculty of Physics, University of Belgrade*

<sup>3</sup>*Institute of Physics – National institute of the Republic of Serbia, University of Belgrade*

e-mail:maricap@vin.bg.ac.rs

In the transmission photoacoustic measurements of transparent samples, using minimum volume cell configuration, a thin protective layer is applied on one surface of the examined samples in order to protect the microphone. The influence of this layer on the recorded photoacoustic response is examined. In this paper, the models of photoacoustic (PA) response for transmission PA setup configurations of two-layered optically transparent samples with thermal memory are analyzed. When the protective layer is illuminated, its influence is significant at high modulation frequencies and it has to be considered in the analysis of the recorded signal. When the layer is not illuminated, its influence is lost.

### REFERENCES

- [1] J. Medina, Yu. G. Gurevich, G. N. Logovinov, P. Rodriguez and G. Gonzalez de la Cruz, *Molecular Physics* 100, 3133-3138 (2002).
- [2] A. M. Mansanares, H. Vargas, F. Galembeck, J. Buijs, D. Bicanic, *J. Appl. Phys.* 70, 7046-7050 (1991).
- [3] S. Galović, D. Kostoski, *J. Appl. Phys.* 93, 3063-3071 (2003).
- [4] M.N. Popovic, D.D. Markushev, M.V. Nesic, M.I. Jordovic-Pavlovic, S.P. Galovic, *J. Appl. Phys.* 129(1):015104 (2021).
- [5] M.N. Popovic, M.V. Nesic, M. Zivanov, D.D. Markushev, S.P. Galovic, *Optical and Quantum Electronics*, 50, 330 (2018)

## Plasma-assisted nitrogen doping of Langmuir-Blodgett self-assembled graphene films

T. Tomasević-Ilić<sup>1</sup>, N. Škoro<sup>1</sup>, N. Puač<sup>1</sup>, M. Spasenović<sup>2</sup>

<sup>1</sup>*Institute of Physics Belgrade, University of Belgrade, Pregrevica 118, 11080 Belgrade, Serbia*

<sup>2</sup>*Center for Microelectronic Technologies, Institute of Chemistry, Technology and Metallurgy, University of Belgrade, Njegoševa 12, 11000 Belgrade, Serbia*  
e-mail:ttijana@ipb.ac.rs

Application of highly transparent films obtained by self-organization of graphene flakes in optoelectronic devices seeks for appropriate surface modification/functionalization, which will adapt their electrical properties to the requirements of the electronic industry. Doping with nitrogen is one of the most promising methods to tailor the electronic properties of graphene [1]. Graphene films prepared from solution and deposited by Langmuir-Blodgett self-assembly (LBSA) [2, 3], were treated with radio-frequency (13.56 MHz) nitrogen plasma in order to investigate the influence of the time of nitrogen plasma exposure on the work function, sheet resistance and surface morphology of LBSA graphene films. Plasma treatments were performed in a chamber with plane-parallel electrode geometry with 5cm electrode gap and at 500 mTorr of N<sub>2</sub>. Tuning parameter in this work was treatment duration. Kelvin probe force microscopy (KPFM) and sheet resistance measurements confirm nitrogen functionalization of our films, with the Fermi level shifting in the direction that indicates binding to a pyridinic and/or pyrrolic site [4], as would be expected for LBSA graphene, where edges are the dominant defect type [5]. We show that by tuning exposure time, we can decrease sheet resistance by a factor of two, without affecting surface morphology. Upon 1 min of nitrogen plasma exposure, the sheet resistance decreases and there is no obvious difference in film morphology. However, plasma exposure longer than 5 min leads to removal of graphene flakes and degradation of graphene films, in turn affecting the flake connectivity and increasing film resistance. Controllability of the plasma technique has an advantage for graphene functionalization over conventional doping techniques such as chemical drop-casting. It allows to controllably tune the work function, surface morphology and sheet resistance of LBSA films, which is substantial for applications in various optoelectronic and electronic devices.

### REFERENCES

- [1] A. Dey, A. Choneos, N. St. J. Braithwaite, R. P. Gandhiraman, S. Krishnamurthy, *Appl. Phys. Rev.* 3, 021301 (2016)
- [2] A. Matković, et al., *2D Mater.* 3, 015002 (2016)
- [3] T. Tomašević-Ilić, J. Pešić, I. Milošević, J. Vujin, A. Matković, M. Spasenović, R. Gajić, *Opt. Quant. Electron.* 48, 319 (2016)
- [4] K. Akada, T. Terasawa, G. Imamura, S. Obata, K. Saiki, *Appl. Phys. Lett.* 104, 131602 (2014)
- [5] T. Tomašević-Ilić, Đ. Jovanović, I. Popov, R. Fandan, J. Pedrós, M. Spasenović, R. Gajić, *Appl. Surf. Sci.* 458, 446–453(2018)

## Enhanced photoluminescence of gamma-irradiated S, N graphene quantum dots

Mila Milenković, Duška Kleut and Svetlana Jovanović

*Vinca Institute of Nuclear Sciences, National Institute of the Republic of Serbia, University of Belgrade P.O.*

*Box 522, 11001 Belgrade, Serbia*

e-mail: mila.milenkovic@vin.bg.ac.rs

Zero-dimensional graphene quantum dots (GQDs) are one of the most promising luminescent carbon-derived nanomaterials with different oxygen-containing functional groups on their surface. They consist of one or few layers of graphene and have a lateral dimension below 100 nm. Some of their distinct and superior physical and chemical properties such as tunable photoluminescence, good biocompatibility, low toxicity, and excellent dispersibility in water, make them a promising candidate for biomedical applications [1]. With the functionalization of GQDs, it is possible to modify their surface structure by adding other functional groups thus altering photoluminescence and enhancing their other properties [2]. Gamma irradiation proved to be a simple and eco-friendly method for subsequent modification of carbon nanomaterials [3, 4].

Here, we present a simple, one-step method for functionalization of GQDs with gamma irradiation in the presence of amino acid L-cysteine as an S, N heteroatom donor and isopropyl alcohol as a radical scavenger. Water dispersion of GQDs with 1 vol% isopropyl alcohol and 2 mass% of L-cysteine was purged with Ar gas for 15 minutes and then exposed to gamma irradiation at doses: 25, 50 and 200 kGy. The optical and structural properties of obtained S, N-GQDs were investigated using Ultraviolet-visible spectroscopy (UV-Vis), Fourier-Transform Infrared spectroscopy (FTIR), Photoluminescence spectroscopy (PL), Atomic force microscopy (AFM) and Dynamic light scattering (DLS). Successful doping of S and N heteroatoms in the structure of irradiated GQDs was confirmed with FTIR analysis through detected S-H, C=S, and N-H stretching vibrations. Also, an improvement in photoluminescence quantum yield (QY) has been proved by PL measurements. The best result was achieved for the sample irradiated with a dose of 25 kGy. PL QY of this sample was 15 times higher compared to non-irradiated p-GQDs, and around 7 times higher up against other irradiated samples. Both AFM and DLS measurements were in correlation and indicated that gamma irradiation increased the layer separation and overall particle diameter of GQDs. The average diameter ranged from 25 nm up to around 30 nm for irradiated samples while the diameter of non-irradiated p-GQDs was 20 nm.

The proposed one-step chemical doping provided an improvement in one of the most characteristic features of GQDs- photoluminescence, as well as in morphological properties. Due to this, the obtained S, N-GQDs have great potential for application in medicine as a bioimaging agent.

**ACKNOWLEDGEMENT:** This work was financially supported by the Ministry of Education, Science and Technological Development of the Republic of Serbia (Grant No. 451-03-9/2021-14/200017).

### REFERENCES

- [1] S. Jovanovic, Handbook of Graphene Set, 267 (2019).
- [2] S. Zhu, et al., Nano Research 8 355 (2015).
- [3] A. Ansón-Casaos, et al., Applied Surface Science 301, 264 (2014).
- [4] S.P. Jovanović, et al., ACS Applied Materials & Interfaces 7, 25865 (2015).

## A cluster of bilayer diodes model for bulk heterojunction organic solar cells

M. Stanojevic<sup>1</sup>, J. Gojanovic<sup>1</sup> and S. Zivanovic<sup>2</sup>

<sup>1</sup>*School of Electrical Engineering, University of Belgrade, Serbia*

<sup>2</sup>*Institute for Micromanufacturing, Louisiana Tech University, USA*

e-mail: sm185019p@student.etf.bg.ac.rs

Organic solar cells (OSCs) possess unique properties such as a low cost, flexibility, lightweight, semitransparency, and compatibility with roll-to-roll fabrication, which make them potential candidates for mass production. The rise in their power conversion efficiency (PCE) over the last few years has been driven by the emergence of new organic semiconductors and the growing understanding of morphological control at both the molecular and aggregation scales resulting in 18% PCE for single junction OSCs [1, 2]. On the other hand, a basic physical concept that singles out dominant processes in these devices and quantifies them is still missing. The clarification of the device physics could open up an additional opportunity for a further PCE increase and the elimination of other shortcomings in OSCs.

The current-voltage (I-V) characteristic of OSCs is usually modeled by the standard drift-diffusion model (DDM) [3]. This model requires a numerical solution that makes it impossible to perceive the influence of individual processes (such as photogeneration, transport, recombination, contact phenomena, etc.) on the shape of the I-V curve. However, what is certain is that OSCs basically behave as photodiodes, implying that their work is based on the physics of heterojunctions. In a standard DDM, a bulk heterostructure active layer of an OSC is considered as a single semiconducting material, and the junction physics is not taken into account.

In this paper we present a new concept of treating the OSC bulk heterostructure as a cluster of spatially arbitrarily oriented small bilayer domains (bilayer diodes). The elementary bilayer domain is described by a one-diode model. The OSC I-V curve is calculated by summing the contributions of all bilayer domains. The resulting I-V dependence is the one-diode equation with parameters (the reverse saturation current and the ideality factor) related to the parameters of the elementary bilayer domain.

The one-diode parameters for the elementary bilayer domains are determined by fitting the one-diode equation to the measured I-V curve of bilayer ITO/PEDOT:PSS/P3HT:PCBM/Al solar cell. The I-V curves of ITO/PEDOT:PSS/P3HT:PCBM/Al bulk heterostructure solar cells with six different P3HT:PCBM thin film thicknesses are then simulated and compared to measured ones. The experimental data are successfully reproduced by the proposed model.

### REFERENCES

- [1] R. Gurney, D. Lidzey, T. Wang, Rep. Prog. Phys. 82, 036601 (2019)
- [2] Q. Liu, Y. Jiang, K. Jin, Science Bulletin 65, 272 (2020)
- [3] G. Li, L. Liu, F. Wei, IEEE Journal of Photovoltaics 2, 320 (2012)

## Influencing on optical properties of buffered TiO<sub>2</sub>-Au thin film systems by deposition and annealing parameters

N. Milicevic<sup>1</sup>, M. Novakovic<sup>1</sup>, J. Potocnik<sup>1</sup>, L. Rakocevic<sup>1</sup>, M. Milovic<sup>1</sup>, N. Abazovic<sup>1</sup> and D. Pjevic<sup>1</sup>

<sup>1</sup>Vinca Institute of Nuclear Sciences - National Institute of the Republic of Serbia, University of Belgrade, Belgrade, Serbia

e-mail: nemanja.milicevic@vin.bg.ac.rs

One of the ways to increase efficiency of TiO<sub>2</sub> thin films is by doping and coating with metals. Metal-doped TiO<sub>2</sub> can reduce electron-hole recombination and increase hydroxyl radical concentration on the surface of TiO<sub>2</sub>, resulting in increase in the photocatalytic activity. Recent studies of J. Li et al. [1] and S. Y. Lee et al. [2] with Au doped TiO<sub>2</sub> thin films showed that these systems have enhanced photocatalytic activity in comparison to pure TiO<sub>2</sub> thin films. Also, recent study [3] showed that Au-doped TiO<sub>2</sub> thin films are great candidates beside photocatalysis for enhancing visible light water splitting. TiO<sub>2</sub> and TiO<sub>2</sub>:Au thin films were obtained by DC magnetron sputtering of Ti target with Ar ions in O<sub>2</sub> atmosphere. In the case of doped TiO<sub>2</sub> thin films with Au, three different systems were deposited for comparison (Fig. 1). Post-deposition annealing for 3 h at 400 °C was carried out in nitrogen atmosphere. For structural analyses XRD, XPS, TEM and AFM methods were used, while for optical characterization UV/Vis method was used. The photo-degradation rate was measured using Rhodamine B which simulated pollutant. Analysis of the binding energy in the corresponding XPS spectra showed that deposited films have good stoichiometry of TiO<sub>2</sub> and that concentration of Au on the surface can be controlled by sputtering and annealing conditions. Post-deposition annealing caused diffusion of Au atoms through the layer as it was shown by TEM and EDS. Obtained TiO<sub>2</sub> thin films before deposition were amorphous-like structured, and after annealing at 400 °C showed that anatase phase dominates in the structure. All Au-doped TiO<sub>2</sub> thin films showed better photo-degradation rates than pure TiO<sub>2</sub>.

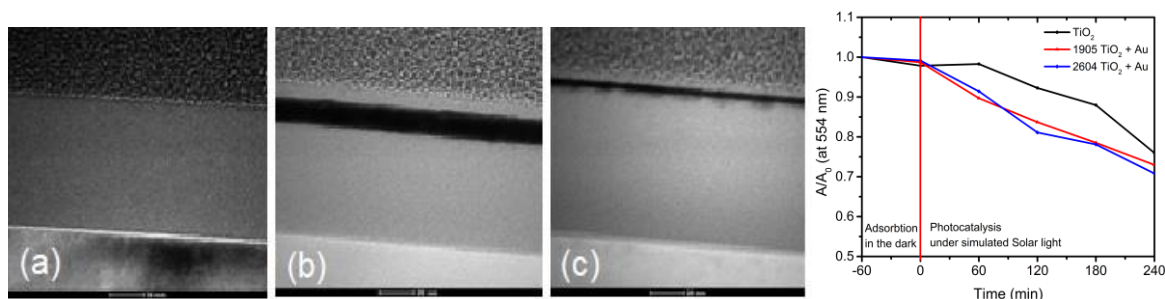


**Fig. 1.** TEM images of as-deposited TiO<sub>2</sub> and buffered TiO<sub>2</sub>-Au systems. **Fig. 2.** Photocatalytic measurement.

### REFERENCES

- [1] J. Li, Z. Chen, J. Fang, Q. Yang, X. Yang, W. Zhao, D. Zhou, X. Qian, C. Liu, J. Shao, Facile synthesis of TiO<sub>2</sub> film on glass for the photocatalytic removal of rhodamine b and tetracycline hydrochloride, *Mater. Express*. 9 (2019) 437–443.
- [2] S. Youl Lee, D. Kang, S. Jeong, H. Tung Do, J. Heon Kim, Photocatalytic Degradation of Rhodamine B Dye by TiO<sub>2</sub> and Gold Nanoparticles Supported on a Floating Porous Polydimethylsiloxane Sponge under Ultraviolet and Visible Light Irradiation, *Cite This ACS Omega*. 5 (2020) 4233–4241.
- [3] A. Sreedhar, I.N. Reddy, J.H. Kwon, J. Yi, Y. Sohn, J.S. Gwag, J.S. Noh, Charge carrier generation and control on plasmonic Au clusters functionalized TiO<sub>2</sub> thin films for enhanced visible light water splitting activity, *Ceram. Int.* 44 (2018) 18978–18986.

## Hard-templated porous Nb<sub>2</sub>O<sub>5</sub> thin films for chemiresistive VOC sensing

Y. Chorbadzhiyska<sup>1</sup>, V. Pavlov<sup>1</sup>, B. Georgieva<sup>1</sup>, R. Georgiev<sup>1\*</sup>,  
<sup>1</sup>*Institute of Optical Materials and Technologies “Acad. J. Malinowski”,  
Bulgarian Academy of Sciences, Acad. G. Bonchev str., bl. 109, 1113 Sofia, Bulgaria*

\*corresponding author’s e-mail address: [rgeorgiev@iomt.bas.bg](mailto:rgeorgiev@iomt.bas.bg)

Nb<sub>2</sub>O<sub>5</sub> is multifunctional material that is interesting for optical applications due to its high refractive index value in the visible region as well as for its chemical stability. The present study aims at investigation of possibility to use porous Nb<sub>2</sub>O<sub>5</sub> in form of thin films as an active medium for detection of organic vapours in air with optical read-out.

The porosity of the films has been generated by hard-template method, where SiO<sub>2</sub> has been used as a porosity-forming agent. The films have been deposited by combination of sol-gel and spin coating techniques. The optical properties of the films have been calculated by using UV-Vis spectroscopy and nonlinear curve fitting methods. The morphology of the films has been studied by Transmission Electron Microscopy (TEM) and the amorphous status of the films has been confirmed by Selected Area Electron Diffraction (SAED). By applying the Bruggeman effective medium approximation the porosity within the films is calculated. The films are then introduced in ambient of different organic vapors - acetone, methanol, and ethanol, etc. The condensed vapors in the films’ pores modify their optical response that has been recorded. The possibility of implementation of these films in optical structures such as Bragg stacks for volatile organic vapors sensing is modelled and discussed.

### **Acknowledgements:**

This research is funded by Bulgarian National Science Fund, Grant No. KP06-M48/26.11.2020

## Determination of refractive index of ultrathin dielectric films prepared via layer-by-layer polyelectrolyte deposition

S. Nedić<sup>1</sup>, S. Aškrabić<sup>1</sup>, B. Vasić<sup>1</sup> and G. Isić<sup>1</sup>

<sup>1</sup> Institute of Physics Belgrade, University of Belgrade, Belgrade, Serbia

e-mail:snedic@ipb.ac.rs

In this work, layer-by-layer polyelectrolyte deposition has been studied by alternately immersing the Si/SiO<sub>2</sub>(300 nm) substrates into successive aqueous solutions of cationic poly(allylamine hydrochloride) (PAH) and anionic poly(sodium 4-styrenesulfonate) (PSS) polyelectrolytes with intermediate rinsing steps [1]. Base piranha approach was adopted for the surface functionalization (SF) of the substrates by dipping them into the NH<sub>4</sub>OH/H<sub>2</sub>O<sub>2</sub> mix for 2 h at 50°C in order to create an OH<sup>-</sup> terminated surface prior to exposing the samples to the positively charged PAH.

Due to their thickness at the nanometer scale, the characterization of polyelectrolyte multilayer films requires highly sensitive techniques such as spectroscopic ellipsometry (SE) and atomic force microscopy (AFM). Both techniques verified the presence of polyelectrolyte multilayer films. Particularly, SE measurements demonstrated consistent shifts in the most prominent tanΨ peak resulting in an increase in the peak's wavelength shift with the increasing number of bilayers (Figure 1), whereas the SF and PAH/PSS bilayer thicknesses were established by AFM scratching and are approximately ~0.5 nm and ~1.1-1.4 nm, respectively.

The empirical Cauchy model can be used for approximation of the real part of the refractive index within spectral regions for which the material has very low or non-existing absorption [2]. Furthermore, complex refractive index of a layer in a multilayer structure can be extracted by direct inversion when the thickness of the layer is known. In accordance with this, the thicknesses of the polyelectrolyte multilayer films established by AFM were used to calculate the complex refractive indices. Finally, direct inversion and parametric fitting based on the Cauchy model have been utilized in order to fully determine the real and imaginary parts of the refractive index of ultrathin polyelectrolyte multilayer films in the wavelength range of 200-800 nm.

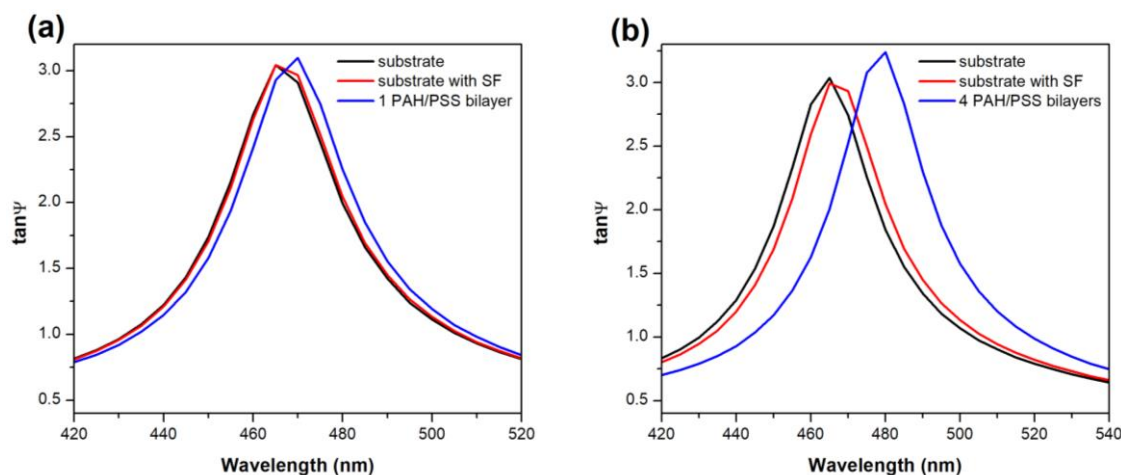


Figure 1. Experimentally measured ellipsometric spectra of two different Si/SiO<sub>2</sub>(300 nm) substrates with SF and (a) one, and (b) four PAH/PSS bilayers.

### REFERENCES

- [1] P. T. Hammond, "Form and function in multilayer assembly: New applications at the nanoscale," *Adv. Mater.* 16, 1271-1293 (2004).
- [2] H. G. Tompkins, E. A. Irene, "Handbook of Ellipsometry," William Andrew Publishing - Springer (2005).

## **Interplay between ordered multilayer structure and randomly distributed nanospheres and nanopillars in dichromated pullulan increases the width of the photonic bandgap**

S. Savic-Sevic<sup>1</sup>, D. Pantelic<sup>1</sup> and B. Jelenkovic<sup>1</sup>

<sup>1</sup>*Institute of Physics, Belgrade, Serbia*

e-mail:savic@ipb.ac.rs

Complex nanostructures with interesting properties for photonic applications received great attention. Initially, highly ordered photonic crystal structures have been manufactured and investigated [1]. Interesting physical phenomena were discovered, such as: complete band gaps, nonlinearities, slow light, negative refraction. Later, attention was drawn to disordered materials [2], random lasing and rediscovering effects like coherent backscattering, Anderson localization [3].

Usually, ordered and disordered photonic structures have been generated and analyzed separately. However, in nature, biological photonic structures are complex and inherently disordered. Here, we present structures having both ordered and disordered components, integrated into novel photonic structure. Ordered Bragg layers are mutually separated and supported by nanopillars, while internal voids are filled with randomly distributed nanospheres. This complex morphology is formed simultaneously by the holographic method and the nonsolvent induced phase separation. Depending on the film thickness, there can be as many as 50 Bragg layers. We show that the interplay between the Bragg regularity and random scattering increases the width of the photonic band-gap significantly, up to a 35% wide band gap, ( $\Delta\lambda_{\max}/\lambda_{\max} = 35\%$ ).

Photonic structures are holographically recorded in pullulan, a linear homopolysaccharide produced by micro-organisms (*Aureobasidium pullulans*), doped with ammonium dichromate. Here we use the dichromated pullulan for volume (Bragg) grating generation using a simple counter-propagating beam configuration.

Our photonic material has both properties of ordered photonic crystals: band gap and high reflectivity; and disordered structures: weak localization [4].

### REFERENCES

- [1] J. D. Joannopoulos, S. G. Johnson, J. N. Winn, R. D. Meade, *Photonic Crystals: Molding the Flow of Light*, 2nd ed., Princeton University Press, Princeton, NJ (2008).
- [2] D. Wiersma, *Nat. Photon.* 7, 188 (2013).
- [3] D. Wiersma, P. Bartolini, A. Lagendijk, R. Righini, *Nature* 390, 671 (1997).
- [4] S. Savic-Sevic, D. Pantelic, D. Grujic, B. Jelenkovic, *Opt Quant Electron* 48:289 (2016).

## Diamond-based nanocomposites as sources of fast X-ray luminescence in the visible and near-IR range

V. Sedov<sup>1</sup>, S. Kuznetsov<sup>1</sup>, I. Kamenskikh<sup>2</sup>, A. Martyanov<sup>1</sup>, D. Vakalov<sup>3</sup>, V. Konov<sup>1</sup>

<sup>1</sup>Prokhorov General Physics Institute of the Russian Academy of Sciences, Moscow, Russia

<sup>2</sup>Physics Faculty of Lomonosov Moscow State University, Moscow, Russia

<sup>3</sup>North Caucasus Federal University, Stavropol, Russia

sedovvadim@yandex.ru

Free-electron lasers allow the generation of coherent electromagnetic radiation in the X-ray range with very high peak power. Thus, there are new challenges in fabricating detectors and visualizers for the “hard” high-power radiation. Diamond is a perfect candidate for the role of X-ray transparent matrix not only due to low X-ray absorption but also due to its high thermal conductivity and chemical/radiation resistance.

Our approach is based on the integration of yttrium-aluminum or gadolinium-aluminum garnets doped with cerium (YAG:Ce and GAG:Ce, accordingly) in form of nanoparticles into robust and X-ray-transparent diamond matrix [1-4]. The solid garnet solutions were synthesized by co-precipitation from aqueous solution technique. Polycrystalline diamond films were grown in microwave plasma in the CVD reactor ARDIS-100. The thickness of composite films was in the range of 3-10 microns with a lateral size of up to 2 inches. The structure and properties of initial powders and obtained composites were studied by scanning electron microscopy, X-ray diffraction patterns, photoluminescence and X-ray luminescence.

The composite films show high-intensity X-ray luminescence with broadband peak at 550 nm (5d → 4f transition in Ce<sup>3+</sup> ion), and a narrow peak of silicon-vacancy (Si-V) centers at 738 nm. The characteristic decay time was measured at  $\tau_{\text{Ce}} < 50$  ns for cerium emission and at  $\tau_{\text{SiV}} \sim 1$  ns for Si-V centers.

The proposed composite material may be engineered to show XRL of desired intensity: from low intensities for high-power free-electron lasers up, which allows preserving the energy of the incident X-ray beam, to high intensities for sensitive X-ray detectors. Thus, the luminescent diamond composites suggest a new way to control X-ray visualization for fast X-ray detectors and screens.

The reported study was funded by RFBR, project №20-32-70074.

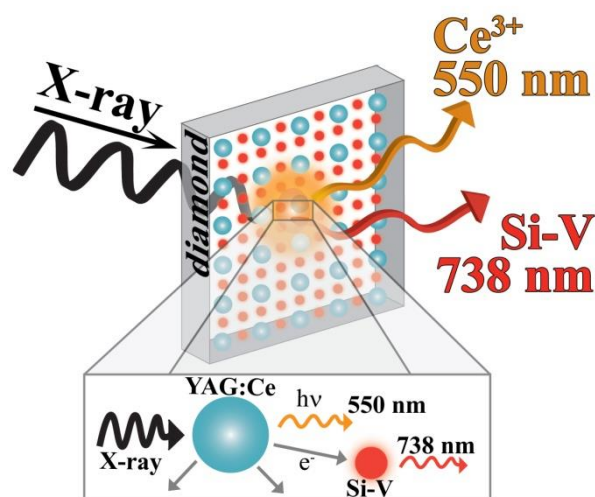


Figure 1. X-ray luminescence mechanism in “Diamond-YAG:Ce” composites.

### REFERENCES

- [1] V.S. Sedov, S.V. Kuznetsov, V.G. Ralchenko et al. *Diam. Relat. Mater.* 72, 47 (2017).
- [2] V. Sedov, S. Kuznetsov, A. Martyanov et al. *ACS Appl. Nano Mater.* 3, 1324 (2020).
- [3] S.V. Kuznetsov, V.S. Sedov, A.K. Martyanov et al. *Ceram. Inter.* 47, 13922 (2021).
- [4] V. Sedov, S. Kuznetsov, I. Kamenskikh et al. *Carbon* 174, 52 (2021).

## High-resolution terahertz and infrared spectroscopy of hybrid perovskite $\text{CH}_3\text{NH}_3\text{PbI}_3$

V. Anikeeva<sup>1,2</sup>, K. Boldyrev<sup>1</sup>, O. Semenova<sup>3</sup>, and M. Popova<sup>1</sup>

<sup>1</sup>*Institute of Spectroscopy of the Russian Academy of Sciences, Troitsk, Moscow, Russia*

<sup>2</sup>*National Research University Higher School of Economics, Moscow, Russia*

<sup>3</sup>*Rzhanov Institute of Semiconductor Physics of the Siberian Branch of the Russian Academy of Sciences, Novosibirsk, Russia*

e-mail: vanikeeva@hse.ru

The hybrid metal-organic perovskite  $\text{CH}_3\text{NH}_3\text{PbI}_3$  belongs to a class of semiconductor compounds with the crystal structure  $\text{ABX}_3$ , where  $\text{A} = \text{CH}_3\text{NH}_3^+$ ,  $\text{NH}_2\text{CH}=\text{NH}_2$ ;  $\text{B} = \text{Pb}, \text{Sn}$ ;  $\text{X} = \text{I}, \text{Br}, \text{Cl}$ . This class of compounds has useful physical properties such as high values of the absorption coefficient, a high carrier mobility, large diffusion lengths, and optical properties optimal for the photovoltaics, making them perspective materials for photodetectors, lasers, LEDs, and thermoelectric devices and especially as transport or/and absorber layers in solar cells [1].

Notwithstanding a large number of studies of optical properties of hybrid perovskites, most of them were carried out on thin films. In this work, high quality large single crystals of methyl ammonia lead iodide ( $\text{CH}_3\text{NH}_3\text{PbI}_3$ ) were investigated by high-resolution (up to  $0.2 \text{ cm}^{-1}$ ) spectroscopy in the wide spectral ( $15 - 650 \text{ cm}^{-1}$ ,  $1750 - 12000 \text{ cm}^{-1}$ ) and temperature ( $5 - 330 \text{ K}$ ) ranges. The  $\text{CH}_3\text{NH}_3\text{PbI}_3$  single crystals were grown from a saturated solution by the method described in [2]. We observed several low-frequency modes and a torsional mode of molecular cation at  $306 \text{ cm}^{-1}$ , which were not previously reported (Figure 1).

Furthermore, an unusual behavior of the transmission spectra was observed across the temperature of the phase transition from an orthorhombic to a tetragonal phase ( $\sim 160 \text{ K}$ ) and when a crystal was cooled down to  $70 \text{ K}$ . An observed splitting of the spectral line at  $2592 \text{ cm}^{-1}$  was attributed to the tunneling dynamics of molecular cation  $\text{CH}_3\text{NH}_3^+$  [3].

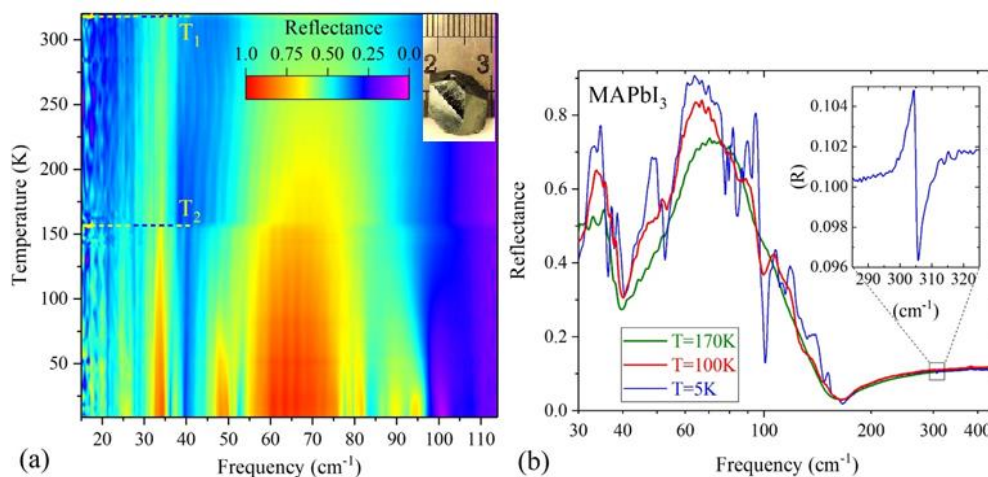


Figure 1.  $\text{CH}_3\text{NH}_3\text{PbI}_3$  reflectance spectra. (a) A map of the reflectance intensity as a function of the frequency and the temperature and (b) single spectra at 5, 100, and 170 K; an enlarged part of the lowest temperature spectrum represents a torsional mode at  $306 \text{ cm}^{-1}$ . The insert in the panel (a) depicts a photo of the investigated single crystal.

This work was supported the Russian Science Foundation (Grant No.19-72-10132).

### REFERENCES

- [1] T. Brenner, D. Egger, L. Kronik, G. Hodes, D. Cahen, *Nat. Rev. Mater.* 1, 15007 (2016).
- [2] O. Semenova, E. Yudanov, N. Yeryukov, Y. Zhivodkov, T. Shamirzaev, E. Maximovskiy, S. Gromilov, I. Troitskaia, *J. Cryst. Growth* 462, 45 (2017).
- [3] K. Boldyrev, V. Anikeeva, O. Semenova, M. Popova, *J. Phys. Chem. C*, 124, 42, 23307 (2020).

## Organic framework engineering for VOC sensing in mesoporous SiO<sub>2</sub> films

V.Pavlov<sup>1</sup>, Y.Chorbadzhiyska<sup>1</sup>, B. Georgieva<sup>1</sup>, R.Georgiev<sup>1\*</sup>,

<sup>1</sup>*Institute of Optical Materials and Technologies "Acad. J. Malinowski",  
Bulgarian Academy of Sciences, Acad. G. Bonchev str., bl. 109, 1113 Sofia, Bulgaria.*

\*corresponding author's e-mail address: [rgeorgiev@iomt.bas.bg](mailto:rgeorgiev@iomt.bas.bg)

Mesoporous materials emerged as an attractive field of interest due to the unique properties of those materials and the possibility to tailor those as per our needs. This gives the opportunity for broad spectrum of applications in fields such as adsorption, catalysis and sensing.

In this work we examine the properties of SiO<sub>2</sub> thin films for application in optical vapors sensing. To do so, thin films are deposited by spin-coating technique. In order to achieve porosity of the films soft-template method is employed via different polymers introduced in different concentrations to generate free volume within the films. The polymers differ in PPG/PEG composition and thus different properties in SiO<sub>2</sub> film are achieved. Thicknesses, refractive indices and extinction coefficients of the films are modelled by using nonlinear curve fitting method using the reflection spectra of the films. The free volume fraction in the film is determined by Bruggeman effective medium approximation. Acetone is used as a probing analyte for determination of medium absorption properties. The optical read-out of the films is recorded prior to and after exposure in acetone environment. Implementation of the most sensitive films in Bragg reflectors for VOC sensing are modelled and discussed.

### **Acknowledgements:**

This research is funded by Bulgarian National Science Fund, Grant No. KP06-M48/26.11.2020.

## Acetone sensing with optical readout using SiO<sub>2</sub> thin films

Y. Chorbadzhiyska<sup>1</sup>, V.Pavlov<sup>1</sup>, B. Georgieva<sup>1</sup>, R.Georgiev<sup>1\*</sup>,

<sup>1</sup>*Institute of Optical Materials and Technologies "Acad. J. Malinowski",  
Bulgarian Academy of Sciences, Acad. G. Bonchev str., bl. 109, 1113 Sofia, Bulgaria.*

\*corresponding author's e-mail address: [rgeorgiev@iomt.bas.bg](mailto:rgeorgiev@iomt.bas.bg)

Engineering properties of metal oxide thin films is of utmost importance for having broader application and better functionality in areas such as catalysis, sensing and energy conversion. Despite of the fact that silica is well studied material it still attracts attention for different photonic applications. One way to tailor its properties and obtain more functionalities is to introduce porosity in the films and thus modulate the refractive index to lower values. In such a way the films become an active media for VOC sensing.

In this study the formation of porous thin films is studied deposited by spin-coating technique. Porosity is generated by soft-template method using the commercially available organic templates and evaporation induced self-assembly method. Optical properties of the films have been calculated by nonlinear curve fitting method and UV-Vis spectroscopy. The morphology of the films has been investigated by Transmission Electron Microscopy. The film reaction to vapors has been recorded prior to and after exposure to acetone as a probe molecule. Bruggeman effective medium has been employed to estimate the physisorbed acetone quantity in the porous medium. The implementation of so-prepared thin films as a building block in Bragg reflectors has been modeled and discussed.

### **Acknowledgements:**

This research is funded by Bulgarian National Science Fund, Grant No. KP06-M48/26.11.2020.

## **4. Biophotonics**

## A new tool for measuring local temperature gradients on a submicron scale

A. Romshin<sup>1</sup>, Vadim Zeeb<sup>2</sup>, Artem K. Martyanov<sup>1</sup>, Igor I. Vlasov<sup>1</sup>

<sup>1</sup>*Prokhorov General Physics Institute of the Russian Academy of Sciences, Vavilov str. 38, Moscow 119991, Russia*

<sup>2</sup>*Institute of Theoretical and Experimental Biophysics of the Russian Academy of Sciences, Pushchino, Moscow Region 142292, Russia*  
e-mail: alex\_31r@mail.ru

Nanodiamonds hosting temperature-sensing centers constitute a closed thermodynamic system. Such a system prevents direct contact of the temperature sensors with the environment making it an ideal environmental insensitive nanosized thermometer. Here we describe a new practical implementation of ultra-local thermometer based on a 500-nm luminescent nanodiamond embedded into the inner channel of a glass submicron pipette. All-optical detection of temperature, based on spectral changes of the emission of “silicon-vacancy” centers with temperature, is used (Fig. 1b). We demonstrate the applicability of the thermometric tool to the study of temperature distribution near a local heater from aggregate of aluminum particles (Fig. 1a), placed in an aqueous medium. The experimental values of temperatures are shown in Fig. 1c. Nanodiamond thermometer reproducibly “senses” temperature changes of 2.1 °C degrees over 200 nm and is capable of monitoring strong temperature gradients  $\Delta T/\Delta X$  on the submicron scale (the drop  $\Delta T \approx 15$  °C is detected within  $\Delta X \approx 500$  nm near  $X = 1$   $\mu\text{m}$ ). Until now, temperature measurements on the submicron scale at such high gradients have not been performed. The new thermometric tool opens up unique opportunities to answer the urgent paradigm-shifting questions of cell physiology thermodynamics.

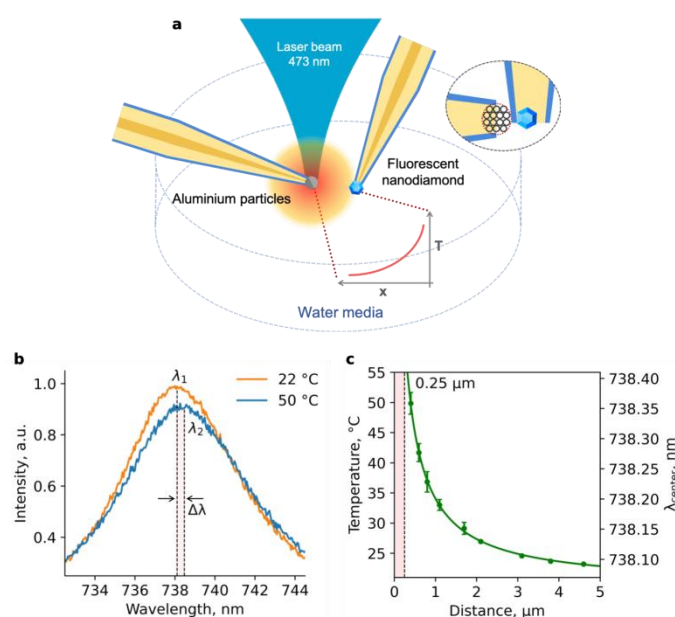


Figure 1. Schematics of temperature distribution evaluation near the local heater: the relative position of the thermometer, heater and laser beam in a cuvette with water (a); PL spectra of the diamond thermometer, measured at different distances from the heater, the positions  $\lambda_1$  and  $\lambda_2$  of SiV ZPL maxima correspond to 22 °C and 50 °C, respectively (b); dependence of the SiV ZPL position and the temperature on the distance  $X$  between the heater surface and the center of the thermometer, dashed line at  $X = 0.25 \mu\text{m}$  corresponds to the distance between the heater surface and the center of the thermometer when they touch each other. The number of measurements in each green point is 7. Corresponding error bars (standard deviations) are minimal (0.3 °C) at distances of 2-5  $\mu\text{m}$  and reach a maximum of 2.5 °C at  $X = 0.41 \mu\text{m}$  (c).

### REFERENCES

[1] Baffou, G., Rigneault, H., Marguet, D., & Jullien, L. A critique of methods for temperature imaging in single cells. *Nature methods*, 11(9), 899-901 (2014).

## Natural waveguides on *Hoplia argentea* elytra

D. Pavlović<sup>1</sup>, B. Salatić<sup>1</sup>, S. Savić-Šević<sup>1</sup>, N. Vesović<sup>2</sup> and D. Pantelić<sup>1</sup>

<sup>1</sup>*Institute of Physics, University of Belgrade, Pregrevica 118, 11080 Belgrade, Serbia*

<sup>2</sup>*University of Belgrade - Faculty of Biology, Studentski Trg 16, 11000 Belgrade, Serbia*  
e-mail: danica.pavlovic@ipb.ac.rs

Light waveguides are structures with a role in receiving and channeling light and filtering certain wavelengths of the electromagnetic spectrum [1]. That's how it comes to light capturing and local reinforcement of its intensity, which can be further utilized for various purposes (e.g. conducting light to pigments in the eye, forming structural coloration, etc.) [2]. Based on their geometric structure waveguides can be planar or linear (banded or fibrous) [3].

Microstructures with a waveguide role have been studied a lot in the living world [4]. Structures with a function of optical waveguides have also been discovered in insects. They can be found on antennae, in complex eyes, on wing scales and other parts of the body [5], and can work as integral part of light or IR receptors, thermoregulatory systems, or can play an important role in the formation of structural coloration [6].

Here we present cuticular structures on beetle elytra (Insecta: Coleoptera) that produce structural coloration thanks to morphology and function of light waveguides. *Hoplia argentea* from family Rutelidae was used as a model organism. We found out that individuals of this species possess linear type of waveguides on its front hardened wings, which are responsible for the production of structurally green coloration.

### REFERENCES

- [1] M. J. Adams, *An introduction to optical waveguides*, 14 (Wiley, New York, 1981).
- [2] A. W. Snyder, R. Menzel, *Photoreceptor optics* (Springer Science & Business Media, 2012).
- [3] G. T. Reed, A. P. Knights, *Silicon photonics: an introduction* (John Wiley & Sons, New Jersey, 2004).
- [4] M. Bass, E. W. Van Stryland, D. R. Williams, *Handbook of optics* (McGrawHill, New York, 1995).
- [5] P. S. Callahan, *Appl. Opt.* **7** (8), 1425-1430 (1968).
- [6] N. N. Shi, C. C. Tsai, F. Camino, G. D. Bernard, N. Yu, R. Wehner, *Science* **349** (6245), 298-301a (2015).

## Thermoresponsive, biocompatible hydrogels for rapid prototyping of biomimetic microchannels

M. Radmilović<sup>1</sup>, B. Murić<sup>1</sup>, D. Grujić<sup>1</sup>, B.Zarkov<sup>2</sup>, M. Nenadić<sup>3</sup> and D. Pantelić<sup>1</sup>

<sup>1</sup>*Institute of Physics, Belgrade, Serbia*

<sup>2</sup>*Directorate for Measure and Precious Metals, Mike Alasa 14, 11000 Belgrade, Serbia*

<sup>3</sup>*Institute for Biological Research "Siniša Stanković" National Institute of Republic of Serbia, University of Belgrade, Serbia*

e-mail: mihajlo.radmilovic@ipb.ac.rs

Single-step prototyping of biophotonic structures that effectively mimic tissue microchannels is a complex task. A wide range of techniques is used for microchannel fabrication such as photolithography, silicon molding, etc. [1] However these techniques possess a high degree of manufacturing complexity and cost [1, 2].

We present technology that is based on locally melted nontoxic, environmentally friendly gels, and a homemade laser writing system. Microchannels are fabricated by local laser irradiation and spatial control is obtained using coordinate stage. The physical properties of microchannels are determined by: gels absorbance, surface tension and laser energy density.

Several *in vitro* assays were performed to establish biocompatibility of the gel materials. *In vitro* studies on the spontaneously immortalized human keratinocytes (HaCaT) cell line showed that the tested material had no toxic effect. Likewise, different ATCC (American Type Culture Collection) and resistant strains of pathogenic bacteria and micromycetes were cultivated. After application of the tested materials no inhibition of bacterial colonies and micromycetes growth was observed.

As a proof of concept, applicability of biomimetic microchannels (BM) was tested using a digital image of a human retinal blood vessels. Digital model is then translated to the set of G-code coordinates and imprinted in gel material by laser writing.

BM has significant potential for a wide range of applications such as noninvasive medical diagnostic, biomedical testing, security, etc. Here we suggest a retinal vascular model to study blood flow in different pathophysiological conditions. Moreover, our gel based material can be used for fast and efficient fabrication of BM and also for micro-optical components generation [3].

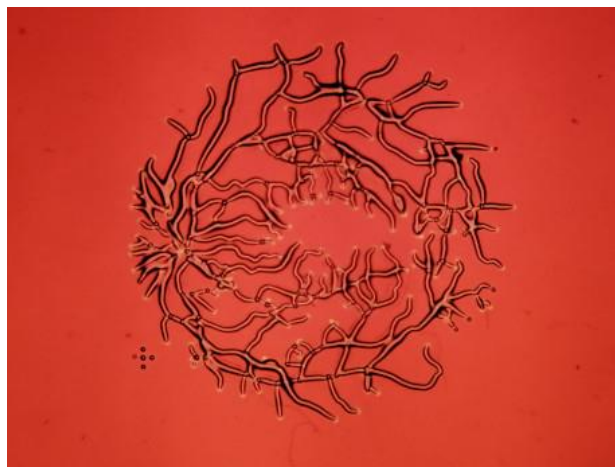


Figure 1. Biomimetic model of human retina blood vessels.

### REFERENCES

- [1] P. Ghassemi, J. Wang, A. Melchiorri, J. Biomed. Opt. 20, 121312 (2015).
- [2] R.Long, T.King, T.Aki, Biomed. Opt. Exp. 2, 1887 (2011)
- [3] B.Murić, D.Pantelić, D.Vasiljević, Appl. Opt. 46 8527 (2007)

## Coupled substitutions of fluorapatite crystals in the engineering of optically-active bionanomaterials

D. Milojkov<sup>1</sup>, V. Manojlovic<sup>2</sup>, D. Mutavdzic<sup>3</sup> and M. Sokic<sup>1</sup>

<sup>1</sup>*Institute for Technology of Nuclear and Other Mineral Raw Materials, Belgrade, Serbia*

<sup>2</sup>*Faculty of Technology and Metallurgy, University of Belgrade, Serbia*

<sup>3</sup>*Institute for Multidisciplinary Research, University of Belgrade, Serbia*

e-mail: d.milojkov@itnms.ac.rs

A wide range of new biomaterials for medical use has been prepared using various coupled ionic substitutions in a fluorapatite (FAP) crystal matrix [1-4]. FAP is present in human enamel, so its synthetic form is often used in the treatment of dental caries or osteoporosis [5]. In recent years, FAP nano-sized particles doped with rare-earth ions have been extensively studied as potential luminescent material for cell labeling, bone imaging in bone tissue engineering, and for cancer therapies [1-4]. Moreover, FAP is a suitable crystal matrix for various substituents that can alter its physicochemical, luminescent, and biological properties [5].

Uniform nanopowders of pure fluorapatite (FAP) and praseodymium-nitrate-carbonate substituted fluorapatite (PrNCFAP) have been successfully synthesized by precipitation reaction, and systematically characterized by XRD, FTIR, SEM, TG and PL methods. Coupled substitution of FAP reduces the crystallite size, and FTIR spectra indicate the presence of nitrate ( $\text{NO}_3^{2-}$ ) and carbonate ( $\text{CO}_3^{2-}$ ) species. Structure thermally analysis confirm decomposition of water,  $\text{NO}_3^{2-}$  and  $\text{CO}_3^{2-}$  species in the range of 100-750 °C. Emission of FAP nanopowder occurred in the violet-blue region of visible part of the spectrum, with redshift to the green color region when  $\text{Pr}^{3+}$ ,  $\text{NO}_3^{2-}$  and  $\text{CO}_3^{2-}$  substituted in the lattice. Analysis of luminescence spectra by MCR-ALS method extract three fluorophores from the samples and showed simultaneous existents of emission-reabsorption between dopants in FAP lattice.

The obtained samples showed a small degree of hemolysis and antibacterial activity and could potentially be candidates for further research in dentistry.

### ACKNOWLEDGMENT

The authors are grateful to the Ministry of Education, Science and Technological Development of the Republic of Serbia (Contract number: 451-03-9/2021-14/200023)

### REFERENCES

- [1] D. Milojkov et al., J. Lumin. 217, 116757 (2020).
- [2] D. Milojkov et al., Acta. Phys. Pol. A. 136, 86 (2019).
- [3] Q. Fan et al., J. Biomater. Appl. 35, 237 (2020).
- [4] X. Hu et al., Biomaterials. 52, 441 (2015).
- [5] N. Leroy and E. Bres, Eur. Cell. Matter. 2, 36 (2001).

## Influence of light guide type on dental composite polymerization shrinkage – a holographic and thermographic study

E. Novta<sup>1</sup>, T. Lainović<sup>1</sup>, S. Savić-Šević<sup>2</sup>, D. Grujić<sup>2</sup>, D. Pantelić<sup>2</sup> and L. Blažić<sup>1,3</sup>  
<sup>1</sup>University of Novi Sad, Faculty of Medicine, School of Dental medicine, Novi Sad, Serbia  
<sup>2</sup>University of Belgrade, Institute of Physics, Belgrade, Serbia  
<sup>3</sup>Dental Clinic of Vojvodina, Novi Sad, Serbia  
 e-mail: evgenije.novta@mf.uns.ac.rs

Polymerization shrinkage stress (PSS) is generated at the tooth-restoration interface, during setting of a dental resin-based composite (RBC) inside a tooth cavity. As a result, various negative clinical outcomes may arise. In addition, the polymerization reaction is followed by heat release due to its exothermic nature. The aim of this study was to investigate the influence of two different light guides on PSS, by detecting tooth model deformation using digital holographic interferometry (DHI). Simultaneously, temperature rise measurements were conducted using infrared thermography (IRT).

Standardized tooth models made of dental gypsum, with a mesial-occlusal-distal (MOD) cavity, were used for the purposes of this study. The specimens were mounted in aluminum blocks and fixed in the custom-made holographic set-up with a Nd:YVO<sub>4</sub> laser at 532nm wavelength and power of 400mW. The cavities were filled with a bulk-fill RBC. Two groups of specimens (n=10) were used. In the first group (G1), a light guide (ϕ 8mm) of a commercial LED light source was used in continuous 40s curing mode. In the second group (G2), three optical fibers (ϕ 1mm), connected to the same light source, were inserted into the dental filling to cure the RBC from within [1] (the first phase–3x40s). After removal of the optical fibers from the RBC, the remaining voids were filled and the specimens were additionally cured (the second phase–40s). Tooth model deformation due to PSS was detected in real-time using DHI, while simultaneously monitoring temperature rise of the RBC using IRT. Statistical analysis was performed using student's t-test for independent samples.

In group G2, the DHI images during the first phase of light curing using optical fibers, demonstrated initiation of the polymerization reaction and tooth model deformation. The final deformation value (after the first and second phase) in group G2 (M=14.3µm) was significantly lower (on average 5.2µm, p<0.05) compared to final deformation value in group G1 (M=9.1µm) (Figure 1.). The resulting IRT images, presented a gradual temperature increase in group G2, postponing the estimated gel-point of the polymerization reaction, which could be related to PSS relaxation (Figure 2.).

Within the limitations of this study, it was concluded that polymerization reaction initiation using optical fibers influenced lower polymerization shrinkage and gradual temperature increase during polymerization. Accordingly, optical fibers could contribute to overcoming the dental PSS problem.

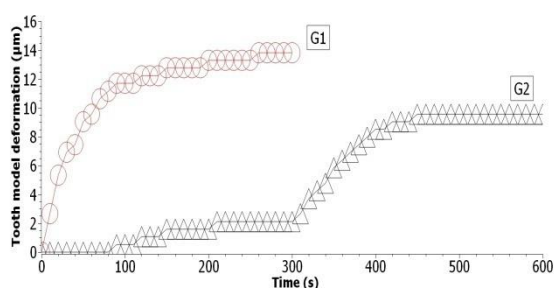


Figure 1. Ellipse-G1 group, standard curing mode; triangle-G2 group, two-phase curing with optical fibers and standard light guide

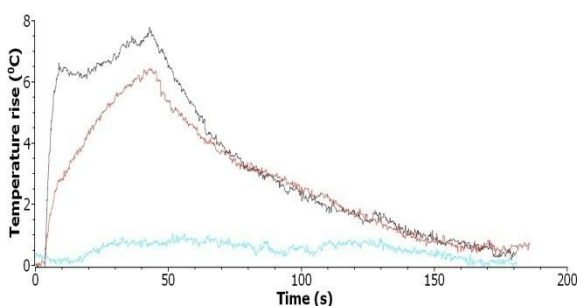


Figure 2. Black-G1 group, standard curing mode; green-G2 group, first phase curing with optical fibers; red-G2 group, second phase-standard curing mode

REFERENCES [1] F.A. Rueggeberg. Dent. Mater. 2011;27(1):39–52.

Supported by the contract NIO200114 and Mikodental, Šabac (distributers of Shofu®, Japan in Serbia)

## The metal-doped TiO<sub>2</sub> nanoparticles as photosensitizers in photodynamic therapy of melanoma

I. D. Miler<sup>1</sup>, M. D. Nešić<sup>1</sup>, J. Žakula<sup>1</sup>, L. Korićanac<sup>1</sup>, M. Radoičić<sup>1</sup>, A. Korać<sup>2</sup>, M. Petković<sup>1</sup>, M. Stepić<sup>1</sup>

<sup>1</sup>Vinča Institute of Nuclear Sciences, National Institute of the Republic of Serbia, University of Belgrade, Belgrade, Serbia; <sup>2</sup>Faculty of Biology, University of Belgrade, Belgrade, Serbia

e-mail: [irenamiler@vin.bg.ac.rs](mailto:irenamiler@vin.bg.ac.rs)

Melanoma is one of the most severe life-threatening diseases with a highly aggressive biologic behavior. Despite all improvements in diagnosis and therapy, most deaths from melanoma are due to metastases that are resistant to conventional treatment modalities [1].

Photodynamic therapy (PDT) is a relatively new treatment modality that has been successfully applied to many diseases and disorders, including skin cancers. PDT uses a combination of a light-sensitive substance (known as a photosensitizer, PS) and light of an appropriate wavelength. After the activation by light, PS reacts with molecular oxygen producing reactive oxygen species (ROS) and radicals, which cause intracellular biochemical changes leading to cell death [2].

Titanium dioxide nanoparticles (TiO<sub>2</sub> NPs) are commonly used PSs in PDT [3], but they absorb strongly in the UV light range. Doping TiO<sub>2</sub> NPs with ions leads to an increase in the absorption edge wavelength and a decrease in the bandgap energy, enabling the application of a less damaging visible light for the NP activation. However, to our best knowledge, metal-doped TiO<sub>2</sub> has not been extensively tested as PSs.

This study aimed to investigate the effects of colloidal TiO<sub>2</sub> NPs and prolate nanospheroids (PNSs) doped with Cu and Ni on melanoma cell lines (A375) in the dark and under blue light irradiation. In general, doped TiO<sub>2</sub> NPs show higher photocatalytic activity than undoped analog. Among them, the best photocatalytic activity showed TiO<sub>2</sub> NPs doped with Cu [4]. However, colloidal TiO<sub>2</sub> NPs have a diameter of 5 nm, whereas PNSs are around 20 nm long. Therefore, the cytotoxicity of cells was dependent on the dopant and the size of NPs. Still, in all cases, it is augmented by the light illumination, implying the potential use of doped TiO<sub>2</sub> NPs with Cu and Ni as a light-sensitive drug in PDT of melanoma. In summary, our results can contribute to the development of more efficient skin cancer treatment modalities.

### REFERENCES

- [1] S. S. Sulaimon, B. E. Kitchell, *J Vet Intern Med.* 17, 760-772 (2003).
- [2] L.B. Josefsen, R.W. Boyle, *Met Based Drugs.* 2008, 276109 (2008).
- [3] S. Cesmeli, C Biray Avci, *J Drug Target.* 27, 762-766 (2019).
- [4] M. Khairy, W. Zakaria, *Egypt. J. Pet.* 23, 419-426 (2014).

## Laser Microsurgery of Filamentous Fungi: The Latest Protocol Enabling Patch-Clamp Amenable Protoplasts

K. Stevanović<sup>1</sup>, T. Pajić<sup>1</sup>, N. Todorović<sup>2</sup>, A. Krmpot<sup>3</sup>, M. Živić<sup>1</sup>, M. Rabasović<sup>3</sup>

<sup>1</sup>University of Belgrade - Faculty of Biology, Serbia

<sup>2</sup>Institute for Biological Research, University of Belgrade, Serbia

<sup>3</sup>Institute of Physics, University of Belgrade, Serbia

e-mail: katarina.stevanovic@bio.bg.ac.rs

We have developed an advanced protocol for laser cell surgery to obtain protoplasts of filamentous fungi, suitable for investigation of ion channels, relying on few attempts already made in the past [1], [2]. Among obtained protoplasts, 32% were shown to be “patchable”, meaning that formation of the gigaseal by the micropipette was possible. Protoplasts were produced by first making an incision on the cell wall of plasmolysed hyphae by a tightly focused femtosecond laser beam (Figure 1). Cell surgery is followed by a reduction of solution osmolarity to promote extrusion of protoplast (or more often, a part of it) through the cut. The two key points- cell surgery parameters and the proper sequence of the solutions used – were subjected to variations to gain insight into parameters that contribute to protoplast production and stability. The proper selection of the pipette size and shape with respect to the protoplast size was also of great importance.

Cell surgery and hyphae imaging was performed by a nonlinear laser scanning microscope. Ti:Sa laser was operating at 730nm, with 76MHz repetition rate and 160fs pulse duration. Water dipping objective lens (40 x 1.0, Zeiss W Plan-Apochromat) on the upright non-linear microscope system made possible to perform laser surgery and patch clamp on two separate systems, while working in the same microscopic chamber. Prior to microsurgery, two-photon excitation fluorescence was used to scan the hyphae cell wall stained with Calcofluor white dye, using the same wavelength as for the surgery.



Figure 1. Hyphae cell surgery a) before laser cutting b) extrusion of the protoplast through the incision after laser cutting c) the pipette on the enlarged protoplast

Two-step plasmolysis, with increased concentration of calcium in the more hyperosmotic solution was both efficient for microsurgery to be performed and had a stabilizing effect on protoplasts. Subtle deplasmolysis prior to the patch clamping effective enough to stimulate protoplasts to exit, without making the membrane overstretched to interact with the pipette was employed. Optimized concentration and type of chemical agents for inhibition of the cell wall production was continuously present in all solutions, as an indispensable factor for success.

Acknowledgement: Project HEMMAGINERO, No. 6066079 from Program PROMIS, Science Fund of the Republic of Serbia; Project „Minimally invasive, selective ablation of dental caries by femtosecond laser“, Move for the science/2019.

### REFERENCES:

- [1] Roberts, S. K., Dixon, G. K., Dunbar, S. J., & Sanders, D. (1997), *New Phytologist*, Vol. 137, 579–585
- [2] Véry, A. A., & Davies, J. M. (1998). *Applied and Environmental Microbiology*, 64(4), 1569–1572

## Boosting surface plasmon resonances of thin golden film by bio photonic crystals

M. Gilic<sup>1</sup>, M. Ghobara<sup>1</sup> and L. Reissig<sup>1</sup>

<sup>1</sup>*Institute for Experimental Physics, Freie Universität Berlin, Arnimallee 14, 14195 Berlin  
martina.gilic@fu-berlin.de*

Diatoms are unicellular biomineralized algae which possess a biosilica shell with a 2D periodic pore structure. Due to their unique physical, chemical and photonic properties, diatoms found numerous application in biochemical sensors contributing to their ultra-high sensitivity [1, 2]. As substrates for Surface Enhanced Raman Spectroscopy (SERS) they proved to be capable of concentrating analyte molecules on their surface as well as assembling metal nanoparticles at pore rims which lead to more controllable hot spot creation. It has been suggested that diatoms enhance the SERS signal additionally with guided mode resonance due to their photonic crystal – like properties. However, current studies are limited to coating diatoms with noble nanoparticles or non-uniform golden films, which hampers interpretation regarding their photonic structure contribution and leads to unsatisfactory reproducibility. Here we present biosilica substrates based on diatom frustules coated with a uniform 10nm thick layer of gold as a candidate for highly reproducible SERS substrates with high enhancement factors. The uniform films spread over the periodic frustule structure enable the study of photonic properties of periodical pore arrays and their role in enhancing optical sensitivity. Rhodamine 6G is used as a typical Raman probe molecule. Our results show that substrates with a gold film over diatom monolayers improve SERS detection of R6G by several times compared to substrates with a gold film on glass. The reproducibility of the measurement was verified with Raman mapping. Surface morphology and the fine structure of the diatoms were investigated with Scanning Electron Microscopy, confirming structural integrity for an expanded analytical study.

### REFERENCES:

- [1] K. Squire, K. Sivashanmugan, B. Zhang, J. Kraai, G. Rorrer, A. Wang, ACS APPLIED NANO MATERIALS 3, 1656 (2020).
- [2] S. Manago, G. Zito, A. Rogato, M. Casalino, E. Esposito, A. De Luca, E. De Tommasi, ACS Appl. Mater. Interfaces 10, 12406 (2018).

## Mapping of fluorescent compounds in lyophilized blackcurrant (*Ribes nigrum L.*) fruits using spectroscopy and nonlinear microscopy

M. S. Rabasovic<sup>1</sup>, D. Sevic<sup>1</sup>, B. P. Marinkovic<sup>1</sup>, A. J. Krmpot<sup>1</sup>, G. Zdunic<sup>2</sup>, K. Savikin<sup>2</sup>,  
M. D. Rabasovic<sup>1</sup>

<sup>1</sup>*Institute of Physics, Belgrade, Serbia*

<sup>2</sup>*Institute for Medicinal Plants Research "Dr Josif Pančić", Tadeuša Košćuška 1, 11 000, Belgrade, Serbia*  
e-mail:majap@ipb.ac.rs

Blackcurrant (*Ribes nigrum L.*) belongs to the important medicinal plants that act preventively and therapeutically on the organism [1, 2]. Bioactive components in fruits and leaves of blackcurrant could have beneficial effects on the skin fibroblasts that produce collagen [3]. The influence of parts and extracts of this plant on erythrocyte membranes has been the subject of research in recent years [4]. Blackcurrants (*Ribes nigrum L.*) contain high levels of polyphenol anthocyanins in fruits and flavonoids in leaves that have beneficial effects on health, owing to antioxidant and anticarcinogenic properties. These compounds are responsible for the coloring of many plants, flowers and fruits. Cyanidin-3-O-glucoside (C3G) is one of the principal types of anthocyanidins and is the most common and abundant one in fruits blackcurrant [5]. Anthocyanidins/anthocyanins can be employed as probes for oxidation processes in biomedical experiments. Their advantages include biocompatibility and the lack of toxicity [6].

The present study aimed to present the analysis and mapping of the Blackcurrants (*Ribes nigrum L.*) components using spectroscopy and imaging measurements [1, 7]. Time resolved optical characteristics were analyzed by using TRLS (Time Resolved Laser Spectroscopy) experimental setup [1]. Nonlinear optical properties of the plant have been studied using two-photon excited autofluorescence (TPEF), and upconversion luminescence (UCL) simultaneously [7]. The benefits of using UCL for biological applications are in reducing the photobleaching and providing photostability. Upconversion emission is also more efficient than the TPEF and SHG. Moreover, UCL could be achieved with a low power continuous wave (CW) laser.

### REFERENCES

- [1] M. S. Rabasovic, B. P. Marinkovic, M. D. Rabasovic, M. G. Nikolic, D. Sevic, Eur. Phys. J. D 75, 180 (2021).
- [2] G. Kendir, I. Süntar, A. O. Çeribaşı, A. Köroğlu, J. Ethnopharmacol. 237,141-148 (2019).
- [3] N. Nanashima, K. Horie, H. Maeda, T. Tomisawa, M. Kitajima T. Nakamura, Nutrients 10, 495 (2018).
- [4] D. Bonarska-Kujawa, S. Cyboran, R. Żyłka, J. Oszmiański, H. Kleszczyńska, BioMed Research International, 2014, 783059 (2014).
- [5] L. Tang, D. Zhang, S. Xu, H. Zuo, C. Zuo, Y. Li, 29, 168-175 (2014).
- [6] G. Bartosz, M. G-Pietrasiewicz, I. S-Bartosz, J. Agric. Food Chem. 68 (43) 12019 (2020).
- [7] M. D. Rabasovic, D.V.Pantelic, B. M. Jelenkovic, S. B. Ćurčić, M. S. Rabasovic, M. D. Vrbica, V. M. Lazovic, B. P.M. Ćurčić, A. J. Krmpot, J. Biomed.Optics 20(1) 016010 (2015).

## Interaction of ultrashort laser pulses with hemoglobin as a tool for selective erythrocytes photo-labeling

M. Radmilovic<sup>1</sup>, I. Drvenica<sup>2</sup>, M. D. Rabasovic<sup>1</sup>, V. Ilic<sup>2</sup>, D. Pavlovic<sup>1</sup>, S. Nikolic<sup>1</sup>, M. Matic<sup>3</sup> and A. Krmpot<sup>1</sup>

<sup>1</sup>Institute of Physics Belgrade, Serbia

<sup>2</sup>Institute for Medical Research, University of Belgrade, Serbia

<sup>3</sup>Institute of Oncology and Radiology of Serbia

e-mail: mihajlo.radmilovic@ipb.ac.rs

Interaction of hemoglobin (Hb) with ultrashort laser pulses is followed by fluorescence detection [1, 2]. The photophysical nature of fluorescence from Hb-containing specimens is not completely understood so far. There is some evidence of photoproduct formation in the process of Hb interaction with ultrashort laser pulses [3].

We measured Uv-Vis and Two-photon emission spectra of formed photoproduct in the way that Hb thin film was previously treated with a femtosecond Ti: Sapphire laser operating on 730nm. A relative relation and position of Uv-Vis Hb characteristic peaks such as Soret peak (410 nm),  $\alpha$  and  $\beta$  peaks (577 nm and 541 nm respectively) served as a marker of structural changes in the laser treated Hb films[4].

Results suggest that the interaction of Hb with ultrashort laser pulses probably leads to the photodegradation of Hb, due to changes in  $\alpha$ ,  $\beta$  peaks relative relation and red shift of Soret peak in photoproduct Fig. 1 a).

Moreover, we emphasize that the photoproduct formed on thin Hb films has long durability, since we were able to detect its fluorescence after several months. This opens a possibility to apply the formed photoproduct as optical data storage and security tag.

We have also induced photoproduct formation in the human healthy erythrocytes Fig. 1 b) in order to selectively “label” and make them fluorescent in a whole blood. Two-photon selective labeling of erythrocytes can be used as a tool for studying red blood cells with different fluorescence detection methods, due to photoproduct fluorescence. This can be potentially applied in studying hemoglobin and erythrocytes in various physiological and pathophysiological states.

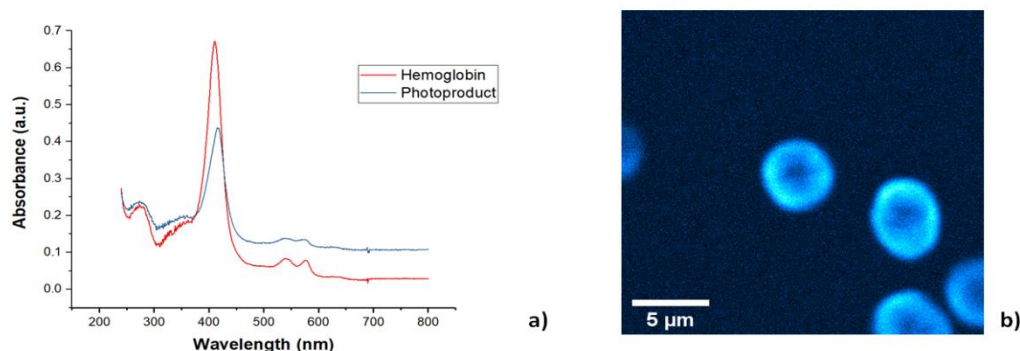


Figure 1. a) Uv-Vis absorption spectra of hemoglobin (red) and formed photoproduct (blue), b) Two-photon fluorescence image of selectively chosen erythrocytes with induced photoproduct formation.

Funding: Project HEMMAGINERO, No 6066079

### REFERENCES

- [1] D. Li, W. Zheng, Y. Zeng, *Optics Lett.* 36, 834 (2011).
- [2] K. Bukara, S. Jovanic, I. Drvenica, *J. Biomed. Opt.* 22.2, 026003 (2017).
- [3] E.A. Shirshin, B.P. Yakimov, S.A. Rodionov, *Laser Phys. Lett.* 15, 075604 (2018).
- [4] E.H. Hanson, J. Ballantyne, *PLoS One* 5, e12830 (2010).

## Discovering abnormal erythrocyte membranes - optical approaches

M. Matic<sup>1</sup>, D. Pavlović<sup>2</sup>, M. Radmilovic<sup>2</sup>, M. D. Rabasovic<sup>2</sup>, V. Ilić<sup>3</sup>, A. Krmpot<sup>2</sup>, I. Drvenica<sup>3</sup>

<sup>1</sup>Institute of Oncology and Radiology of Serbia, <sup>2</sup>Institute of Physics, Belgrade, Serbia

<sup>3</sup>Institute for Medical Research, University of Belgrade

e-mail: milica.matic1210@gmail.com

Due to their complex physiological role, erythrocytes have naturally very elastic membranes, however, extremely susceptible to various endogenous and exogenous factors. Therefore, it has been speculated that abnormalities in erythrocyte membrane deformability and shape can be seen as an early sign of some acute and chronic pathological states/diseases [1,2]. In the project HEMMAGINERO [3], we are exploring whether optical methods, ektacytometry, and Two-Photon Excitation Fluorescence (TPEF) microscopy, can be used as potential diagnostics tools in identifying any changes in the shape/deformability of erythrocytes. Using ektacytometry (RheoScan D-300, RheoMeditech Inc., South Korea) we calculate the cell deformability from the intensity pattern of the laser light which is scattered by a suspension of red blood cells exposed to shear stress [4]. Our previous research already demonstrated that in-house TPEF microscopy set-up is an effective tool for label- and fixation -free imaging of erythrocytes and their membranes [5], based on a peculiar feature of hemoglobin to produce a fluorescent molecule upon interaction with ultrashort laser pulses [6,7].

In the first phase of the project, we have used blood from healthy volunteer donors and *in vitro* made environments that simulate different conditions to which erythrocytes can be exposed in pathological processes (hyper- and hypo-osmolarity; acidosis, alkalosis). The obtained data on erythrocyte morphology by TPEF and erythrocytes deformability by ektacytometry are correlated with the results of routinely used biochemical tests for oxidative stress assessment, and mechanical and osmotic fragility indices.

Our results show that both ektacytometry and TPEF microscopy are sensitive and reliable in determining that membranes of erythrocytes have suffered under non-ideal (meaning non-physiological) conditions of the *in vitro* environment. Further investigation is needed to conclude the precision of these optics methods in discovering abnormal erythrocyte membranes in actual patients' blood.

Funding: Project HEMMAGINERO No 6066079 from Program PROMIS, Science Fund of the Republic of Serbia

### REFERENCES:

- [1] H. Chen, W. Yunpeng, C. Shaoxi, et al. Clin. Hemorheol. Microcirc. 16,2 (1996).
- [2] S. Shin, Y. H. Ku, J.X. Ho, et al. Clin. Hemorheol. Microcirc. 36, 3(2007).
- [3] <http://www.hemmagero.rs/hemmagero.html>
- [4] A.E.O. Finkelstein. Design and evaluation of a new diagnostic instrument for osmotic gradient ektacytometrie. PhD Thesis, Université Paris-Est (2017).
- [5] K.S. Bukara, S.Z. Jovanić, I.T. Drvenica, et al. Mapping of hemoglobin in erythrocytes and erythrocyte ghosts using two photon excitation fluorescence microscopy J. Biomed. Optics 22(2), 026003 (2017).
- [6] W. Zheng, D. Li, Y. Zeng, et al. Two-photon excited hemoglobin fluorescence, Biomed. Opt. Express 2, 71-79 (2011).
- [7] E.A. Shirshin, B.P. Yakimov, S.A. Rodionov et al. Formation of hemoglobin photoproduct is responsible for two-photon and single photon-excited fluorescence of red blood cells. Laser Phys. Lett. 15, 075604 (2018).

## Visible light-responsiveness of the nanocarrier/drug complex based on the TiO<sub>2</sub> nanoparticles and Ru complex

M. Matijević<sup>1</sup>, M. Stepić<sup>1</sup>, M. Radojičić<sup>1</sup>, M. Petković<sup>1</sup> and M. D. Nešić<sup>1</sup>

<sup>1</sup>VINČA Institute of Nuclear Sciences, National Institute of the Republic of Serbia, University of Belgrade  
e-mail: milica.m@vin.bg.ac.rs

TiO<sub>2</sub> nanoparticles (NPs) have great potential for implementing photodynamic therapy (PDT) as a part of drug delivery therapeutical systems. PDT is an emerging anti-cancer therapy that involves the administration of photosensitizer (PS), which undergoes reversible changes upon light exposure. Next, PS can release a cytostatic drug and/or transfer its energy to molecular oxygen, generating reactive oxygen species (ROS), consequently leading to cancer cell ablation [1].

In this work, we assessed photocytotoxicity to the HeLa cell line of the nanocarrier/drug complexes–nanocomposite systems (NCSs) made of different types of carriers, TiO<sub>2</sub> NPs, for the delivery of Ru complex (cis-dichlorobis (2,2'-bipyridyl-4,4'-dicarboxylic acid)ruthenium(II)). One tested NCS consists of colloid TiO<sub>2</sub> NPs, whereas the other consists of the TiO<sub>2</sub> prolate nanospheroids (PNSs). Previously in our work, both TiO<sub>2</sub> NPs demonstrated good biocompatibility in the dark [2,3], whereas the Ru complex exhibited notable anti-proliferative, genotoxic, and antitumor effects [4]. As TiO<sub>2</sub> NPs are photo-active in the UV range, and the Ru complex absorbs in both UV and visible spectrum [3], herein, we have determined the optical bandgaps of the synthesized NCSs with Tauc's plot.

Calculated bandgaps of the synthesized NCSs proved that the Ru complex extends the responsiveness of TiO<sub>2</sub> to visible light while acts as a medicament in photo-active NCSs, allowing the absorption of the NCSs in the visible range. Thus, we have examined the photocytotoxicity of the combined treatment of the HeLa cells with NCSs and visible light. The preliminary results show that visible light, which is not harmful when applied alone to the cells, can effectively induce a cytotoxic effect in the combined therapy with the NCSs.

### REFERENCES

- [1] S. S. Lucky, K. C. Soo, Y. Zhang, Chem. Rev. 115, 1990-2042 (2015)
- [2] M. Matijević, Nakarada, Đ. Liang, X. et al. J. Nanoparticle Res. 22, 1–12 (2020).
- [3] Nešić, M. Žakula, J; Stepić, M. et al. J. Photochem. Photobiol. A Chem. 347, 55–66 (2017).
- [4] Nešić, M. Popović, I. Leskovic, A. Petković, M. BioMetals 29, 921–933 (2016).

## The use of Raman microspectroscopy for characterization of tumor and tumor margin cell populations

M. Lazarevic<sup>1</sup>, M. Milosevic<sup>1</sup>, M. Jaksic<sup>1</sup>, I. Pecinar<sup>2</sup> and J. Milasin<sup>1</sup>

<sup>1</sup>*School of Dental Medicine, University of Belgrade, Serbia*

<sup>2</sup>*Faculty of Agriculture, University of Belgrade, Serbia*

e-mail: milos.lazarevic@stomf.bg.ac.rs

**Introduction.** Squamous and basal cell carcinoma (SCC, BCC) are the most common cancers in the maxillofacial region. Both types of tumors remain a considerable medical challenge, despite important advances in treatment and diagnosis that occurred during the last decades. Finding new tools for a more reliable and timely diagnosis would be of substantial importance and would improve therapy outcome. Raman microspectroscopy has emerged as a promising technique for *in vitro* and *in vivo*, non-destructive detection and biochemical characterization of several types of cancer.

**Aim.** To compare Raman spectra of cells originating from oral squamous cell carcinoma (OSCC), basal cell carcinoma (BCC) and their surgical margins (SM), with the aim of evaluating the ability of Raman spectroscopy to detect differences between the two types of neoplasms and their surgical margins, as well as between tumor cells and control cells.

**Methods.** OSCC, BCC and SM cell cultures were generated. The cells from the 3<sup>rd</sup> passage were used for the experiment. After passing and counting cells,  $1 \times 10^6$  cells of each culture was separated in centrifuge tubes in culture medium. After centrifugation, the precipitate was transferred without fixation directly to a gold microscope plate for Raman microspectroscopy. Raman signals were obtained by the HORIBA Jobin Yvon Xplora spectromicroscopic apparatus (HORIBA Jobin Yvonne S.A.S., Villeneuve-d'Ascq, France) equipped with microscope BKS51 (Olympus, Tokyo, Japan). Laser diode at a wavelength of 785 nm and power of 90 mW, magnification of 100x, focus size of 2  $\mu\text{m}$  and a time exposure of 100s was used. CCD camera (Syncerity, HORIBA Scientific, Edison, New Jersey, USA) was used for spectrum recording. All cell samples were recorded 30 times, by random selection of points. Raman cell spectra were observed in the range of 400-2600  $\text{cm}^{-1}$ . Acquisition of Raman spectra was performed using LabSpec 6 software (HORIBA Jobin Yvon S.A.S., Villeneuve-d'Ascq, France).

**Results.** The study showed considerable similarities between the spectra of the tumors cells and their respective margins and controls. However, differences of Raman spectra between the different cells cultures could be observed as well. Analysis of BCC Raman spectrum showed high levels of type I collagen, amino acids proline, hydroxyproline and valine (921-984  $\text{cm}^{-1}$ ) as well as amide III (peak 1238  $\text{cm}^{-1}$ ). The intensity of the 1635  $\text{cm}^{-1}$  peak indicates an increased amount of protein and lipids in tumor cells compared to margin cells. The analysis of OSCC showed that amide peak (1242  $\text{cm}^{-1}$ ) was more prominent in tumor cells than in margins; similarly, the amount of protein and lipids (peaks 1433 and 1648  $\text{cm}^{-1}$ ) was higher in tumor cells than in margin cells. On the other hand, DNA / RNA levels (peak 781  $\text{cm}^{-1}$ ) were higher in surgical margins.

**Conclusion.** The analyzed tumor, tumor margin, and control cells displayed remarkable similarities, with however occasional differences sufficient to distinguish normal from cancer cells.

## First glance at a multitude of ion currents on filamentous fungus *P. blakesleeanus* protoplasts obtained by femtosecond laser microsurgery

M. Zivic<sup>1</sup>, K. Stevanovic<sup>1</sup>, T. Pajic<sup>1</sup>, M. D. Rabasovic<sup>2</sup>, A. Krmpot<sup>2</sup>, N. Todorovic<sup>3</sup>

<sup>1</sup>University of Belgrade - Faculty of Biology, Serbia

<sup>2</sup>Institute of Physics, Belgrade, Serbia

<sup>3</sup>Institute for Biological Research "Sinisa Stankovic, University of Belgrade, Serbia

e-mail:mzivic@bio.bg.ac.rs

Electrophysiology of cell membrane ion channels in filamentous fungi, unlike that in yeast, plant and animal cells is still in its infancy. The only two reports on single channel patch clamp recordings from native cell membrane of filamentous fungi were made on protoplasts obtained after cell wall microsurgery with UV pulsed laser more than 20 years ago [1, 2]. Both pioneering papers reported fairly high success rates of obtaining gigaohm contacts, but neither was followed by more studies. Advanced imaging techniques that enable more controllable surgery process and utilizing the femtosecond pulses, after optimizing the protocol, could result in minimally damaging cell wall microsurgery. The end result would be reproducibly high quality membrane of "de-walled" protoplasts. The membrane quality, property that is of utmost importance for application of patch clamp method, is a term describing not only mechanical integrity and cleanliness of the membrane, but the physiological fitness of the cell as well, as cells about to enter apoptosis or necrosis, or that were subjected to oxidative stress do not have it.

We are presenting here, to the best of our knowledge, the first electrophysiological snapshot obtained on filamentous fungi protoplast after cell wall removal by a femtosecond laser microsurgery. Utilization of the Ti:Sa femtosecond laser with optimizations of the cell wall microsurgery protocol explained in [3], this conference, resulted in protoplasts that were prone to form contacts of high electrical resistance ( $G\Omega$ ) with a patch pipette. Ti:Sa laser operating at 730 nm (76 MHz, 160 fs pulse duration) combined with homemade nonlinear laser scanning microscope, physiological 40x 1.0 NA objective was employed for microsurgery and imaging. Standard patch-clamp set up was used for electrophysiology. In single channel recordings from more than 30 patches, 11 different channel types were distinguished, based on the reversal potential in asymmetric ionic conditions and on the conductance. By far, the most frequent types of conductance were anionic. We have found four groups of ion channel currents, based on ion selectivity:

1. Unselective anion currents (not discriminating between chloride and glutamate) 44% of all recorded currents.
2. Anionic currents selective for chloride (carried exclusively or mostly by chloride) 35%.
3. Organic acid permeable anionic currents (discriminating for glutamate over chloride) 17%;
4. Calcium cationic current was recorded once.

The range of conductance size (g) was variable, with unselective anionic currents encompassing the smallest (5 pS) and largest (160 pS) recorded conductances. Calcium conductance was small (6 pS), while organic acid conductances and Cl<sup>-</sup>-selective conductances had similar ranges (10-60 pS). Most of the conductances displayed linear current-voltage relationships.

### REFERENCES

- [1] SK. Roberts, GK. Dixon, SJ. Dunbar and D. Sanders. *New Phytol.* 137, 579 (1997).
- [2] AA. Véry, JM. Davies. *Appl Environ Microbiol.* 64,1569 (1998).
- [3] K. Stevanovic, et al. <http://www.photonica.ac.rs/> (2021)

## Surface roughness and topography of dentin characterized by AFM

N. Pecikozić<sup>1</sup>, T. Lainović<sup>1</sup>, L. Blažić<sup>1,2</sup>, Z. Bobić<sup>3</sup>, P. Terek<sup>3</sup>, B. Škorić<sup>3</sup>

<sup>1</sup>Faculty of Medicine Novi Sad, University of Novi Sad, Serbia

<sup>2</sup>Dental Clinic of Vojvodina, Novi Sad, Serbia

<sup>3</sup>Faculty of Technical Sciences, University of Novi Sad, Serbia

e-mail:nevena\_pecikozić@uns.ac.rs

Dentin is a mineralized tissue constituent of a human tooth, which, in addition to the mineral component, contains an organic matrix organized into tubules, surrounded by the peritubular and intertubular dentin. Various dental treatments lead to changes in dentinal surface properties. Contemporary adhesive dental procedures consider dentinal etching by using the orthophosphoric acid to remove a smear layer and to open dentinal tubules to achieve conditions for adequate adhesion of the restorative material [1].

Atomic force microscopy (AFM) is proven as a valuable tool for characterizing the dentinal surface at the nanoscale after any chosen dental conventional or experimental surface treatment methods [2]. It can be used after different chemical treatments, as well as after physical methods used for surface preparation, such as conventionally or experimentally used lasers for dental treatment.

This study aimed to analyze the influence of conventional phosphoric acid treatment on dentinal surface topography and 3D roughness parameters using AFM.

The intact mandibular canine, extracted for orthodontic reasons, was cut into horizontal slices using a diamond saw disk. The samples were etched with orthophosphoric acid for 15 seconds and stored in a moist medium until examination. The structure of the dentin was examined by Veeco CP-II Atomic Force Microscope. Sample's surface was scanned in contact mode with symmetrically etched silicon tip at 0.5 Hz scan rate. Areas of  $20\ \mu\text{m} \times 20\ \mu\text{m}$  were scanned with resolution of  $256 \times 256$  pixels. The obtained topography data were processed by image analysis software (SPIP, Image metrology) and the following 3D roughness parameters were obtained: average surface roughness (Sa), root mean square height (Sq), maximum height (Sz), and surface skewness (Ssk).

Topography of dentinal surface will be presented by AFM 3D images. The Sa parameter of acid-etched dentin was 246.53 nm, and the  $Sq=307.23$  nm,  $Sz = 2047.8$  nm – presenting the existence of deep open tubular structures. The Ssk parameter had mainly negative values (-0.431), which indicates a negative surface dominated with holes which could be considered as a favourable functional surface property for better load-bearing and adhesive-lubrication properties.

AFM is a valuable tool for quantitative functional roughness characterization and 3D presentation of the dentinal topography. The results presented in this study could be used as reference measurements, since the AFM could be used in determination of dentinal surface changes after different experimental laser treatments, or following the cold atmospheric plasma (CAP) surface modification, since CAP is a promising experimental method used in dental medicine research. Future perspectives offer potential new possibilities of “site-matching” analysis, giving the parallel 3D imaging and chemical fingerprinting on certain areas of interest by means of AFM-IR, which is a perspective of our further research.

### REFERENCES

- [1] Pelin I.M, Piednoir A, Machon D, Farge P, Pirat C, Ramos S.M.M. Adhesion forces between AFM tips and superficial dentin surface. *J Colloid Interface Sci.* 2012;376:262-8.
- [2] Kubinek R, Zapletalova Z, Vujtek M, Novotny R, Kolar H, Chmelickova H. Examination of dentin surface using AFM and SEM. In: Méndez-Vilas A, Diaz J, editors. *Modern Research and Educational Topics in Microscopy*. Badajoz, Spain: Formatex; 2007. p.593-8.

## Secondary structure of *Ginkgo biloba* chlorophyll catabolites by circular dichroism spectroscopy

N. Djapic<sup>1</sup>

<sup>1</sup>University of Novi Sad, Technical Faculty "Mihajlo Pupin"

Zrenjanin, Serbia

e-mail:nidjapic@gmail.com

Circular dichroism (CD) spectroscopy is an experimental technique used in the characterization of chiral molecules in solution. This technique measures the differential absorption of molecules to left- and right-handed circularly polarized light (CPL) excitation, permitting the characterization of the biomolecules' secondary structure. It is used to determine the enantiopurity of pharmaceutical drugs and natural products [1, 2].

*Ginkgo biloba* chlorophyll catabolites exhibit the electronic absorption (UV/VIS) and circular dichroism (CD). The absorption bands correlate with the macrocyclic chromophores and are optically active, exhibiting Cotton effects in the optical rotatory dispersion (ORD). The *Ginkgo biloba* chlorophyll catabolite epimers show virtually identical UV/VIS spectra, while their CD spectra are to a great extent different. The molar extinction coefficients of the epimers are unequal in circularly polarized light. These differences in absorption were measured as a function of wavelength, and the obtained were CD curves. Half of them had positive, the other negative signs (Cotton effect) to an equal degree as for ORD curves.

The recorded UV/VIS, CD and proton magnetic resonance (<sup>1</sup>H NMR) spectra for *Ginkgo biloba* chlorophyll catabolites were analyzed in detail. Found were the differences in configurations on two carbon atoms. Those differences were evident in the <sup>1</sup>H NMR spectra. The differences in the CD bands and epimer configuration can only be proposed.

### REFERENCES

[1] L. D. Barron, *Molecular Light Scattering and Optical Activity*, 2<sup>nd</sup> ed.; Cambridge University Press, 2004.

[2] H. Wolf, H. Scheer, *Ann. N. Y. Acad. Sci.* 206, 549 (1973).

## **Altered organization of collagen fibers in the uninvolved human colon mucosa 10 cm and 20 cm away from the colorectal cancer**

S.Despotović<sup>1</sup>, Đ. Milićević<sup>2</sup>, A. Krmpot<sup>3</sup>, A. Pavlović<sup>4</sup>, V. Živanović<sup>4</sup>, Z. Krivokapić<sup>5</sup>, V. Pavlović<sup>6</sup>, S. Lević<sup>6</sup>, G. Nikolić<sup>7</sup>, M. D. Rabasović<sup>3</sup>

*1 University of Belgrade, Faculty of Medicine, Institute of Histology and embryology, Belgrade, Serbia*

*2 Saarland University, Department of Internal Medicine V- Pulmonology, Allergology, Intensive Care Medicine, Homburg/Saar, Germany*

*3 University of Belgrade, Institute of Physics Belgrade, Belgrade, Serbia*

*4 University Hospital Center "Dr Dragiša Mišović Dedinje", Belgrade, Serbia*

*5 Clinic for Abdominal Surgery- First surgical clinic, Clinical Center of Serbia, Belgrade, Serbia*

*6 University of Belgrade, Faculty of Agriculture, Belgrade, Serbia*

*7 University of Belgrade, Faculty of Medicine, Institute of Pathology, Belgrade, Serbia*

e.mail: sanjadesp@gmail.com

Remodelling of collagen fibers has been described during every phase of cancer genesis and progression. Changes in morphology and organization of collagen fibers contribute to the formation of microenvironment that favors cancer progression and development of metastasis. However, there are only few data about remodelling of collagen fibers in healthy looking mucosa distant from the cancer. Using SHG imaging, scanning electron microscopy (SEM) and specialized softwares (CT-FIRE, CurveAlign and FiberFit), we objectively visualized and quantified changes in morphology and organization of collagen fibers. SHG polarization anisotropy was used to quantify alignment of collagen molecules inside fibers. Using immunohistochemistry (staining with anti-alphaSMA, anti-LOX, anti-MMP2 and anti-MMP9) we investigated possible causes of collagen remodelling (change in syntheses, degradation and collagen cross-linking) in the colon mucosa 10 cm and 20 cm away from the cancer in comparison with healthy mucosa. We showed that in the lamina propria this far from the colon cancer, there were changes in collagen architecture (width, straightness, alignment of collagen fibers and collagen molecules inside fibers), increased representation of myofibroblasts and increase expression of collagen-remodelling enzymes (LOX and MMP2). Thus, the changes in organization of collagen fibers, which were already described in the cancer microenvironment, also exist in the mucosa far from the cancer, but smaller in magnitude.

### REFERENCES:

- [1] S. Despotović, Đ. Milićević, A. Krmpot et al. Sci Rep 10, 6359 (2020).
- [2] M. Rabasović et al. J Biomed Opt 20, 016010 (2015).

## Label-free Third Harmonic Generation Imaging of Lipid Droplets in Live Filamentous Fungi

T. Pajić<sup>1</sup>, N. Todorović<sup>2</sup>, M. Zivić<sup>1</sup>, M. D. Rabasović<sup>3</sup>, A.H.A. Clayton<sup>4</sup>, and A. Krmpot<sup>3</sup>

<sup>1</sup>University of Belgrade – Faculty of Biology, Belgrade, Serbia

<sup>2</sup>Institute for Biological Research “Siniša Stanković”, University of Belgrade, Serbia

<sup>3</sup>Institute of Physics, Belgrade, Serbia

<sup>4</sup>Optical Sciences Centre, Swinburne University of Technology, Victoria, Australia

e-mail:tpajic@bio.bg.ac.rs

Oleaginous fungi can accumulate significant amounts of lipids in their mycelium (up to 80% of their biomass), primarily in the form of lipid droplets (LDs). LDs have optical properties that differ from the surrounding aquatic environment, which causes sudden changes in the refractive index. Here, we present *in vivo* and label-free imaging of individual hyphae of the oleaginous filamentous fungus *Phycomyces blakesleeanus* by Third Harmonic Generation (THG) microscopy method [1], where LDs are the main source of contrast [2] (Figure 1). The LDs quantification from THG images was performed by two image analysis techniques: Image Correlation Spectroscopy (ICS) and software particle counting – Particle Size Analysis (PSA). ICS measures the spatial variation of fluorescence intensity fluctuations in the images, which can then be related to particle density and aggregation state. In order to test and compare the two methods, we used hyphae that undergo nitrogen starvation, which is known to cause alterations in lipid metabolism and the increase in LDs number.

For *in vivo* THG imaging of label-free, > 24-hour old hyphae, we used 1040 nm, 200 fs pulses from Yb KGW laser. Detection was performed in the transmission arm by PMT through Hoya glass UV filter with peak transmission at 340nm. The laser beam was focused with the Zeiss Plan Neofluar 40x1.3 objective lens. For the imaging, the fungi were placed between two cover glasses of 0.17  $\mu\text{m}$  thickness to match the objective lens requirements and for better transmission of the THG signal.

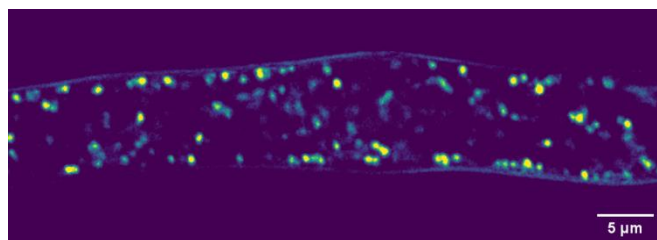


Figure 1. THG image of lipid droplets in hyphae of the fungus *Phycomyces blakesleeanus*. The bright objects are lipid droplets.

An increased number of LDs under nitrogen starvation was observed in THG images and their number and size were analyzed using two quantification methods. The comparison of LDs number and size obtained by ICS and PSA shows that the number of LDs is approximately the same on average, but that ICS consistently detects slightly larger LD number in older group. The mean ICS measured diameter was slightly lower. Using the THG method *in vivo* and label-free, we can accurately and reliably, over time, detect changes in the localization, total number, and size of LDs in hyphae of the oleaginous filamentous fungus *Phycomyces blakesleeanus*.

Acknowledgement: Project HEMMAGINERO, No. 6066079 from Program PROMIS, Science Fund of the Republic of Serbia, and Project „Minimally invasive, selective ablation of dental caries by femtosecond laser “Move for the science/2019

### REFERENCES

[1] R. W. Boyd, Academic Press (2008).

[2] D. Débarre, W. Supatto, A. M. Pena, A. Fabre, T. Tordjmann, L. Combettes, E. Beaurepaire, *Nature Methods*, 3(1), 47–53. (2006).

## Nonlinear Imaging of Dentin-Adhesive Interface Treated by Cold Atmospheric Plasma

T. Lainović<sup>1</sup>, A. Krmpot<sup>2</sup>, M. D. Rabasović, N. Selaković, I. Plešić<sup>1</sup>, L. Blažić<sup>1,3</sup>, N. Škoro<sup>2</sup>, N. Puač<sup>2</sup>

<sup>1</sup>*Faculty of Medicine, School of Dental Medicine, University of Novi Sad, Novi Sad, Serbia*

<sup>2</sup>*Institute of Physics, University of Belgrade, Belgrade, Serbia*

<sup>3</sup>*Dental Clinic of Vojvodina, Novi Sad, Serbia*

e-mail: [tijana.lainovic@mf.uns.ac.rs](mailto:tijana.lainovic@mf.uns.ac.rs)

The Nonlinear Laser Scanning Microscopy (NLSM) could be considered as a useful tool for the analysis of hard dental tissues, and tissue-material interfaces in dental medicine. Two-photon excitation fluorescence microscopy (TPEF) is able to detect the two-photon excited autofluorescence of dental tissues, and the second harmonic generation (SHG) can detect second-order nonlinear susceptibility of collagen type I, the most abundant dentinal organic substance [1,2].

The objective of this study was to microscopically test the effect of Cold Atmospheric Plasma (CAP) [3,4] on the morphology of the dentin-adhesive interface, using NLSM.

Human molar teeth were cut in half for the CAP-treated and control samples. The influence of CAP on standard etch-and-rinse (ER) or self-etch (SE) procedures was investigated. The following CAP configurations were used: feeding gas He, gas flow 1 slm, deposited power in the plasma power input 1 W or 2 W, and tip-to-surface distance 2 mm or 4 mm. The CAP-treated ER group was firstly etched and treated by CAP, before adhesive application. The SE group was treated by CAP before the adhesive placement. The control groups underwent the same process omitting the CAP phase. NLSM was used to image the morphology of hybrid layers.

The results demonstrated that the CAP causes the removal of the smear layer and opens the tubules. The tubules are not only more open but changed by CAP regarding their surface properties so that the permeation of the adhesive is highly favored. Compared to the control groups of around 20-30  $\mu\text{m}$  hybrid layers, the length of resin tags in the CAP treated ER group was measured to even up to 600  $\mu\text{m}$ , and in the CAP-treated SE group they were extended up to 100  $\mu\text{m}$ .

CAP treatment of dentin drastically changes the morphology of the hybrid layer and the extension of resin tags. There is a need for additional analysis in the field to examine the influence of these changes on the quality of the dentin-adhesive interface.

Acknowledgment: Supported by the Ministry of Education, Science and Technological Development of Republic of Serbia (under contract No. NIO 200114 and No. 451-03-68/2021-14/200024), Project HEMMAGINERO, No. 6066079 from Program PROMIS, Science Fund of the Republic of Serbia and by the program "Start up for science. Explore. Make a change.", Funded by Leadership Development Center, Phillip Morris for Serbia, 2019.

### REFERENCES

- [1] T. Lainović, J. Margueritat, Q. Martinet, X. Dagany, L. Blažić, D. Pantelić, M.D. Rabasović, A.J. Krmpot and T. Dehoux, *Acta Biomater* 105, 214-222 (2020).
- [2] T. Cloitre, I.V. Panayotov, H. Tassery, C. Gergely, B. Levallois and F.J.G. Cuisinier, *J Biophotonics* 6, 330-337 (2013)
- [3] J.N. Stašić, N. Selaković, N. Puač, M. Miletić, G. Malović, Z.Lj. Petrović, D.N. Veljović and V. Miletić, *Clin Oral Invest* 23, 1383–1396 (2019).
- [4] A. Stancampiano, D. Forgione, E. Simoncelli, R. Laurita, R. Tonini, M. Gherardi and V. Colombo, *J Adhes Dent* 21, 229-237 (2019).

## **5. Devices and components**

## Modeling of intersubband transitions in ZnO/ZnMgO Coupled Quantum Wells

A. Atić<sup>1,2</sup>, J. Radovanović<sup>2</sup>, N. Vuković<sup>2</sup>  
<sup>1</sup>Vinča Institute of Nuclear Sciences, Belgrade Serbia  
<sup>2</sup>School of Electrical Engineering,  
 University of Belgrade, Serbia  
 e-mail:atic@vin.bg.ac.rs

In recent years ZnO has become a popular semiconductor with many potential applications in infra-red and THz optical devices owing to a wide direct bandgap (3.4 eV) in combination with relatively high exciton binding energy (60 meV) [1]-[2]. In this work, we model the electronic structure of coupled oxide-semiconductor quantum wells by numerically solving the system of coupled Schrödinger-Poisson equations self-consistently (Fig. 1). We compare the obtained results with the recent experimental data [3] and analyze how the variation of the layers' thicknesses affects the energy states. In addition, we examine the influence of doping to assess the differences between single well and two wells' cases, for the purpose of designing more complex multi-well optical system in the future.

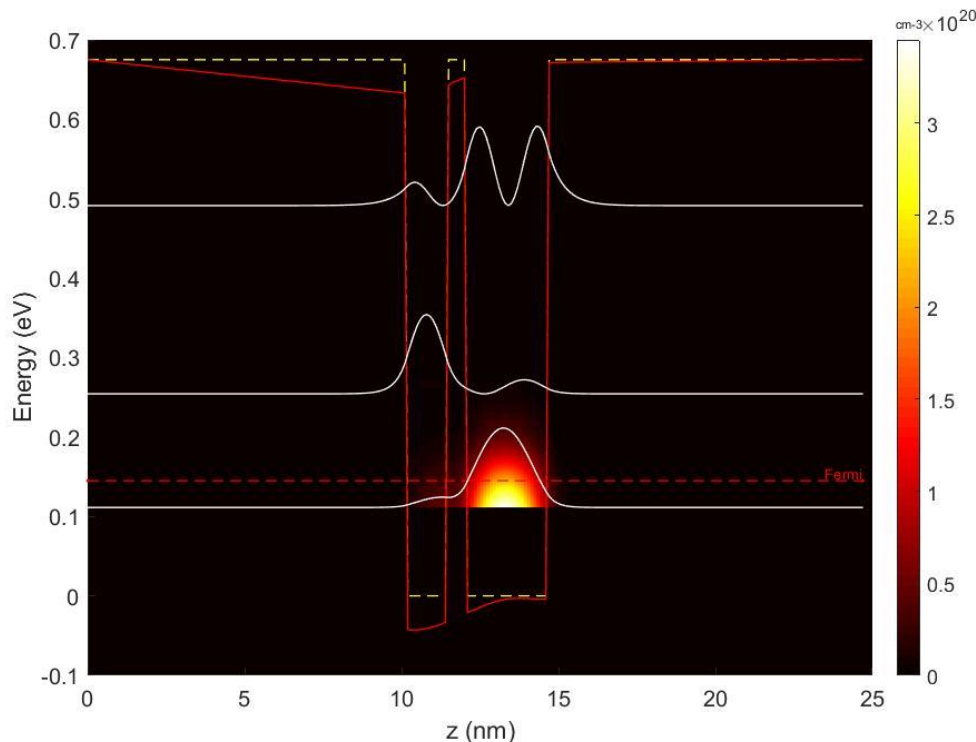


Fig 1. Calculated conduction band of a double well ZnO/ZnMgO structure, together with wavefunctions squared, for a structure with 0.5 nm thick barrier at room temperature (300 K) with uniform layer doping  $n \cong 10 \times 10^{18} \text{ cm}^{-3}$  [3].

### REFERENCES

- [1] M. Belmoubarik, K. Ohtani, and H. Ohno, "Intersubband transitions in ZnO multiple quantum wells," *Appl. Phys. Lett.*, 2008.
- [2] N. Le Biavan *et al.*, "Homoepitaxy of non-polar ZnO/(Zn,Mg)O multi-quantum wells: From a precise growth control to the observation of intersubband transitions," *Appl. Phys. Lett.*, 2017.
- [3] B. Meng *et al.*, "Observation of Intersubband Absorption in Zn O Coupled Quantum Wells," *Phys. Rev. Appl.*, 2019.

## Surface recombination influence on photocurrent spectra of organic photovoltaic devices

Ali R. Khalf<sup>1</sup>, Jovana P. Gojanović<sup>1</sup>, Sandra Živanović<sup>2</sup>

<sup>1</sup>School of Electrical Engineering, University of Belgrade, Serbia

<sup>2</sup>Institute for Micromanufacturing, Louisiana Tech University, Ruston, LA 71272, USA

e-mail: alirkhalf@yahoo.com

Organic solar cells (OSCs) have attracted extensive attention in the past decade as one of the promising photovoltaic technologies offering unique advantages over their inorganic counterparts, such as lightweight, low cost, flexibility, semitransparency, and solution-processing fabrication [1]. The design of novel narrow-bandgap donor and acceptor materials, interface engineering, novel processing methods, innovative device structures, and light management led to a significant improvement in power conversion efficiency (PCE), which exceeded 17% for single bulk heterojunction devices [2]. Still, the full photoconversion potential of these devices has not been reached because of the unresolved OSCs physics and the lack of adequate physical models describing devices' operation.

It was established that surface processes, particularly a surface recombination as the loss mechanism have tremendous influence on the OSCs performance [3]. It is of a great importance to distinguish between the influence of the majority and minority carriers surface recombinations. Also, the impact of surface recombination (of majorities and minorities) is not identical at the anode and cathode contact, since the device is illuminated through the one of them. The surface recombination effects differ for the front and back electrode. The comprehensive study of surface recombination effects can be conducted through photocurrent spectra (PCS) analysis.

In this paper, a standard drift-diffusion model (DDM) that accounts for surface recombination and thermionic emission on electrode contacts through boundary conditions was used for PCS calculation [3]. The photogeneration rate profile in the photovoltaic device was determined from the Beer-Lambert law. The PCS were simulated for three cases: 1) electron dominated transport, (assuming electron mobility  $\mu_n$  is much larger than hole mobility  $\mu_p$ ), 2) balanced transport ( $\mu_n \sim \mu_p$ ), and 3) hole dominated transport ( $\mu_n \ll \mu_p$ ). For each type of transport, the effect of minority and majority carriers surface recombination at the anode and cathode was considered. This was done by taking the appropriate surface recombination velocity (SRV) to be reduced while other SRVs were assumed to tend to infinity. A detailed analysis of the obtained results was performed by taking into account different penetration depths for different light wavelengths which were determined from absorption coefficient spectrum. Also, the interplay between the bulk and surface recombination was considered, having in mind that the influence of the bulk recombination is significantly reduced at high reverse bias voltages, making the effects of surface recombination visible in the simulated PCS. In the zero-biased devices, the bulk recombination is almost completely dominant compared to the surface recombination.

The measured PCS for ITO/PEDOT:PSS/P3HT:PCBM/Al devices with eight different thicknesses of active P3HT:PCBM layer were compared to the ones calculated by described DDM. Excellent match between theory and experiment was accomplished indicating that there was no pronounced surface recombination in the fabricated devices.

### REFERENCES

- [1] J. Gao, J. Wang, C. Xu, Z. Hu, X. Ma, X. Zhang, L. Niu, J. Zhang, F. Zhang, "A Critical Review on Efficient Thick-Film Organic Solar Cells", *Sol. RRL*(2020), 2000364 (1–26).
- [2] Q. Liu, Y. Jiang, K. Jin, J. Qin, J. Xu, W. Li, J. Xiong, J. Liu, Z. Xiao, K. Sun, S. Yang, X. Zhang, L. Ding, "18% efficiency organic solar cells", *Science Bulletin* 65, 272–275 (2020).
- [3] A. Khalf, J. Gojanović, N. Ćirović, S. Živanović, "Two different types of S-shaped J-V characteristics in organic solar cells", *Optical and Quantum Electronics* 52, 121 (2020).

## Measuring the Spectrally-Resolved Linewidth Enhancement Factor

Florian Pilat<sup>1</sup>, Nikola Opačak<sup>1</sup>, Dmitry Kazakov<sup>1,2</sup>, Sandro Dal Cin<sup>1</sup>, Georg Ramer<sup>3</sup>, Bernhard Lendl<sup>3</sup>, Federico Capasso<sup>2</sup>, Gottfried Strasser<sup>1</sup> and Benedikt Schwarz<sup>1,2</sup>

<sup>1</sup> Institute of Solid State Electronics, TU Wien, Gusshausstrasse 25-25a, 1040 Vienna, Austria

<sup>2</sup> John A. Paulson School of Engineering and Applied Sciences, Harvard University, Cambridge, Massachusetts

<sup>3</sup> Institute of Chemical Technologies and Analytics, TU Wien, Getreidemarkt 9/164, A 1060 Vienna, Austria

e-mail: florian.pilat@tuwien.ac.at

Semiconductor frequency comb lasers are gaining more and more attention in the last two decades due to their various applications such as high-precision spectroscopy for medical and chemical sensing. The devices are compact and electrically pumped - ideal for miniaturization and integration. The linewidth enhancement factor (LEF) plays a key role in the description of these devices and understanding the dynamic processes like laser linewidth broadening, modulation response and frequency comb formation [1]. Therefore, knowing its value in a real device is of utmost importance. However, as of yet, experimental schemes to determine the LEF were limited to measurements below the lasing threshold or single-mode laser operation. Here we present a novel and universally applicable modulation technique, capable of measuring the LEF of a laser source during operation [2]. For a frequency comb we can infer the LEF over the whole laser spectrum, for each comb mode, in a single-shot measurement. The technique utilizes “Shifted Wave Interference Fourier Transform Spectroscopy” (SWIFTS), a phase-sensitive measurement scheme [3]. Fig. 1a shows a sketch of the experimental setup.

Extensive Maxwell-Bloch simulations are applied to investigate the theoretical model [4]. Then an experimental demonstration is performed on a quantum cascade laser frequency comb. The frequency comb spectrum and the corresponding extracted LEF values are depicted in Fig. 1b.

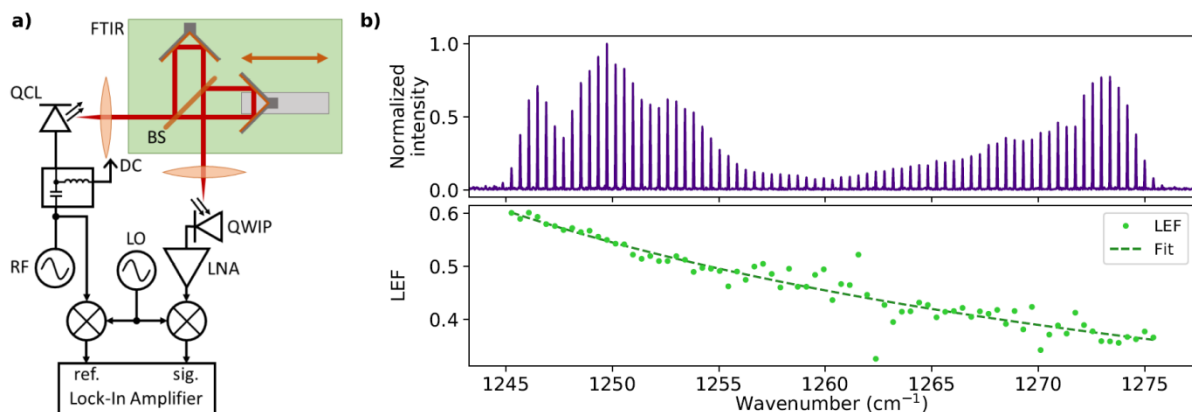


Figure 1. a) Sketch of the experimental setup, b) Intensity spectrum of the laser frequency comb (top), Spectrally-resolved LEF for each comb mode with fit (bottom).

### REFERENCES

- [1] M. Osinski et al, “Linewidth broadening factor in semiconductor lasers: An overview”, IEEE J. Quant. Electron., (1987)
- [2] N. Opačak et al, “Spectrally resolved linewidth enhancement factor of a semiconductor frequency comb”, arXiv:2104.05747 [physics.optics], (2021)
- [3] D. Burghoff et al, “Terahertz laser frequencycombs,” Nat. Photonics, (2014)
- [4] N. Opačak et al, “Theory of Frequency-Modulated Combs in Lasers with Spatial Hole Burning, Dispersion, and Kerr Nonlinearity”, Phys. Rev. Lett., (2019)

## Interband cascade lasers: overcoming intersubband transitions in the valence band

H. Knötig<sup>1</sup>, R. Weih<sup>2</sup>, N. Opacak<sup>1</sup>, S. Höfling<sup>3,4</sup>, J. Koeth<sup>2</sup>, G. Strasser<sup>1</sup> and B. Schwarz<sup>1</sup>

<sup>1</sup>Institute of Solid State Electronics and Center for Micro- and Nanostructures, TU Wien, Vienna, Austria

<sup>2</sup>nanoplus Nanosystems and Technologies GmbH, Gerbrunn, Germany

<sup>3</sup>Physikalisches Institut and Wilhelm Conrad Röntgen-Research Center for Complex Material Systems, University Würzburg, Germany

<sup>4</sup>SUPA, School of Physics and Astronomy, University of St Andrews, United Kingdom

e-mail:hedwig.knoetig@tuwien.ac.at

Interband cascade lasers (ICLs) [1] are gaining increasing attention as reliable laser sources in the mid-infrared spectral region. They are especially valued due to their low threshold current densities and low power consumption. Continuous-wave (cw) operation at room temperature has been demonstrated at wavelengths from 2.8-5.6  $\mu\text{m}$  in the GaSb material system [2,3] with a performance sweet spot around 3-4  $\mu\text{m}$ . However, extending this range towards longer wavelengths has proven difficult for ICLs, partly originating in a still insufficient understanding of the internal device physics.

Here, we present our recent results on the impact of intersubband absorption in the valence band on the performance of ICLs. We use a numerical model employing the eight-band  $k\cdot p$  method to calculate the wavelength-dependent intersubband absorption in the W-quantum well (QW) of the ICL active region. The calculated electronic band structure of an exemplary W-QW is shown in Figure 1. Here, we use a generalized momentum matrix element model, which can explain all contributions to the absorption in the W-QW, regardless of being interband or intersubband transitions.

We experimentally observe a clear performance dependence on the thickness and composition of the  $\text{Ga}_{1-x}\text{In}_x\text{Sb}$  hole- QW, reflecting in the characteristic temperature  $T_0$  as well as the threshold current density  $J_{\text{th}}$ , which is supported by our model. By careful design of the active W-QW the intersubband absorption in the valence band can be tailored and even completely avoided, allowing us to enhance ICL performance outside of the sweet spot 3-4  $\mu\text{m}$  region, paving the way towards higher cw operating temperatures and output powers.

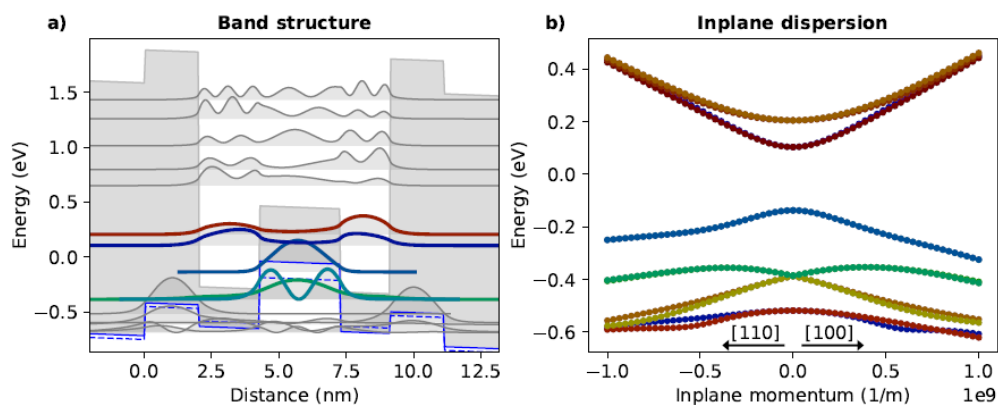


Figure 1. a) Calculated band structure at the  $\Gamma$ -point of an exemplary W-QW consisting of AlSb/InAs/Ga<sub>0.65</sub>In<sub>0.35</sub>Sb/InAs/AlSb layers. b) Same band structure in dependence on wave vector  $k$

### REFERENCES

- [1] J.R. Meyer et al., Photonics 7, 75 (2020).
- [2] J. Scheuermann et al., Applied Physics Letters 106, 161103 (2015).
- [3] W.W. Bewley et al., Optics Express 20, 3235 (2012).

## Bend-free photonic integrated circuits with the crosstalk as a resource

J. Petrovic<sup>1,2</sup>, J. Krsic<sup>2</sup>, J.J.P Veerman<sup>3</sup>, A. Maluckov<sup>2</sup>

<sup>1</sup>*Institut für Optik und Atomare Physik, Technische Universität Berlin, Germany*

<sup>2</sup>*"VINCA" Institute of Nuclear Sciences, University of Belgrade, Serbia*

<sup>3</sup>*Fariborz Maseeh Department of Mathematics and Statistics, Portland State University, Portland, OR, USA*

e-mail: jovana.petrovic@tu-berlin.de

We challenge the current thinking and approach to design of photonic integrated circuits (PICs), which are marked as drivers of the future information processing.

Standard quantum PICs are composed of the unit cells based on directional couplers. The couplers typically consist of two waveguides bent to exhibit coupling in the proximity region. They conveniently produce the maximally entangled Bell state and have been used to construct functional optical quantum PICs [1]. However, their full exploitation faces the conceptual and technical challenges including the non-intrinsic scalability that requires waveguide branching, the radiation loss at waveguide bends and the therewith associated high-density packaging limit [2].

Arrays of linearly coupled parallel waveguides have been considered a viable alternative. However, the intricate inverse design of the corresponding Hamiltonians has limited their applications to the particular instances of the quantum logic gates obtained by numerical optimization procedures and machine learning [3, 4] and the simulators of the condensed matter systems, such as spin and Bloch arrays with the Wannier-Stark ladder spectrum [5]. A generic design solution based on a common physical and mathematical principle has not been reached.

We propose a new concept for the design of bend-free high-density PICs composed exclusively of the linearly coupled *commensurable* waveguide arrays (CWGA). Their operation is based on the *periodic continuous quantum walk of photons* and leverages on the engineered waveguide coupling. We discuss the class of analytically accessible designs with the eigenspectra that randomly sample the Wannier-Stark ladder [6, 7]. *The free choice of eigenfrequencies marks a clear distinction from the current photonic simulators and provides a variety of novel circuit layouts and functionalities.* In particular, we rework the designs of interconnects for qubits and qudits, multiport couplers, entanglement generators and interferometers. The analytical results are corroborated numerically. Finally, we test the robustness of the proposed building blocks to the random variations in design parameters, with a view to defining acceptable fabrication tolerances.

### REFERENCES

- [1] J. Wang, et al. *Science* 360, 285 (2018).
- [2] W. Song, et al., *Nat. Commun.* 6, 2027 (2015).
- [3] Y. Lahini, et al., *npj Quantum Inf.* 4, 2 (2018).
- [4] A. Youssry, et al., *Quant. Sci. Technol.* 5, 025001 (2020).
- [5] M. Gräfe, A. Szameit, *J. Phys. B: Atom. Mol. Opt. Phys.* 53, 073001 (2020).
- [6] J. Petrovic, J. J. P. Veerman, *Ann. Phys.* 392, 128 (2018).
- [7] J. Petrovic, *Opt. Lett.* 40, 139 (2015).

## Influence of vacancy defects on electronic structure of graphene nanoribbons

J. R. Vlahović<sup>1</sup>, V. V. Arsoški<sup>1</sup>, M. V. Milošević<sup>2</sup>, M. Ž. Tadić<sup>1</sup>, and F. M. Peeters<sup>2</sup>

<sup>1</sup>*School of Electrical Engineering, University of Belgrade,  
P.O. Box 35 – 54, 11120 Belgrade, Serbia*

<sup>2</sup>*Department of Physics, University of Antwerp,  
Groenenborgerlaan 171, B – 2020 Antwerp, Belgium  
e-mail: jovana.vlaha@gmail.com*

Graphene emerges as a promising novel material for post-silicon electronic devices due to its excellent transport properties, such as ballistic conduction at room temperature and high carrier mobility [1]. The basic prerequisite for applications in field effect transistors is the existence of the band gap that enables a device to be switched between the off and on states. However, this criterion is not fulfilled for large single-layer graphene. Yet, it can be circumvented by patterning large graphene sheets into narrow-width nanoribbons [2]. As experimentally verified a common type of intrinsic defect in this graphene is vacancy [3] whose presence largely affects the nanoribbons electronic and magnetic properties [4]. A vacancy can take place at an arbitrary position in the crystal and arise due to high-energy electrons or ions [5]. It paves the way for engineering the electronic properties, such as the band-gap.

We theoretically investigate the electronic and transport properties of graphene nanoribbons with periodic defects. Modeling of the electron states was performed by using a single-particle tight-binding model. The limitations of the adopted model restrict our calculations to the case when the bonds due to atom removal are dangling. Hence, we do not consider bond reconstruction, which is an effect discovered in a recent experimental work [6]. Furthermore, the state-of-the-art nanoribbons manufacturing indicate that the vacancies positions can be efficiently controlled [5]. Therefore, we assume that vacancies are distributed periodically along a nanoribbon.

We found that the electronic structure is dependent on size, lateral position, and periodicity of vacancies. It in turn brings about the in-gap states, regardless of the type of edges. The local density of states in narrow-width zig-zag nanoribbons show that there is a strong coupling between the edge and defect states. Moreover, we show that the electronic and transport properties can be efficiently controlled by means of an applied in-plane electric field.

### REFERENCES

- [1] X. Du, I. Skachko, A. Barker, E.Y. Andrei, *Nat. Nanotechnol.* **3**, 491-495 (2008).
- [2] M. Y. Han, B. Özyilmaz, Y. Zhang, and P. Kim, *Phys. Rev. Lett.* **98**, 206805 (2007).
- [3] M. M. Ugeda, I. Brihuega, F. Guinea, and J. M. Gómez-Rodríguez, *Phys. Rev. Lett.* **104**, 096804 (2010).
- [4] M. Topsakal, E. Aktürk, H. Sevinçli, and S. Ciraci, *Phys. Rev. B* **78**, 235435 (2008).
- [5] K. Nordlund, J. Keinonen, and T. Mattila, *Phys. Rev. Lett.* **77**, 699 (1996).
- [6] Y. Zhang, S.-Y. Li, H. Huang, W.-T. Li, J.-B. Qiao, W.-X. Wang, L.-J. Yin, K.-K. Bai, W. Duan, and L. He, *Phys. Rev. Lett.* **117**, 166801 (2016).

## High-power diffraction-limited laser systems oscillating in middle infrared spectral range on strontium atomic self-terminating transitions

I. Kostadinov<sup>1</sup>, K. Temelkov<sup>1</sup>, B. Ivanov<sup>2</sup>, S. Slaveeva<sup>1</sup>, G. Yankov<sup>1</sup>

<sup>1</sup>*Institute of Solid State Physics, Bulgarian Academy of Sciences, 72 Tzarigradsko Chaussee, 1784 Sofia, BULGARIA*

<sup>2</sup>*Department of Chemical and Biomolecular Engineering, Vanderbilt University, 2201 West End Ave, Nashville, Tennessee, TN 37235, USA*  
e-mail: temelkov@issp.bas.bg

Efficient and precise laser ablation of soft and hard tissues with minimal thermal collateral damage with tunable laser sources delivering laser radiation at the wavelength 6.45  $\mu\text{m}$ , namely free electron lasers [1] and optical parametric oscillators [2], justifies great efforts made to improve the Sr vapor laser performance. A large-bore Sr vapor laser excited in a nanosecond pulsed longitudinal discharge is reported. The optimal discharge conditions for achieving a maximal average output power at several Sr atom and ion lines in the mid-IR spectral range are determined. High average output power of 29 W (at 25 kHz pulse repetition frequency) and laser pulse energy of 2.9 mJ (at 5 kHz pulse repetition frequency) are obtained at the multiline operation. These values are more than two times better than the ones achieved so far with a single-tube strontium or strontium halide vapor lasers.

Except for energy laser characteristics, efficiency and accuracy of high-precision microprocessing of various materials including biological tissues via laser ablation crucially depend on the laser beam quality, which is quantitatively determined with  $M^2$  (M-squared), so called beam propagation factor (or times-diffraction-limited factor). High-power diffraction-limited ( $M^2 = 1$ ) master oscillator–power amplifier (MO–PA) system is also developed and studied. A new optical arrangement is utilized for MO, as follows: two laser tubes are placed in a negative branch unstable resonator with magnification  $M = 17$ . First laser tube is with copper bromide and windows made of  $\text{CaF}_2$ . Laser oscillation at 510.6- and 578.2-nm copper atomic lines is used to visualize the optical path. The second laser tube is the actual MO with strontium. For spatial adjustment of the MO beam and the aperture of PA and spatial filtering, a mirror telescope with magnification  $M = 1.9$  and a 0.5-mm diaphragm in its confocal plane is also applied. A large-volume sealed-off gas-discharge tube for Sr vapor laser, which was studied with a stable cavity and was used as an amplifier in the MO–PA system in [3], had the a lifetime of several tens of hours that was definitely not satisfying. Using the MO laser tube construction ensuring 400-hour lifetime, a new sealed-off laser tube is developed and studied with a stable cavity and is applied as a power amplifier. For precise material processing laser beam is focused by an objective on samples, which are placed on X-Y stage. The MO–PA system is applied in microprocessing of quartz, glass, biological tissues, etc.

A compact mobile 5-15 W Sr vapor laser is also developed using all-solid-state power supply based on a new innovative bipolar excitation scheme.

**ACKNOWLEDGEMENTS:** This work was supported by the Project “Basic research and development of high-beam-quality high-power laser system oscillating in middle infrared spectral range” of Bulgarian National Science Fund under grant KP-06-H27/5.

### REFERENCES

- [1] J. M. Auerhammer, R. A. Walker, F. G. van der Meer, B. Jean, *Applied Physics B: Lasers and Optics* **68**, 111 (1999).
- [2] M. A. Mackanos, D. Simanovskii, K. M. Joos, H. A. Schwettman, E. D. Jansen, *Laser in Surgery & Medicine* **39**, 230 (2007).
- [3] I. K. Kostadinov, D. N. Astadjov, G. P. Yankov, L. T. Popova, S. I. Slaveeva, Yu. I. Fedchenko, and K. A. Temelkov, *Journal of Physics: Conference Series* **1859**, art. No. 012054 (2021).

## Fiber optic sensor system for intrusion location detection based on Sagnac interferometer

M. Vasiljevic Toskic<sup>1</sup>, L. Manojlovic<sup>2</sup>, J. Bajic<sup>1</sup>

<sup>1</sup>Faculty of technical sciences, University of Novi Sad, Novi Sad, Serbia

<sup>2</sup>Zrenjanin Technical College, Zrenjanin, Serbia

e-mail: markovt@uns.ac.rs

Sensors based on Sagnac interferometers have widespread usage in acoustic, temperature, acceleration, and strain sensing. Devices based on the Sagnac interferometer can also find applications in the characterization of light sources and optical fibers[1]. Basic Sagnac interferometer consists of various optical components which course light in opposite directions around a common optical path and then merge it on a detector, where the interference pattern can be captured [2].

In this paper, a simple novel sensor system based on a Sagnac interferometer is presented. The structure of the system is presented in Figure 1. The system consists of a dual Sagnac interferometer, where the larger interferometer is longer for the fiber delay line ( $L_D$ ). A low coherence source (LCS) is modulated using pulse modulation. By exerting pressure on the fiber at a specific location, a small phase shift occurs. By observing the ratio of the electrical signals obtained by subtraction of the currents of photodetectors PD1 and PD2 the precise location of intrusion can be determined.

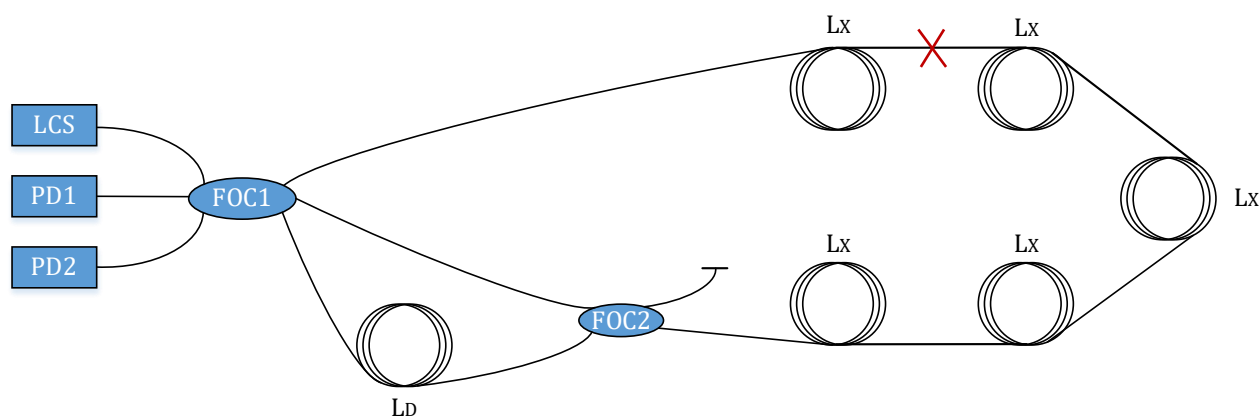


Figure 1. Basic concept of fiber optic sensor system for intrusion location detection

### REFERENCES

- [1] Eric Udd; William B. Spillman, "Fiber Optic Sensors Based on the Sagnac Interferometer and Passive Ring Resonator," in *Fiber Optic Sensors: An Introduction for Engineers and Scientists*, Wiley, 2011, pp.199-230, DOI: 10.1002/9781118014103.ch9.
- [2] S. J. Russell, K. C. Brady, and J. P. Dakin, "Real-Time location of multiple time-varying strain disturbances, acting over a 40-km fiber section, using a novel dual-Sagnac interferometer," *Journal of Lightwave Technology*, vol. 19, no. 2, pp. 205-213, Feb 2001.

## Frequency combs generated by a Bloch gain induced giant Kerr nonlinearity

N. Opačak<sup>1</sup>, S. D. Cin<sup>1</sup>, J. Hillbrand<sup>2</sup>, G. Strasser<sup>1</sup> and B. Schwarz<sup>1</sup>

<sup>1</sup>Institute of Solid State Electronics, Technische Universität Wien, Gußhausstraße 25-25a Vienna, Austria

<sup>2</sup>Institute for Quantum Electronics, ETH Zurich, 8093 Zurich, Switzerland

e-mail:nikola.opacak@tuwien.ac.at

Optical nonlinearities are known to coherently couple the amplitude and the phase of light, which can lead to the formation of perfectly periodic waveforms – known as frequency combs (FCs). Recently, self-starting frequency combs that do not rely on the emission of short pulses are appearing in numerous semiconductor laser types, among which is the quantum cascade laser. This novel type of combs is gaining vast attention from researchers due to their self-starting nature and compactness, making them an ideal platform for further development of spectroscopic applications. Their spontaneous formation was explained through an interplay of phenomenological nonlinearity and dispersion in the laser active region [1], although the actual physical processes remained unclear until now. Here we show that Bloch gain – a phenomenon described by Bloch and Zener in the 1930s – plays an essential role in their formation.

We develop a self-consistent theoretical model which couples every aspect of the laser operation – from the electronic band structure and carrier transport, to the spatio-temporal evolution of the electric field inside the laser cavity [2]. We demonstrate that a Bloch gain contribution is present in any laser and becomes dominant under saturation, shown in Fig. 1a). It deviates the gain strongly towards an asymmetric shape, which yields a giant Kerr nonlinearity of  $\sim 10^{-15}$  m<sup>2</sup>/W and explains the nonzero linewidth enhancement factor [3]. The induced Kerr nonlinearity serves as an efficient locking mechanism and results in the formation of FCs in Fabry-Perot laser cavities (Fig. 1.b). In ring resonators, it leads to the emission of localized structures [4], akin to dissipative Kerr solitons.

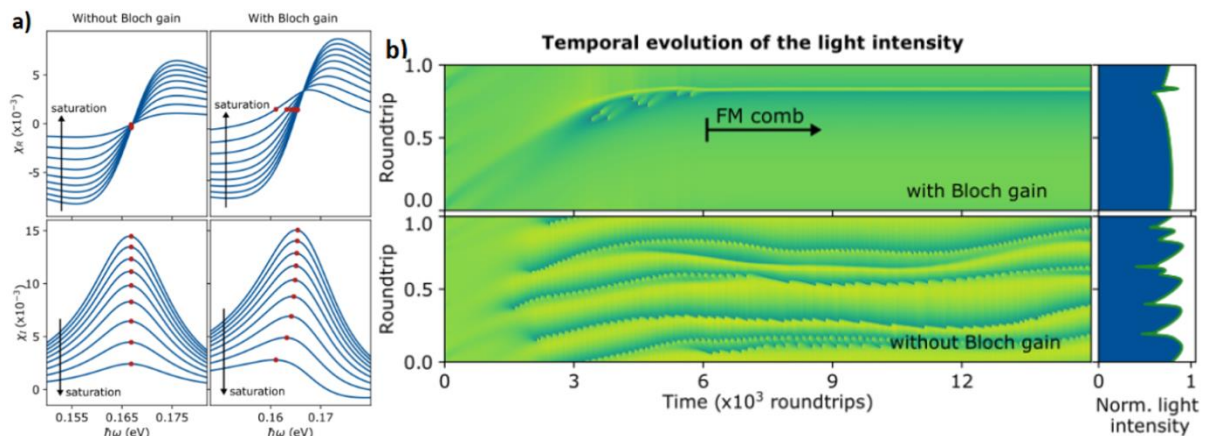


Figure 1. a) Complex susceptibility of the laser active medium with the increase of the laser intensity. b) Temporal evolution of the light intensity inside the laser cavity. Inclusion of the Bloch gain leads to the formation of a stable frequency modulated (FM) comb. Omitting it results in an unlocked state.

### REFERENCES

- [1] N. Opačak, B. Schwarz, Phys. Rev. Lett. 123, 243902 (2019).
- [2] N. Opačak, S. D. Cin, J. Hillbrand et al., arXiv 2102.08167 (2021).
- [3] N. Opačak, F. Pilat, D. Kazakov et al., arXiv 2104.05747 (2021).
- [4] M. Piccardo, B. Schwarz, D. Kazakov et al. Nature 582, 360 (2020).

## Advanced model of Mid-IR quantum cascade laser active region with anisotropy effects included

N. Vukovic<sup>1</sup>, B. Petrovic<sup>1</sup>, J. Radovanovic<sup>1</sup>, and V. Milanovic<sup>1</sup>

<sup>1</sup>*School of Electrical Engineering,  
University of Belgrade, Serbia  
e-mail: nvukovic@etf.bg.ac.rs*

In this communication, we present an enhanced theoretical model of the active region of a quantum cascade laser based on GaAs/AlGaAs semiconductor system, modified with respect to existing conventional models present in the literature in which the effects of dielectric constant anisotropy and its dependence on structure design (layer parameters) are neglected [1], [2]. The aim is to determine the scattering rates due to the interaction of electrons with longitudinal optical phonons within the anisotropic model and to implement the results in a structure that emits radiation in the mid-infrared region of the spectrum. Scattering rates and electron sheet densities are calculated through an iterative procedure that will be demonstrated on the example of a three-level system in a structure with LO-phonon depopulation [3]. Finally, the optical gain will be calculated and the results compared with the predictions of the isotropic model of dielectric permittivity.

### REFERENCES

- [1] M. A. Strosio and M. Dutta, "Phonons in nanostructures," in *Phonons in Nanostructures*, Cambridge University Press, (2001).
- [2] C. Jirauschek and T. Kubis, "Modeling techniques for quantum cascade lasers," *Appl. Phys. Rev.* 1, p. 011307, (2014).
- [3] C. N. Atkins, "New Developments in GaAs-based Quantum Cascade Lasers," PhD Thesis, University of Sheffield. October, (2013).

## GST loaded silicon-on-insulator diffraction grating

R. Minnullin<sup>1,2</sup>, M. Makarov<sup>1,3</sup>, and M. Barabanenkov<sup>1,3</sup>

<sup>1</sup>Moscow Institute of Physics and Technology (National Research University), Dolgoprudny, Russia

<sup>2</sup>JSC Molecular Electronics Research Institute, Moscow, Zelenograd, Russia

<sup>3</sup>Institute of Microelectronics Technology of RAS, Chernogolovka, Russia

e-mail: [ramil.minnullin@phystech.edu](mailto:ramil.minnullin@phystech.edu)

It is well known that progress in modern nanoelectronics through the scaling of standard planar CMOS technology is becoming more complicated with transition to feature sizes below 100 nm [1]. One of the prominent alternatives is nanophotonics, in particular, integrated silicon photonics due to its compatibility with CMOS manufacturing process. For over the decades extensive research in this field has resulted in a number of photonic applications in datacom, sensing and some other fields. Recently, it has been a great interest in photonics-based non-volatile data storage and neuromorphic applications that naturally incorporate phase-change materials such as Ge-Sb-Te (GST) alloys [2, 3].

In this paper, we start with a consideration of a thin-film GST diffraction grating deposited on a silicon-on-insulator (SOI) waveguide with 220 nm thick silicon and 1  $\mu\text{m}$  thick buried oxide layer. Earlier in [4], we have mentioned several advantages such diffraction-grating-like GST formation can have beyond regular continuous film deposition. These are: i) lowering energy budget for optically induced GST phase transition utilizing resonant properties of the grating; ii) providing a simple way of GST phase verification on the basis of the grating reflection spectra; iii) and also, enabling an alternative input of light into the structure with different efficiencies depending on the GST phase.

However, considering the diffraction grating solely as an input (output) element, optimization of a certain number of parameters is needed. These parameters include input angle of incidence, grating period (pitch), filling factor (duty cycle), and height, which is also an etching depth. Since GST is typically deposited as thin films with thickness 10–30 nm because of its strong light absorption, the resulting grating height can be inadequate for the efficient coupling to the waveguide. Hence, we propose to etch further in the silicon layer, which will lead to the formation of a composite structure – SOI diffraction grating “loaded” with GST (Fig. 1a). We demonstrate that even shallow additional etching of silicon (5–30 nm) yields significant increase in the excited mode profile (Fig. 1b).

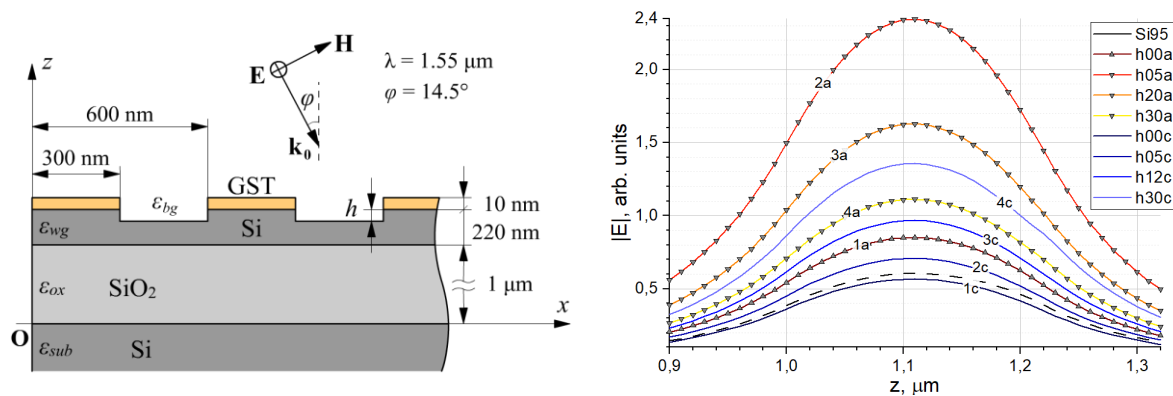


Figure 1. (a) Considered structure – composite GST+SOI diffraction grating; (b) excited mode profiles without additional silicon etching (lines 1a,c) and with etching to depths 5 nm (2a,c), 20 and 12 nm (3a,c), 30 nm (4a,c).

This study was supported by the Russian Foundation for Basic Research, project No.19-29-03040.

## REFERENCES

- [1] G. Ya. Krasnikov, N. A. Zaitcev, Nano and Microsystem Technique, **1**, 2 (2009) (in Russian)
- [2] M. Wuttig, H. Bhaskaran, T. Taubner, Nature Photonics, **11**, 465 (2017)
- [3] J. Wang, L. Wang, J. Liu, IEEE Access, **8**, 121211 (2020)
- [4] R. T. Minnullin et al., IOP Conf. Ser.: Mater. Sci. Eng., **840**, 012008 (2020)

## The electron coherent transport in nonpolar m-plane ZnO/MgZnO resonant tunneling diodes

X. Wang, A. Demić, Z. Ikonić, R. W. Kelsall and D. Indjin  
*School of Electronic & Electrical Engineering, University of Leeds,  
 Woodhouse Lane, Leeds, LS2 9JT, U.K.  
 e-mail: el17xw@leeds.ac.uk ; d.indjin@leeds.ac.uk*

GaAs-based quantum cascade lasers (QCLs) are the most promising devices emitting in terahertz frequency range, but they lack significant improvements within recent years and are still limited to operation at low temperatures ( $\sim 250\text{K}$ ). They are fundamentally limited by electron-optical LO-phonon resonance at around  $36\text{meV}$  in GaAs, causing parasitic non-radiative depopulation of the upper laser level at room temperature. Promising alternative semiconductors to solve this problem include new material systems like ZnO with their larger LO-phonon energy ( $\sim 72\text{meV}$ ) [1]. ZnO-based semiconductor compounds are promising materials not only because their high LO-phonon energy, but also due to their large bandgap and conduction band offset energy and resistance to the high breakdown electric field [1]. Moreover, it was established [2] that the ZnO-based terahertz sources can cover the spectral region of  $5\text{--}12\text{ THz}$ , which is very important for THz imaging and detection of explosive materials, and which could be not covered by conventional GaAs-based terahertz devices. Recent progress in growth of non-polar m-plane ZnO-based heterostructures and devices with low density defects [3], opens a wide perspective towards design and fabrication of non-polar m-plane ZnO-based unipolar intersubband structures capable of operation at elevated temperature. We present the results of a simulation of coherent electron transport in non-polar m-plane ZnO/MgZnO double-barrier resonant tunneling diode by solving Schrödinger-Poisson equations self-consistently. It is found that in current density-voltage characteristics of such devices a region is present with negative differential resistance. We simulated the different combinations of ZnO/MgZnO resonant-tunneling diodes at room temperature. Calculation shows a high sensitivity of the tunneling current peak on monolayer-scale barrier structure fluctuation which strongly affects peak to valley ratio in the structure.

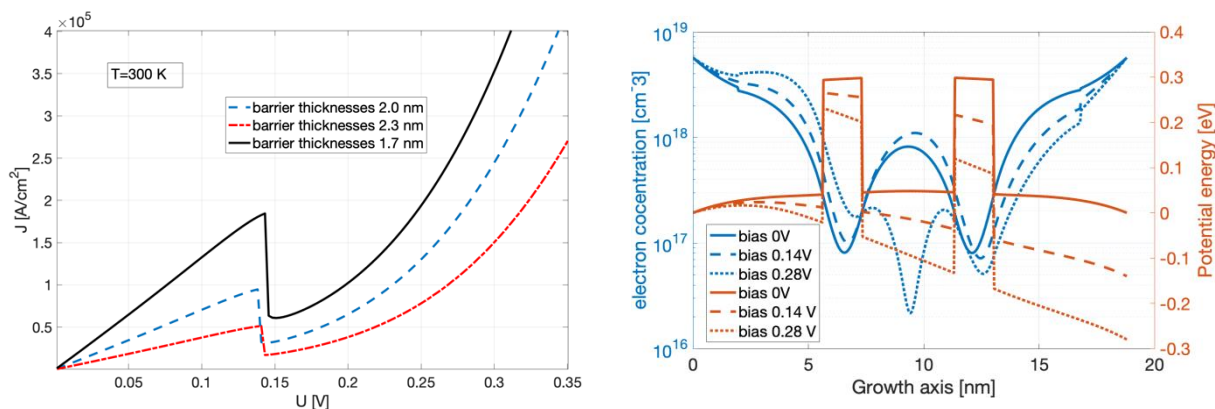


Figure 1. Left: Current density-voltage characteristics of ZnO/Mg<sub>0.15</sub>Zn<sub>0.85</sub>O resonant tunneling diodes with monolayer-scale fluctuation of barrier thickness. Nominal layer thickness in nanometers are 5.7/2.0/4.0/2.0/5.7

Right: Self-consistent potential and corresponding electron concentration for three different biasing conditions. Emitter and collector layers (underlined) doping is used to be  $1 \times 10^{18} \text{cm}^{-3}$

[1]. V.P. Sirkeli, H.L. Hartnagel, Opto-Electronics Review, **27**, 119-122(2019).

[doi:10.1016/j.opelre.2019.04.002]

[2] B. Meng et al, ACS Photonics, **8**, 343–349 (2021);

[https://dx.doi.org/10.1021/acsp Photonics.0c01641]

[3] N. LeBiavan et al, Appl. Phys. Lett. **111**, 231903 (2017); [https://doi.org/10.1063/1.5003146]

## High-power high-beam quality laser systems oscillating in visible spectral range on copper atomic self-terminating transitions

I. Kostadinov, K. Temelkov, D. Astadjov, S. Slaveeva, G. Yankov

*Institute of Solid State Physics, Bulgarian Academy of Sciences, 72 Tzarigradsko Chaussee, 1784 Sofia, BULGARIA*

e-mail: temelkov@issp.bas.bg

The most attractive characteristics of metal vapor lasers operating on atomic self-terminating transitions, such as copper, gold, lead and strontium vapor lasers, are their high gain, scalability to large dimensions, high average and peak pulsed laser powers, high efficiency, as well as high-beam-quality and high-brightness output. Among them copper vapor laser is the most powerful and efficient laser source in the visible spectral range ( $\lambda 510.6$  nm and  $\lambda 578.2$  nm) and has remained so to date [1]. A large-volume single-tube copper bromide (CuBr) vapor laser excited in a nanosecond pulsed longitudinal discharge and oscillating on atomic copper self-terminating transitions is described. The optimal discharge conditions for achieving a maximal average output power at the atomic copper lines, such as the excitation scheme parameters, the pressure of the buffer-gas mixture, the commutated electrical power, the charging voltage, and the pulse repetition frequency, are found. A record average output power of 140 W for the atomic CuBr vapor lasers is obtained. The average output power of 131 W achieved with commutation of just 10 kV is also superior for the atomic CuBr vapor lasers.

Laser application in various fields in science and technology, including medicine and human health, is one of the leading problems in laser physics. The ultimate aim of laser ablation is to efficiently remove a defined amount of material with the least amount of collateral damage. One standard application of lasers is in industry for cutting, welding, drilling, etc. of materials. The range of application of laser radiation is determined by the radiation properties as power, wavelength, beam geometry, divergence, etc. The precision of many operations done via lasers is concomitant of the so called beam quality, which is quantitatively determined with  $M^2$  (M-squared), so called beam propagation factor (or times-diffraction-limited factor). High-beam-quality sealed-off master oscillator–power amplifier (MO–PA) system, based on a copper bromide vapor laser and oscillating on copper atomic self-terminating transitions was described in [2]. A detailed study on the laser beam divergence was carried out demonstrating production of near-diffraction-limited laser beams ( $M^2 = 1.2$ ) from CuBr vapor laser systems [2] that was well in the range of recently announced second harmonic Nd:YAG laser systems produced by Spectra-Physics and Coherent yielding single transverse mode TEM<sub>00</sub> laser oscillation at the wavelength of 532 nm with beam propagation factor  $M^2$  of about 1.1-1.3. Unfortunately, the average output power of the MO–PA system was insufficient. High-power high-beam-quality sealed-off master oscillator–power oscillator–power amplifier (MO–PO–PA) system, which is based on a copper bromide vapor laser and oscillating on copper atomic self-terminating transitions is reported. Keeping the beam-quality high, a considerable increase in the average laser power is obtained. The MO–PO–PA laser radiation is used in precise microprocessing of various conductors, semiconductors and dielectrics, such as aluminum, copper, silicon, stainless steel, glass, fused silica, etc. A compact mobile 10-W CuBr vapor laser is also developed using all-solid-state power supply based on a new innovative bipolar excitation scheme.

**ACKNOWLEDGEMENTS:** This work was supported by the Project “Basic research and development of high-beam-quality high-power laser system oscillating in visible spectral range” of Bulgarian National Science Fund under Grant No. KP-06-H37/2 of 06.12.2019.

### REFERENCES

- [1] R. P. Hackel, B. E. Warner, Proc. of SPIE 1859, 120 (1993).
- [2] I. K. Kostadinov, D. N. Astadjov, G. P. Yankov, L. T. Popova, S. I. Slaveeva, Yu. I. Fedchenko, K. A. Temelkov, Journal of Physics: Conference Series 1859, art. No. 012056 (2020).

## **6. Optical communications**

## Experimental observation of edge states in dimerized Stub photonic lattices

G. Cáceres-Aravena<sup>1</sup>, B.Real<sup>2</sup>, C. Cid, D. Guzmán-Silva<sup>1</sup>, and R.A. Vicencio<sup>1</sup>

<sup>1</sup>Departamento de Física and MIRO, Facultad de Ciencias Física y Matemáticas, Universidad de Chile, Chile<sup>2</sup>Université de Lille, CNRS, Laboratoire de Physique des Lasers Atomes et Molécules (PhLAM), Lille, France

e-mail: gabriel.caceres@ug.uchile.cl

Inspired by the work of Su-Schrieffer-Heeger [1], we study theoretically and experimentally a dimerized Stub lattice, as shown in Fig.1(a). This lattice has a flat band[2] at  $\beta_z = 0$  for any value of  $\delta = t_1/t_2$  and edge localized states for  $\delta < 1$  at  $\beta_z = \pm \mathbf{t}_3$ , as shown in Fig. 1(b). By using a femtosecond-laser written technique [3], we fabricate several photonic lattices as the one shown in Fig.1(c). We analyze these photonic lattices using an experimental setup sketched in Fig. 1(d), where we excite edge “ $w_n$ ” waveguides and observe localization for  $\delta < 1$  and transport for  $\delta > 1$ . Fig.1(e) summarizes all our experimental results and show quite clearly the predicted transition. Numerical edge states are shown in Figs.1(f) and (g), for  $\beta_z = 1$  and  $\beta_z = -1$ , respectively. Finally, we find a basis change that transform the dimerized Stub model into a SSH model including site energies, giving us some insights of the edge mode origin.

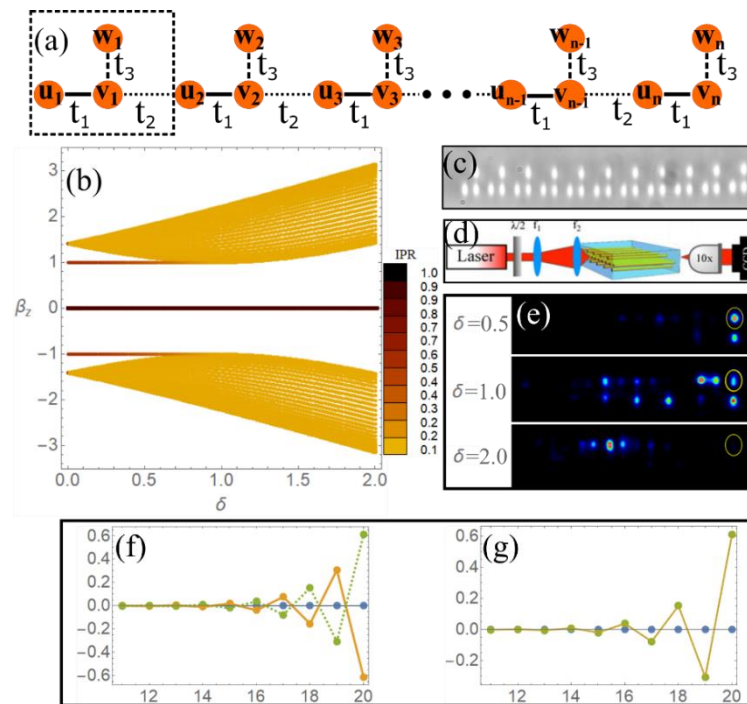


Figure 1.(a) A dimerized Stub lattice. (b) Numerical spectrum for a finite lattice,  $\mathbf{t}_3 = ?$ . Color represents an inverse participation ratio (IPR). (c) Microscope image at the output facet of a photonic lattice. (d) Experimental characterization setup. (e) Experimental output intensity for a  $w_n$  input excitation. (f) and (g) Numerical edge states for  $\delta = 0.5$ . Blue, orange and green dots are for “ $u$ ”, “ $v$ ” and “ $w$ ” sites.

### REFERENCES

- [1] W. P. Su, J. R. Schrieffer, and A. J. Heeger, Phys. Rev. Lett. 42, 1698 (1979).
- [2] R. Vicencio. Advances in Physics: X, 6, 1878057 (2021).
- [3] A. Szameit et al., Opt. Express 13, 10552 (2005).

## An estimation of the far-field intensity distribution for novel hollow photonic crystal optical fibers

M. S. Kovačević<sup>1</sup>, Lj. Kuzmanović<sup>1</sup>, M. M. Milošević<sup>1</sup> and A. Djordjevich<sup>2</sup>

<sup>1</sup>Faculty of Science, University of Kragujevac, Serbia

<sup>2</sup>City University of Hong Kong, Hong Kong

e-mail: [kovac@kg.ac.rs](mailto:kovac@kg.ac.rs)

In this paper, the far-field intensity distribution of hollow photonic crystal optical fibers (HPCF) is thoroughly analyzed using an analytical approach based on the normalized frequency ( $V$  parameter) and normalized attenuation constant ( $W$  parameter). Utilizing a three-layered structure of HPCF with a central air hole, the characteristic M-shaped index profile is obtained by forming a silica ring core with its own value of the effective index corresponding to the distinct size and/or spacing of air holes in it. By altering the hole-to-hole spacing ( $\Lambda$ ) and hole diameter ( $d$ ) in the selected fiber layer, the effective index profile can be adjusted for the cladding region. Using the empirical relations for the  $V$  and  $W$  parameters of photonic crystal fibers (PCF), the dependence of the far-field intensity distribution on two structural parameters - the air hole diameter and the air hole pitch is calculated and presented. The results displayed here can find their utilization in the design and development of a sensor system based on HPCFs for potential application involving structural health monitoring, medicine, environmental monitoring sensors, multimode fiber (MMF) mode convertor for gigabit LAN, higher-order-mode (HOM) dispersion compensation, tunable bandpass filters, etc.

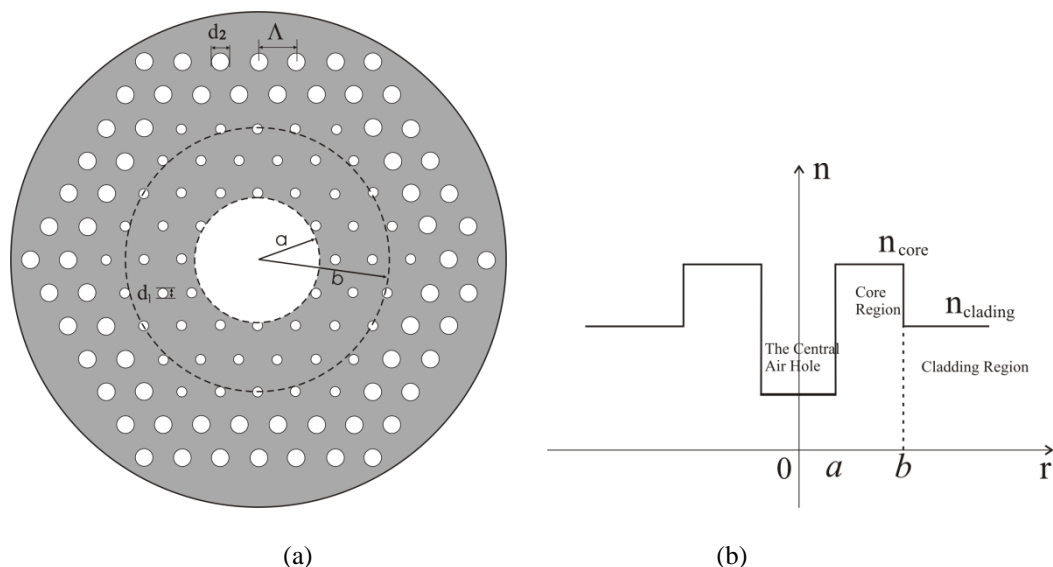


Figure 1. (a) Cross section of a three-layered structure of M-type PCF (central air hole, ring core region and cladding region); (b) refractive index profile of the referent M-type PCF.

### REFERENCES

- [1] S. Lee, J. Park, Y. Jeong, H. Jung, and Kyunghwan Oh, *J. Light. Technol.* **27** (22), 4019 (2009).
- [2] Kyunghwan Oh, *J. Light. Technol.* **23** (2), 524 (2005).
- [3] P. St. J. Russell, *Science* **299**, 358 (2003).
- [4] J. C. Knight, *Nature* **424** (14), 847 (2003).
- [5] Knight J. C., J. Broeng, T. A. Birks, and P. S. J. Russell, *Science* **282**, 1476 (1998).
- [6] Knight J. C. and P. S. J. Russell, *Science* **296** (2002).
- [7] M. S. Kovačević, L. Kuzmanović, A. Simović, S. Savović, and A. Djordjevich, *J. Light. Technol.* **35** (20), 4352 (2017).
- [8] M. S. Kovačević, Lj. Kuzmanović, A. Simović, S. Savović, B. Drljača, A. Djordjevich, *Opt. Commun.* **427**, 348 (2018).

## **7. Laser spectroscopy and metrology**

## Time-spatial resolved LIBS of atomic and molecular carbon in laser ablation plasma

A. Nevar<sup>1</sup>, M. Nedelko<sup>1</sup>, A. Radomzev<sup>1</sup>, N. Tarasenko<sup>1</sup>, J. Savovic<sup>2</sup>, M. Kuzmanovich<sup>3</sup>,  
D. Rankovic<sup>3</sup>

<sup>1</sup>B. I. Stepanov Institute of Physics, National Academy of Sciences of Belarus, Minsk, Belarus

<sup>2</sup>Vinca Institute of Nuclear Sciences, Belgrade, Serbia

<sup>3</sup>Faculty of Physical Chemistry, University of Belgrade, Belgrade, Serbia

e-mail: a.nevar@ifanbel.bas-net.by

For elucidation a possibility to use molecular emission spectra in LIBS analysis of carbon containing materials time and space resolved spectra of laser ablation plasma from graphite were studied.

Laser plasma was produced on a rotated graphite target by fundamental harmonic of YAG: Nd<sup>3+</sup> laser (Lotis TII) in air at atmospheric pressure. The optical emission spectra were analyzed using a GSM-850 Lotis TII monochromator/spectrograph equipped with a CCD detector. The atomic and molecular spectra in the region of emission of molecules C<sub>2</sub> ( $\lambda = 516,52$  nm) and CN ( $\lambda = 421,16$  nm) were registered by photomultiplier placed behind the interference filter to record the intensity of the selected plasma emission line.

The temporal and spatial characteristics of the plasma spectra with special attention to molecular carbon including molecules CN and C<sub>2</sub> were analyzed. It was found that the time range of dominance of the C<sub>2</sub> and CN emission is related to the stage of the plasma decay (10–20  $\mu$ s after the action of the laser pulse, depending on the conditions for plasma creating).

The atomic emission spectra of the plasma were used to estimate the concentration of electrons and the electron temperature of the plasma. The vibrational temperature of the carbon plasma was determined from the molecular spectrum of the radical CN ( $(\Delta v = 0, -1)$ ). The plasma electron concentration and electron temperature as well as vibrational temperature were determined in different zones of the expanding plasma and at different values of laser power densities ( $2,2 \cdot 10^8 \div 3,7 \cdot 10^8$  W/cm<sup>2</sup>) used in experiments. The electron temperature varied in the range 9700 – 10300 K, the electron concentration was estimated to be in the range from  $0,8 \cdot 10^{18}$  cm<sup>-3</sup> to  $8,0 \cdot 10^{18}$  cm<sup>-3</sup>, the vibrational temperature of the plasma was 4560 - 7350 K depending on the experimental conditions (laser power density, spatial zone of the plasma plume).

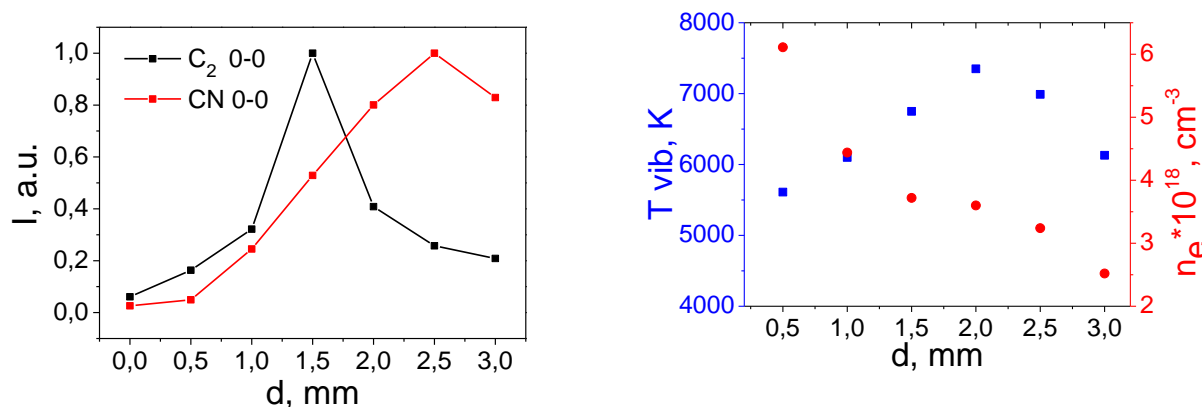


Figure 1. Spatial distribution of C<sub>2</sub> (0-0) and CN (0-0) band heads intensities (left) as well electron concentration and vibrational temperature (right)

## Colorimetric system based on CCD array spectrometer

Boban Zarkov<sup>1</sup>, Kolja Bugarski<sup>2</sup>

<sup>1</sup>*Directorate of Measures and Precious Metals (DMDM), Serbia*

<sup>2</sup>*University of Belgrade School of Electrical Engineering, Belgrade, Serbia*

e-mail: zarkov@dmdm.rs

For the needs of the new realization scale of luminous intensity through radiometric detectors in the laboratory for optical quantities of the Metrological Institute of the Republic of Serbia, a measuring colorimetric system was developed to determine chromatic coordinates and correlation color temperature - CCT of light sources. The system is based on a spectrometer with a toroidal grating manufactured by Ocean Optics, model Torus, slit width 25 $\mu$ m, which contains a Sony ILX511B linear CCD-array detector with a resolution of 0.265nm. The receiving optical part consists of fiber 400 $\mu$ m, length 2m and integration sphere with a diameter of 38.1 mm. Application Software is written in virtual instruments - VI LabVIEW environment. The spectral responsivity of the spectrometer was performed on the primary spectrophotometric system by the method of comparison with standard radiometric silicon detectors with an extended uncertainty of 0.6% for ( $k = 2$ ). Wavelength accuracy of spectrometer was checked via arc lamps with maximum deviation of 0.2nm.

The VI Chromaticity 2021.vi program acquires data from the spectrometer via the USB bus and executes certain mathematical operations and calculations. The main form of the program shows the intensity of the source as a function of wavelength, the normalized spectral power distribution – SPD of the light source, the values of the calculated chromatic coordinates for the standard CIE observer 1931 as well as the CCT value shown on the chromatic diagram. The user also has the ability to visually compare normalized SPD curves for the measured light source and blackbody at the same temperature. Additional advanced features of the colorimetric system enable compensation of dark current, possibility of adjusting spectrometer parameters in real time, recording of obtained values and graphics in a file as well as recording of spectral transmittance of optical filters and their determination of chromatic coordinates.

The system was validated with three bulbs at different color temperatures (2800K, 2856K and 2965 K) where is maximum measured deviation was 3K. The intensity-integration time curve was recorded where it was shown that there is a nonlinearity above 75% of the maximum intensity value. A significant influence of temperature change during measurement on measurement results was noticed, which we managed to limit by temperature stabilization of the spectrometer in the temperature interval of  $\pm 0.2$  °C.

The colorimetric system based on CCD arrays was developed to determine the chromatic coordinates of light sources, transparent filters and reflective plates as well as CCT of light sources with measurement uncertainty of 10K ( $k = 2$ ). Based on this system, which performs real-time measurements, we are able to correct the deflection of the lamp from CCT = 2856K during the new realization scale of luminous intensity (candela) via radiometric detector.

### REFERENCES

- [1] Münevver Nehir, Carsten Frank, Steen Aßmann, Sensors, 19 (12, Article 2833)
- [2] Boban Zarkov, Slavica Simic, Optical and Quantum electronics (2018), vol.50(8)

## Effects of laser heating on luminescent properties of Gd<sub>2</sub>O<sub>3</sub>:Er,Yb nanophosphor

D. Sevic<sup>1</sup>, M.S. Rabasovic<sup>1</sup>, J. Krizan<sup>2</sup>, S. Savic-Sevic<sup>1</sup>, M.D. Rabasovic<sup>1</sup>, B.P. Marinkovic<sup>1</sup>  
and M.G. Nikolic<sup>1</sup>

<sup>1</sup>Institute of Physics, Belgrade, Serbia

<sup>2</sup>AMI d.o.o., Ptuj, Slovenia

e-mail:sevic@ipb.ac.rs

In this study we analyze effects of laser heating on luminescent properties of nanocrystalline Gd<sub>2</sub>O<sub>3</sub> doped with Er<sup>3+</sup> and Yb<sup>3+</sup> cations. Material was synthesized by combustion method, as described in [1]. Our experimental setup is presented in detail in [2,3,4]. In this study we have used pulsed laser diode excitation at 980 nm. Variable laser pulse energy was obtained by varying the laser pulse duration. Used laser diode has both continual and pulse mode. In continual mode its power is 1 W; in pulse mode it is possible to tune pulse duration and repetition, thus obtaining different average excitation powers. Here, we have used repetition rate of 200 Hz, with varying pulse duration between 20 μs and 200 μs, so average excitation power is between 8 mW and 80 mW.

Generally, laser power heating effects are unwanted and should be avoided in luminescence thermometry experiments; external heater and thermometer are used to calibrate the temperature sensing curve. Interestingly enough, the thermometry system, based on laser heating of sample, applicable for biomedical purposes, is described in [5].

Luminescence spectra of Gd<sub>2</sub>O<sub>3</sub>:Er<sup>3+</sup>,Yb<sup>3+</sup> excited at room temperature with different laser excitation powers are shown in Figure 1. It should be noted that excitation power is intentionally much higher than used in [3]. Based on temperature sensing calibration curve presented in [3] for the same sample it could be estimated that the material is locally heated to about 375 K for pulse time of 200 μs.

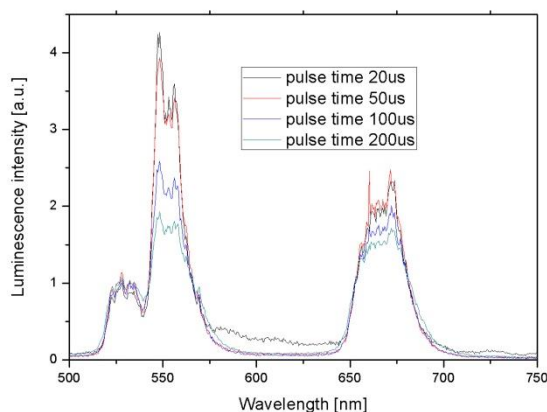


Figure 1. Luminescence spectra of Gd<sub>2</sub>O<sub>3</sub>:Er<sup>3+</sup>,Yb<sup>3+</sup> excited at room temperature with different laser powers.

### REFERENCES

- [1] J. Krizan, M. Mazaj, V. Kaucic, I. Bajsic, J. Mozina, Acta Chim. Slov. 61, 608 (2014).
- [2] A. Vlastic, D. Sevic, M.S. Rabasovic, J. Krizan, S. Savic-Sevic, M.D. Rabasovic, M. Mitric, B.P. Marinkovic, M.G. Nikolic, Journal of Luminescence, 199, 285 (2018).
- [3] D. Sevic, M.S. Rabasovic, J. Krizan, S. Savic-Sevic, M.D. Rabasovic, B.P. Marinkovic, M.G. Nikolic, Optical and Quantum Electronics 52, 232 (2020).
- [4] D. Sevic, M.S. Rabasovic, J. Krizan, S. Savic-Sevic, M.G. Nikolic, B.P. Marinkovic, M.D. Rabasovic, J. Phys. D: Appl. Phys. 53, 015106 (2020).
- [5] M.F. Ferreira, K.Z.R. de Sousa, W.L. Massarotto, E.G. Ricci, E.H. de Faria, K.J. Ciuffi, D. Sevic, L.A. Rocha, E.J. Nassar, J. Braz. Chem. Soc., 32(2) 376 (2021).

# Optical Phase Locked Loop for Quantum Cascade Laser Frequency Combs

Sandro Dal Cin<sup>1</sup>, Johannes Hillbrand<sup>1,3</sup>, Pitt Allmendinger<sup>2</sup>, Pierre Jouy<sup>2</sup>, Gottfried Strasser<sup>1</sup> and Benedikt Schwarz<sup>1</sup>

<sup>1</sup> Institute of Solid State Electronics and Center for Micro- and Nanostructures, TU Wien, Vienna, Austria

<sup>2</sup> IRsweep AG, Laubisruetistrasse 44, 8714 Staefa, Switzerland

<sup>3</sup> Quantum Optoelectronics Group, ETH Zürich, Zürich, Switzerland

e-mail: sandro.cin@tuwien.ac.at

Dual comb spectroscopy employing Quantum Cascade Laser (QCL) frequency combs can be used to evaluate and analyze optical absorption features in the easily accessible radio-frequency (RF) domain. This conversion from the optical – to the RF domain has great potential for integration of spectroscopic applications like chemical sensing [1, 2]. A challenge hindering fast reproducible measurements is imposed by temperature fluctuations and electronic noise leading to often highly unstable heterodyne beating signals. We present a simple, yet reliable phase locking technique based on a dual feedback Optical Phase Locked Loop (OPLL). Stable locking bandwidths exceeding 600 kHz for a heterodyne QCL frequency comb setup were achieved (see Figure 1). For loop-filter parameter prediction, a simplified theoretical model is applied. The model relies on two initial measurements, namely the measurement of the phase-frequency-detector (PFD) sensitivity and frequency modulation gain of one frequency comb.

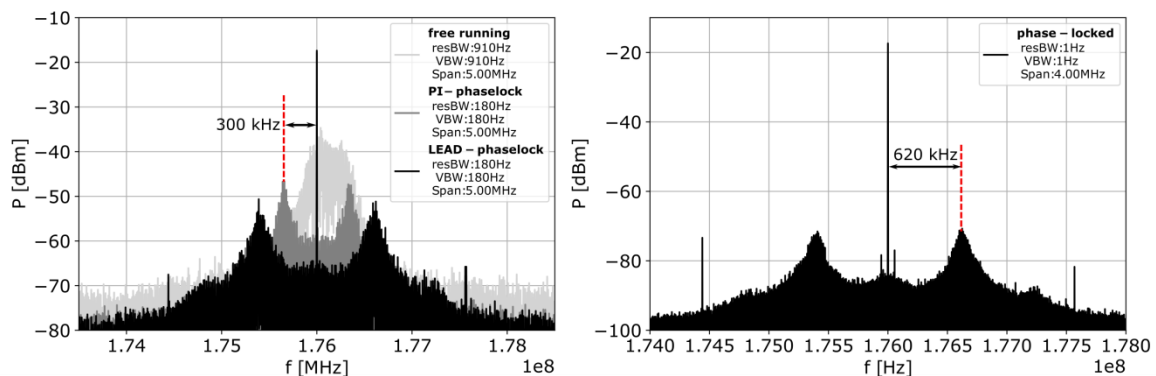


Figure 1. Left: Comparison of one free running beatnote comb tooth (light grey), 300 kHz locking bandwidth with slow loop-filter path active (grey) and 620 kHz locking bandwidth with slow and fast loop-filter path active (black). Right: Higher resolution plot of locked beatnote tooth with 620 kHz locking bandwidth

## REFERENCES

- [1] Geiser, M. et al. Single-shot microsecond-resolved spectroscopy of the bacteriorhodopsin photocycle with quantum cascade laser frequency combs. *Biophys. J.* 114, 173a (2018)
- [2] Villares, G. et al. On-chip dual-comb based on quantum cascade laser frequency combs. *Appl. Phys. Lett.* 107, 251104 (2015).

## Approaching the Heisenberg limit in a many-spin system

S. Colombo<sup>1</sup>, E. Pedrozo-Peñafiel<sup>1</sup>, A. Adyatullin<sup>1</sup>, Z. Li<sup>1</sup>, E. Mendez<sup>1</sup>, C. Shu<sup>1,2</sup>, V. Vuletić<sup>1</sup>

<sup>1</sup>*Department of Physics, MIT-Harvard Center for Ultracold Atom sand Research Laboratory of Electronics, Massachusetts Institute of Technology, Cambridge, MA, United States of America*

<sup>2</sup>*Department of Physics, Harvard University, Cambridge, MA, United States of America*  
e-mail:colombos@mit.edu

A long-sought in the field of Quantum Metrology is the creation of exotic quantum states that allow atomic sensors to operate far beyond the Standard Quantum Limit (SQL), where the precision scales with square root of the number of involved particles  $N^{1/2}$ . Gaussian Spin Squeezed States have been used to overcome the SQL in atomic sensors but offer limited quantum metrological advantages. To approach the Heisenberg Limit, Non-Gaussian Entangled States (NGES) that carry larger statistical information have to be engineered. However, the fragility of highly entangled states against decoherence and single-particle state resolution requirements have made difficult their experimental realization and application to atomic sensors with today's technology.

We present here the implementation of a robust Signal Amplification through Time-reversal Interaction (SATIN) protocol that allows for the generation of NGESs and the efficient use of their quantum resource. In particular, we report the largest sensitivity improvement beyond the SQL demonstrated in any interferometer to date [2]. This is achieved by experimentally demonstrating for the first time a previously proposed effective time-reversal protocol [1], where a NGES is generated through a nonlinear Hamiltonian. When this state is subjected to a small signal (phase shift), the application of the negative nonlinear Hamiltonian ("time reversal") generates a large amplification of the interferometric signal that can be read out easily.

Our work presents a new paradigm of nonlinear atomic sensors where the time-reversal protocol enables robust operation far beyond the SQL, and close to the Heisenberg limit with precision improving in proportion to atom number. Potential applications include searches for dark matter and for physics beyond the standard model, tests of the fundamental laws of physics, timekeeping, and geodesy.

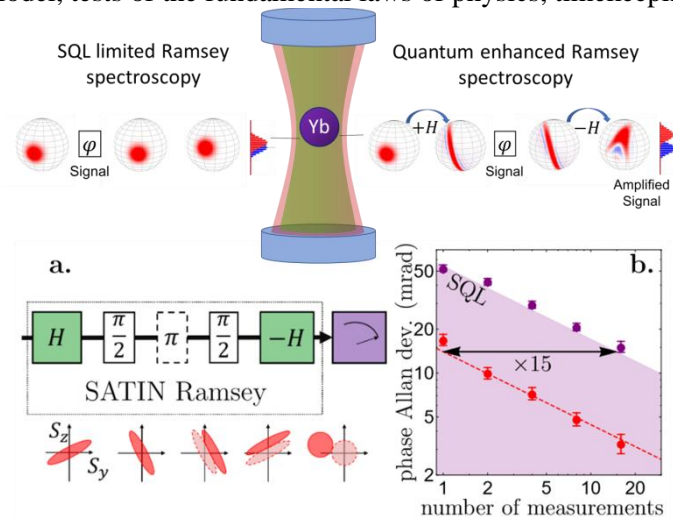


Figure 1. SATIN protocol principle and its application to Ramsey spectroscopy.

### REFERENCES

- [1] E. Davis, G. Bentsen, Schleier-Smith, Phys. Rev. Lett. 116(5), 053601 (2016).  
[2] S. Colombo, E. Pedrozo-Peñafiel, *et. al.*, arXiv:2106.03754 (2021).

## **8. Ultrafast optical phenomena**

## Ultrashort quasi-non-diffracting long-range Gauss-Bessel beams

L. Stoyanov<sup>1,2</sup>, Y. Zhang<sup>1</sup>, A. Dreischuh<sup>2</sup> and G. G. Paulus<sup>1,3</sup>

<sup>1</sup>*Institute of Optics and Quantum Electronics, Friedrich Schiller University,  
Max-Wien-Platz 1, D-07743 Jena, Germany*

<sup>2</sup>*Department of Quantum Electronics, Faculty of Physics, Sofia University,  
5, J. Bourchier Blvd., Sofia-1164, Bulgaria*

<sup>3</sup>*Helmholtz Institute Jena, Helmholtzweg 4, D-07743 Jena, Germany  
e-mail: l.stoyanov@phys.uni-sofia.bg*

Bessel beams (BBs) are one of the four known types of exact solutions of the Helmholtz equation describing non-diffracting beams in circular cylindrical coordinates [1,2]. Non-diffracting means that the central maxima of these beams are remarkably resistant to diffractive spreading [3,4]. Precisely speaking, the BB has an infinite number of rings carrying infinite power/energy, and hence, cannot be generated in the exact sense. However, Durnin and co-authors showed first [5] that one can generate its reasonable approximation by placing an annular slit in the back focal plane of a lens.

Here we demonstrate a straightforward yet efficient method for generating zeroth- and first-order Gauss-Bessel beams (GGBs) using a single reflective spatial light modulator (SLM). These GGBs can be generated in the fields of few-cycle femtosecond laser pulses by initially nesting and subsequently annihilating multiple-charged optical vortices (OVs) and finally Fourier-transforming the resulting ring-shaped beam with a large ring radius-to-width ratio by a thin lens.

Even in the sub-8-fs range there are no noticeable consequences for the measured pulse duration [6]. The only effect is a weak “coloring” of the outer-lying satellite rings of the beams due to the spectrum spanning over more than 300 nm. The obtained beams have diffraction half-angles below 40  $\mu$ rad and reach propagation distances in excess of 1.5 m. At large propagation distances, the quality of the generated GGBs significantly surpass this of GGBs created by low angle axicons. Detailed results will be presented and discussed.

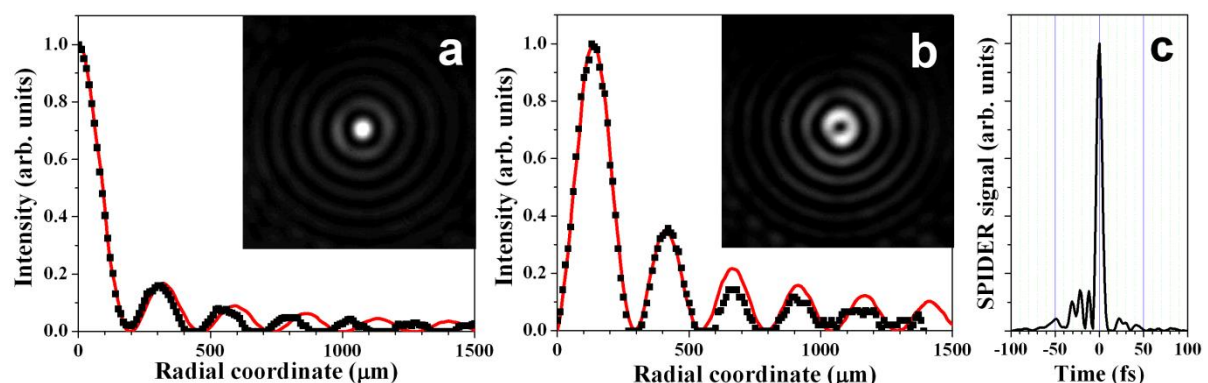


Figure 1. Radial cross-section of the experimentally and theoretically obtained zeroth- (a) and first-order (b) GGBs. Inset frames – experimentally recorded energy density distribution of these GGBs obtained by the creation and subsequent annihilation of an OV with topological charges  $|TC|=30$  (a) and of an OV with  $TC = 31$  and  $-30$  (b). Typical reconstructed GGB pulse profile (pulse duration  $\sim 7.5(\pm 0.5)$  fs), retrieved from SPIDER device (c) [6].

### REFERENCES

- [1] J. Durnin, *Opt. Soc. Am. A* 4, 651–654 (1987).
- [2] S. N. Khonina, A. V. Ustinov, S. Chávez-Cerda, *J. Opt. Soc. Am. A* 35, 1511–1517 (2018).
- [3] Z. Bouchal, *J. Phys.* 53, 537–578 (2003).
- [4] D. McGloin, K. Dholakia, *Contemp. Phys.* 46, 15–28 (2005).
- [5] J. Durnin, J. J. Miceli Jr., J. H. Eberly, *Phys. Rev. Lett.* 58, 1499–1501 (1987).
- [6] L. Stoyanov, Y. Zhang, A. Dreischuh, G. G. Paulus, *Optics Express* 29, 10997–11008 (2021).

## Femtosecond laser spectroscopy for Exploration of Space: Introduction of new research group at German Aerospace Center

N. Stojanovic<sup>1</sup>, M. Gensch<sup>1,2</sup>

<sup>1</sup> *Institut für Optische Sensorsysteme, DLR, Berlin, Germany*

<sup>2</sup> *Technische Universität Berlin, Berlin, Germany.*

e-mail: nikola.stojanovic@dlr.de

The Time-Domain Spectroscopy group (TLS - ZS) in the department of Terahertz and Laser Spectroscopy (TLS) has a long track record in instrumentation development and has in recent years pioneered terahertz time-domain set-ups demonstrating world-wide unique sensitivity levels [1,2]. It is currently working on developing compact laser-based spectroscopy techniques based on short-pulse lasers for future applications in e. g. robotic missions to extraterrestrial objects in our solar system. Scientific applications range from planetary research to nonlinear spectroscopy of novel quantum materials with applications in space instruments (e. g. topological insulators or Graphene[3]). The group is furthermore contributing its expertise in laser spectroscopy, optic design, detector development and qualification of spectroscopy components to different cross-sectoral projects within TLS.

### Time domain Spectroscopy Group

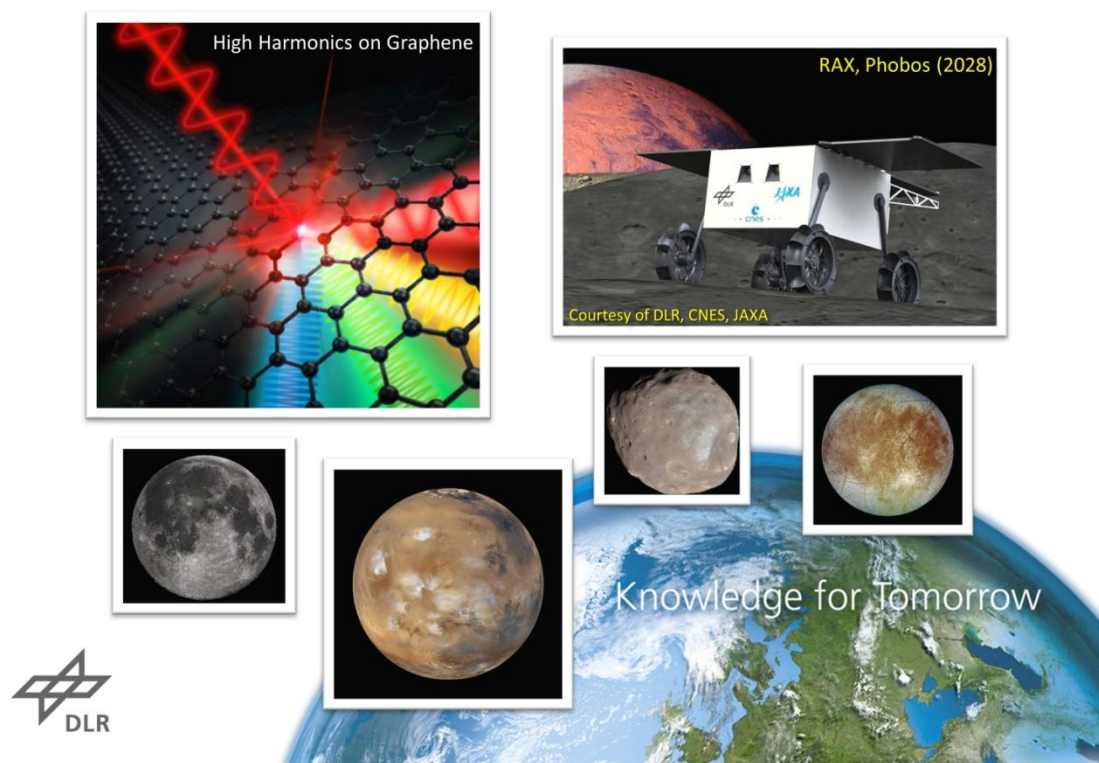


Figure 1. Towards new research enabled by space ready ultrafast lasers

#### REFERENCES

- [1] R. Pan, et. al. *J. Synchrotron Radiat.* 26 (3) (2019) 700–707.
- [2] B. Green, et. al., *Sci. Rep.* 6, 22256 (2016).
- [3] H. A. Hafez et. al., *Nature*, 561, 507 (2018)

## Ultrafast Laser Control of Interatomic-Coulomb-Decay Dynamics

C. W. Hogle<sup>1</sup>, L. Martin<sup>1</sup>, X-M. Tong<sup>2</sup>, K. Ueda<sup>3</sup>, T. Miteva<sup>4</sup>, L. S. Cederbaum<sup>5</sup>, H. C. Kapteyn<sup>1</sup>, M. M. Murnane<sup>1</sup>, and P. Ranitovic<sup>1,6</sup>

<sup>1</sup>JILA and Department of Physics, University of Colorado and NIST, Boulder, CO 80309, USA

<sup>2</sup>Center for Computational Sciences, University of Tsukuba, Ibaraki 305-8573, Japan

<sup>3</sup>Institute of Multidisciplinary Research for Advanced Materials, Tohoku University, Sendai 980-8577, Japan

<sup>4</sup>Sorbonne Université, CNRS, Laboratoire de Chimie Physique—Matière et Rayonnement, Paris, France

<sup>5</sup>Theoretical Chemistry, PCI, Universität Heidelberg, 69120 Heidelberg, Germany

<sup>6</sup>Physics Department, University of Belgrade, Serbia

p.ranitovic@ff.bg.ac.rs

Ultrafast Interatomic-Coulomb-Decay (ICD) processes play an important role during an interaction of X-rays and biological samples. Here, we present the first successful experimental demonstration that enables, and precisely times the outcome of an ICD process in an argon dimer, utilizing ultrafast XUV and IR radiation [Fig. 1]. Since the experimental work first identifying the ICD process a decade ago, extensive studies have unraveled its complex character [1-3]. Following X-ray ionization, an ultrafast interaction of the irradiated site with its environment produces a low-energy ICD electron that follows the initial direct-ionized electron. In contrast to the better-known Auger relaxation process where the electron that fills the X-ray ionization hole originates from the same atom, and the decay rate is essentially independent of environment, ICD is intrinsically complex in nature and the low energy electron (LEE) exhibits a broad energy spectrum due to the coupling of the ICD rate with the motion of the molecular nuclear wave-packet. This provides the opportunity for control over the energy and ICD electron ejection site—which could, for example, lead to new approaches for radiation therapy. To develop a better understanding of the potential control over core-relaxation processes, in past work resonant Auger decay was used as an intermediate step and a precursor to ICD. This work allowed us to demonstrate a laser-enabled ICD (LE-ICD) process—a sophisticated control mechanism over the last step of the relaxation mechanism, involving a valence, Rydberg, and an inner-valence electron transition, allowing us to control bond breaking in the Ar dimer.

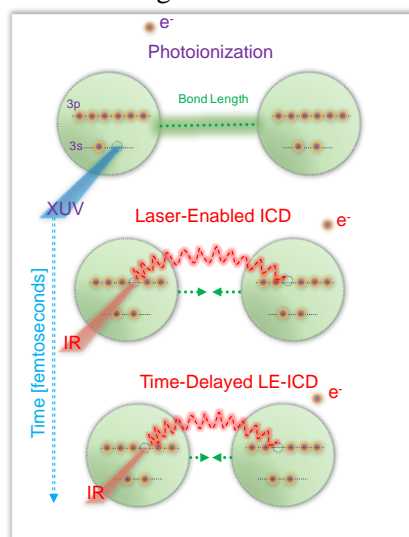


Figure 1. Schematically shown the laser-enabled control of ultrafast ICD process in Ar dimer.

### REFERENCES

- [1] L. S. Cederbaum, J. Zobeley and F. Tarantelli, Phys. Rev. Lett. 79, 4778–4781 (1997).
- [2] N. Sisourat, N. Kryzhevoi, P. Kolorenc, et al., Nature Physics 6, 508–511 (2010).
- [3] K. Nagaya, D. Lablonskyi, N. V. Golubev, et al., Nat. Communications 7, 13477 (2016).

## Upgrading of the THz beamline for pump-probe experiments in FLASH2020+

Rui Pan<sup>1</sup>, Seung-gi Gang<sup>1</sup>, Marc Temme<sup>1</sup>, Nikola Stojanovic<sup>1,2</sup>, Elke Plönjes<sup>1</sup>

<sup>1</sup>*Deutsches Elektronen-Synchrotron (DESY), Hamburg, Germany*

<sup>2</sup>*DLR – Institute for Optical Sensor Systems, Berlin, Germany*

e-mail: rui.pan@desy.de

FLASH at DESY has a unique FEL scheme providing soft X-ray beam and intense THz beam simultaneously with only a few femtosecond timing jitter. The two beams can be used to study matter by pump-probe techniques. FLASH2020+, a project to upgrade FLASH, is ongoing at DESY[1]. After the upgrade, a THz beam with over 250  $\mu\text{J}/\text{pulse}$  and a broad THz bandwidth is expected to be transported through the beamline and provided to the endstation with high repetition rate. The THz undulator source, tunable in wavelength and currently inline with the XUV undulator, will be separated from the XUV undulator, which will allow a completely parastic operation for THz only experiments, such as non-linear THz spectroscopy. At the same time, photon energy loss in the currently complex separation of THz and XUV photon beams will be avoided in the future.

A new beamline FL11 shall be equipped with bendable KB optics[2] and provide photon energies beyond the carbon K-edge. In addition, a dedicated experimental end-station for THz-XUV pump-probe experiments for studying solid state physics, and femtomagnetism at FL11 is under development. The THz doubler, a special FLASH operation mode producing double pulses for pump-probe experiments [3, 4], will be further developed. This will significantly enhance the capability and flexibility for THz-XUV pump-probe experiments at FL11.

### REFERENCES

[1] 'FLASH2020+ Conceptual Design Report' (CDR), (2020).

[2] L. Raimondi, M. Manfredda, and et al., 'Kirkpatrick-Baez active optics system at FERMI: system performance analysis', *J. Synchrotron Rad.* 26, 1462-1472, (2019).

[3] E. Zapolnova, T. Golz and et al., 'THz pulse doubler at FLASH: double pulses for pump-probe experiments at X-ray FELs', *J Synchrotron Radiat.*, 1; 25(Pt 1): 39–43, (2018).

[4] E. Zapolnova, R. Pan, and et al., 'XUV-driven plasma switch for THz: new spatio-temporal overlap tool for XUV-THz pump-probe experiments at FELs', *J. Synchrotron Rad.* 27, 11-16., (2020).

## Single-shot THz characterization for a new THz/XUV endstation in FLASH2020+

S. Gang<sup>1</sup>, R. Pan<sup>1</sup>

<sup>1</sup> *Deutsches Elektronen-Synchrotron (DESY), Notkestraße 85, D-22607 Hamburg, Germany*  
e-mail: seung-gi.gang@desy.de

The FLASH1 THz beamline at DESY provides intense THz pulses simultaneously to the FLASH1 soft X-ray beam with only a few femtosecond timing jitter for THz/XUV pump-probe experiments. As a part of the FLASH upgrading project, FLASH 2020+ [1], the FLASH1 will provide flexible polarization and enhanced XUV photon energy beyond carbon K-edge and separation of THz undulator will enable complete independent operation of XUV and THz. A new semi-permanent endstation for THz-XUV pump-probe experiments will be implemented and aim at various scientific researches such as solid state- and surface physics, surface chemistry, and especially femtomagnetism by various experimental geometries such as reflection- (for transverse magneto-optic Kerr effect, T-MOKE) or transmission (for magnetic small-angle X-ray scattering, SAXS) geometry. Online photon diagnostics for the THz pulses are under development and will provide the THz temporal- and spectral profile on a single-shot basis. For this purpose, single-shot diagnostics employing electro-optic sampling has been experimentally carried out [2,3]. A reflective echelon mirror with size of 30 mm by 30 mm was employed to introduce a series of probe pulses with 50 fs of timing interval as a temporal resolution. The probe pulses cover the temporal range of 10 ps which is employed for single-shot diagnostics of THz. Measured temporal profile and spectrum of THz pulse from single-shot method proves the practical availability of the single-shot diagnostics of THz pulse at FLASH1 after the FLASH 2020+ project.

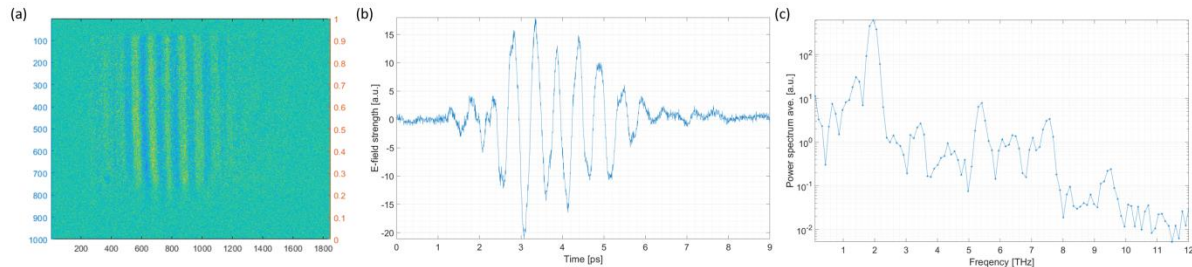


Figure 1. Results of single-shot THz diagnostics (a) Image of probe laser pulse after intensity modulation by THz field (b) Electric field of THz pulse (c) Measured THz (155  $\mu\text{m}$ ) spectrum in frequency.

### REFERENCES

- [1] 'FLASH2020+ Conceptual Design Report' (CDR), (2020).
- [2] K. Y. Kim, B. Yellampalle, and et al., 'Single-shot terahertz pulse characterization via two-dimensional electro-optic imaging with dual echelons', *Opt. Lett.* 32, 1968-1970 (2007)
- [3] G. Timothy Noe, I. Katayama, and et al., 'Single-shot terahertz time-domain spectroscopy in pulsed high magnetic fields', *Opt. Express* 24, 30328-30337 (2016)

## **9. Laser - material interaction**

## Sulphur concentration influence on morphology and optical properties of MoS<sub>2</sub> monolayers

A.Senkic<sup>1,2,3</sup>, A.Supina<sup>1,2,3</sup>, J.Bajo<sup>4</sup>, V. Jadrisko<sup>1,3</sup>, B. Radatovic<sup>1,3</sup> and N. Vujicic<sup>1,3</sup>

<sup>1</sup>Institute of Physics, Zagreb, Croatia

<sup>2</sup>Department of Physics, University of Rijeka, Rijeka, Croatia

<sup>3</sup>Center of Excellence for Advanced Materials and Sensing Devices, Institute of Physics, Zagreb, Croatia

<sup>4</sup>Department of Applied Physics, KTH Royal Institute of Technology, Stockholm, Sweden

e-mail: asenkic@ifs.hr

MoS<sub>2</sub> in its two-dimensional (2D) form is one of the most studied materials in the last decade due to its promising applications in semiconducting industry (photosensors [1], optoelectronics [1], photovoltaics [1] etc.). One of the main approaches in synthesis of semiconducting 2D materials is chemical vapour deposition (CVD) technique, schematically shown in Fig. 1. In this work we have systematically investigated how synthesis parameters (growth temperature  $T_G$ , sulphur temperature  $T_S$  and carrier gas flow) influence sample quality. As a result, correlation between synthesis parameters and sample's morphology and optical response were obtained.

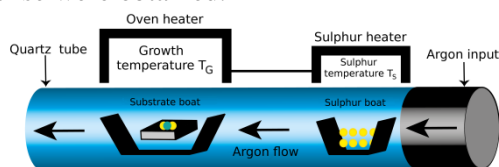


Figure 2. Schematic illustration for the CVD setup.

By changing mentioned synthesis parameters, the Mo:S ratio was consistently tuned which, in turn, modified both morphology and optical response of the sample (Fig. 2). As the ratio is approaching to the ideal value of 1:2, the morphology of samples becomes more symmetric, triangular with even edges while the PL and Raman spectra intensities for given sample increase. If the sulphur concentration is increased compared to the ideal stoichiometric ratio, the samples become dendritic with uneven edges and optical response is poor. On the other hand, if the molybdenum concentration is increased by increasing  $T_G$  vertical growth is preferred rather than lateral, and bilayers or multiple-layered islands are formed.

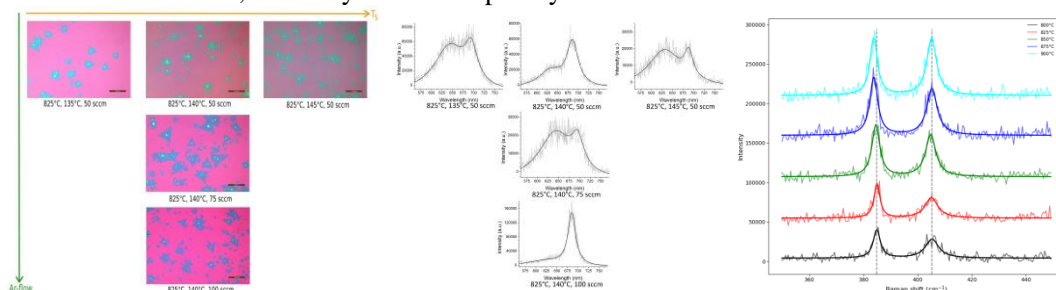


Figure 2: Left: Morphological evolution of CVD grown MoS<sub>2</sub> islands. Given synthesis parameters are in following order: growth temperature, sulphur temperature, argon flow. Scale bar is 100  $\mu\text{m}$ . Middle: Evolution of photoluminescence spectra of MoS<sub>2</sub> islands. Solid black lines represent non-linear fit using two Lorentzian functions. Right: Raman spectra of samples made at different growth temperatures. Sulphur temperature is 140°C and argon flow 75 sccm. Solid lines represent non-linear fit using two Lorentzian functions. Vertical grey lines are only eye-guides.

Raman spectra of samples grown at different  $T_G$  (800-900°C) are shown on the right side of Fig. 2. The difference between centers of these two Raman modes increases with the growth temperature increase [2]. One possible explanation for this behavior is increased induced tensile strain resulting from the high-temperature growth process. Complementary structural characterization by atomic force microscope (AFM) and scanning electron microscope (SEM) were used to determine existence of grain boundaries and cracks in crystal basal plane, showing that optimization of synthesis parameters leads to high-quality crystal morphology. Our further work will focus on exploring the optical properties of crystals in low-temperature limit.

### REFERENCES

- [1] Q.H. Wang, K. Kalantar-Zadeh, A. Kis et al. *Nature Nanotech* **7**, 699-712 (2012).
- [2] Zusong Zhu et al. *Mater. Res. Express* **6** 095011 (2019).

## Optical breakdown of liquid media triggered by a wide range of laser pulse durations and its analytical application

H. Delibašić Marković<sup>1</sup>, V. Petrović<sup>1</sup> and I. Petrović<sup>2</sup>

<sup>1</sup> Faculty of Science, University of Kragujevac, Serbia

<sup>2</sup> Academy of Professional Studies Šumadija, Department in Kragujevac, Serbia

e-mail: hristina.delibasic@pmf.kg.ac.rs

The generation of plasmas in liquid media was investigated to derive a closed-form mathematical expression describing the free electron density and energy density of the laser-induced plasma (LIP) [1] for laser pulse durations in the range of a few nanoseconds to a few tens of femtoseconds. In doing so, we postulated that a critical seed electron density exists due to the joined effects of multiphoton ionization (MPI) [2] and cascade ionization (CI) [3]. The effect of electron losses contributed to thermal ionization (TI) [4], electron diffusion (ED) [5], and electron-ion recombination (E-IR) [6] are also taken into account. The obtained results were verified via numerical simulation. This enabled us to analyze the interplay between MPI, CI, and joined effects of losses (TI, ED, and E-IR) during the laser pulse. After an extensive research on the subject, our results indicated that for longer laser pulses the generation of free electrons is always initiated by MPI but afterward dominated by CI, while for shorter pulse duration, MPI predominates. It is also important to note that during short and ultrashort pulses, losses due to TI, ED, and E-IR during breakdown almost completely diminish. By analytically solving the free-electron density rate equation [7], we were also able to calculate the energy density of the created plasmas in a wide range of pulse durations. A good overall quantitative agreement was found between calculated and available experimental values for the free electron density and plasma energy density [8-10].

### REFERENCES

- [1] A. De Giacomo and J. Hermann, *J. Phys. D: Appl. Phys.* 50(18), 183002 (2017).
- [2] A. Sharma, M. N. Slipchenko, M. N. Shneider, X. Wang, K. A. Rahman, and A. Shashurin, *Sci. Rep.* 8(1), (2018).
- [3] D. Woodbury, A. Goffin, R. M. Schwartz, J. Isaacs, and H. M. Milchberg, *Phys. Rev. Lett.* 125(13), (2020).
- [4] Y. R. Davletshin and J. C. Kumaradas, *Beilstein J. Nanotechnol.* 7, 869 (2016).
- [5] N. Linz, S. Freidank, X. X. Liang, H. Vogelmann, T. Trickl, and A. Vogel, *Phys. Rev. B.* 91(13), 134114 (2015).
- [6] P. K. Kennedy, D. X. Hammer, and B. A. Rockwell, *Prog. Quantum. Electron.* 21(3), 155 (1997).
- [7] H. Delibasic, V. Petrovic, and I. Petrovic, *Journal of the Physical Society of Japan* 89(11), 114501 (2020).
- [8] J. Noack and A. Vogel, *IEEE J. Quantum Electron.* 35(8), 115 (1999).
- [9] J. Jiao and Z. Guo, *Appl. Phys. B* 103(1), 195 (2010).
- [10] E. I. Mareev, B. V. Rumiantsev, E. A. Migal, A. S. Bychkov, A. A. Karabutov, E. B. Cherepetskaya, V. A. Makarov, and F. V. Potemkin, *Meas. Sci. Technol.* 31(8), 085204 (2020).

## Morphological study of silver in the conditions of ultrashort laser ablation in liquid

J. Stašić<sup>1</sup>, M. Trtica<sup>1</sup>, D. Batani<sup>2</sup>, R. Benocci<sup>3</sup>, V. Narayanan<sup>4</sup>, A. Žekić<sup>5</sup>

<sup>1</sup>*“Vinča” Institute of Nuclear Sciences – National Institute of the Republic of Serbia, University of Belgrade, Belgrade, Serbia*

<sup>2</sup>*Université Bordeaux, CNRS, CEA, CELIA (Centre Lasers Intenses et Applications), Bordeaux, France*

<sup>3</sup>*Dipartimento di Scienze dell’Ambiente e del Territorio e di Scienze della Terra-Università degli Studi di Milano-Bicocca, Milano, Italy*

<sup>4</sup>*Indian Institute of Technology Jodhpur, Jodhpur, Rajasthan, India*

<sup>5</sup>*Faculty of Physics, University of Belgrade, Belgrade, Serbia*

The study deals with morphological effects on the silver target irradiated with ultrashort laser pulses in liquid (water). Synthesis of metal nanostructures (NS) by laser ablation in liquid is a relatively new method with benefits including clean production, without the use of additional chemicals necessary in conventional techniques, obtaining of pure particles with no surfactants, and good stability of the colloid. There are fewer studies, however, concerning the effects on the target itself during the laser action, and this type of research could lead to a better understanding of the physics involved and therefore better control of the process by linking the induced morphological features with NS synthesis results – yield, size distribution, etc. Also, reports on the laser ablation parameters of silver in liquid environment are scarce and significant for every particular set of parameters (laser pulse length, other laser parameters, liquid type). In this work, Ag target was irradiated with laser pulses 40 ps long, at 1064 nm wavelength and 10 Hz repetition rate. Irradiation time was 5 min, and pulse energies ranged from 0.5 mJ to around 22 mJ. Submicron particles were synthesized for all energies above 1 mJ and their size varied from tens of nanometers to ~200 nm. Optimum results were obtained for energies ~14-17 mJ. Ablation depths were in the range of 30 to 100 μm for the above mentioned energy range. Damage threshold fluence was determined to be around 0.7 J/cm<sup>2</sup>. Surface features were distinctly different than in air with sponge-like structure.

### REFERENCES

- [1] J. Stašić, Lj. Živković, M. Trtica, J. Nanopart. Res. 18, art. no. 366 (2016).
- [2] R. Nadarajah, S. Barcikowski, B. Gökce, Opt. Express 28, 2909 (2020).

## Analysis of Chitosan/ Hydroxyapatite spin-coated fs microstructured Poly Lactic Acid (PLA) temporary cell scaffolds

L. Angelova<sup>1</sup>, A. Daskalova<sup>1</sup>, E. Filipov<sup>1</sup>, R. Mincheva<sup>2</sup>, X. Carette<sup>2</sup>, D. Miano<sup>3</sup>, D. Aceti<sup>1</sup>, A. Trifonov<sup>4</sup>, I. Buchvarov<sup>4</sup>

<sup>1</sup>*Institute of Electronics, Bulgarian Academy of Sciences, Sofia, Bulgaria*

<sup>2</sup>*Laboratory of Polymeric and Composite Materials (LPCM), University of Mons, Mons, Belgium*

<sup>3</sup>*Faculty of Physics, University of Calabria, Calabria, Italy*

<sup>4</sup>*Physics Department, Sofia University "St. Kliment Ohridski", Sofia, Bulgaria*

e-mail:lily1986@abv.bg

In the field of bone tissue engineering, temporary cell scaffolds, based on biocompatible and degradable biopolymers, are emerging as one of the most powerful tools for guided self-regeneration of injured, diseased or malfunctioning tissues. These cell environmental structures serve as mechanically stable supporting platforms for patient's own cells attachment and proliferation and are gradually displaced by the newly formed bone tissue in an absolutely natural way. In recent years scientists are in constant search and optimization of the best materials for restoring, maintaining and improving cell scaffold function - their biocompatibility and "extracellular matrix qualities", such as surface roughness, wettability, hierarchical interconnected porosity, anti-inflammatory properties, and at the same time, avoiding cell cytotoxicity changes in their chemical composition. In order to fulfill the cells viability needs, additional functionalization of the temporary cell platforms is an absolute requirement. Femtosecond laser surface modification is a non-thermal and precisely controlled cell scaffold optimization technique, which does not change the chemical composition of the material treated, while finely tunes its topography properties, like wettability, charge, roughness and porosity. Due to its biocompatibility, biodegradability, mechanical stability and strength, poly-lactic acid (PLA) is gradually being established as a basic biomaterial in the design of temporary tissue engineered bone cell matrices. It is thermoplastic polyester of lactic acid, a natural non-toxic metabolic product, subject to carboxylic acid degradation pathway in the body. On the other hand, chitosan (Ch) is a natural biocompatible polysaccharide, characterized with high antimicrobial activity and superior affinity to cell proteins, making it a promising cell adhesion non-inflammatory biomaterial. Hydroxyapatite (HAp), the form in which calcium phosphate is naturally found in bones, is known for its osteoconductive properties and it is a key component in implants "bonding glue" with surrounding tissues, as it makes strong connection with them.

In the current study, CPA Ti:sapphire fs laser system ( $\tau = 150\text{fs}$ ,  $\lambda = 800\text{ nm}$ ,  $\nu = 0.5\text{ kHz}$ ) was used for surface modification of PLA samples at fluence  $F = 0.8\text{ J/cm}^2$  and scanning velocity  $V = 3.8\text{ mm/s}$ . Additional thin layer of chitosan (CH)/ hydroxyapatite (HAp) (up to 30nm) was deposited on the treated PLA matrices by the precise spin coating method for cell scaffolds surface additional functionalization. In order to monitor their complementary impact on the PLA scaffolds properties, both surface modification methods were applied on the PLA samples, prepared by compression molding. Each laser processed PLA scaffold was analyzed in respect to control - laser treated and untreated surface, covered with Ch or HAp, respectively. The microstructured scaffolds were investigated by SEM, EDX, FTIR, AFM and WCA analyses. Preliminary cell viability studies were performed. The results obtained show that such combined methods application for functionalization of the bone PLA scaffolds can essentially improve the bioactivity properties of the as created PLA-Chitosan and PLA- hydroxyapatite hybrid cell matrices.

### ACKNOWLEDGMENTS:

This research was funded by BULGARIAN NATIONAL SCIENCE FUND (NSF) under grant number No. **KP-06-H48/6 (2020–2023)**, „Development of hybrid functional micro/nanoporous biomaterial scaffolds by ultra-fast laser modification"; EUROPEAN UNION'S H2020 research and innovation programme under the Marie Skłodowska-Curie Grant Agreement No. **861138** and H2020 FET Open METAFast Grant Agreement No. **899673**.

## Neodymium-doped ZnO nanoparticles for NIR II biomarkers

N. Tarasenka<sup>1</sup>, V. Kornev<sup>1</sup> and N. Tarasenko<sup>1</sup>

<sup>1</sup>B.I. Stepanov Institute of Physics of the National Academy of Sciences of Belarus

Minsk, Belarus

e-mail: natalie.tarasenka@dragon.bas-net.by

Recently, design and preparation of the nanoparticles (NPs) suitable for labeling of the living cells has become an important task of modern nanotechnology. Among the requirements to this type of nanomaterials is their biocompatibility and luminescence in the NIR region because biological tissues have a maximum light transmission in the 850-1100 nm range [1]. This work is focused on the laser-assisted method for Nd-doped ZnO NPs preparation and testing their luminescent properties. ZnO nanocrystals doped with Nd<sup>3+</sup> ions, which have several important luminescent bands in the NIR region, can be of interest for applications as luminescent biomarkers. The preparation method is based on laser ablation of zinc target in Nd(NO<sub>3</sub>)<sub>3</sub> solution using ns-pulsed Nd:YAG laser (1064 nm, 10 ns, 10 Hz).

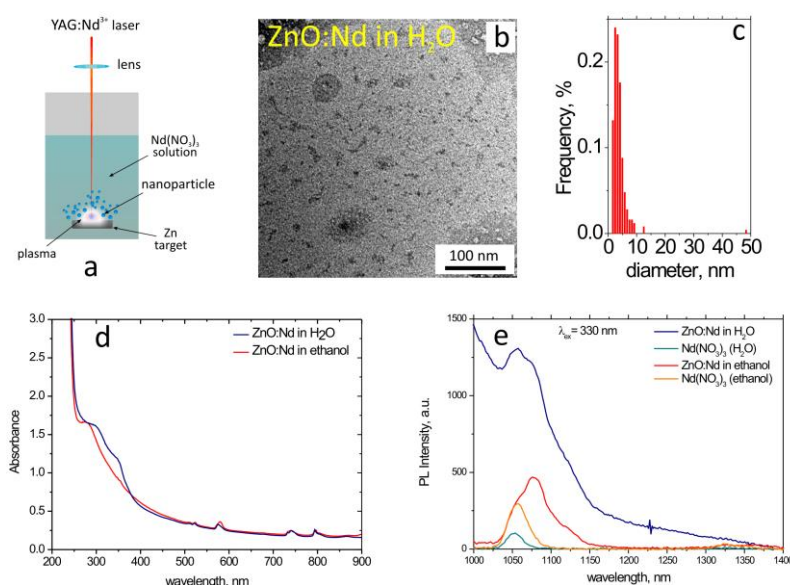


Figure 1. Scheme of the setup used for the ZnO:Nd nanoparticles preparation (a), TEM image of the particles prepared in water (b) and their size distribution (c). The figures (d) and (e) show the optical absorption and photoluminescence spectra of the prepared colloids in water and ethanol.

It was shown that Nd<sup>3+</sup> ions can be incorporated into ZnO NPs that is confirmed by the results of XRD, TEM characterization and observation of the characteristic NIR luminescence of Nd<sup>3+</sup> ions in the obtained ZnO nanocrystals. Upon excitation at 578 and 808 nm, three luminescence bands were observed with centers at 887, 1060, and 1334 nm, attributable to the radiative transitions from the ground <sup>4</sup>F<sub>3/2</sub> level of Nd<sup>3+</sup> to the <sup>4</sup>I<sub>9/2</sub>, <sup>4</sup>I<sub>11/2</sub> and <sup>4</sup>I<sub>13/2</sub> levels, respectively. The position and shape of these peaks in the recorded luminescence spectrum differ from the peaks of Nd<sub>2</sub>O<sub>3</sub> nanocrystals spectrum, which confirms the inclusion of Nd<sup>3+</sup> ions in ZnO nanocrystals instead of the formation of an impurity Nd<sub>2</sub>O<sub>3</sub> phase. UV-Vis absorption spectra indicated a decrease in the optical band gap of the doped ZnO that can be attributed to the distortion of the crystal structure of zinc oxide upon doping due to the difference in the ionic radii of Nd<sup>3+</sup> (0.99 Å) and Zn<sup>2+</sup> (0.74 Å).

### REFERENCES

- [1] Y. Liu, W. Luo, R. Li, H. Zhu, X. Chen, Optics Express 17, 9748 (2009).

## Dynamic interference of photoelectrons at multiphoton ionization of atoms by short laser pulses

A. Bunjac, D. B. Popović and N. S. Simonović  
*Institute of Physics, Belgrade, Serbia*  
 e-mail:simonovic@ipb.ac.rs

The dynamics of atomic levels resonantly coupled by an intense short laser pulse is studied by calculating numerically the time-dependent amplitudes for the populations of atomic states (both discrete and continuum) [1, 2]. Here we consider the resonant multiphoton ionization of atoms which can be described within the single active electron approximation (hydrogen, alkali), studied earlier using other methods [3, 4]. It is demonstrated that the laser pulse gives rise to two wave packets emitted with a time delay with respect to each other (at the rising and falling sides of the pulse) which interfere in the time domain (see Fig. 1). The interference effects are observed in the energy spectrum and momentum distribution of photoelectrons.

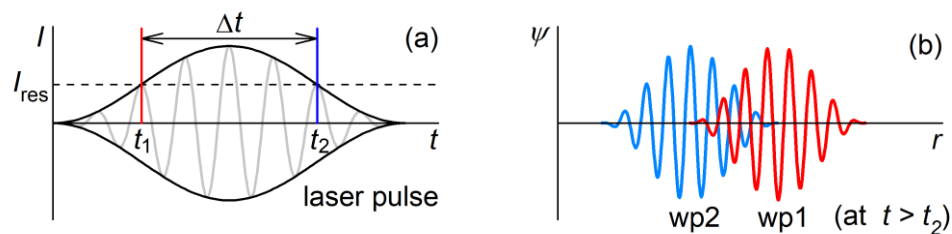


Figure 1. (a) If the intensity  $I$  of applied laser field varies, an atomic state can (due to the dynamic Stark shift) transiently shift into resonance, that occurs two times during the pulse (at  $t_1$  and  $t_2$  when  $I = I_{\text{res}}$ ). (b) Then the photoelectrons emitted at the rising and falling sides of the pulse (electron wave packets wp1 and wp2, respectively) interfere due to a time delay  $\Delta t = t_2 - t_1$ .

### REFERENCES

- [1] P. V. Demekhin and L. S. Cederbaum, *Phys. Rev. A* **83**, 023422 (2011).
- [2] P. V. Demekhin and L. S. Cederbaum, *Phys. Rev. A* **86**, 063412 (2012).
- [3] A. Bunjac, D. B. Popović and N. S. Simonović, *Phys. Chem. Chem. Phys.* **19**, 19829 (2017).
- [4] A. Bunjac, D. B. Popović and N. S. Simonović, *Phys. Lett. A* **394**, 127197 (2021).

## Laser surface texturing of Ti/Cu/Ti/Si and Ti/Cu/Zr/Ti/Si multilayer thin films

<sup>1</sup>N. Božinović, <sup>2</sup>D. Milovanović, <sup>1</sup>V. Rajić, <sup>1</sup>L. Rakočević, <sup>1</sup>J. Savović, <sup>1</sup>S. Petrović

<sup>1</sup> Department of Atomic Physics, „VINČA" Institute of Nuclear Sciences - National Institute of the Republic of Serbia, University of Belgrade, Belgrade, Serbia<sup>2</sup>School of Electrical Engineering, University of Belgrade, Serbia

<sup>3</sup> Institute of General and Physical Chemistry, Studentski trg 12-16, 11158 Belgrade, Serbia  
e-mail: [nevena.bozinovic@vin.bg.ac.rs](mailto:nevena.bozinovic@vin.bg.ac.rs)

Design of surface patterning with the co-existence of micro- and nanoscale features by picosecond laser processing is investigated in order to improve cell integration. New biomedical Ti alloys with a high concentration of  $\beta$ -stabilizer elements (zirconium) are developed, as potential solutions to the mismatch between the Young's modulus of the implant and the surrounding hard tissues. On the other hand, in order to enhance the tribological and antimicrobial properties of Ti/Zr coating, a novel titanium-copper and titanium-copper-zirconium thin film systems were designed in this work. Novel composite structure composed of subsurface distributed Cu and Zr layers (thickness of 10 nm), with satisfying mechanical properties and moderate biocompatibility, were deposited by ion sputtering on Si substrate to the total thickness of 300 nm. The multilayer thin films were irradiated by focused linearly p-polarised picosecond pulses with following characteristics: repetition rate of 10 Hz, pulse duration equal to 150 ps, central wavelength of 1064 nm and 120  $\mu$ m Gaussian spot diameter. The changes of the composition and surface morphology in the Ti/Cu/Ti/Si and Ti/Cu/Zr/Ti/Si multilayer thin films were monitored by X-ray photoelectron spectroscopy (XPS), by scanning electron microscopy (SEM) and by profilometry.

The main part of the absorbed laser energy was rapidly transformed into heat, producing intensive modifications of composition and morphology on the multilayer surface [1,2]. The results show an increase in surface roughness, formation of a specific surface topography, appearance of hydrodynamic features and ablation of surface material. XPS analysis revealed that laser modification was induced intermixing between the Cu and Zr layers, but also with dominant Ti component. During the laser processing of Ti/Cu/Ti/Si and Ti/Cu/Zr/Ti/Si multilayer thin films, delivered energy was sufficient to cause solid-state reactions, the formation of alloy between components.

Laser processing of Ti/Cu/Ti/Si and Ti/Cu/Zr/Ti/Si multilayer thin films is used to create the arrayed surface structure, such as laser-induced periodic surface structures (LIPSS) and at the same time to induce mixing of components inside the thin film structures, as well as the formation of ultrathin oxide layer at the laser-treated surfaces [3,4]. Laser surface patterns are organized as networks and parallel lines, where lines formed of LIPSS are wide up to 100  $\mu$ m and distance between lines are less than 300  $\mu$ m. The average periodicity between LIPSSs was about 900 nm, which would correspond to the formation of low spatial frequency LIPSS (LSFL).

### REFERENCES

- [1] S. Petrović, D. Peruško, "Laser Modification of Multilayer Thin Films," in *Advances in Optics*, Y. Y. Sergey, Ed. International Frequency Sensor Association Publishing, 2019, pp. 169–201.
- [2] Bäuerle, D. (2013). *Laser processing and chemistry*. Springer Science & Business Media.
- [3] V. Stranak, H. Wulff, H. Rebl, C. Zietz, K. Arndt, R. Bogdanowicz, B. Nebe, R. Bader, A. Podbielski, Z. Hubicka, and R. Hippler, "Deposition of thin titanium-copper films with antimicrobial effect by advanced magnetron sputtering methods," *Mater. Sci.Eng. C*, vol. 31, no. 7, pp. 1512–1519, Oct. 2011, doi: 10.1016/j.msec.2011.06.009.
- [4] Yu, Z., Yang, G., Zhang, W., Hu, J., "Investigating the effect of picosecond laser texturing on microstructure and biofunctionalization of titanium alloy," *Journal of Materials Processing Technology*, vol. 255, pp. 129–136, May 2018, doi: 10.1016/j.jmatprotec.2017.12.009.

## Raman spectroscopy and multivariate classification as a tool for different ketchup samples discrimination

S. Kolasinac<sup>1</sup>, I. Pecinar<sup>1</sup>, Z. Dajic-Stevanovic<sup>1</sup>

<sup>1</sup> Faculty of Agriculture, Department of Agricultural Botany, Belgrade, Serbia  
e-mail: stefan.kolasinac@agrif.bg.ac.rs

The main aim of this paper is to test PCA-LDA (Principal Component Analysis – Linear Discriminant Analysis) coupled with Raman spectroscopy for discrimination of two ketchups commercially available at the local markets in Serbia. Raman spectra were recorded at two different wavelengths (785 and 532 nm) and 30 spectra per sample are obtained. The data were divided into the training (3/4 of samples) and validation (1/4 of samples) data. Two types of pre-processing methods which were applied and results of discrimination are represented in table 1. Obtained results showed that second-order derivative did not improve discrimination power. On the other hand, laser at 785 nm provided a better classification of samples which can be related to the fact that 785 nm laser reveals bands that are masked by the high fluorescence background seen when using the 532 nm laser and consequently gives wider chemical information about the sample (Haraa et al., 2018). Pre-processing analysis of the spectra was performed using the software The Unscrambler X version 10.4 (Camo Software, Oslo, Norway) while supervised classification models were performed using the Python software.

Table 1. Classification results of training and test sets of PCA-LDA

Excitation wavelength			785 nm		532 nm	
Pre-processing methods			Smoothing + baseline correction + normalization + principal component analysis	Smoothing + baseline correction + normalization + 2 <sup>nd</sup> order derivative + principal component analysis	Smoothing + baseline correction + normalization + principal component analysis	Smoothing + baseline correction + normalization + 2 <sup>nd</sup> order derivative + principal component analysis
Correct classified (%)	Training data	Sample 1	95.45	95.45	95.45	90.91
		Sample 2	100.00	95.45	95.45	95.45
	Test data	Sample 1	87.50	87.50	62.50	37.50
		Sample 2	100.00	87.50	37.50	37.50

### REFERENCES

[1] R. Haraa, M. Ishigakib, Y. Kitahamab, Y. Ozakib, T. Genkawaa. Food Chem. 258, 308 (2018)

## Implementation of general Bessel beam scattering using the discrete dipole approximation

S. A. Glukhova<sup>1,2</sup>, M. A. Yurkin<sup>1,2</sup>

<sup>1</sup>Voevodsky Institute of Chemical Kinetics and Combustion, SB RAS,  
Novosibirsk, Russia

<sup>2</sup>Novosibirsk State University, Novosibirsk, Russia  
stefgluhova@gmail.com

Among various types of structured light with orbital angular momentum Bessel beams hold leading positions in many fields. One of the most prominent advantages of Bessel beams is their ability to propagate maintaining the profile near the beam axis. These beams are actively used in such areas as optical manipulation (tweezing), material proceeding, imaging, etc.

In many physical problems, it is crucial to consider the scattering of Bessel beams, which is predominantly studied for spherical particles with the use of the generalized Lorenz-Mie theory (GLMT) than for arbitrary particles. This work aims to classify various types of high-order vector Bessel beams and develop the capability to simulate the scattering of such beams by arbitrary particle using the discrete dipole approximation (DDA).

Thus, a new general classification of all existing Bessel beam types was developed. Next, we implemented these beams in ADDA code – an open-source parallel implementation of the DDA [1]. The code is available for everyone on a separate branch on GitHub [2] and enables easy and efficient simulation of Bessel beams scattering by arbitrary-shaped particles. One of the possible applications includes scattering of the circular symmetric (CS) type of Bessel beam by a red blood cell presented in Figure 1. The results of this work pave the way for the following research related to the Bessel beam scattering by particles near a substrate and optical forces.

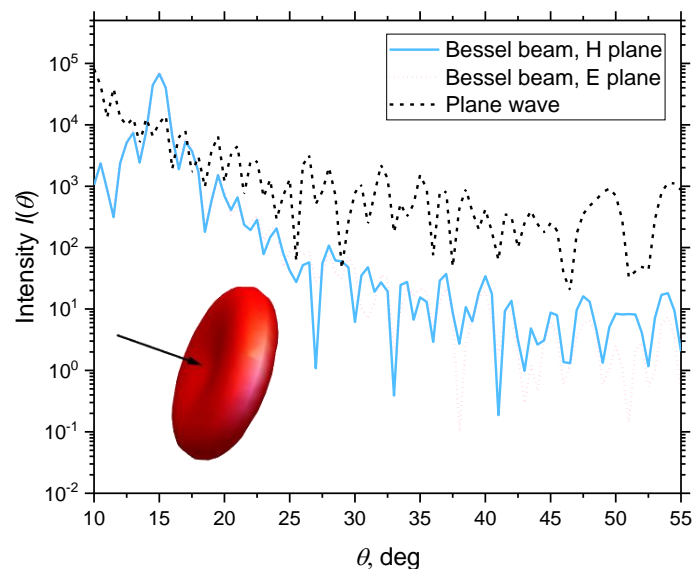


Figure 1. Example of zero-order CS Bessel beam scattering simulation by a red blood cell (cell characteristics are taken from [3]).

### REFERENCES

- [1]. M.A. Yurkin and A.G. Hoekstra, *J. Quant. Spectrosc. Radiat. Transf.* **112**, 2234–2247 (2011).
- [2]. <https://github.com/stefaniagl/adda>
- [3] M.A. Yurkin, *Discrete Dipole Simulations of Light Scattering by Blood Cells*, PhD thesis, University of Amsterdam, (2007).

## The surface array structures induced by femtosecond laser modifications of Ti/Cr multilayer thin films for biomedical applications

<sup>1</sup>Suzana Petrović, <sup>1</sup>D. Peruško, <sup>2</sup>A. Mimidis, <sup>2</sup>P. Kavatzikidou, <sup>2</sup>A. Manousaki, <sup>1</sup>N. Božinović,  
<sup>1</sup>V. Rajić, <sup>2</sup>E.Stratakis

<sup>1</sup>Vinča Institute of Nuclear Sciences, University of Belgrade, P.O.Box 522, 11001 Belgrade, Serbia

<sup>2</sup>Institute of Electronic Structure and Laser (IESL), Foundation for Research and Technology (FORTH), N. Plastira 100, Vassilika Vouton, 70013 Heraklion, Crete, Greece

e-mail: [spetro@vin.bg.ac.rs](mailto:spetro@vin.bg.ac.rs)

The experimental study of the static and dynamic femtosecond laser ablation of the multilayer 15x(Ti/Cr)/Si system is reported. The layer-by-layer selective laser ablation mechanism was studied by analysis of the surface morphology and elemental composition in static single pulse irradiation in a range of pulse energy from 10 – 17  $\mu$ J. The selective ablations as number of concentric circles in modified spots are increased with the pulse energy. The boundary between the circles was shown a change in the depth, comparable to the thickness of the individual layers. Changes in the elemental composition at the edges are associated with the removal of the layer by layer. Due to the intermixing of components and higher content of oxygen in the central area of ablated spots, it is expected that an ultra-thin layer composed of Ti and Cr oxide phases is formed at the bottom of the ablated center. The dynamic multi-pulse irradiation was observed via the production of lines with laser-induced periodic surface structures (LIPSS) at different laser parameters (scan velocities and laser polarization). The spatial periodicity of the formed LIPSS depends on changes in the effective number of pulses and laser polarization, as well as the nature of the material. The formation of LIPSS is followed with the significant ablation of multilayer 15x(Ti/Cr)/Si system, without visible hydrodynamic features, but ripples are somewhere covered with nanoparticles dimension up to 100 nm.

The main focus of this experimental study was examined a novel Ti/Cr nanolayered composite in order to create a biomimetic surface with suitable composition and structure for cell integration. Using SEM and confocal microscopy images of the laser modified surfaces with seeded cell culture (NIH 3T3 fibroblasts) was found that cell adhesion and their growth depend on the surface composition and morphological forms. These results indicated a good adhesion and proliferation of cells after two and four days, with some tendency of grouping of cells on the laser modified surfaces.

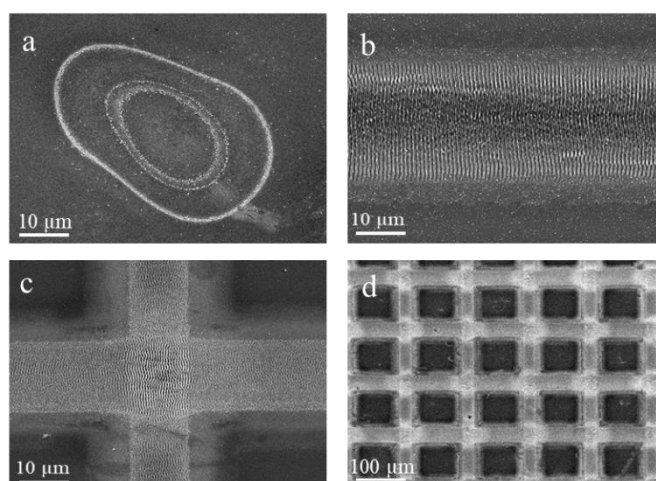


Figure 1. SEM images of 15x(Ti/Cr)/Si multilayer thin film after fs modification at the pulse energy of 15  $\mu$ J for the created: (a) spot, (b) lines, (c) crossed lines and (d) network-like structure on a larger surface.

## Direct laser writing waveguides in CR-39 polymer

S. Gündogdu<sup>1,2,3</sup>, and T. Schröder<sup>1,2</sup>

<sup>1</sup>*Department of Physics,*

*Humboldt-Universität zu Berlin, Berlin, Germany*

<sup>2</sup>*Ferdinand Braun Institut, Berlin, Germany*

<sup>3</sup>*Center for Theoretical Physics of Complex Systems,*

*Institute for Basic Science, Daejeon, South Korea*

e-mail: sinang@physik.hu-berlin.de

We present a simulation model for laser writing waveguides into a bulk polymer using a low-power UV laser. CR-39, an organic polymer commonly used as a lens material, is transparent to visible light and has a small extinction coefficient in the ultraviolet spectral range ( $k \sim 0.004$  at 400 nm). Its refractive index and ultraviolet extinction coefficient, however, increase when thermally heated. Previous experiments involving oven annealing showed an up to 10% refractive index change at 600 nm [1]. Such an intrinsic index change can be optically explored, making CR-39 an interesting candidate as a direct laser writing medium. To model the induced refractive index change under laser illumination, we use the Arrhenius equation for the rate with which the absorption coefficient changes for a moving Gaussian beam as a heat source. We calculate the refractive index profiles of the annealed zones using finite element methods. Our simulations show the feasibility of writing 3D embedded waveguides with a CW laser in contrast to high-power pulsed lasers that are commonly used in laser writing. At high laser powers, catastrophic instabilities can occur. We discuss a stabilization mechanism which may prevent instability and enable even higher index contrasts. This platform could offer a low-cost alternative to femtosecond laser writing techniques [2].

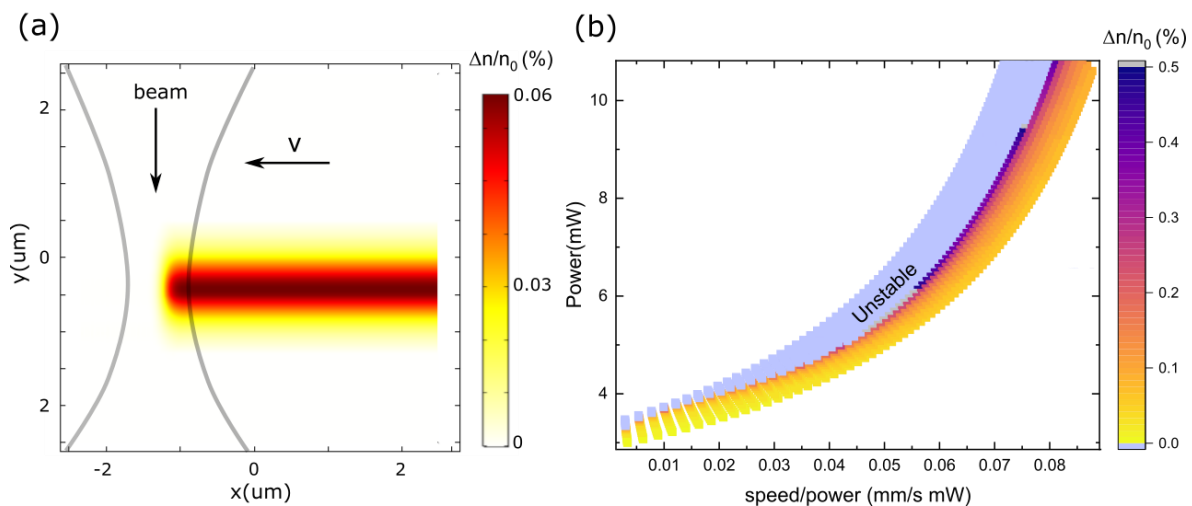


Fig.1 (a) Simulated steady-state change of refractive index of CR-39 due to a moving Gaussian laser beam. (b) Change of refractive index as a function of laser power and writing speed/power ratio for a 410 nm beam with a numerical aperture of 0.5.

### REFERENCES

- [1] V. Kumar and P. K. Goyal and S. Mahendia and R. Gupta and T. Sharma and S. Kumar, Radiation Effects and Defects in Solids 166, 109-113 (2011).
- [2] K. M. Davis, K. Miura, N. Sugimoto, and K. Hirao, Optics Letters 21, 1729-1731 (1996).

## **10. Optical metamaterials and plasmonics**

## Active terahertz metamaterial for polarization manipulation and biosensing

D. B. Stojanovic<sup>1</sup>, V. Milosevic<sup>2</sup>, U. Ralevic,<sup>2</sup> Lj. Hadzievski<sup>1</sup>

<sup>1</sup>*Vinca Institute of Nuclear Sciences, University of Belgrade  
Belgrade, Serbia*

<sup>2</sup>*Institute of physics, University of Belgrade, Belgrade, Serbia  
e-mail: dankas@vin.bg.ac.rs*

Controlling states of circular polarization with metamaterials [1] enables diverse applications in information processing, spectroscopy and communications. Furthermore, strong modulation of polarization of terahertz (THz) electromagnetic waves can be achieved by integrating active material (such as graphene) with metamaterials [2,3]. The chiral effects can be tuned and metamaterial sensing capabilities can be improved by dynamical modulation of the graphene conductivity. Nowadays, there is a need for rapid and reliable detection of biological samples, especially viruses. The advantage of active metamaterials is precise distinction in between viruses, which is challenging due to their nearly comparable refractive indices. This makes them appropriate for biosensor applications [4,5].

In this work, we numerically investigate THz electromagnetic wave propagation through metamaterial composed of resonant elements based on metallic strips embedded with gated graphene layer. The analysis is provided by calculation of cross- and co-reflection coefficients and efficiency of linear to circular polarization conversion with the change of the Fermi energy of graphene. In addition, the sensitivity of reflection spectra is tested for variations of refractive index, using the data available in the literature for several types of viruses, which is indicative for performance of the proposed metamaterial as a potential biosensor. We expect that proposed structure will enable easier biosensor fabrication with enhanced detection sensitivity compared to previously numerically investigated structures.

### REFERENCES

- [1] D. B. Stojanović, G. Gligorić, P. P. Beličev, M. R. Belić, Lj. Hadžievski, *IEEE J. Sel. Top. Quantum Electron.*, 27, 4700506 (2020).
- [2] S. J. Kindness et al, *Adv. Optical. Mater.* 2020, 1000581 (2020).
- [3] T-T. Kim et al, *Sci. Adv.* 3(9), e1701377 (2017).
- [4] Y. Zhang, Y. Feng, J. Zhao, *Carbon* 163, 244-252 (2020).
- [5] M. Amin, O. Siddiqui, H. Abutarboush, M. Farhat, R. Ramzan, *Carbon* 176, 580-591 (2021).

## Light absorption in two-dimensional crystals covered by randomly distributed plasmonic nanoparticles

G. Isić<sup>1,2</sup>, U. Ralević<sup>1</sup> and M. R. Belić<sup>2</sup>

<sup>1</sup>*Institute of Physics Belgrade, University of Belgrade, Belgrade, Serbia*

<sup>2</sup>*Texas A&M University at Qatar, Doha, Qatar*

e-mail:isicg@ipb.ac.rs

The discovery of many thermodynamically stable two-dimensional crystals attainable, amongst others, by the mechanical exfoliation method [1] has, since the 2000s, been inspiring the investigation of a range of electronic and, more recently, optoelectronic systems featuring such atomically thin layers either individually or stacked into so-called van der Waals heterostructures. In case of van der Waals heterostructure photovoltaics [2], light trapping strategies gain in significance as the active layer thickness is typically two orders of magnitude smaller than the wavelength.

We pursue ways to increase the light absorption efficiency using plasmonic nanoparticles randomly distributed on top of two-dimensional crystals [3]. To study the light absorption in disordered systems, we employ Smuthi [4,5], an open-source T-matrix based Python package for simulating light scattering on particles embedded in arbitrary layered systems. In numerical simulations, we assume that a number  $N_p$  of nanoparticles is arranged over a square area  $A$  with a uniform distribution. As macroscopic clusters (such that  $A \sim 1 \text{ mm}^2$  or more) are way too large to simulate numerically, our method relies on simulating sufficiently large (typically  $N \sim 100$ ) ensembles of smaller randomly generated clusters and estimating the absorption enhancement of a macroscopic system from the ensemble average. In the example shown in Fig. 1, we study how the nanoparticle concentration  $n$  affects the observed enhancement and find that, typically, the enhancement grows with increasing  $n$ , but, somewhat unexpectedly, only to a certain point after which it starts to decrease.

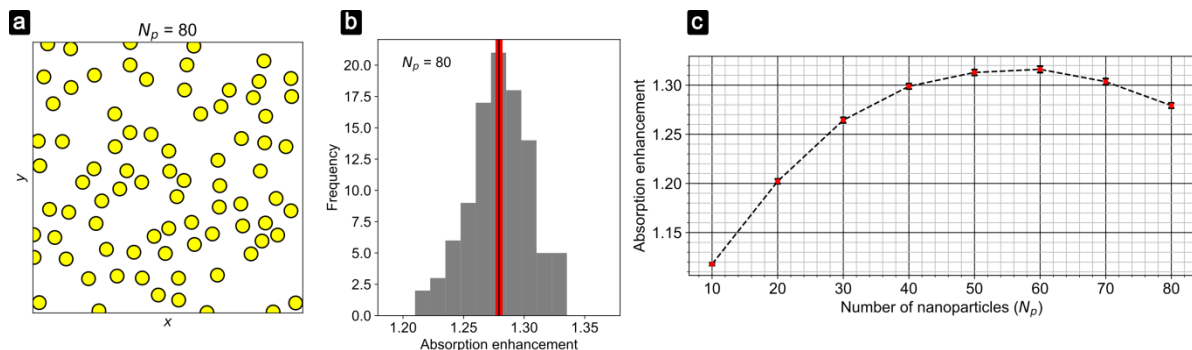


Figure 1. Absorption enhancement at  $\lambda = 550 \text{ nm}$  in a  $1 \text{ nm}$  layer of  $\text{MoS}_2$  sitting on top of a gold film (a) A typical cluster of 80 gold  $100 \text{ nm}$  nanoparticles randomly distributed over an area of  $2 \times 2 \text{ }\mu\text{m}^2$ . (b) Absorption enhancement histogram obtained by simulating 100 randomly generated clusters. The vertical black line represents the ensemble mean, while the mean error is indicated by the red band. (c) Absorption enhancement (ensemble mean) as a function of the number of nanoparticles with  $A = 4 \text{ }\mu\text{m}^2$ . The mean error is indicated by error bars which are hardly visible on this scale.

### REFERENCES

- [1] K. S. Novoselov, D. Jiang, F. Schedin, T. J. Booth, V. V. Khotkevich, S. V. Morozov, A. K. Geim, PNAS **102**, 10451 (2005)
- [2] D. Jariwala, A. R. Davoyan, J. Wong, H. A. Atwater, ACS Photonics **4**, 2962 (2017)
- [3] <http://pv-waals.com>
- [4] SMUTHI Available: <https://smuthi.readthedocs.io> [Accessed June 22, 2021]
- [5] Amos Egel: "Accurate optical simulation of disordered scattering layers for light extraction from organic light emitting diodes", Dissertation, Karlsruhe, DOI: 10.5445/IR/1000093961 (2018)

## Fibonacci sequence design for MXene based metasurface with enhanced optical absorption in the visible range

M. Obradov, Z. Jakšić, D. Tanasković, I. Mladenović, D. Vasiljević Radović

Centre of Microelectronic Technologies, Institute of Chemistry, Technology and Metallurgy - National Institute of the Republic of Serbia

University of Belgrade, Njegoseva 12, 11000 Belgrade, Serbia

e-mail: marko.obradov@nanosys.ihm.bg.ac.rs

In this contribution we aim to extend the use of fractal sequences in broadband Bragg grating superabsorbers to ultrathin metasurface-based superabsorbers utilizing plasmonic effects.

Bragg gratings in our case represent 1D metamaterials with their dispersive properties tailored by the thickness and the number of the grating lines. Additional tailoring of optical properties for broadband applications can be achieved by embedding in-plane truncated sequences of various infinite series, i.e. Cantor or Fibonacci sequences, to form quasi periodic fractal metasurfaces [1, 2]. These structures are further optimized towards enhanced optical absorption by utilizing various conductive materials. Here, we utilize MXenes as a class 2D materials characterized by free-electron conductivity instead of more commonly utilized plasmonic materials like noble metals or graphene [3].

An alternative approach to the superabsorber design is to utilize two thin conductive sheets separated by a thin dielectric layer. By structuring one of the conductive layers as a 1D diffraction grating the incident light couples with the plasmonic modes that are localized within the dielectric layer, thus achieving enhanced optical absorption on the subwavelength level [4].

We theoretically and numerically analyze a metamaterial absorber structure consisting of thin MXene (titanium carbide) strips as presented in Fig.1.a. The top layer is patterned by thin strips of MXene separated by narrow air gaps. Both narrow gap and MXene strip widths follow the Fibonacci sequence starting with 10 nm. The middle layer is silica glass, and bottom layer is a thin MXene sheet. Fig.1.b presents widening of useful absorption spectra by increasing the number of embedded sequence elements. We believe our proposal extends the toolbox for the design of plasmonic metamaterial-based superabsorbers, but one could also envision its use for other applications.

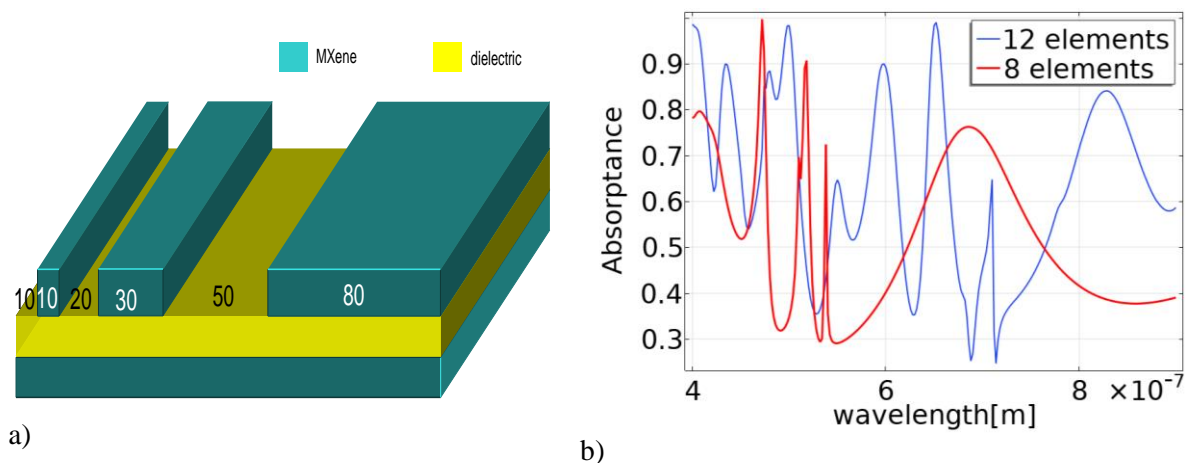


Figure 1. MXene metamaterial with striped top surface. a) unit cell consisting of strips and gaps whose widths are following a finite Fibonacci sequence. (numbers given in the picture represent widths of the elements in nm). Thickness of each layer is 50 nm. b) Absorption spectra depending on the order of the Fibonacci sequence.

### REFERENCES

- [1] R. Ning, S. Liu, H. Zhang, X. Kong, B. Bian, J. Bao, *J. Opt.*, 16(12), 125108, 2014.
- [2] M. Maksimović, Z. Jakšić, *J. Opt. A-Pure Appl. Opt.*, 8(3), 355-362, 2006.
- [3] Z. Jakšić, M. Obradov, D. Tanasković, O. Jakšić, D. V. Radović, *Opt. Quant. Electron.*, 52(2), 1-10, 2020.
- [4] K. Aydin, V. E. Ferry, R. M. Briggs, and H. A. Atwater, *Nature Comm.*, 2, 517, 2011.

## Hyperbolic Metamaterials via Hierarchical Block Copolymer Nanostructures

Marwan Channab<sup>1,2</sup>, Irdi Murataj<sup>1,2</sup>, Eleonora Cara<sup>2</sup>, Candido F. Pirri<sup>1</sup>, Luca Boarino<sup>2</sup>, Angelo Angelini<sup>2</sup>, Federico Ferrarese Lupi<sup>2</sup>

<sup>1</sup>*Dipartimento di Scienza Applicata e Tecnologia, Politecnico di Torino, Turin, Italy*

<sup>2</sup>*Advanced Materials and Life Sciences, Istituto Nazionale di Ricerca Metrologica (INRiM), Turin, Italy*

e-mail: [marwan.channab@polito.it](mailto:marwan.channab@polito.it)

Extremely exotic optical properties unattainable in natural materials can be shown by an innovative class of materials: hyperbolic metamaterials (HMMs). Exploiting HMMs, it is possible to obtain the confinement of light at the nanoscale and the enhancement of spontaneous emission of a coupled emitter. Most of the HMMs are fabricated by sequential deposition of alternating metal/dielectric layers to obtain a multilayer structure. In this case, the optical axis lies in the out-of-plane direction. This particular feature causes many issues for their exploitation into more complex integrated photonic devices such as a difficult radiation outcoupling. Since in-plane orientation of the optical axis is desirable for different applications in nanophotonics and imaging, we present a method for fabricating localized HMMs with in-plane optical axis based on the dewetting of block copolymer (BCP)/homopolymer blend thin films [1]. We obtained droplets composed of highly ordered lamellar nanostructures in hierarchical configuration by exploiting the blend film instability over topographically defined substrates, see figures 1.a–1.c. The pattern transfer process onto a flexible substrate creates an Au/air HMM with hyperbolic dispersion in broad wavelength range in the visible spectrum. Moreover, we obtained a strong reduction in the measured fluorescence lifetime of NV centers in nanodiamonds placed on top of the HMM. This measurement is supported by computed Purcell factor as high as 32 at 580 nm, see figures 1.d and 1.e. To conclude, we proposed a method to obtain hybrid metal/dielectric nanopatterned substrates in a fast and low-cost way with in-plane optical axis whose spectral response can be further tuned.

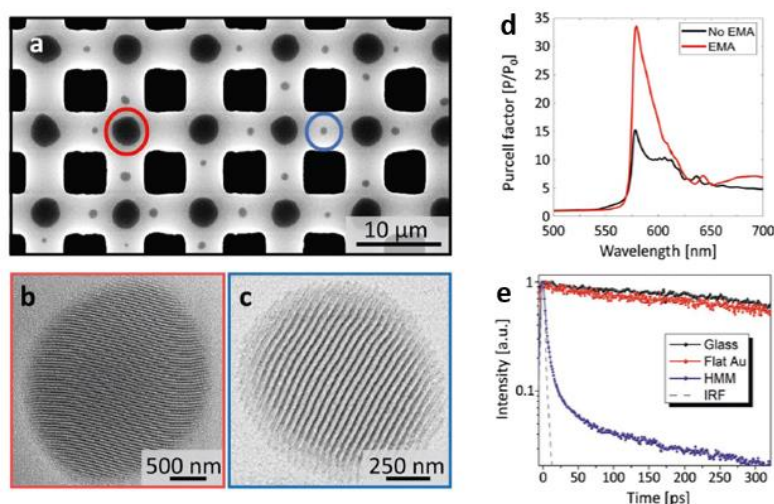


Figure 1. **a**) SEM image of BCP blend dewetting over a large-area substrate. **(b,c)** SEM images of lamellar nanostructured droplets in a single grain configuration related to highlighted areas in figures 1.a. **d**) Simulated Purcell factor for a vertically oriented dipole located 5 nm above the HMM. It has been computed for both the effective medium approximation (EMA) and the real lamellar structure for comparison. **e**) Lifetime fluorescence measurements for NV centers in nanodiamonds on glass (black), flat Au (red), and HMM (blue).

### REFERENCES

[1] Murataj, I.; Channab, M.; Cara, E.; Pirri, C.F.; Boarino, L.; Angelini, A.; Ferrarese Lupi, F. Hyperbolic Metamaterials via Hierarchical Block Copolymer Nanostructures. *Adv. Optical Mater.* 2021, 2001933. doi:10.1002/adom.202001933.

## Optical properties of surface plasmon polaritons launched via metallic grooves

U. Ralević<sup>1</sup>, G. Isić<sup>1,2</sup>

<sup>1</sup>*Institute of Physics Belgrade, University of Belgrade, Belgrade, Serbia*

<sup>2</sup>*Texas A&M University at Qatar, Doha, Qatar*

e-mail: [uros@ipb.ac.rs](mailto:uros@ipb.ac.rs)

The optical properties of surface plasmon polaritons (SPPs) including field enhancement, subwavelength field confinement, and high sensitivity to the structure of the dielectric/metal interfaces where they exist have been exploited for numerous applications ranging from sensors to optical integrated circuits [1]. One of the key requirements for building a SPP based device is a controllable and efficient conversion of the free-space light to the SPPs. In the last two decades, isolated nano-sized slits and grooves perforated in metal films have been utilized as efficient SPP launchers in novel, compact SPP based devices, where high density of integration, amongst other properties, plays an important role [2].

In this work we investigate the SPPs launched on a metal groove using finite element method numerical simulations. In particular, we study the effects of various parameters such as groove shape and the incident angle on the properties of launched SPPs and the launching efficiency. The launching efficiency of the SPPs exhibits maxima (minima) whenever the scattering into SPPs is in constructive (destructive) interference with the scattering arising via the groove mode excitation. The extremal points position is found to be dependent on the groove shape and virtually independent on the incident angle. We show that the rotation of the plane of incidence modifies the SPP wavevector by introducing an offset between the amplitude and phase fronts of the launched SPP. The former becomes slanted with respect to the Poynting vector, while the latter remains perpendicular to it.

### REFERENCES

- [1] W.L. Barnes, A. Dereux, T.W. Ebbesen, *Nature* 424, 824 (2003)
- [2] H. J. Lezec, A. Degiron, E. Devaux, R. A. Linke, L. Martin-Moreno, F. J. Garcia-Vidal, T. W. Ebbesen, *Science* 297, 820 (2002)

## Dependence of loss parameters on circularly polarized terahertz wave propagation through graphene gated metamaterial

V.Milosevic<sup>1</sup>, U.Ralevic<sup>1</sup>, D. B. Stojanovic<sup>2</sup>,

<sup>1</sup>*Institute of physics, University of Belgrade, Belgrade, Serbia*

<sup>2</sup>*Vinca Institute of Nuclear Sciences, University of Belgrade  
Belgrade, Serbia*

e-mail:vojislav@ipb.ac.rs

Polarization is an important characteristic of electromagnetic waves and manipulation of polarization plays pivotal role in different areas such as communications, imaging and sensing. On the other hand, the ability to dynamically modify the state of polarization with metamaterials enables control of circular dichroism and optical activity in terahertz frequency range [1,2]. This dynamic control can be realized by incorporating graphene layer into the metasurface, whose conductivity can be controlled by applying gate voltage.

In this work, the effect of graphene conductivity on chiral effects of the metasurface will be analyzed using temporal coupled-mode theory [3,4]. In this frame, each resonant mode is characterized with its resonant frequency, radiative and non-radiative coupling coefficients. These parameters will be retrieved from simulated reflection and transmission spectra for left and right circular polarizations. In such way, theoretical model for tunable chiral effects in graphene metasurface will be given, enabling further improvement of its properties.

### REFERENCES

- [1] D. B. Stojanović, P. P. Beličev, G. Gligorić, Lj. Hadžievski, *J. of Phys. D: Appl. Phys.* 51 (4), 045106 (2018).
- [2] S. J. Kindness et al, *Adv. Optical. Mater.* 2020, 1000581 (2020).
- [3] T-T. Kim et al, *Sci. Adv.* 3(9), e1701377 (2017).
- [4] M. Masyukov et al, *Sci. Rep.* 10, 3157 (2020).

## Bio-inspired holey submicrometer plasmonic core-shell particles as generalized synthetic brochosomes

Z. Jakšić, M. Obradov, O. Jakšić, D. Tanasković

Centre of Microelectronic Technologies

Institute of Chemistry, Technology and Metallurgy - National Institute of the Republic of Serbia

University of Belgrade, Njegoseva 12, 11000 Belgrade, Serbia

e-mail:jaksa@nanosys.ihtm.bg.ac.rs

Brochosomes are aperture-riddled submicrometer hollow spherical particles consisting of proteins and lipids (Fig. 1a) that are produced by some insects (e.g. leafhoppers) and that simultaneously perform a role of superhydrophobic protection against sticking the insect to plants sap and serving as antireflective coatings in the visible to reduce observability by predatory species [1]. Attracting researchers' attention by their multifunctionality, brochosomes had been artificially produced in various materials, including among others plasmonic materials. From the photonics point of view, so far they have been used as ultra-antireflective diffractive coatings [2] and as photoanodes in photoelectrochemistry [3].

In this work we propose generalized geometries (Fig. 1b,c) of synthetic brochosomes containing free-electron conductors (i.e. plasmonic materials) that can be nanofabricated by first depositing small spheres on the plasmonic shells of core-shell submicrometer particles at various depths and then subtracting them from the shell material, as described in detail in [1]. We performed simulation of the electromagnetic parameters of the novel structures using the finite element method. We succeeded in obtaining ultralow reflection coefficients in an extended wavelength range while simultaneously achieving high geometry-based control over frequency shifting and shape of the spectral characteristics of scattering parameters (Fig.1d). The main advantage of using our plasmonic-based artificial brochosomes is their multifunctional applicability (at the same time they serve as antireflective, superhydrophobic and highly porous structures with parameters controllable by design), which is highly convenient for numerous microoptoelectromechanical (MOEMS) systems.

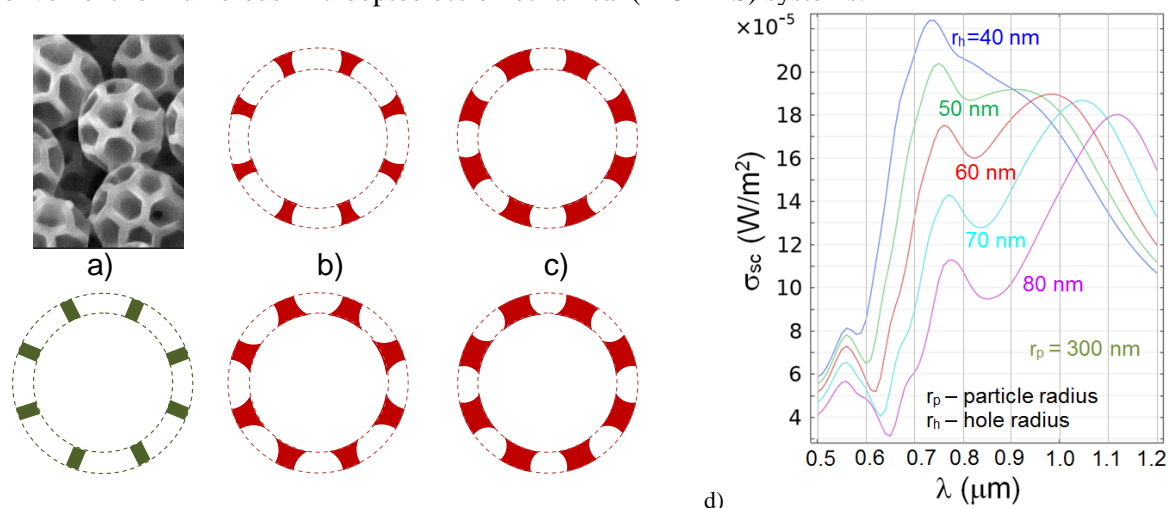


Figure 1. Brochosome geometries. a) top: Electron micrograph of leafhopper brochosomes; bottom: schematics of its cross-section. b-c: our alternative geometries; red: metal. Positions and diameters of spheres subtracted from the starting core-shell plasmonic particle are used as varying parameters. d) FEM-calculated spectral scattering cross-section of the structure shown in b-top, plasmonic shell material is gold.

### REFERENCES

- [1] S. Yang, N. Sun, B. Stogin, J. Wang, Y. Huang, T. S. Wong, *Nature comm*, 8(1), 1-8 (2017).
- [2] C. W. Lei, R. Y. Chen, H. Yang, *Langmuir*, 36(19), 5296-5302 (2020).
- [3] Q. Pan, H. Zhang, Y. Yang, C. Cheng, *Small*, 15(28), 1900924, (2019).

# **11. Machine learning in photonics**

## Deep learning for analysis of optical maps of CVD-grown TMDs

A. Supina<sup>1</sup>, A. Senkić<sup>1</sup>, A. L. Brkić<sup>1</sup>, M. Jaklin<sup>2</sup> and M. Kralj<sup>1</sup>

<sup>1</sup>*Institute of Physics, Zagreb, Croatia*

<sup>2</sup>*Universidade de Santiago de Compostela, Spain*

e-mail: asupina@ifs.hr

The study of atomically thin transitional metal dichalcogenides (TMDs) is a new and vibrant research field. Due to their advantageous electronic and optical properties, these materials show great promise for use in electronic and photonic devices. In particular, chemical vapor deposition (CVD) synthesis has a good potential to grow large and uniform monolayer islands, while still exhibiting sufficient crystallinity [1]. However, synthesis does not typically produce homogenous distribution of island shapes and properties with respect to lateral position on the growth substrate. To tackle this problem, we propose a low-cost upgrade to existing optical microscope used to inspect synthesized samples. The upgrade consists of an x-y motorized stage based on the Arduino microcontroller and MARLIN [2], an open-source software for 3D printers, as well as the Raspberry Pi and camera for image acquisition. This allows us to acquire high magnification optical image maps and extract distribution maps of different features over the whole substrate area.

Typically, in data analysis of 2D samples, processing is done on a few representative areas. However, in recent years, different machine learning algorithms are employed to map over the entire substrate area in setups similar to ours. However, to the best of our knowledge, all previous work is mainly focused on exfoliated samples of 2D materials in an effort to extract the number of layers and size of the exfoliated flakes [3]. In this work, we use CVD grown crystals of different TMDs and employ neural networks for feature extraction. We employ a YOLO-like architecture [4] to localize and assess the size of crystal islands, allowing us to get a lateral distribution of island density and island size for each grown sample. We also employ a modified UNET neural network [5] with adversarial augmentation for segmentation of material from the substrate area to extract the distribution of material coverage.

We anticipate our work will extend this principle to other mapping techniques such as AFM, SEM and Raman spectroscopy. Furthermore, we plan to extract maps of morphological information from individual islands. Using this information, we can correlate CVD parameters to different growth mechanisms and optimise the synthesis to be more homogeneous, while retaining good quality of the samples.

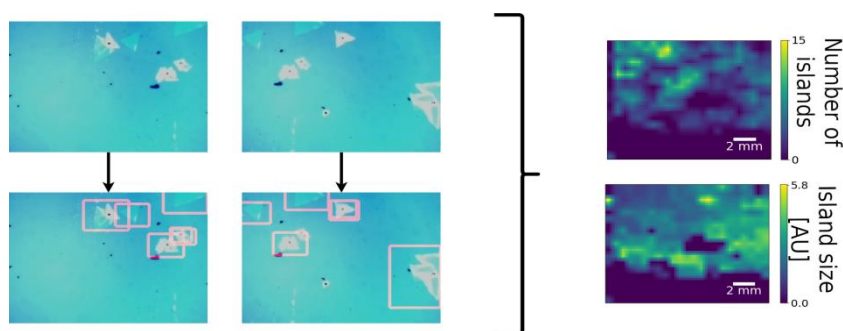


Figure 1. Top left: examples of two neighbouring imaged areas with significant overlap. Bottom left: localizing individual islands and finding their respective bounding box. Right: extracted island density and distribution of island size over the whole sample.

### REFERENCES

- [1] D. Dumcenco, D. Ovchinnikov, K. Marinov, et al, *ACS Nano*. 9, 4611–4620 (2015).
- [2] <https://github.com/MarlinFirmware/Marlin>
- [3] B. Han, Y. Lin, Y. Yang, et al., *Advanced Materials*. 32, 2000953 (2020).
- [4] O. Ronneberger, P. Fischer, T. Brox, arXiv:1505.04597 [Cs]. (2015).
- [5] J. Redmon, S. Divvala, R. Girshick, A. Farhadi, [arXiv:1506.02640](https://arxiv.org/abs/1506.02640) [cs.CV], (2016).

## Design and optimization of fiber-optic colorimetric probe based on ANN for estimating spectrum of color samples

B. Batinić<sup>1</sup>, J. Bajić<sup>1</sup>, M. Arbanas<sup>1</sup> and M. Vasiljević Toskić<sup>1</sup>  
<sup>1</sup>Faculty of technical sciences, University of Novi Sad, Novi Sad, Serbia  
 e-mail: banebb@uns.ac.rs

A new, optimized colorimetric probe used for color estimation of printed samples obtained using digital printing is presented in this paper. Colorimetric probe is based on non-contact measurement of the intensity of light transmitted by optical fibers from light sources to a measuring point and then reflected to a photo-detector. ANN (Artificial Neural Networks) based algorithm is used in order to predict the shape of the spectral curve in the range of 380-730 nm with resolution of 10 nm [1].

Given that the way the light reflects depends on the texture and gloss of the surface, reflection can be roughly divided into two types: specular and diffuse reflection. The first one represents reflection from a smooth surface at a definite angle, and the second one from rough surfaces that tend to reflect light in a multitude of directions. Even though the law of reflection is completely valid in both cases, during the diffuse reflection the incident angle is changing as the beams of incident light hit the rough surface at different angles.

The proposed colorimetric probe [2] is designed to measure the color of printed samples obtained using digital printing, which was performed using calibrated Xerox Versant 80 Press machine. Identical 9x9 mm color patches were printed on matte and gloss coated white papers, according to the ISO Fogra Coated 39 profile.

Specular reflection can have significant impact in case of measuring gloss samples, since the specular light reflected from a gloss surface follows the same angle from the normal, as the incident light. Fig. 1a shows the previous design of the probe which was used to measure color on matte coated white paper. The probe consists of plastic optical fibers which transmit light from six discrete LED sources (arranged in a circle) whose wavelengths are equidistantly distributed within the visible range to color patches and returns the reflected part of the light from the color patches to a single wideband photo-detector positioned in a center of the probe [2]. All LED sources, as well as the photo-detector, are perpendicular to the illuminated surface, therefore the reflected light returns at the same angle as the incident light. This set-up is not suitable for measurement on gloss coated paper since it would cause a mirror-like reflection of light from the surface. Furthermore, since the used LED sources are discrete components without heatsinks, the temperature effect should be taken into account. By increasing the temperature, peak wavelengths shift to longer wavelength [3,4]. Instead of the aforementioned limited concept, a new colorimetric probe with implemented geometry 45/0 and integrated LED sources with common heatsink (Fig. 1b), optimized for measurement on both matte and gloss coated paper will be presented in this paper.

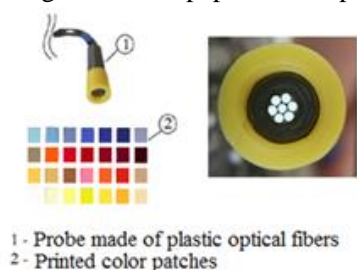


Figure 3a) Basic concept of colorimetric probe designed in our previous work [1]

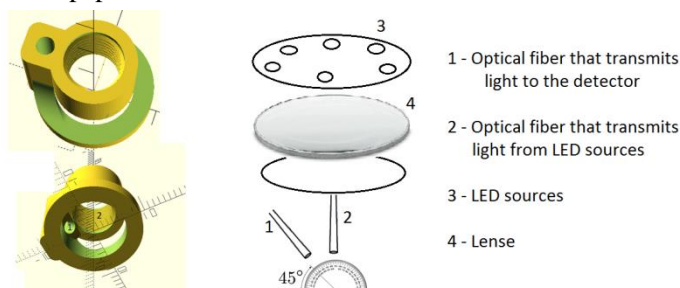


Figure 1b) Proposed colorimetric probe design with implemented geometry 45/0

### REFERENCES

- [1] Batinić, B.; Arbanas, M.; Bajić, J.; Dedijer, S.; Rajs, V.; Laković, N.; Kulundžić, N. (2020). IEEE Transactions on Instrumentation and Measurement, (), 1–1. doi:10.1109/TIM.2020.3011763
- [2] Batinić, B.; Bajić, J.; Dedijer, S.; Kulundžić, N.; Joza, A.; Laković, N.; Rajs, V. (2020). Optical and Quantum Electronics, 52(7), 342–. doi:10.1007/s11082-020-02458-7.
- [3] Yadav, A.; Titkov, I. E.; Sokolovskii, G. S.; Karpov, S. Y.; Dudelev, V. V.; Soboleva, K. K.; Strassburg, M.; Pietzonka, I.; Lugauer, H-J.; Rafailov, E. U. (2018). J. Appl. Phys. 124(1), 013103
- [4] Reynolds, K. J.; De Kock, J. P.; Tarassenko, L.; Moyle, J. T. B. (1991). BJA: British Journal of Anaesthesia, 67(5), 638–643. doi:10.1093/bja/67.5.638

## Electronic Semiconductor Characterization Using Reverse-Back Procedure Based on Neural Networks and Photoacoustic Response

K.Lj. Djordjevic<sup>1</sup>, S.P. Galović<sup>1</sup>, Ž.M. Čojbašić<sup>2</sup>, D.D. Markushev<sup>3</sup>,  
D.K. Markushev<sup>4</sup>, S.M. Aleksic<sup>4</sup>, D.S. Pantic<sup>4</sup>

<sup>1</sup>University of Belgrade, „VINČA“ Institute of Nuclear Sciences - National Institute of the Republic of Serbia,  
PO box 522, 11000 Belgrade, Serbia

<sup>2</sup>University of Niš, Mechanical Engineering Faculty, Aleksandra Medvedeva 14, 18000 Niš, Serbia

<sup>3</sup>University of Belgrade, Institute of Physics Belgrade, National Institute of the Republic of Serbia, Pregrevice  
118, 11080 Belgrade (Zemun), Serbia

<sup>4</sup>University of Niš, Faculty of Electronic Engineering, Aleksandra Medvedeva 14, 18000 Niš, Serbia

e-mail: [katarinaljdjordjevic@gmail.com](mailto:katarinaljdjordjevic@gmail.com)

In this paper, electronic semiconductor characterization using reverse-back procedure was applied to different photoacoustic (PA) responses aiming to find effective ambipolar diffusion coefficient and a bulk life-time of the minority carriers. The main idea was to find the small fluctuations in investigated parameters due to detecting possible unwanted sample contaminations and temperature variations during the measurements. The mentioned procedure was based on the application of neural networks [1]. Knowing that in experiments the contaminated surfaces of the sample can play a significant role in the global recombination process that we are measuring and that the unintentionally introduced defects of the sample crystal lattice could vary the carrier lifetime by several orders of magnitude, a method of PA signal adjustment by the reverse-back procedure is developed, based on the changes of the carrier electronic parameters. Such changes are detected (Fig.1) and calculated here by analyzing PA signal amplitude ratios  $A^{\text{ANN}} / A^{\text{exp}}$  and phase differences  $\Phi^{\text{ANN}} - \Phi^{\text{exp}}$  obtained using experimental (exp) and network predicted (ANN) thermal and geometrical parameters of the sample [2]. The values of photogenerated carrier lifetime and ambipolar diffusion coefficient obtained by the presented method can be used in the quality control procedure of the investigated samples, active control of the experimental conditions and within the general characterization process of semiconductors.

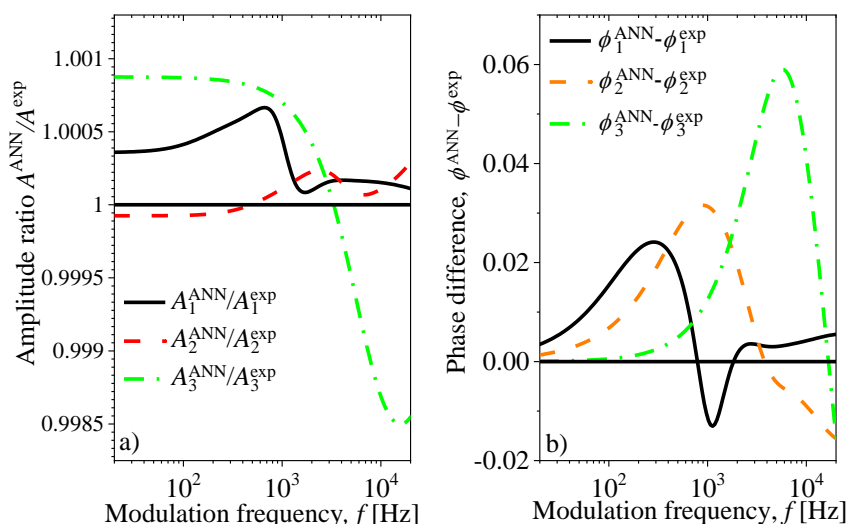


Fig. 1.a) Amplitude ratios and b) phase differences between ANN and experimental (exp) photoacoustic signal prediction of different sample thicknesses in frequency domain used for electronic parameters calculations.

### REFERENCES

- [1] DjordjevicKLj, Markushev DD, Čojbašić ŽM, Galović SP, Inverse Problems in Science and Engineering 29(2020)<https://doi.org/10.1080/17415977.2020.1787405>  
[2] DjordjevicKLj, Galovic SP, Jordovic-Pavlovic MI, Nestic MV, Popovic MN, Čojbašić ŽM, Markushev DD, Optical and Quantum Electronics 52(2020)<https://doi.org/10.1007/s11082-020-02373-x>

## Deep learning solutions for cross-phase modulation dominated channels

Lazar S. Stojković<sup>1</sup>, Velimir M. Ilić<sup>2</sup> and Ivan B. Djordjević<sup>3</sup>

<sup>1</sup>*Faculty of Science and Mathematics, University of Niš, Serbia*  
e-mail: lazar.stojkovic@pmf.edu.rs

<sup>2</sup>*Faculty of Science and Mathematics, University of Niš, Serbia*  
e-mail: velimir.ilic@pmf.edu.rs

<sup>3</sup>*Department of Electrical and Computer Engineering,  
College of Engineering, University of Arizona, USA*  
e-mail: ivan@email.arizona.edu

Optical fiber, unlike other transmission media, features significant change of light propagation properties with increasing signal power, known as Kerr-nonlinear effect, which induces self-phase modulation (SPM) of the transmitted signal [1, 5]. Moreover, the wavelength of light in one wavelength channel can affect the phase of the wavelength of light in nearby channels, inducing a nonlinear optical effect known as cross-phase modulation (XPM) [2]. We hereby present the artificial neural networks (ANN) as an efficient solution for symbol detection and constellation design problems for the XPM-dominated systems as in [2].

In case of symbol detection, some already proposed constellations have been considered for a wide range of nonlinearity intensities, and our ANN detector has been compared to some established detectors such as minimum-distance and two-stage detectors [2, 3], where it exhibits performance superiority while preserving low complexity. In addition, we advance auto-encoder technique previously used for SPM dominated channels [4] and adapt it for the XPM case, which allows precise learning of constellations for specific fiber channel settings and power constraints, in significant improvements in symbol error rates (SER).

### REFERENCES

- [1] R. J. Essiambre, G. Kramer, P. J. Winzer, G. J. Foschini, B. Goebel, "Capacity Limits of Optical Fiber Networks", *Journal of Lightwave Technology*, vol. 28, no. 4, pp. 662-701, Feb.15, 2010, doi:10.1109/JLT.2009.2039464.
- [2] T. Liu, I. Djordjevic, M. Li, "Signal constellation design for cross-phase modulation dominated channels", *ICTON 2015 - 17th International Conference on Transparent Optical Networks*, 2015, doi:1-4. 10.1109/ICTON. 2015.7193299.
- [3] L. Beygi, E. Agrell, M. Karlsson, "Optimization of 16-point Ring Constellations in the Presence of Nonlinear Phase Noise", *Optical Fiber Communication Conference and Exposition (OFC) and The National Fiber Optic Engineers Conference (NFOEC)*, 2011, doi:10.1364/OFC.2011.OThO4.
- [4] S. Li, C. Häger, N. Garcia and H. Wymeersch, "Achievable Information Rates for Nonlinear Fiber Communication via End-to-end Autoencoder Learning", *2018 European Conference on Optical Communication (ECOC)*, 2018, pp. 1-3, doi:10.1109/ECOC.2018.8535456.
- [5] L. Mo, N. Stojanovic, V. Ilic, I. Djordjevic, F. Kupperts, "Target constellation diagram determination method, data sending method, and apparatus", EP3490207A4 *European Patent Office*, Jul. 24, 2019.

## Using SOLO software package for classification of temperature dependent luminescence spectra

D. Sevic<sup>1</sup>, M.S. Rabasovic<sup>1</sup>, J. Krizan<sup>2</sup>, S. Savic-Sevic<sup>1</sup>, M.D. Rabasovic<sup>1</sup>, M.G. Nikolic<sup>1</sup>  
and B.P. Marinkovic<sup>1</sup>

<sup>1</sup>Institute of Physics, Belgrade, Serbia

<sup>2</sup>AMI d.o.o., Ptuj, Slovenia

e-mail:sevic@ipb.ac.rs

In this study we use SOLO software package (Version 8.8, Eigenvector Research Inc, USA) for classification of temperature dependent luminescence spectra of nanocrystalline Gd<sub>2</sub>O<sub>3</sub>:Er<sup>3+</sup>,Yb<sup>3+</sup> at different temperatures using K-Nearest Neighbor and K-Means Nearest Group algorithms. Our experimental setup is presented in detail in [2,3]. In [4,5] we have used Principal Component Analysis of luminescence spectra of thermophosphors; here, we use classification tools based on more sophisticated K-Nearest Neighbor and K-Means Nearest Group algorithms.

Classification results (shown as dendrograms) of luminescence spectra of Gd<sub>2</sub>O<sub>3</sub>:Er<sup>3+</sup>,Yb<sup>3+</sup> at different temperatures using K-Nearest Neighbor and K-Means Nearest Group algorithms are shown in Figure 1. Although dendrograms are different, the groups determined by both methods are the same; moreover, the test luminescence spectra are also classified in temperature groups where they belong. So, the machine could be trained to differentiate spectral data obtained on different temperatures.

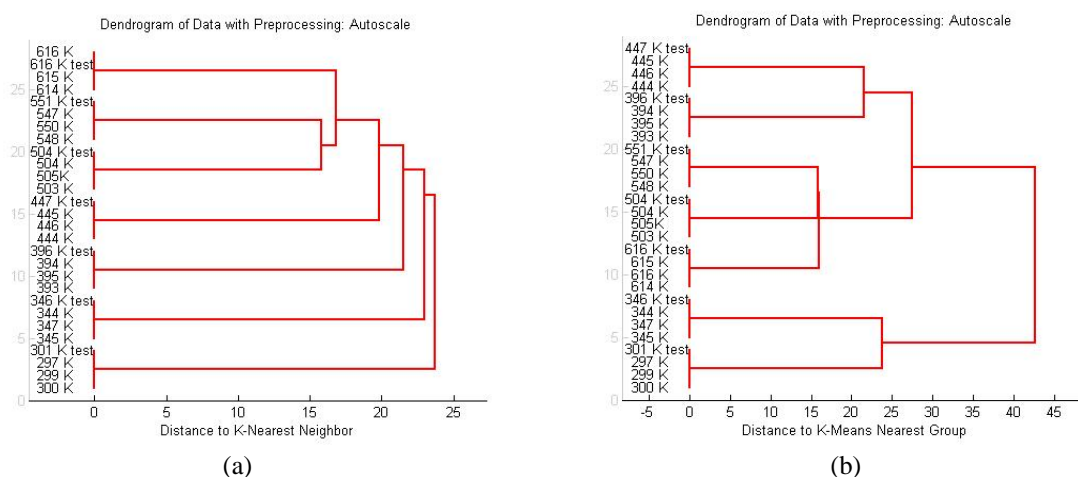


Figure 1. Classification results (shown as dendrograms) of luminescence spectra of Gd<sub>2</sub>O<sub>3</sub>:Er<sup>3+</sup>,Yb<sup>3+</sup> at different temperatures using (a) K-Nearest Neighbor and (b) K-Means Nearest Group algorithms.

### REFERENCES

- [1] J. Krizan, M. Mazaj, V. Kaucic, I. Bajsic, J. Mozina, Acta Chim. Slov. 61, 608 (2014).
- [2] D. Sevic, M.S. Rabasovic, J. Krizan, S. Savic-Sevic, M.D. Rabasovic, B.P. Marinkovic, M.G. Nikolic, Optical and Quantum Electronics 52, 232 (2020).
- [3] D. Sevic, M.S. Rabasovic, J. Krizan, S. Savic-Sevic, M.G. Nikolic, B.P. Marinkovic, M.D. Rabasovic, J. Phys. D: Appl. Phys. 53, 015106 (2020).
- [4] D. Sevic, A. Vlastic, M.S. Rabasović, S. Savic-Sevic, M.D. Rabasović, M.G. Nikolić, B. D. Muric, B. P. Marinković, J. Križan, Tehnika 75(3), 279 (2020).
- [5] D. Sevic, J. Krizan, M. S. Rabasovic, B.P. Marinkovic, Eur. Phys. J. D 75, 56 (2021).

## Reducing number of measuring points for estimating reflected spectrum of colorimetric probe

M. Arbanas<sup>1</sup>, B. Batinić<sup>1</sup>, J. Bajić<sup>1</sup>, M. Vasiljević-Toskić<sup>1</sup>, M. Brkić<sup>1</sup> and V. Rajs<sup>1</sup>

<sup>1</sup>Faculty of Technical Sciences,

Novi Sad, Serbia

e-mail: milos.arbanas@uns.ac.rs

*Abstract* – As the world of IoT, and sensor-data gathering is becoming more widespread, reducing the cost of each sensor system is becoming an important factor. In this paper reducing the number of necessary measuring points for estimating a reflected electromagnetic spectrum is presented. In our previous work [1], a machine learning-based method was proven to be superior to Cubic Hermite interpolation in estimating spectrum based on six measured values. Now the new hypothesis is that the number of measuring points could be decreased without the significant loss of spectrum estimation. The output of the system is formed out of thirty-six points in the range of 380-730 nm.

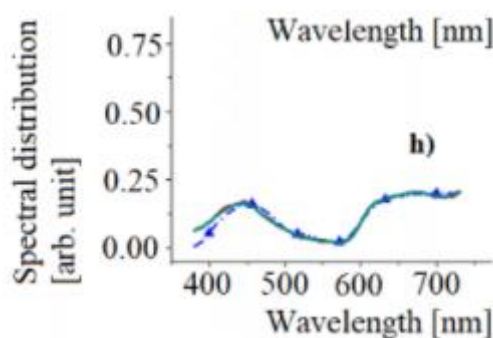


Figure 1. Example of spectrum estimation based on six LED sources.

The spectral radiation power of six proposed LED sources is at 400 nm, 457 nm, 517 nm, 572 nm, 632 nm and 700 nm. In Figure 1. the blue triangles present measured values, blue line estimated spectrum and green line presents spectrum attained from a commercial spectrophotometer.

This paper analyses the usage of different combinations of measuring points and using different machine learning methods with the end goal of significantly reducing the number measuring points, therefore the number of LED sources. The different combinations of measuring points are used as inputs to ANN (Artificial Neural Networks), the network is then trained using dataset generated by spectrophotometer.

Colorimetric capabilities of the different combinations of the measuring points are compared with each other as well as with a commercial spectrophotometer.

### REFERENCES

- [1] B. Batinić, M. Arbanas, J. Bajić, S. Dedijer, V. Rajs, N. Laković, N. Kulundžić., Using machine learning for improvement of reflected spectrum estimations of colorimetric probe; IEEE Transactions on Instrumentation and Measurement PP(99), August 2020
- [2] Haykin, S., Neural Networks: A Comprehensive Foundation, 2nd ed.; Prentice-Hall, Englewood Cliffs, NJ, USA, 1999.

## Influence of data scaling and normalization on overall neural network performances in photoacoustics

K.Lj. Djordjevic<sup>1</sup>, M.I. Jordović-Pavlović<sup>2</sup>, Ž.M. Čojbašić<sup>3</sup>, S.P. Galović<sup>1</sup>,  
M.N. Popović<sup>1</sup>, M.V. Nešić<sup>1</sup>, D.D. Markushev<sup>5</sup>

<sup>1</sup>University of Belgrade, Vinca Institute of Nuclear Sciences-National Institute of the Republic of Serbia, Belgrade, Serbia

<sup>2</sup>Western Serbia Academy of Applied Studies, Užice, Trg Svetog Save 34, Užice, Serbia

<sup>3</sup>University of Niš, Faculty of Mechanical Engineering, Niš, Serbia

<sup>5</sup>University of Belgrade, Institute of Physics Belgrade- National Institute of the Republic of Serbia, Belgrade-Zemun, Serbia

e-mail: [katarinaljdjordjevic@gmail.com](mailto:katarinaljdjordjevic@gmail.com)

In our previous articles [1,2] we have shown that the application of artificial neural networks (ANNs) in photoacoustics could improve experimental procedures in many ways: better accuracy and precision in investigated sample parameters prediction, better control of the experimental conditions together with approaching to the real-time characterization of the investigated sample, etc. Here we will try to show why the different types of scaling and normalization procedures could be beneficial to the accuracy, precision and numerical stability of the network predicted parameters and network training speed. To do that numerical (Fig.1) or logarithmic scaling and min-max and max normalizations are applied on experimental input data used in the ANNs training process. At the same time, specific numerical scaling is used for network output data (predicted sample thermal and geometric parameters such as thermal diffusivity, linear coefficient of thermal expansion, thickness) to find possible benefits to ANNs performances. Our analysis of training, stability, and accuracy of network prediction will rely on the ANNs trained with or without scaling and/or normalization to find their influence on overall network performances.

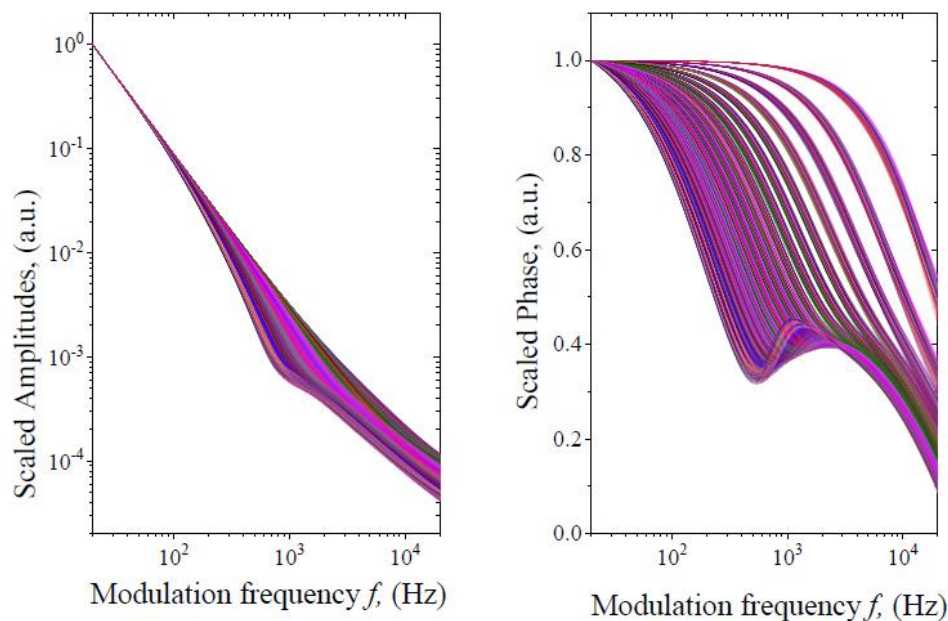


Fig.1. Numerically scaled a) amplitudes and b) phases of the photoacoustic signals used as an input data for network training base formation in frequency domain aimed for electronic parameters calculations.

### REFERENCES

[1] Djordjevic KLj, Markushev DD, Čojbašić ŽM, Galović SP, Inverse Problems in Science and Engineering 29(2020) <https://doi.org/10.1080/17415977.2020.1787405>

[2] Djordjevic KLj, Galovic SP, Jordovic-Pavlovic MI, Nesic MV, Popovic MN, Čojbašić ŽM, Markushev DD, Optical and Quantum Electronics 52(2020) <https://doi.org/10.1007/s11082-020-02373-x>

[X](#)

## Trace gases analysis in pulsed photoacoustics based on swarm intelligence optimization

M. Lukić<sup>1</sup>, Ž. Čojbašić<sup>2</sup>, D. D. Markushev<sup>3</sup>

<sup>1</sup>Faculty of Occupational Safety, University of Niš, Černojevića 10a, Niš 18000, Serbia.

<sup>2</sup>Mechanical Engineering Faculty, University of Niš, Aleksandra Medvedeva 14, Niš 18000, Serbia.

<sup>3</sup>Institute of Physics, University of Belgrade, Pregrevica 118, Belgrade-Zemun 11080, Serbia.

e-mail:mladena.lukic@zrnrfak.ni.ac.rs

The application of pulsed photoacoustic spectroscopy (PAS) in in-situ measurements of trace gases with variable spatial and temporal distribution of concentrations requires high sensitivity, selectivity, as well as a simple, easily portable apparatus. In order to improve PAS characteristics in trace gases measurements, we have applied artificial intelligence techniques [1,2] which can not only increase the efficiency and precision of measurements but also enable the interaction of the system with its environment, through online training. The swarm intelligence optimization techniques simultaneously determined the unknown parameters of the photoacoustic (PA) signal: radius of the laser beam spatial profile ( $r_L$ ) and vibrational-to-translational relaxation time ( $\tau_{V-T}$ ). Experimental PA signals were generated in the SF<sub>6</sub>+Ar mixture in the multiphoton regime. Two swarm intelligence algorithms were applied: particle swarm optimization (PSO)[3] and artificial bee colony optimization (ABC) [4]. Selected algorithms differ in terms of space being searched, the operators who use them, etc. [2-4].

Due to the convenience in calculations, the dimensionless parameters  $\varepsilon$  ( $\varepsilon \propto \frac{1}{\tau_{V-T}}$ ) and  $r^*$  ( $r^* \propto \frac{1}{r_L}$ ), were used, where  $r_L$  is the radius of Gaussian, top-hat or Lorentzian spatial profile of the laser beam. The parameter  $r^*$  is selected from the interval [10, 50], and  $\varepsilon$  from the interval [0.2, 5]. The lower and the upper bounds of the interval values of the selected parameters are the smallest and highest values of the parameters  $\varepsilon$  and  $r^*$ , which can be expected in the experiment. The performances of the applied algorithms are based on the criteria: the precision of the result (%) and the number of function evaluations. The number of evaluations of PSO and ABC algorithm functions is similar. PSO algorithm precisely defines the unknown parameters of photoacoustic (PA) signal with a small number of function evaluations, while the ABC algorithm determines the least number of parameters to be set. A small number of function evaluations and a relatively simple implementation make swarm intelligence algorithms an efficient and extremely perspective tool for in-situ measurements.

### REFERENCES

- [1] M. Lukić, Ž. Čojbašić, M.D. Rabasović, D.D. Markushev, Meas. Sci. Technol. 25(12), 125203 (2014)
- [2] A.P. Engelbrecht, Computational Intelligence, 2nd edn.(John Wiley and Sons 2007)
- [3] K. Parsopoulos, M.Vrahatis, Particle swarm optimization and intelligence: Advances and applications, (IGI Global Joannina, Greece2010)
- [4] D.Karaboga, B. Gorkemli, C. Ozturk, N. Karaboga, Artif. Intell. Rev.42(1), 21-57 (2014)

## **12. Other topics in photonics**

## Localization-delocalization transition in compressed Lieb ribbon lattices

D. Román<sup>1</sup>, G. Fadic<sup>1</sup>, C. Cid<sup>1</sup>, B. Real<sup>2</sup>, D. Guzmán-Silva<sup>1</sup>, and R.A. Vicencio<sup>1</sup>

<sup>1</sup>*Departamento de Física and MIRO, Facultad de Ciencias Física y Matemáticas, Universidad de Chile, Chile*

<sup>2</sup>*Université de Lille, CNRS, Laboratoire de Physique des Lasers Atomes et Molécules (PhLAM), Lille, France*  
e-mail:rvicencio@uchile.cl

A Lieb photonic ribbon lattice corresponds to a quasi-1D version of the well known 2D Lieb lattice [1]. Its unit cell is composed by five sites [see Fig.1(a)] and, therefore, the linear spectrum is formed by five bands. Relevant nearest-neighbor interactions are described by horizontal  $V_x$ , vertical  $V_y$ , and diagonal  $V_d$  coupling constants. Depending on the magnitude of coupling interactions, the linear spectrum induce localization or delocalization dynamics. We use a femtosecond-laser writing technique [2], as sketched in Fig.1(b), to fabricate several dimer configurations (vertical, horizontal and diagonal) and characterize the coupling constants versus distance. We identify the vertical separation distance as a critical parameter and find that horizontal and vertical couplings become equal for a constant difference of  $1 \mu\text{m}$ . Then, we fabricated 14 ribbon lattices as the example shown in Fig.1(c). We analyze all fabricated photonic lattices by focusing a HeNe laser beam at the B-bulk site and measure intensity profiles at the output facet, after a propagation of 50 mm. Figs.1(e) show the output profile for different vertical distances, where we observe quite clearly how light is localized for distances larger than  $18 \mu\text{m}$ , while it spreads out for smaller distances. This localization-delocalization transition is generated by a lattice compression that produces a homogeneous reduction of all lattice dimensions, implying an increment of the Fourier linear spectrum.

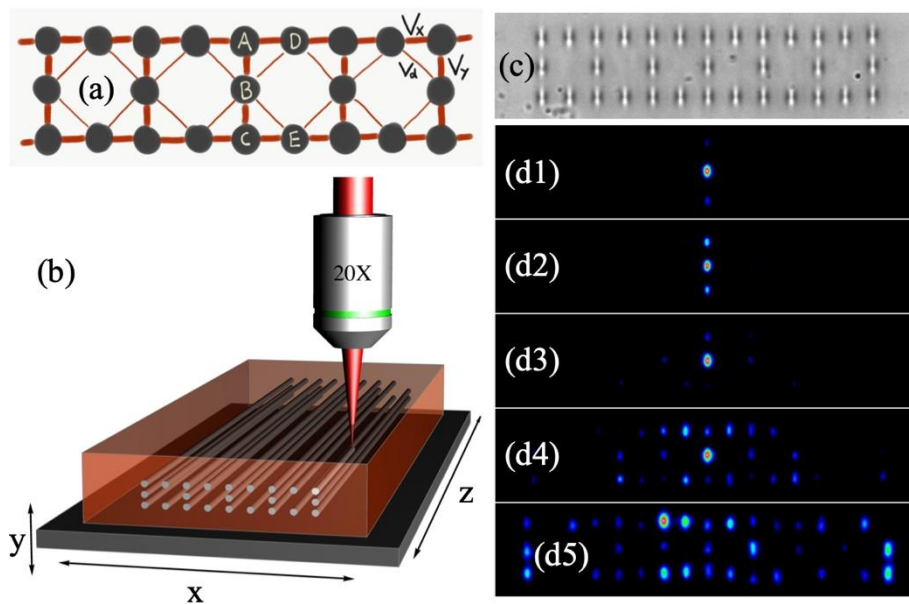


Figure 1. (a) Lieb ribbon lattice. (b) Femtosecond-laser writing technique. (c) White-light image of a Lieb ribbon photonic lattice. (d1)-(d5) Output intensity profiles for a nominal distance  $d = 22, 20, 18, 16, \text{ y } 14 \mu\text{m}$ .

### REFERENCES

- [1] R.A. Vicencio. *Advances in Physics*: X, 6, 1878057 (2021).  
[2] A. Szameit, et al., *Opt. Express* 13, 10552 (2005).

## Transport properties and localized edge modes arising at imperfect kagome lattices

Guillermo Fadic, Diego Román, Javier Cubillos, and Rodrigo A. Vicencio

*Departamento de Física and MIRO, Facultad de Ciencias Físicas y Matemáticas, Universidad de Chile, Chile*  
 e-mails: guillermo.fadic@ug.uchile.cl, diego.roman.c@ug.uchile.cl

Physical lattices are generally assumed to be theoretically infinite, which implies that they are boundless. This theoretical assumption is impossible to recreate experimentally. Specific borders, which appear due to the finite size of real lattices, could prove to be a useful tool in the search for localization of light in specific regions of a given photonic lattice [1]. Inspired by imperfect kagome photonic systems which are available in our laboratory [see Fig.1(a)], we aimed to study the borders of this lattice and the effect of removing some specific lattice sites. To do this, we analyzed the linear modes arising due to a modification of lattice borders and their dependence when considering different system sizes.

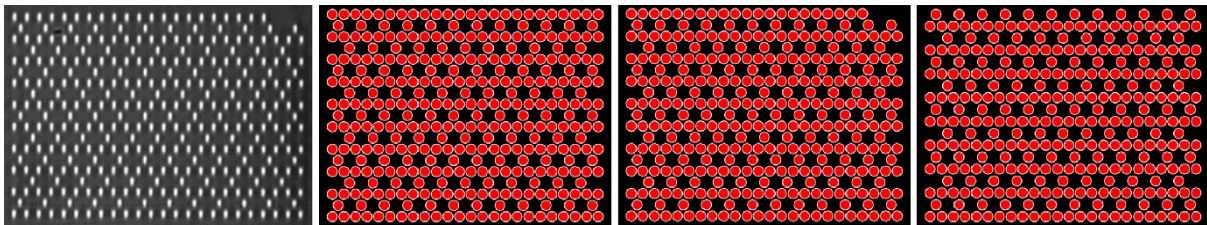


Figure 1. (a) White-light image of an imperfect kagome lattice (see top right corner). Transverse view of different kagome lattices: (b) Perfect, (c) corner-defected, (d) missing--row kagome lattice.

Femtosecond-laser written waveguides [2], as the ones shown in Fig.1(a), have an elliptical profile which induces an effective anisotropy in coupling constants, destroying the well-known flat band properties of kagome lattices [3,4]. In this work, we are interested on studying the effect of anisotropy by considering non-symmetric diagonal and horizontal coupling constants. Additionally, we notice that a modification of lattice edges [see Figs. 1(b)-(d)] gives rise to 1D-like line modes, edge localized modes and side-to-side light oscillations. Imperfections and defects could appear in photonic lattices fabricated using femtosecond-laser writing techniques. We take this not as a problem itself, but as a chance to study photonic lattices considering specific defects, which could offer new possibilities to observe enhanced localization as well as better transport on a given photonic system.

### REFERENCES

- [1] F. Lederer et al., *Phys. Rep.* 463, 1 (2008).
- [2] A. Szameit et al., *Opt. Express* 13, 10552 (2005).
- [3] Y. Zong et al., *Opt. Express* 24, 8877 (2016).
- [4] R. Vicencio. *Advances in Physics: X*, 6, 1878057 (2021).

## Bipartite lattice of domain wall junction states in photonic lattices

Esteban Flores<sup>1</sup>, Francisco Muñoz<sup>2,3</sup> and Rodrigo A. Vicencio<sup>1</sup>

<sup>1</sup>*Departamento de Física and MIRO, Facultad de Ciencias Física y Matemáticas, Universidad de Chile, Chile*

<sup>2</sup>*Departamento de Física, Facultad de Ciencias, Universidad de Chile, 9170124 Santiago, Chile*

<sup>3</sup>*Center for the Development of Nanoscience and Nanotechnology (CEDENNA), 9170124 Santiago, Chile*  
e-mail:esteban.flores@ug.uchile.cl

The similarities between the Schrödinger equation in quantum mechanics and the paraxial wave equation in optics have allowed scientists to study quantum phenomena in photonic lattices [1,2]. The possibility of imaging the wave function directly using a CCD camera has emerged as a key advantage in optics in comparison to electronics systems [3].

This work suggests the observation of localized states of topological origin in waveguide arrays. In particular, we use a generalized Su-Schrieffer-Heeger (SSH) model [4,5]. The primitive cell of SSH model is composed of two sites interacting between an intracell ( $t$ ) and an intercell ( $v$ ) coupling constant. The hopping ratio defines the topology of edge wavefunctions from a trivial insulator to a topological insulator.

The generalized SSH consists in a domain wall defect created by concatenating SSH arrays with different topology. This generates localized states in the junctions that govern the near-zero energy physics. If the domain walls are replicated periodically, topologically protected modes and the band structure of the SSH model can be recovered in a longer scale [5]. In this context, the main purpose is to study the effect of the length of the chains and the number of repetitions of the different chains.

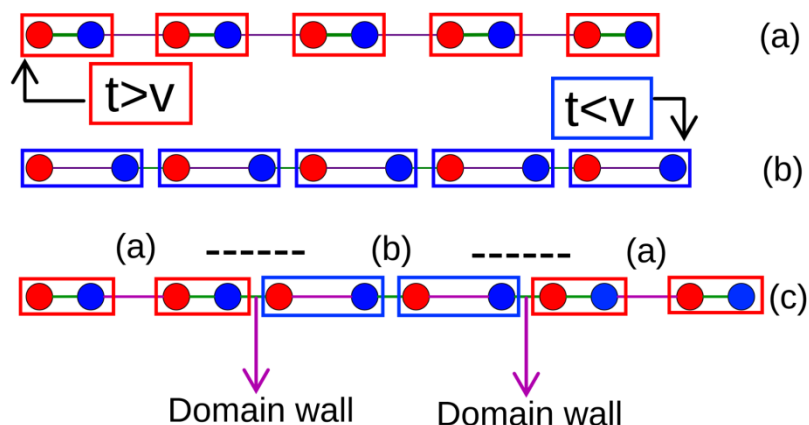


Figure 1. (a), (b) represents the SSH model for an intracell coupling greater than the intercell ( $t > v$ ) and the opposite ( $v > t$ ), respectively (each box is a unit cell). They have different winding numbers that define their topology. Both chains can be concatenated (c) and the junction between them is known as domain wall defect.

This research focuses on the interaction between these defects.

### REFERENCES

- [1] F. Lederer et al., Phys. Rep. 463, 1 (2008).
- [2] Malkova, N., Hromada, I., Wang, X., Bryant, G., Chen, Z., Opt. Lett. 34, 1633-1635 (2009).
- [3] Szameit, A., Nolte, S. J. Phys. B: At. Mol. Opt. Phys. 43 163001 (2010).
- [4] W. P. Su, J. R. Schrieffer, A. J. Heeger. PhysRevLett.42.1698 (1979).
- [5] Munoz, F., Pinilla, F., Mella, J., Molina, M. Sci Rep 8, 17330 (2018).

## Calculation of transition amplitude in two levels systems by application of an adiabatic approximation

M. Kurtovic<sup>1</sup>, H. Delibasic Markovic<sup>1</sup>, I. Petrovic<sup>2</sup> and V. Petrovic<sup>1</sup>

<sup>1</sup>Faculty of Science, University of Kragujevac, Serbia

<sup>2</sup>Academy of Professional Studies Sumadia, Department in Kragujevac, Serbia

e-mail:kurtovicmaida@gmail.com

In this paper, we will analyze the transition between atomic states of neon under the influence of an adiabatic approximation. We examined transition in two-level systems because the majority of the semiclassical calculations can be brought to a final result [1-3]. This was achieved using the well-known equation for transition amplitude [4]:  $A_{mn} = i \text{Exp} \left[ i \int_{t_1}^{\tau} \omega_{mn} dt \right]$ , where  $\omega_{mn}$  is the distance between levels,  $t_1$  denotes the point on the real-time axis and  $\tau$  is the upper half-plane of complex time that satisfies equality between the initial,  $E_n$ , and the final,  $E_m$ , energies [5]:  $E_n(\tau) = E_m(\tau)$ . To compare our results with other theoretical and experimental findings [6-8], we included the influence of the perturbed ionization potential in our investigation. In addition, we performed calculations with linear and time-dependent laser profiles. Our results clearly indicated that change of the above-mentioned parameters, i.e., perturbation of ionization potential and change of the laser pulse, significantly influences the transition amplitude of ejected photoelectrons.

### REFERENCES

- [1] M. V. Ammosov, Sov. Phys. JETP 64, 1191 (1987).
- [2] V. S. Popov, Phys.-Uspekhi. 47(9), 855 (2004).
- [3] N. I. Shvetsov-Shilovski, M. Lein, L. B. Madsen, E. Räsänen, C. Lemell, J. Burgdörfer, and K. Tórkési, Phys. Rev. A 94(1), 013415 (2016).
- [4] N. B. Delone, *Basics of interaction of laser radiation with matter*, Atlantica Séguier Frontières, (1993).
- [5] V. P. Krainov and A. V. Sofronov, Phys. Rev. A 77(6), 063418 (2008).
- [6] A. S. Kornev, I. M. Semiletov, and B. A. Zon, J. Phys. B. 47(20), 204026 (2014).
- [7] J. E. Calvert, H. Xu, A. J. Palmer, R. D. Glover, D. E. Laban, X. M. Tong, and R. T. Sang, Sci. Rep. 6(1), 1-9 (2016).
- [8] T. Shaaran, N. Camus, J. Dura, L. Fechner, A. Thai, A. Britz, and R. Moshhammer, Phys. Rev. A 99(2), 023421 (2019).

## Influence of UV radiation on the time response of a resistive gas sensor based on liquid-phase exfoliated graphene

M. V. Bošković<sup>1</sup>, S. Andrić<sup>1</sup>, M. Frantlović<sup>1</sup>, I. Jokić<sup>1</sup>, M. Sarajlić<sup>1</sup>, T. Vićentić<sup>1</sup>, and M. Spasenović<sup>1</sup>  
 University of Belgrade - Institute of Chemistry, Technology and Metallurgy - Department of Microelectronic Technologies - National Institute of the Republic of Serbia, Belgrade, Serbia  
 e-mail: boskovic@nanosys.ihtm.bg.ac.rs

Graphene as an active surface for gas sensors attracts increasing attention. It has excellent intrinsic properties, such as high electrical conductivity and low electrical noise, and, since it is two-dimensional, all carbon atoms can react with the analyte [1]. These properties reduce the detection limit of graphene-based sensors down to a single molecule [2]. However, the aforementioned statement holds only for ideal graphene, without any impurities [3]. These impurities are typically a consequence of chemicals used for the synthesis and/or transfer process [3]. During the transfer process to the target substrate and before a gas-sensing experiment, graphene is in the ambient atmosphere, which inevitably results in the adsorption of water and other molecules from the air on its surface. Annealing at high temperatures (above 200 °C) is a well-established procedure for cleaning graphene surface [3]. As an alternative, exposing graphene films to the UV radiation of appropriate intensity was proposed [2].

Herein we investigate the influence of UV irradiation on the time response of a resistive gas sensor with a liquid-phase exfoliated graphene [4] as the active material. The effect of exposure to UV light on the baseline electrical resistance (in inert atmosphere) will be compared with the effect of the annealing process. The influence of various intensities of UV radiation on the response and recovery time, repeatability and detection limit of graphene will be discussed.

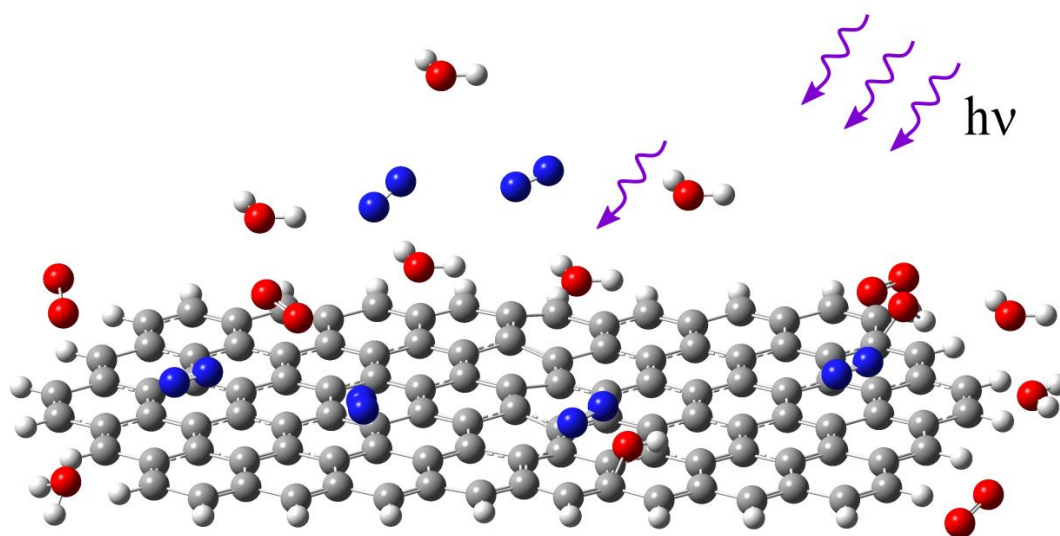


Figure 1. Illustration of UV-induced gas desorption from graphene surface

### REFERENCES

- [1] F. Schedin, A. K. Geim, S.V. Morozov, E.W. Hill, P. Blake, M.I. Katsnelson, and K.S. Novoselov, *Nat. Mater.* United Kingdom, 6 652 (2007)
- [2] C.-M. Yang, T.-C. Chen, Y.-C. Yang, and M. Meyyappan, *RSC Adv.* United Kingdom. 9 23343 (2019)
- [3] X. Yan, Y. Wu, R. Li, C. Shi, R. Moro, Y. Ma, and L. Ma, *ACS OMEGA*, USA. 4, 14179 (2019)
- [4] S. Andrić, T. Tomašević-Ilić, M. V Bošković, M. Sarajlić, D. Vasiljević-Radović, M. M Smiljanić, M. Spasenović, *Nanotechnology* United Kingdom. 32 025505 (2020)

## Observation of inter-orbital coupling

Diego Guzmán-Silva, Gabriel Cáceres-Aravena, Christofer Cid, and Rodrigo A. Vicencio

<sup>1</sup>*Departamento de Física and MIRO, Facultad de Ciencias Física y Matemáticas, Universidad de Chile, Chile*  
e-mail:rvicencio@uchile.cl

In lattice science, physicists, chemists and material scientists focus on wave propagation considering different lattice geometries and different – linear and nonlinear – interactions to visualize new solutions for improving localization and transport of energy across a given system [1]. The most standard theory is written assuming a tight-binding approximation, where every lattice site possesses a given state which, in most of the cases, corresponds to the fundamental symmetric ground state (typically called S wave-function). Therefore, most of the theory and experiments found in literature assume this wave-function at every site and construct a full lattice by inserting nearest-neighbor interactions plus different effects coming from magnetic and electric fields, spin-orbit, dipole-dipole interactions, self-focusing, among many others. Although it has been suggested theoretically the possibility of studying lattice interactions by assuming higher-order states as, for example, P or D wave-functions, solid experiments showing this interaction and direct control are still missing.

In this work [2], we explore theoretically, numerically and experimentally an orthogonal coupling interaction, focused on S and P wave-functions. We demonstrate a simple method which proposes the creation of asymmetric double-well like potentials in order to effectively tune the states energies. We specifically focus on a photonic context, where the theory perfectly coincides with a single-particle picture from quantum mechanics. We construct a full analogy between these two different scenarios and demonstrate, first, by numerical integration of a paraxial wave equation, that a perfect transfer of energy is possible between S and P wave-functions and, even further, between S and D states. We experimentally characterize the fabrication of single and multi-mode waveguides, using a femtosecond laser writing technique [3], and construct asymmetric photonic dimers (double-well potentials) to directly show the excitation of P wave-functions by a direct inter-orbital coupling from an initially S state. We show sinusoidal transfer dynamics by scanning the propagation distance along waveguides and perfectly show the oscillation of energy between S and P states. We characterize the coupling versus distance for S-S, S-P and P-P interactions to stimulate further research on extended lattice systems [1]. At the end, as a concrete application, we implement a phase beam splitter ( $\pi$ -BS) which splits an input S-wave-function into two S states, but having a  $\pi$ -phase difference. From a more applied point of view, our proposal is a device itself which perfectly works as a mode converter, which is quite relevant nowadays for classical and quantum information spatial multiplexing techniques, that are expected to be an answer for the increasing internet demand along optical fiber networks [4]. Also, the  $\pi$ -BS gives a new solution for quantum protocols where a phase beam splitter could be an important tool for concatenated operations.

### REFERENCES

- [1] F. Lederer, et al., Phys Rep. 463, 1 (2008).
- [2] D. Guzmán-Silva, G. Cáceres-Aravena, and R.A. Vicencio, submitted (2021).
- [3] A. Szameit, et al., Opt. Express 13, 10552 (2005).
- [4] R.G.H. Van Uden, et al., Nat. Phot. 8, 865 (2014).

## Microstructural characterization of Al-Cu alloy with optical microscopy in bright field and polarized light

S.Dikić<sup>1</sup>, M.Filipović<sup>1</sup>

<sup>1</sup>*Faculty of Technology and Metallurgy, University of Belgrade  
Karnegijeva 4, Belgrade, Serbia  
e-mail:sdikic@tmf.bg.ac.rs*

Precipitation hardening is characteristic for aluminium-copper (Al-Cu) alloys [1]. Main characteristics of Al-Co alloys, series 2xxx, are: wide range of mechanical properties and reduced corrosion resistance [1,2]. Corrosion resistance and mechanical properties of the Al alloy, depend on its microstructure [3]. As corrosion resistance properties can be improved by some technological processes, these alloys, because of their high strength, hardness and fatigue failure resistance, have found the application even in the most extreme conditions such as aircraft, vehicles and shipbuilding industries [1].

In this paper, the effects of homogenization annealing on the microstructure of the hypoeutectic Al-Cu alloys DC cast billets have been explored. Optical microscopy in bright field and polarized light were used in order to examine and characterize microstructure. In aluminum alloys, the best resolution of individual grains is achieved by the examination of electrolytically anodized samples in a polarized light microscopy. Segregations in microstructure causes not only the inhomogeneity of the microstructure, but also creates, the weak spots, places with different mechanical properties which may degrade material performances. In order to improve material properties, providing homogeneous microstructure was the initial goal. Homogenization was performed at 500°C for a different holding times (3h, 6h, 8h, 10h, 12h, 14h and 16h).

Microstructural changes are visible even after shortest homogenization times and microsegregations are reduced to a large extent during it. Otherwise, results have shown that macrosegregation can not be completely eliminated from the structure even after the longest homogenization times. Intermetallic Al<sub>2</sub>Cu phase dissolves and remains in the structure only in the traces.

### REFERENCES

- [1] J.E. Hatch, Aluminium: Properties and Physical metallurgy. Metals Park, OH: Am Soc Metals, 1984.
- [2] R. Nadella, D.G. Eskin, Q. Du, L. Kategerman, Prog. Mater. Sci., 53, 241-280 (2008).
- [3] M.A. Talamantes-Silva, A. Rodrigez, J. Talamantes-Silva, S. Valteierra, R. Colas, Mater Charact, 59, 1434-1439 (2008).

## Tracking of the temporal dependency of fading of the human footprint temperature contrast

S. Djenedic<sup>1</sup>, Lj. Tomic<sup>2</sup>, V. Damnjanovic<sup>1</sup>, D. Vasiljevic<sup>3</sup>, D. Pavlovic<sup>3</sup>

<sup>1</sup>University of Belgrade, Faculty of Mining and Geology, Djusina 7, Belgrade, Serbia

<sup>2</sup>Military Technical Institute, Ratka Resanovica 1, Belgrade, Serbia

<sup>3</sup>University of Belgrade, Institute of Physics, Photonics Center, Pregravica 118, Belgrade, Serbia

e-mail: [stevan.djenadic@rgf.bg.ac.rs](mailto:stevan.djenadic@rgf.bg.ac.rs)

In certain situations, it is extremely important to determine the exact time “someone” entered or crossed the forbidden zone of a military or strategic installation, a red zone of radioactive, chemical or biological contamination, a bank or similar structure. Standard security measures include ordinary video surveillance using cameras that operate in the visible range of the electromagnetic spectrum, as well commercial thermal imaging cameras [1, 2]. The paper presents the results of experiments that suggest another possible use of infrared (IR) thermography – tracking of the time dependency of fading of the human footprint temperature contrast.

The results are based on analyses of thermal images captured by a FLIR SC620 camera with an uncooled microbolometer detector VOx of  $640 \times 480$  pixels. The standard field of view of the camera is  $24^\circ \times 18^\circ$ , the spatial resolution 0.65 mrad and the NETD sensitivity less than 40 mK. The thermal imaging frequency was set at 30 Hz. Two of the thermal images of the surface of a carpet, after it was stepped over or after heat was transferred to the cold surface of the flooring, are shown in Figure 1. Several IR sequences and a series of thermal images were selected to analyze the temperature contrast in the zone of interest over time. The temperature contrast history, or the difference between the surface temperature of the footprint and the floor, shows “when the intruder invaded the forbidden zone”.

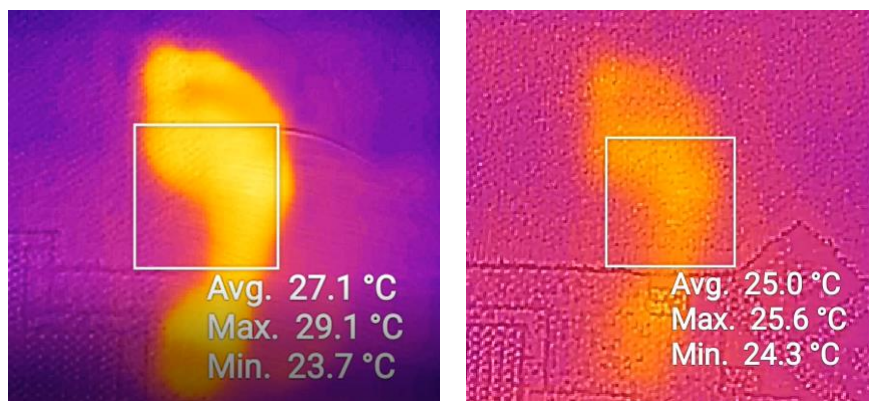


Figure 1. Thermal image of footprint on carpet:

Left 1 s after beginning of imaging;

Right – 30 s after beginning of imaging.

### REFERENCES

- [1] S. W. Harmer, C. I. Johnson, D. Wheeler, and H. Bhabha. *PIER M.* 88, 83-89 (2020).  
 [2] L. Tomić, V. Damnjanović, G. Dikić, and B. Milanović. *Appl. Sci.* 9, 1854 (2019).

## Optimization of Optoelectronic Properties of Electrochemically Exfoliated Graphene by Cascade Centrifugation

T. Vićentić<sup>1</sup>, S. Andrić<sup>1</sup>, M. Bošković<sup>1</sup>, J. Stevanović<sup>1</sup>, I. Pašti<sup>2</sup> and M. Spasenović<sup>1</sup>

<sup>1</sup>Center for Microelectronic Technologies, Institute of Chemistry, Technology and Metallurgy, University of Belgrade, Serbia

<sup>2</sup>Faculty of Physical Chemistry, University of Belgrade, Serbia  
e-mail: teodora@nanosys.ihm.bg.ac.rs

Graphene dispersions produced by the process of electrochemical exfoliation were used for preparing multi-layered graphene films for transparent conductor applications. In order to achieve homogeneous films with defined particle sizes from a solution with a wide distribution of initial particle sizes, cascade centrifugation was used. The particle size was selected by low-speed centrifugation, with rate values: 2, 3, 3.5, 4 and 5 krpm. After each step of centrifugation, supernatants were used as initial solutions for the following steps, while the sediments were collected and redispersed by using N-methyl-2-pyrrolidone as a solvent [1]. To study optical properties of produced graphene films, the dispersions were deposited onto glass substrates and UV/VIS spectroscopy was performed. Films with the best optical properties were selected and the same dispersions were deposited onto substrates with electrodes, to examine electronic properties of the films. Films had an optical transparency of ~83% in the visible part of the spectrum, and initial resistances between  $8 \cdot 10^3$  and  $1.6 \cdot 10^7$  Ohms. In order to improve electronic properties, the active surface was treated with nitric acid. After the treatment, sheet resistance decreased by a factor of 1,000, which makes these films good candidates for transparent electrodes. Scanning electron microscopy was used to analyze the surfaces of both treated and non-treated films.

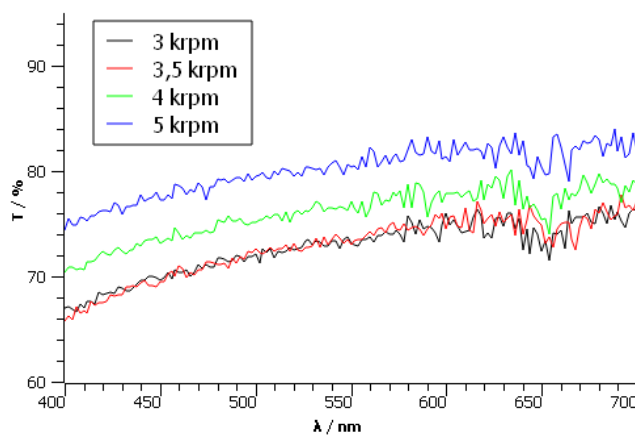


Figure 1. UV/VIS spectra for different graphene films.

### REFERENCES

[1] C. Backes et al, Production of Highly Monolayer Enriched Dispersions of Liquid-Exfoliated Nanosheets by Liquid Cascade Centrifugation, ACS Nano 10, 1, 1589–1601 (2016).

## Relevance of incoherent light-induced coherences for photosynthetic energy transfer

V. Janković<sup>1</sup>

<sup>1</sup>*Institute of Physics Belgrade, University of Belgrade, Serbia*  
e-mail: veljko.jankovic@ipb.ac.rs

The interpretation of oscillatory features in experimental signals from photosynthetic pigment–protein complexes excited by laser pulses [1] has been motivating vigorous interest in quantum effects in photosynthetic energy transfer (ET) [2]. However, electronic dynamics triggered by natural light, which is stationary and incoherent, is generally substantially different from the one observed in pulsed laser experiments. It has been suggested that the physically correct picture of photosynthetic ET should be in terms of a nonequilibrium steady state (NESS) [3], which is formed when a photosynthetic complex is continuously photoexcited and continuously delivers the excitation energy to the reaction center (RC), in which charge separation takes place.

We study ET in a molecular aggregate that is driven by weak incoherent radiation and coupled to its immediate environment and the RC. We combine a second-order treatment of the photoexcitation with an exact treatment of the excitation–environment coupling and formulate the hierarchy of equations of motion (HEOM) that explicitly takes into account the photoexcitation process [4]. We develop an efficient numerical scheme that respects the continuity equation for the excitation fluxes to compute the NESS of the aggregate [5]. The NESS is most conveniently described in the so-called preferred basis, in which the excitonic density matrix is diagonal. The preferred basis, which is analogous to the set of normal modes of a system of coupled harmonic oscillators, is singled out by the interplay between excitation generation, energy relaxation, dephasing, and excitation delivery to the RC. Having established the proper NESS description, we are in position to critically reassess the involvement of stationary coherences in the photosynthetic ET and claims that stationary coherences may enhance the ET efficiency. Focusing on a model photosynthetic dimer, we examine the properties of the NESS. In the limit of slow delivery to the RC, we find that the NESS is quite similar to the excited-state equilibrium in which the stationary coherences originate from the excitation–environment entanglement. When the excitation delivery is slower than energy relaxation processes, we establish a general relationship between the NESS picture and time-dependent description of an incoherently driven, but unloaded system.

### REFERENCES

- [1] G. S. Engel et al., *Nature* **446**, 782–786 (2007).
- [2] J. Cao et al., *Sci. Adv.* **6**, eaaz4888 (2020).
- [3] P. Brumer, *J. Phys. Chem. Lett.* **9**, 2946–2955 (2018).
- [4] V. Janković and T. Mančal, *J. Chem. Phys.* **153**, 244122 (2020).
- [5] V. Janković and T. Mančal, *J. Chem. Phys.* **153**, 244110 (2020).

## Coupled waveguide arrays ring resonators

Paloma Vildoso, Scarlett Plaza, and Rodrigo A. Vicencio

*Departamento de Física and MIRO, Facultad de Ciencias Física y Matemáticas, Universidad de Chile, Chile*  
 paloma.vildoso@ug.uchile.cl

The study of optical ring resonators (RR) has had a great deal of attention from the scientific community the last years due to there are lot of possible applications for them in laser fabrication, interferometry, telecommunications, optical parametrical oscillators, among others [1]-[3]. There are several works describing the dynamics in systems fabricated in Silicon [4]-[6] as well as in Photonic Crystal configurations [7]-[9]. However, RR using waveguide arrays configurations have not been still developed and our main aim is to explore this possibility. Interestingly, although the coupling mechanism in between the input straight waveguide and the ring resonator itself is based on an evanescent coupling, no relation or analogy with coupled waveguide arrays has been establish up to now.

In this work, we propose to theoretically and numerically investigate the possibility of a RR analog based on waveguide arrays (WARR). In order to implement this, we propose to use engineered coupling constants with functionality in the propagation coordinate  $z$  [see Fig.1(a)]. This is necessary to define a rotation direction as it would happen in a standard RR configuration producing a rotational power increment as shown in Fig.1(b). We compare our main findings with standard RR results in terms of transmission dependence with respect to the coupling in between the detection waveguide and the waveguide ring and, also, with respect to the specific ring size.

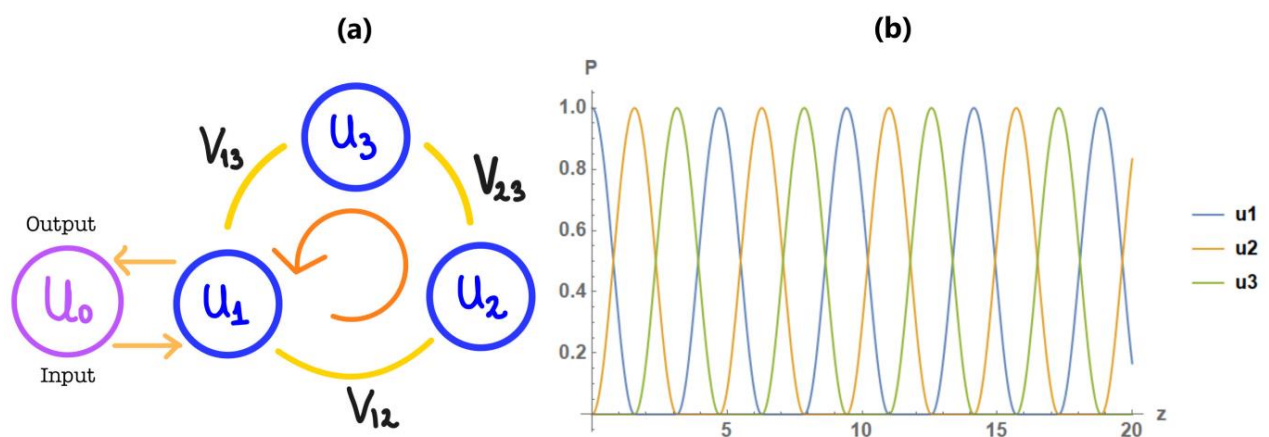


Figure 1. (a) WARR using three waveguides as a ring and other as a detection waveguide. (b) Power vs  $z$  for each waveguide in the ring.

### REFERENCES

- [1] C.L.Linsal et al, APL 106,131101(2015)
- [2] Zhenyu Li, Jun Zou, Huihui Zhu et al, *ACS Sensors* **2020** 5 (8), 2448-2456
- [3] S. Azzini, D.Grassani,M.J. Strain et al, *Opt. Express* **20**, 23100-23107 (2012)
- [4] W.Bogaerts,P.De Heyn, T.Van Vaerenbergh et all, *Laser Photonics Rev.* 6, No. 1, 47–73 (2012).
- [5] John D. Orlet and Ryan C. Bailey, *Analytical Chemistry* **2020** 92 (2), 2331-2338
- [6] A. Mirza, F. Sunny, S. Pasricha and M. Nikdast, 2020 Design, Automation & Test in Europe Conference & Exhibition (DATE), 2020, pp. 484-489, doi: 10.23919/DATE48585.2020.9116201.
- [7] V. Dinesh Kumar, T. Srinivas, A. Selevarajan, <https://doi.org/10.1016/j.photonics.2004.11.001>.
- [8] Zexuan Qiang, Weidong Zhou, and Richard A. Soref, *Opt. Express* **15**, 1823-1831 (2007)
- [9] Wei-Yu Chiu, Tai-Wei Huang, Yen-Hsiang Wu et al, *Opt. Express* **15**, 15500-15506 (2007)

## Index

### A

Abazovic N.....	89
Aceti D.....	150
Adyatullin A.....	139
Aleksić B. N.....	64
Aleksić N. B.....	64, 72
Aleksic S.M.....	169
Allmendinger Pitt.....	138
Altan Hakan.....	22
Alwashahi S. B. A.....	72
Andjus Pavle.....	44
Andrejić N.....	57
Andrić S.....	180, 184
Angelakis D. G.....	28
Angelini Angelo.....	162
Angelova L.....	150
Anglin J.....	54
Anikeeva V.....	94
Arbanas M.....	168, 172
Arsenovic D.....	66
Arsoski V. V.....	77, 123
Arsov Z.....	47
Ashour O. A.....	72
Aškrabić S.....	81, 91
Astadjov D.....	130
Atić A.....	118

### B

Bagabas Reem.....	36
Bajić J.....	125, 168, 172
Bajo J.....	147
Balaž A.....	59
Barabanenkov M.....	128
Batani D.....	149
Batinić B.....	168, 172
Belić M. R.....	64, 72, 160
Beličev P. P.....	71
Benocci R.....	149
Bijelić Dunja.....	44
Biswas Anjan.....	73
Blažić L.....	102, 112, 116
Bluvstein D.....	19
Boarino Luca.....	162
Bobić Z.....	112
Boldyrev K.....	83, 94

Boltasseva Alexandra.....	10
Boscolo Sonia.....	23
Bošković M. V.....	180, 184
Božanić D. K.....	46
Božanić Dušan K.....	76
Bozhikoliev Ivan.....	68
Božinović N.....	153, 156
Božović P.....	77
Braatz Thomas.....	38
Brehove Matthew S.....	36
Brkić A. L.....	167
Brkić M.....	172
Buchvarov I.....	150
Budimir M. D.....	40
Bugarski Kolja.....	136
Bulgakova N.M.....	24
Buljan Hrvoje.....	25
Bunjac A.....	152
Buss Jan Heye.....	38
Busuladžić M.....	65

### C

Cáceres-Aravena Gabriel.....	132, 181
Cantillano Camilo.....	67
Çapar Abdulkерim.....	44
Capasso Federico.....	120
Čapeta D.....	81
Cara Eleonora.....	162
Carette X.....	150
Cederbaum L. S.....	143
Changeux J.-P.....	45
Channab Marwan.....	162
Chen Z.....	51
Chin S. A.....	72
Choi S.....	19
Chorbadzhiyska Y.....	90, 95, 96
Cid Christofer.....	132, 176, 181
Cin S. D.....	126
Clayton A.H.A.....	14, 45, 115
Ćojbašić Ž.M.....	169, 173, 174
Colombo S.....	139
Cubillos Javier.....	177
Ćurčić M.....	58, 66

### D

Dajic-Stevanovic Z.....	154
-------------------------	-----

Dakova Aneliya .....	68, 73
Dakova Diana .....	73
Dal Cin Sandro .....	120, 138
Damnjanovic V. ....	183
Danilović Danijela .....	76
Das Saumya .....	36
Daskalova A. ....	150
Dean P. ....	41
Delibašić Marković H. ....	148, 179
Demić A. ....	41, 129
Desaules J.-Y. ....	42
Despotović S. ....	114
Dikić S. ....	182
Djapic N. ....	113
Djenadic S. ....	183
Djoković Vladimir .....	46, 76
Djordjevic Ivan B. ....	170
Djordjevic K.Lj. ....	85, 169, 173
Djordjevich A. ....	133
Dojčilović Radovan .....	46, 76
Dreischuh A. ....	141
Drvenica I. ....	107, 108
Dudley J. M. ....	15
<b>E</b>	
Ebadi S. ....	19
Eggeling C. ....	11
Endo M. ....	26
Ersen Kerman Bilal .....	44
<b>F</b>	
Fadic Guillermo .....	176, 177
Ferrarese Lupi Federico .....	162
Filipov E. ....	150
Filipovic J. ....	55
Filipović M. ....	182
Filipović N. ....	61
Finot Christophe .....	15, 23
Flores Esteban .....	178
Frantlović M. ....	180
<b>G</b>	
Galović S.P. ....	85, 169, 173
Gang Seung-gi .....	144, 145
Gazibegović-Busuladžić A. ....	65
Gensch M. ....	142
Genty G. ....	15
Georgiev R. ....	90, 95, 96
Georgieva B. ....	90, 95, 96
Ghobara M. ....	105
Gilić M. ....	78, 105
Gligorić G. ....	71
Glukhova S. A. ....	155
Gojanović Jovana P. ....	88, 119
Golz Torsten .....	38, 51
Greiner M. ....	19
Grujić D. ....	51, 100, 102
Grujić Z. D. ....	62
Gündogdu S. ....	69, 157
Guzmán-Silva Diego. ....	132, 176, 181
Gvozdiovas E. ....	27
<b>H</b>	
Habibović D. ....	65
Hadzibabic Zoran .....	16
Hadžievski Lj. ....	71, 159
Hillbrand Johannes .....	126, 138
Ho W.W. ....	19
Höfling S. ....	121
Hogle C. W. ....	143
Hudomal A. ....	42
<b>I</b>	
Ikonić Z. ....	41, 129
Ilić V. ....	107, 108
Ilić Velimir M. ....	170
Indjin D. ....	41, 129
Isić G. ....	91, 160, 163
Ivanov B. ....	124
<b>J</b>	
Jačimovski S.K. ....	80
Jadrisko V. ....	147
Jaklin M. ....	167
Jaksic M. ....	110
Jakšić O. ....	165
Jakšić Z. ....	161, 165
Janković V. ....	185
Jelenković B. ....	58, 66, 75, 92
Jokić I. ....	180
Jones Veronica .....	36
Jordović-Pavlović M.I. ....	173
Jouy Pierre .....	138
Jovanović Svetlana. ....	87
Jovanovic-Talisman Tijana .....	36
Juzeliūnas G. ....	27
<b>K</b>	
Kamenskikh I. ....	93
Kapteyn H. C. ....	143
Kasapeteva Zara .....	73
Kaščakova S. ....	46
Kavatzikidou P. ....	156
Kazakov Dmitry .....	120
Keesling A. ....	19
Kelsalland R. W. ....	129

Khalf Ali R. ....	119
Kisic D. ....	43
Kleut Duška ....	87
Knötig H. ....	121
Koeth J. ....	121
Koklič T. ....	47
Kolasinac S. ....	154
Konov V. ....	93
Korać A. ....	103
Korenić Andrej ....	44
Korićanac L. ....	103
Kornev V. ....	151
Kostadinov I. ....	124, 130
Kovacevic A. ....	75
Kovačević M. S. ....	133
Kovachev Lubomir ....	73
Kowalska K. ....	82
Kralj M. ....	167
Krasteva Stefka ....	73
Krebs O. ....	55
Krivokapić Z. ....	114
Krizan J. ....	137, 171
Krmpot A.J. ....	45, 66, 104, 106, 107, 108, 111, 114, 115, 116
Krsic J. ....	56, 122
Kurtovic M. ....	179
Kuwik M. ....	82
Kuzmanović Lj. ....	133
Kuzmanovich M. ....	135
Kuznetsov S. ....	93
<b>L</b>	
Lagerholm C. ....	11
Lainović T. ....	102, 112, 116
Lapre C. ....	15
Lazarevic M. ....	110
Lekic M. ....	75
Lemaîtreand A. ....	55
Lendl Bernhard ....	120
Lennon Kathleen M. ....	36
Lević S. ....	114
Levine H. ....	19
Leykam D. ....	28
Li Z. ....	139
Lidorikis E. ....	29
Loza-Alvarez Pablo ....	30
Lukić M. ....	174
Lukin M. ....	19
<b>M</b>	
Mabed M. ....	15
Maddox Adam L. ....	36
Makarov M. ....	128
Maluckov A. ....	56, 69, 71, 122
Manojlovic L. ....	125
Manojlovic V. ....	101
Manousaki A. ....	156
Marinkovic B.P. ....	106, 137, 171
Marković Z.M. ....	40
Markushev D.D. ....	85, 169, 173, 174
Markushev D.K. ....	169
Martella D. ....	20
Martin L. ....	143
Martyanov Artem K. ....	93, 98
Matić M. ....	107, 108
Matijević M. ....	109
Matković A. ....	31
Mendez E. ....	139
Meng F. ....	15
Miano D. ....	150
Milanovic V. ....	127
Milasin J. ....	110
Milenković Mila. ....	87
Miler I. D. ....	103
Milićević Đ. ....	114
Milicevic N. ....	89
Miljkov D. ....	101
Milosavljević Aleksandar R. ....	76
Milošević D. B. ....	65
Milosevic M. ....	110
Milošević M. M. ....	133
Milošević M. V. ....	123
Milosevic V. ....	159, 164
Milovanović D. ....	153
Milovic M. ....	89
Mimidis A. ....	156
Mincheva R. ....	150
Minnullin R. ....	128
Miteva T. ....	143
Mitrić J. ....	78
Mladenović I. ....	161
Mortimer Joanne ....	36
Muñoz Francisco. ....	178
Mur J. ....	47
Murataj Irdi ....	162
Murić B. ....	100
Murnane M. M. ....	143
Mutavdzic D. ....	101
<b>N</b>	
Nagaoka Hiroki ....	26
Narayanan V. ....	149
Nedelko M. ....	135
Nedić S. ....	91
Nenadić M. ....	100
Nenadovic M. ....	43

Nešić M. D.....	103, 109
Nešić M.V.....	85, 173
Nevar A. ....	135
Nikitović Ž.....	66
Nikolić G. ....	114
Nikolic M.....	51
Nikolic M.G.....	137, 171
Nikolić S.N. ....	45, 72, 75, 107
Nocentini S. ....	20
Novakovic M.....	43, 84, 89
Novta E.....	102
<b>O</b>	
Oasa S. ....	45
Obradov M.....	161, 165
Obradović J.....	81
Omran A. ....	19
Opačak Nikola.....	120, 121, 126
<b>P</b>	
Pajić T.....	75, 104, 111, 115
Pajović J.....	46
Pan Rui .....	51, 144, 145
Pantelić D. ....	92, 99, 100, 102
Pantic D.S.....	169
Papić Z.....	42
Parmeggiani C. ....	20
Pašti I. ....	184
Paulus G. G.....	141
Paunović N. ....	78
Pavlov V. ....	90, 95, 96
Pavlović A. ....	114
Pavlović D. ....	75, 99, 107, 108, 183
Pavlović V. ....	61, 114
Pecikozić N.....	112
Pecinar I.....	110, 154
Pedrozo-Peñafiel E. ....	139
Peeters F. M.....	77, 123
Pelster A. ....	54, 59, 60
Peng Junsong.....	23
Peruško D. ....	156
Pešić I. ....	78
Pešić J. ....	78
Petković M.....	103, 109
Petkovšek R.....	47
Petrovic B. ....	127
Petrović I. ....	148, 179
Petrovic J. ....	56, 122
Petrović M. S.....	64
Petrović S.....	153
Petrović Suzana .....	156
Petrović V.....	148, 179
Petrović Zoran Nikola .....	70
Pichler H. ....	19
Pilat Florian.....	120
Pirri Candido F.....	162
Pisarska J.....	82
Pisarski W.A. ....	82
Pjevic D.....	89
Plaza Scarlett.....	186
Pleštić I. ....	116
Plönjes Elke .....	144
Podlipec R.....	47
Popova M.....	94
Popović D. B.....	152
Popović M.....	79, 84
Popović M.N.....	85, 173
Potočnik J.....	43, 79, 89
Prandolini Mark J.....	38
Ptasinska Sylwia .....	76
Puač N.....	86, 116
Pustelny Szymon.....	32
<b>Q</b>	
Quidant R.....	17
<b>R</b>	
Rabasović M. D. .	51, 104, 106, 107, 108, 111, 114, 115, 116, 137, 171
Rabasović M. S. ....	106, 137, 171
Račkauskas P. ....	27
Radatovic B.....	147
Radenković M.....	77
Radmilović M. ....	100, 107, 108
Radoičić M.....	103
Radojičić M.....	109
Radomzev A. ....	135
Radonjić Milan .....	60
Radovanović J.....	118, 127
Radulaski Marina.....	33
Rajić V. ....	84, 153, 156
Rajs V. ....	172
Rakočević L. ....	89, 153
Ralević U. ....	81, 159, 160, 163, 164
Ramer Georg.....	120
Ranitovic P.....	143
Rankovic D. ....	135
Real B. ....	132, 176
Refregiers M. ....	46
Reina F.....	11
Reissig L. ....	105
Riedel Robert.....	38
Rigler R.....	45
Román Diego .....	176, 177
Romčević N. ....	78
Romshin A. ....	98

Ronning Carsten .....	18	Stojanović M. G. ....	69
<b>S</b>		Stojanovic Nikola.....	51, 142, 144
Sachdev S. ....	19	Stojković Lazar S. ....	170
Saftics Andras.....	36	Stoyanov L. ....	141
Salatić B.....	99	Štrancar J.....	47
Salinas Ignacio V.....	67	Strasser Gottfried .....	120, 121, 126, 138
Samajdar R. ....	19	Stratakis E. ....	156
Sapkota Pitambar.....	76	Strinić A. I.....	64
Sarajlić M. ....	180	Supina A. ....	147, 167
Savić-Šević S.....	92, 99, 102, 137, 171	<b>T</b>	
Savikin K. ....	106	Tadić M. Ž. ....	77, 123
Savović J.....	135, 153	Tanasković D. ....	161, 165
Schmolze Daniel.....	36	Tarasenska N. ....	151
Schröder T. ....	157	Tarasenko N. ....	135, 151
Schulz Michael .....	38	Temelkov K. ....	124, 130
Schwarz Benedikt.....	120, 121, 126, 138	Temme Marc.....	51, 144
Sedov V. ....	93	Terek P.....	112
Selaković N. ....	116	Terenius L. ....	45
Semeghini G. ....	19	Tobin Steven J. ....	36
Semenova O.....	94	Todorović Marković B.....	40
Senkić A. ....	147, 167	Todorović N.....	104, 111, 115
Štrajčić I.J. ....	80	Toleikis S. ....	51
Štrajčić J.P. ....	80	Tomasević-Ilić T.....	49, 86
Štrajčić-Tomić A.J. ....	80	Tomic Lj. ....	183
Sevic D. ....	106, 137, 171	Tong X-M. ....	143
Shu C. ....	139	Topalović D. B.....	77
Simonović N. S.....	152	Topić S.....	62
Šindik M. ....	51, 59	Tošić Dragana.....	76
Singh Gagandeep.....	36	Trifonov A. ....	150
Škorić B. ....	112	Trtica M. ....	149
Škoro N.....	86, 116	Tserevelakis G.J.....	37
Slavchev Valeri .....	68, 73	Tsigelny I.F.....	45
Slaveeva S. ....	124, 130	Turitsyn S.....	71
Šljivančanin Ž.....	48	Turner C. J. ....	42
Smirnova Daria.....	34	<b>U</b>	
Smit Meint K. ....	12	Ueda K. ....	143
Sokic M. ....	101	Urbančić I. ....	47
Šolajić A. ....	78	<b>V</b>	
Šoškić B. N.....	48	Vakalov D. ....	93
Spasenović M. ....	49, 86, 180, 184	Van Keuren-Jensen Kendall.....	36
Stanciu George A.....	35	Vasić B.....	91
Stanic M.....	75	Vasiljevic D. ....	183
Stanojevic M.....	88	Vasiljević Radović D. ....	161
Starosielec Sebastian .....	38	Vasiljević-Toskić M.....	125, 168, 172
Stasić J. ....	149	Veerman J.J.P .....	56, 122
Stavrić S.....	48	Vesović N. ....	99
Stepić M.....	69, 103, 109	Vicencio Rodrigo A. ...	67, 132, 176, 177, 178, 181, 186
Stevanović J.....	184	Vićentić T. ....	180, 184
Stevanović K. ....	104, 111	Vildoso Paloma.....	186
Stevanović Lj.....	57		
Stojanovic D. B. ....	159, 164		
Stojanović Krasić M. ....	69		

Vlahović J. R. ....	123
Vlasov Igor I. ....	98
Vojnović N.R. ....	80
Vučenović S.M. ....	80
Vudragović Dušan ....	50
Vujčić N. ....	147
Vukmirović Nenad ....	76
Vukojević V. ....	45
Vuković N. ....	118, 127
Vuletić V. ....	19, 139

**W**

Wakefield Devin L. ....	36
Wamba E. ....	54
Wang T.T. ....	19
Wang X. ....	129
Wani Fumio ....	26
Weih R. ....	121
Wiersma D.S. ....	20

**Y**

Yankov G. ....	124, 130
Yurkin M. A. ....	155

**Z**

Žakula J. ....	103
Zamanev Zhelyazko ....	68
Zapolnova Ekaterina ....	38, 51
Zarkov Boban ....	100, 136
Zdunic G. ....	106
Zeeb Vadim. ....	98
Žekić A. ....	149
Zhang Y. ....	141
Živanović Sandra ....	88, 119
Živanović V. ....	114
Živić M. ....	104, 111, 115
Zlatković B. ....	66